2012

Methods of optimizing the gas exchange process to improve fuel efficiency of small carbureted spark ignition engines

Cory Hannibal Huck

Department:

METHODS OF OPTIMIZING THE GAS EXCHANGE PROCESS TO IMPROVE FUEL EFFICIENCY OF SMALL CARBURETED SPARK IGNITION ENGINES

by

CORY HANNIBAL HUCK

A THESIS

Presented to the Faculty of the Graduate School of the

MISSOURI UNIVERSITY OF SCIENCE AND TECHNOLOGY

In Partial Fulfillment of the Requirements for the Degree

MASTER OF SCIENCE IN MECHANICAL ENGINEERING

2012

Approved by

James A. Drallmeier, Advisor
Kelly O. Homan
Arindam Banerjee

ABSTRACT

Fuel efficiency of internal combustion engines long has been a topic of concern. Much effort has been made to optimize the fuel efficiency of large automotive type engines. However, for small engine manufactures subject to tight cost constraints, this has only recently become an area of great focus. A method by which the fuel efficiency of an engine can be improved is through optimization of the intake process. Specifically, reductions in flow losses and the choice of appropriate valve event timings can provide ways to make gains towards more fuel efficient operation. The challenge arises when the focus is on carbureted engines where the flow rate of air and the flow rate of fuel are coupled. At this point, and for the focus of this thesis, it is important to reduce the amount of energy required of the engine to induct the fuel and air mixture. Several experiments and testing methodologies are introduced that look at ways of minimizing these losses, as well as a look at optimizing the timing of valve events for key operating points. A look at how valve timing events effect the distribution of energy throughout the engine using first law principles was also examined.

AKNOWLEDGEMENTS

I would first like to express my appreciation and gratitude to my advisor Dr. James Drallmeier, whose support, advice, and guidance has enabled this thesis to come to fruition. The vast knowledge and problem solving techniques he has imparted will continue to help me succeed throughout my career. I would also like to thank my graduate committee members Dr. Kelly Homan and Dr. Arindam Banerjee who have been excellent teachers and mentors throughout my collegiate career.

I would also like to express my thanks to my friends and mentors who have driven me to succeed through my time at this University: Jeff Massey who provided much needed guidance and leadership in my early graduate career; Josh Bettis, Shawn Wildhaber, Avinash Singh, Aaron Attebery, and Allen Ernst for their assistance and friendship over the last two years.

Lastly, I would like to thank my family, particularly my parents Stan and Sandy Huck who have helped provide this opportunity to me. The support and moral values they have instilled in me for my entire life has made this possible. Most importantly, I would like to thank my fiancé, Katy Whites, who has been encouraging, supportive, patient, and understanding throughout this long process.

TABLE OF CONTENTS

Page

ABSTRACT iii

AKNOWLEDGEMENTS iv

LIST OF ILLUSTRATIONS x

LIST OF TABLES xvi

ABBREVIATIONS xviii

SECTION

1. INTRODUCTION 1

2. LITERATURE REVIEW 5

2.1 GAS EXCHANGE PROCESS IN A FOUR STROKE ENGINE. 5

2.1.1 Poppet Valve Characteristics 7

2.1.2 Valve Event Timings and their Effects on Engine Operation. 8

2.2 EXPERIMENTAL ANALYSIS OF THE GAS EXCHANGE PROCESS. 11

2.2.1 Steady State Flow Bench Testing 12

2.2.1.1 Flow and discharge coefficients 14

2.2.1.2 Internal flow loss in the intake system 15

2.2.2 Engine Performance Measurements 16

2.2.2.1 Collection of pressure data 17

2.2.2.2 Measurement of pumping work by means of cylinder pressure ... 19

2.3 MODELING OF THE GAS EXCHANGE PROCESS. 21

2.3.1 Thermodynamic Formulation. 22

2.3.2 Fluid Dynamic Model 23

2.3.3 Application of Engine Simulations 24

2.4 SMALL ENGINE DESIGN 26

3. EXPERIMENTAL FACILITY 28

3.1 STEADY STATE FLOW BENCH AND TESTING PROCEDURE. 28

3.1.1 Steady Sate Flow Bench 28

3.1.2 Steady State Flow Bench Testing Procedure 36

3.1.3 Steady State Flow Bench Data Reduction 37

3.2 ENGINE STAND TESTING AND PROCEDURE. 38

3.2.1 The Engine Stand 38

3.2.2 Engine Instrumentation 38

3.2.3 Engine Testing Procedure 39

3.2.4 Engine Data Reduction 41

3.3 EXPERIMENTAL ERROR ANALYSIS 43

4. INITIAL DESIGN CONSIDERATIONS 46

4.1 FOCUS ON DESIGN CONCERNS 46

4.1.1. Stock Head Comparison 46

4.1.2 The Stock Port Design and Proposed Modifications 47

4.1.3 Experimental Valve Characteristics 48

4.2 CYLINDER DISCREPANCIES 52

4.2.1 Test Engine Cylinder Setup 52

4.2.2 Cylinder Pressure versus Cylinder Volume Diagrams 54

5. COMPUTATIONAL FLUID DYNAMICS AND INITIAL FLOW TESTING 59

5.1 COMPUTATIONAL FLUID DYNAMICS. 59

5.1.1 Motivation 59

5.1.2 Computational Fluid Dynamic Model 59

5.2 STEADY STATE TESTING FOR FLOW AND DISCHARGE COEFFICIENTS 65

5.2.1 Flow Bench Testing 65

5.2.2 Experimental Error Range of Flow Bench Testing 66

5.2.3 Results for Flow and Discharge Coefficient Tests 67

5.2.4 Integrated Flow Coefficient and Mach Index 70

6. STEADY STATE PRESSURE LOSS COEFFICIENT 75

6.1 PRESSURE LOSS COEFFICIENT FORMULATION AND PROCEDURE.. 75

6.1.1 Fluid Dynamic Formulation 75

6.1.2 Accounting for Major and Minor Losses in Steady State Flow Testing. . 85

6.1.3 Pressure Loss Testing Procedure 87

6.2 PRESSURE LOSS COEFFICIENT RESULTS 90

7. BASELINE ENGINE TESTING 97

7.1 BASELINE PRESSURE DATA. 97

7.1.1 Trends in Cylinder Pressure Data with Respect to Crank Angle 97

7.1.2 Trends in Cylinder Pressure Data with Respect to Cylinder Volume 106

7.2 MEAN EFFECTIVE PRESSURE ANALYSIS 112

7.3 CRANKSHAFT ACCELERATION 114

7.4 COMPARISON OF THE STOCK AND MODIFIED HEADS FOR BASELINE PRESSURE TESTING 116

8. STAGING OF THE TEST ENGINE'S CAMSHAFT 118

8.1 CAMSHAFT STAGING 118

8.1.1 Camshaft Staging Experimental Procedure 118
8.2 EXPERIMENTAL RESULTS AND ANALYSIS 120
8.2.1 Comparison of Cylinder Pressure Trends for the Staged Camshaft 120
8.2.2 Comparison of Experimental Parameters Based on Cylinder Pressure .. 132
8.2.3 Comparison of Experimental Parameters Based on Energy Flow..... 140
8.2.4 Performance of Modified Cylinder Heads for Camshaft Staging Tests.. 156
8.3 FIRST LAW ENERGY BALANCE. 158
8.3.1 Combustion Stoichiometry 158
8.3.2 Energy Pathways..... 160
8.3.3 Energy Balance Calculations. 161
8.3.4 Energy Balance Results Between Camshaft Staging Tests 162
9. ENGINE SIMULATION PROGRAM 169
9.1 INTRODUCTION TO THE ENGINE SIMULATION PROGRAM 169
9.1.1 ESP Governing Models and Assumptions..... 169
9.1.2. ESP Model Limitations..... 171
9.2 COMPARISON AND RESULTS OF SIMULATED DATA..... 172
9.2.1 Comparison of Experimental and Simulated Data..... 172
9.2.2 Camshaft Staging Simulation 176
9.2.3 The Variation of Individual Valve Events..... 180
9.2.4 Mass Flow Across System Boundaries..... 183
10. CONCLUSIONS..... 195
10.1 METHODS OF ANALYSIS. 195
10.2 OPTIMIZATION OF INTAKE GEOMETRY..... 195

10.3 OPTIMIZATION OF VALVE EVENTS 196

10.4 SUMMARY OF CONCLUSIONS AND RECOMMENDATIONS 199

APPENDICES

A. ADDITIONAL PLOTS RELATING TO ENGINE TESTING RESULTS 201

B. ENGINE SIMULATION INPUT DATA 207

BIBLIOGRAPHY 212

VITA 214

LIST OF ILLUSTRATIONS

Figure Page

2.1: Typical intake system of a small engine 6

2.2: Intake manifold pressure with respect to engine crank angle degrees 7

2.3: Depiction of valve curtain area and minimum port area 8

2.4: Typical valve event timings plotted as cylinder pressure versus crank angle 9

2.5: Depiction of pumping work for the test engine 20

3.1: Flow bench diagram with all instrumentation included 29

3.2: Front pannel instrumentation for steady state flow bench setup 30

3.3: Top side of the flow bench 31

3.4: Cylinder head with bell-mouth and valve control mechanism attached 32

3.5: Settling tank fixture 33

3.6: Meriam laminar flow element and associated instrumentation 34

3.7: Liquid ring vacuum pump setup 35

3.8: Vacuum pump relief valve used to control pressure drop 36

3.9: Engine test stand and instrumentation 40

3.10: Intake manifold pressure and uncorrected cylinder pressure 42

3.11: Intake manifold and properly referenced cylinder pressure 43

4.1: Visual comparison of the test engine's cylinder heads 46

4.2: Typical valve lift profile with lift sections depicted 49

4.3: Intake and exhaust valve lift profile for both cylinders of the test engine 50

4.4: Cylinder pressure versus crank angle degrees for cylinder 1 and cylinder 2 53

4.5: Cylinder process diagram for the test engine 53

4.6: Typical pressure-volume plot for the pumping loop of th test engine 55

4.7: Pressure-volume diagram depicting valve events and cylinder processes 56

4.8: Representation of the valve timings for a camshaft staging test 57

5.1: Cross-section of the three-dimensional mesh featuring the valve at full lift 60

5.2: Pressure contours and streamlines of airflow through base head intake port 62

5.3: Modified head internal geometry used in CFD simulation. 63

5.4: Airflow streamlines through engine head modified with 7mm radius. 64

5.5: Repeatability testing results for flow and discharge coefficients 67

5.6: Flow and discharge coefficients for varying pressure drops and valve lifts 68

5.7: A comparison of flow and discharge coefficients for head 1 and head 2 69

5.8: Flow and discharge coefficients for stock head compared to modified head 69

6.1: Depiction of the steady state flow bench. 85

6.2: Critical areas of pressure loss testing 88

6.3: Component pressure loss contribution for the additive testing procedure 93

6.4: Stock cylinder head subsystem pressure loss contribution 94

6.5: Modified cylinder head subsystem pressure loss contribution 95

7.1: Cylinder and intake manifold pressure comparison for mode 1 operation 99

7.2: Cylinder and intake manifold pressure comparison for mode 6 operation 100

7.3: Compilation of cylinder pressure for all 6 modes of cylinder 1 101

7.4: Gas exchange processes for all 6 modes of cylinder 1 102

7.5: Compilation of manifold pressure for all 6 modes of cylinder 1 103

7.6: Compilation of cylinder pressure for all 6 modes of cylinder 2 104

7.7: Gas exchange processes for all 6 modes of cylinder 2 105

7.8: Compilation of intake manifold pressure for all 6 modes of cylinder 2 106

7.9: Mode 1 pumping loop for cylinder 1 and cylinder 2 108

7.10: Mode 2 pumping loop for cylinder 1 and cylinder 2 108

7.11: Mode 3 pumping loop for cylinder 1 and cylinder 2 109

7.12: Mode 4 pumping loop for cylinder 1 and cylinder 2 109

7.13: Mode 5 pumping loop for cylinder 1 and cylinder 2 110

7.14: Mode 6 pumping loop for cylinder 1 and cylinder 2 110

7.15: Motored pumping loop for cylinder 1 and cylinder 2 111

7.16: Pumping work values for cylinder 1 and cylinder 2; modes 1-6 113

8.1: Internal configuration of the test engine 119

8.2: Cylinder 1 mode 1 pressure versus volume for all camshaft staging tests 123

8.3: Cylinder 1 mode 2 pressure versus volume for all camshaft staging tests 124

8.4: Cylinder 1 mode 3 pressure versus volume for all camshaft staging tests 125

8.5: Cylinder 1 mode 4 pressure versus volume for all camshaft staging tests 126

8.6: Cylinder 1 mode 5 pressure versus volume for all camshaft staging tests 126

8.7: Cylinder 1 mode 6 pressure versus volume for all camshaft staging tests 127

8.8: Cylinder 2 mode 1 pressure versus volume for all camshaft staging tests 129

8.9: Cylinder 2 mode 2 pressure versus Volume for all camshaft staging tests 129

8.10: Cylinder 2 mode 3 pressure versus volume for all camshaft staging tests 130

8.11: Cylinder 2 mode 4 pressure versus volume for all camshaft staging tests 130

8.12: Cylinder 2 mode 5 pressure versus volume for all camshaft staging tests 131

8.13: Cylinder 2 mode 6 pressure versus volume for all camshaft staging tests 131

8.14: Shaft torque comparison for full engine of 6-Mode camshaft staging tests 133

8.15: Shaft output comparison for full engine of 6-Mode camshaft staging tests 134

8.16: Comparison of pumping work between camshaft staging tests for cylinder 1 137

8.17: Comparison of pumping work between camshaft staging tests for cylinder 2 137

8.18: Comparison of net imep between camshaft staging tests for cylinder 1 139

8.19: Comparison of net imep between camshaft staging tests for cylinder 2 139

8.20: Comparison of air mass flow rate between 6-Mode camshaft staging tests 141

8.21: Intake manifold pressure for 10 crank angle degrees retarded and 10 crank angle degrees advanced camshaft timings (mode 1) 142

8.22: Comparison of air mass flow rate between 6-Mode camshaft staging tests 143

8.23: Air to fuel ratio for cylinder 1 for 6-Mode camshaft staging tests 146

8.24: Air to fuel ratio for cylinder 2 for 6-Mode camshaft staging tests 147

8.25: Cylinder 1 exhaust gas temperatures for 6-Mode camshaft staging tests 149

8.26: Cylinder 2 exhaust gas temperatures for 6-Mode camshaft staging tests 149

8.27: Combustion efficiency for 6-Mode camshaft staging tests 151

8.28: Fuel conversion efficiency for 6-Mode camshaft staging tests 152

8.29: Brake specific fuel consumption for 6-Mode camshaft staging tests 154

8.30: Typical energy pathways for an internal combustion engine 161

8.31: 6-Mode energy distribution for camshaft staging of 10 degrees advanced 164

8.32: 6-Mode energy distribution for the stock camshaft setting 165

8.33: 6-Mode energy distribution for camshaft staging of 10 degrees retarded 165

8.34: Mode 1 comparison of energy for camshaft staging tests 166

8.35: Mode 6 comparison of energy for camshaft staging tests 167

9.1: Comparison between experimental and simulated data of cylinder 1 mode 1 174

9.2: Comparison between experimental and simulated data of cylinder 2 mode 1 174

9.3: Simulated camshaft staging for cylinder 1 177

9.4: Camshaft staging for cylinder 2 178

9.5: Staging of the exhaust valve opening event 181

9.6: Staging of the exhaust valve closing event 181

9.7: Staging of the intake valve opening event 182

9.8: Staging of the intake valve closing event 182

9.9: Effects of the IVO event on mass flow rate across the valves 185

9.10: Intake mass flow rate for IVO valve event 186

9.11: Exhaust mass flow rate for IVO valve event 187

9.12: Effects of the EVC event on mass flow rate across the valves 188

9.13: Intake mass flow rate for EVC valve event 189

9.14: Exhaust mass flow rate for EVC valve event 190

9.15: Intake mass flow rate for IVC valve event 192

9.16: Exhaust mass flow rate for EVO valve event 193

A.1: Cylinder and intake manifold pressure comparison for mode 2 operation 202

A.2: Cylinder and intake manifold pressure comparison for mode 3 operation 202

A.3: Cylinder and intake manifold pressure comparison for mode 4 operation 203

A.4: Cylinder and intake manifold pressure comparison for mode 5 operation 203

A.5: 6-Mode energy distribution for camshaft staging of 5 degrees advanced 204

A.6: 6-Mode energy distribution for camshaft staging of 5 degrees retarded 204

A.7: Mode 2 comparison of energy for camshaft staging tests 205

A.8: Mode 3 comparison of energy for camshaft staging tests 205

A.9: Mode 4 comparison of energy for camshaft staging tests..... 206

A.10: Mode 5 comparison of energy for camshaft staging tests..... 206

LIST OF TABLES

Table Page

3.1: Test Engine Specifications 38

3.2: Cycle B Six-Mode test procedure 40

4.1: Critical valve geometry properties 48

4.2: Test engine valve event timings 51

5.1: Mass flow rate comparison for the validation of the CFD simulation 61

5.2: CFD comparison of base and modified heads for key performance parameters 65

5.3: Integrated C_f and Mach indices at three different valve pressure drops 73

5.4: Experimental comparison of key parameters for base and modified heads 73

6.1: Typical experimental results from pressure loss flow testing 91

6.2: Reynolds numbers for each component from the experimental data 91

6.3: Pressure loss coefficient results for the additive testing procedure 92

6.4: Pressure loss coefficient results for the stock and modified heads 95

7.1: Mode 1 mean effective pressures for both cylinders of two data sets 114

7.2: Time of induction process of both cylinders 115

7.3: Test engine air mass flow rate comparison of stock and modified heads 117

8.1: Shaft torque of full engine for 6-Mode camshaft staging tests 133

8.2: Shaft output of full engine for 6-Mode camshaft staging tests 134

8.3: Pumping mean effective pressure for all 6-Mode camshaft staging tests 136

8.4: Net indicated mean effective pressure for all 6-Mode camshaft staging tests 138

8.5: Mass flow rate of air for full engine 6-Mode camshaft staging tests. 140

8.6: Mass flow rate of fuel for full engine 6-Mode camshaft staging tests. 143

8.7: Air to fuel ratio for 6-Mode camshaft staging tests 146

8.8: Exhaust gas temperatures for 6-Mode camshaft staging tests 148

8.9: Combustion efficiency for 6-Mode camshaft staging tests 151

8.10: Fuel conversion efficiency for 6-Mode camshaft staging tests 152

8.11: Brake specific fuel consumption for 6-Mode camshaft staging tests 154

8.12: Volumetric efficiency comparison for mode 1 of camshaft the staging tests..... 156

8.13: Comparison of stock and modified heads for the camshaft staging test of 10 cranke angle degrees advanced..... 157

8.14: Comparison of stock and modified heads for the camshaft staging test of 10 crank angle degrees retarded..... 157

9.1: Volumetric efficiency comparison between simulated and experimental tests..... 176

9.2: Comparison of simulated and experimental pumping mean effective pressure 176

9.3: Volumetric efficiency comparison of simulated camshaft staging tests..... 179

10.1: Weighted fuel conversion efficiency for the camshaft staging tests 198

B.1: Engine simulation input data..... 208

ABBREVIATIONS

A/F	Air to Fuel Ratio
BDC	Bottom Dead Center
bmep	Brake Mean Effective Pressure
bsfc	Brake Specific Fuel Consumption
CAD	Crank Angle Degrees
CFD	Computational Fluid Dynamics
EGR	Exhaust Gas Recirculation
EVC	Exhaust Valve Closed
EVO	Exhaust Valve Open
fmep	Frictional Mean Effective Pressure
$imep_{,g}$	Gross Indicated Mean Effective Pressure
$imep_{,n}$	Net Indicated Mean Effective Pressure
IVC	Intake Valve Closed
IVO	Intake Valve Open
LFE	Laminar Flow Element
MAP	Manifold Absolute Pressure
mep	Mean Effective Pressure
pmep	Pumping Mean Effective Pressure
RPM	Rotations Per Minute
sfc	Specific Fuel Consumption
TDC	Top Dead Center

1. INTRODUCTION

The ability of an engine to breathe, that is to expel all of its exhaust gas and induct the maximum amount of fresh charge possible, is of the utmost importance to maintaining a high engine operating efficiency. This has long been an area of concern with the automotive industry, but has only recently become an area of focus for manufacturers of smaller engines. With rising energy prices, increasing engine performance while decreasing fuel consumption has become a key goal of efficient engine design.

Due to cost constraints, many small engines typically used in powered equipment and generators are still air cooled and carbureted. Carburetors operate with the assistance of a venturi effect; flow through the venturi is generated by a pressure drop. Therefore, with a larger pressure drop or a higher mass flow rate of air, more fuel will be pulled into the system. In light of this, it is important to conduct a study that does not simply increase the flow rate within the engine, but ensures the flow of air and fuel are being utilized optimally. The reduction of flow friction and flow losses throughout the induction process and introducing flow into the cylinder at a desirable time are the key focuses of such an investigation.

The valve geometry and the timing of valve events play a critical role in determining overall engine efficiencies. The size and lift characteristics of poppet valves determine the amount of time available for flow as well as the overall flow area. The timing of valve events determines when in the engine cycle a valve opens and closes; this has a considerable effect on engine performance.

It is not possible within the current cost constraints of small engine applications to use advanced engine control schemes such as variable valve timing. That is, the ability to adjust the timing of certain valve events during real time engine operation based on speed and loading conditions. Thus, a tradeoff between high and low speed operation as well as high and low load operation must be made in the attempt to maximize the efficiency of the engine under all operating conditions.

There are several different methods available by which to test the performance of an engine's intake and exhaust system. Computational fluid dynamics (CFD) uses a geometrical mesh and either an explicit or implicit scheme to solve fluid dynamic based problems both spatially and temporally. Steady state flow bench testing allows for experimental measurements to be obtained in a controlled environment. Engine simulations are available that use thermodynamic and fluid dynamic based models to analyze energy and mass transfer in an engine cycle. Engine cell testing allows for the observation of real performance improvements in a dynamic environment under normal engine operation.

All of these methods will be considered within the scope of this investigation. Each method provides a different analysis tool and the ability to focus on certain aspects of the engine. For example, CFD allows the effects of flow separation around the valves to be modeled based on upstream geometry and flow conditions. Steady state testing can aid in the determination of flow loss throughout the intake system by analyzing each intake component. An engine simulation can provide insight on how changing valve events and other metrics will alter the performance of the engine. Lastly, engine testing will prove or disprove the results obtained in other tests as well as provide insight to

actual improvements in engine operation. This analysis is done with the ultimate goal of determining improvements that can be made within the intake and exhaust system of a small air cooled carbureted engine. This investigation will be focused on protocols and methods which can be used to reduce flow friction and increase output performance by making improvements to the geometry of the intake system and the timing of engine valve events. This is done with the goal of decreasing operational costs of these small industrial type engines.

Discussion of these methodologies will begin with a review on past and current literature that parallels the topics of interest, as well as design guidelines and typical engine operating characteristics primarily concerning the intake system. The testing facility will be discussed and described in detail including the proper instrumentation and the testing procedures used. Consideration will be given to initial design concerns of typical small engines.

To evaluate the losses in the current design and consider the potential improvement possible with new designs, the base engine head and intake manifold will be investigated on a steady state flow bench. Discharge, flow, and pressure loss coefficients will be measured and calculated as a function of valve lift. To establish a potential for improvement, a CFD model of the test engine's stock port design will be used and benchmarked to the flow data collected from the steady state flow bench.

Initial baseline engine testing will be presented, as well as concerns with regards to the stock design. The pumping loop of the stock engine will be measured using an in-cylinder pressure transducer and shaft encoder. The camshaft will be staged at different timings and the resulting pumping loops will be measured to discern the impact of intake

and exhaust valve events on various load conditions. Volumetric flow into the engine will be measured using a laminar flow element. Based on the valve timing experiment, optimal valve timings will be discussed with regards to the test engine. An engine simulation will be calibrated and compared to the results of the test engine to prove the simulation's viability as tool that can be used in the preliminary design of engine intake systems. Additional analysis and methodologies will be proposed to assist with the initial design of these small industrial type engines.

2. LITERATURE REVIEW

2.1 GAS EXCHANGE PROCESS IN A FOUR STROKE ENGINE

The gas exchange process of a four stroke engine is made up of the exhaust and intake strokes. The purpose is to expel burned gases during the exhaust stroke and induct the fresh charge during the intake stroke. The key goal of the exhaust stroke is to dispel all of the burned gases out of the cylinder before the intake valve opens. The goal of the intake process is to induct the maximum amount of fresh charge and retain it in the cylinder without allowing any to escape through the exhaust manifold or allowing burned gases to dilute the fresh charge.

In Figure 2.1 can be seen a diagram of a typical small engine's intake system. Flow enters from the air cleaner through the hose and into the plenum. From the plenum, if the engine is carbureted and multi-cylinder the flow will split through the throttle body. If the engine is carbureted fuel will be introduced at the throttle body. The fuel and air mixture will then proceed through the manifold, across the intake valve and into the combustion chamber.

The geometries of both the intake manifold and intake port are very important to maintaining optimal flow conditions at all engine operating points. The flow performance of the manifold and port are difficult to model. Inlet manifold and port air flow offers a complicated fluid dynamics problem due to turbulent effects and the unsteady nature of the flow. The gas dynamics problem uses the complete three dimensional Navier-Stokes equations to model the real flow. The full set of equations consists of ten unknowns; it is not clear, however, that a complete solution is necessary in

order to model the significant flow features [1]. Assumptions, such as axisymmetric flow, are made to reduce the complexity of the gas dynamics problem while still maintaining the integrity of the solution.

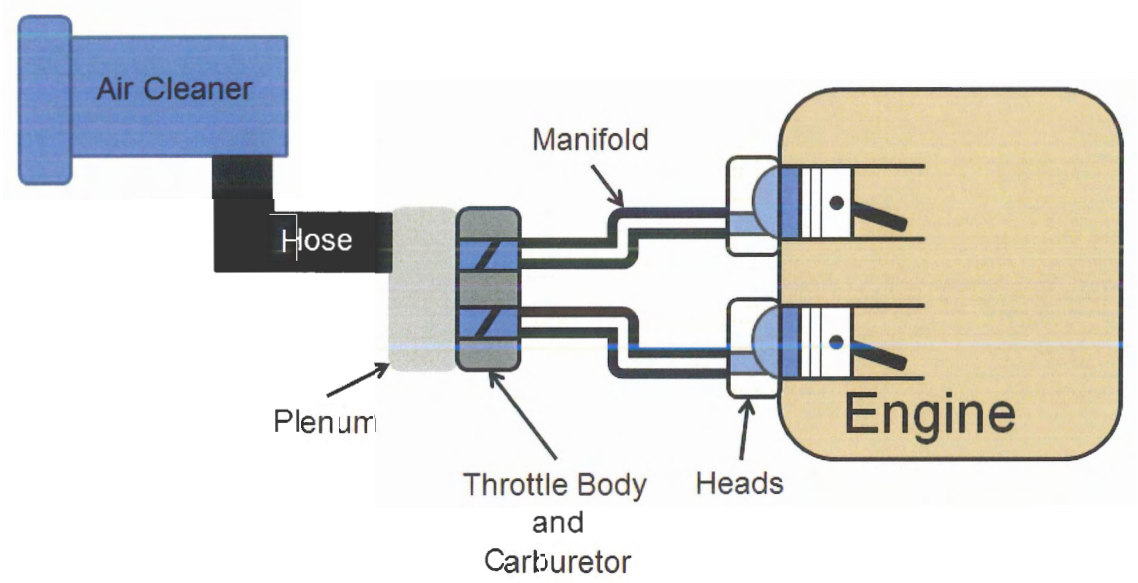

Figure 2.1: Typical intake system of a small engine

Another contributing factor to the complexity of the intake flow is the valve events of the engine. Typical valve profiles follow a sinusoidal shape; when a valve opens it produces a variable flow area and with the assistance of the piston motion creates a pressure differential between the manifold and the cylinder. This pressure drop forces air to flow either into cylinder from the manifold or out of the cylinder into the manifold.

A plot of intake manifold pressure measured just above the intake valve can be seen in Figure 2.2 for a wide open throttle case and a throttled case. It must be

understood that the real intake process of an internal combustion engine is highly dynamic and highly unsteady.

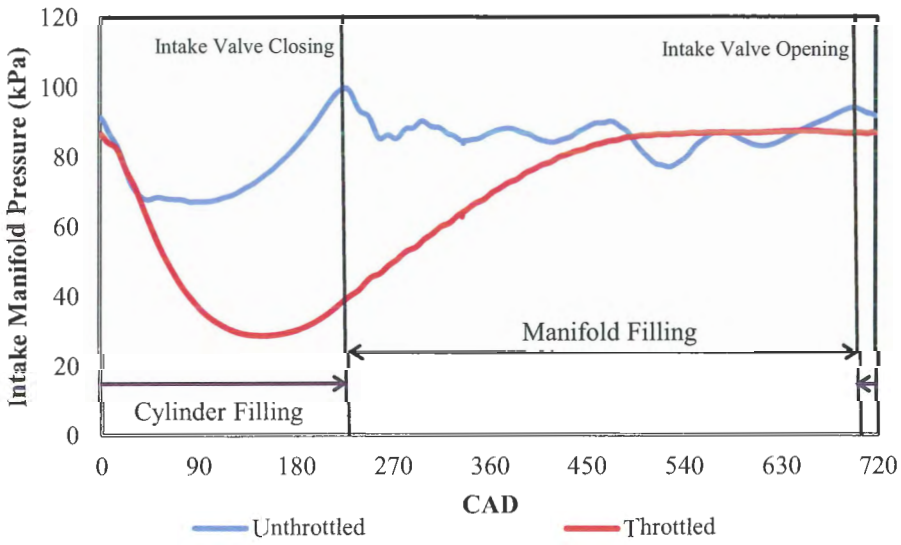

Figure 2.2: Intake manifold pressure with respect to engine crank angle degrees

The geometries of the poppet valves play a key role in determining flow performance during the early stages of the valve lift profile. The timing and size of the valves are the largest contributors to determining the volumetric efficiency of the engine, that is, the effectiveness of the engine to induct and retain fresh charge. In Figure 2.3, can be seen a depiction of the valve and port geometry of an engine.

2.1.1 Poppet Valve Characteristics. The valve, or valve and port together, is usually the most important flow restriction in the intake and exhaust system of four-stroke engines [2]. The lift of a poppet valve is controlled by the camshaft within an engine. Both the intake valve and exhaust valve open and close once per cycle. The timing of these events is controlled by the shape of the lobes on the camshaft. The shape

of each lobe determines how long the valve stays open, how quickly the valve opens or closes, to what lift the valve opens, and when in the cycle the valve events occur. The size of the valve depends on the geometry of the cylinder and the available space on the engine head. Heywood [2] mentions that a rule of thumb for a typical valve lift is 12 percent of the cylinder bore and the typical valve head diameter is 45 percent of the cylinder bore.

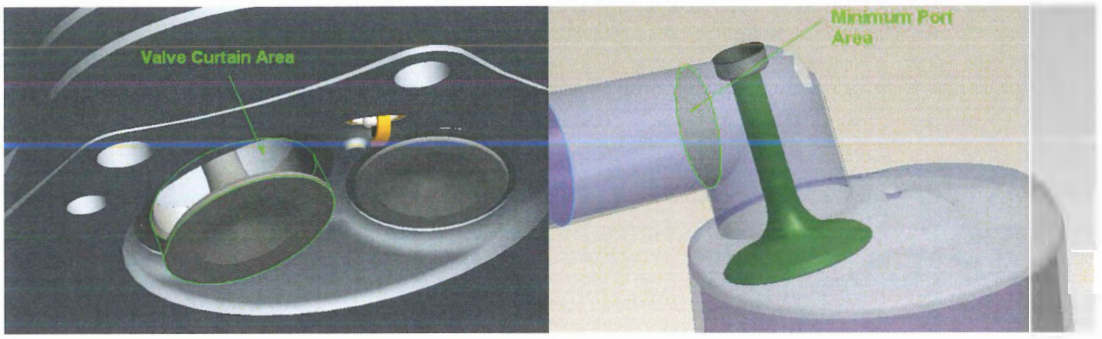

Figure 2.3: Depiction of valve curtain area and minimum port area

2.1.2 Valve Event Timings and their Effects on Engine Operation. In order to understand the gas exchange process it is important to grasp how each valve event can effect engine operation. There are four individual valve events that take place in one engine cycle. They are, in order of appearance after the combustion process: exhaust valve opening (EVO), intake valve opening (IVO), exhaust valve closing (EVC), and intake valve closing (IVC). Much work has been done over the last few decades in trying to understand how these timings affect the performance of an engine under a regime of operating conditions. Of particular interest have been volumetric efficiency and residual gas fraction (amount of fuel and exhaust gases from the previous cycle) as well as how

they can be optimized to improve the fuel efficiency and power output of the engine while reducing emissions. Below can be seen Figure 2.4, depicting a cylinder pressure versus crank angle degree diagram annotated with typical valve events and cylinder processes.

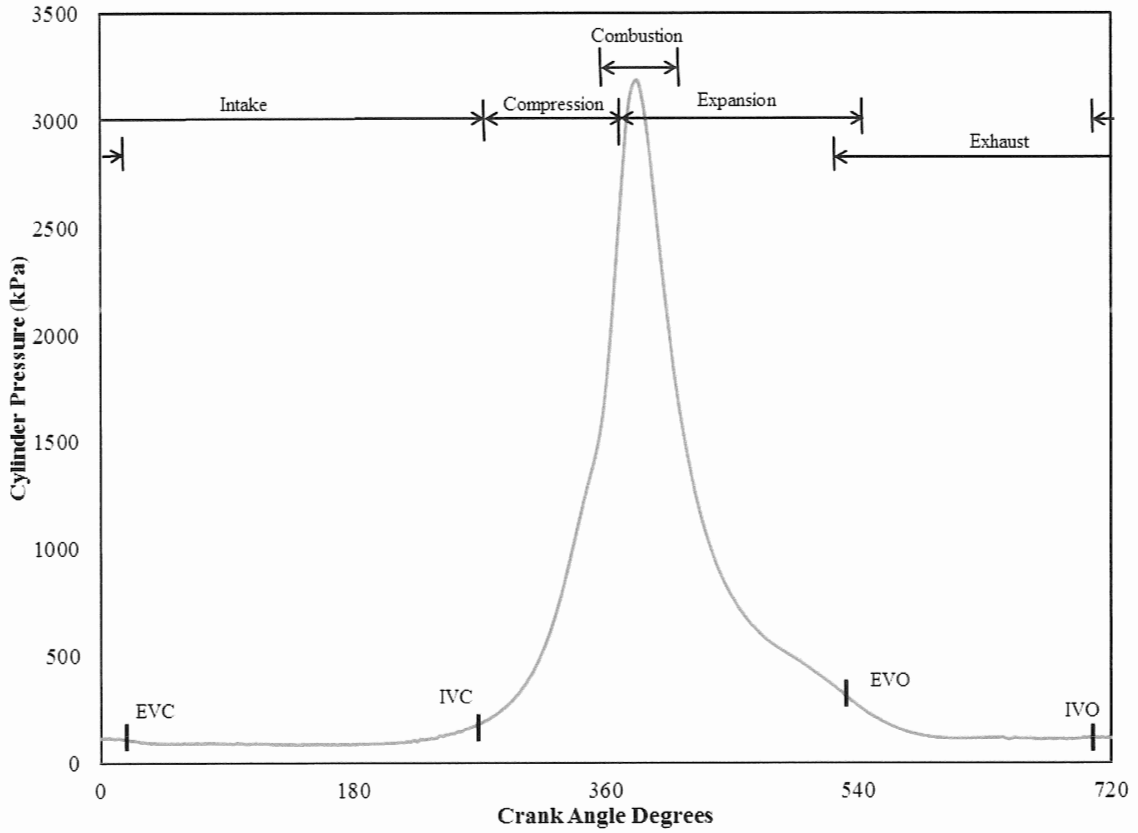

Figure 2.4: Typical valve event timings plotted as cylinder pressure versus crank angle

Heywood [2] discusses the importance of each valve timing individually, considering typical event timings and their effect on flow. In the order as stated above; EVO generally occurs 50 to 60° before bottom dead center of the expansion stroke, so that blow down can assist in expelling the exhaust gases to reduce the cylinder pressure

to manifold exhaust pressure as close to BDC as possible. Exhaust valve opening can influence the expansion ratio and thus the cyclic thermal efficiency. It can also affect the temperature of the exhaust products and consequently the rate at which hydrocarbons and carbon monoxide may be able to oxidize in the exhaust stream.

The IVO event typically occurs 10 to 25° before top dead center so the cylinder pressure does not dip too early in the intake stroke. Engine performance is relatively insensitive to this timing. Exhaust valve closing ends the exhaust process and determines the duration of the valve overlap period; it generally falls in the range of 8 to 20° after top dead center. Finally, IVC usually falls in the range of 40 to 60° after bottom dead center of the compression stroke to allow for additional cylinder filling under high speed conditions. Intake valve closing is one of the principle factors that determine high speed volumetric efficiency; it also adversely affects low speed volumetric efficiency by allowing cylinder gases to flow back into the intake manifold [2].

Asmus [3] discusses some key points when considering the timing of valve events. The principal determinants of high-speed volumetric efficiency are the timing of IVC and the valve overlap (IVO and EVC). The timing of EVC should happen sufficiently far beyond top dead center, such that cylinder pressure does not rise near the end of the exhaust stroke. The timing of IVO should occur sufficiently before top dead center so that cylinder pressure does not dip early in the intake stroke. Lastly, valve overlap is recognized as a factor which can influence the amount of residual gas fraction in the cylinder.

Asmus [3] writes, on the topic of valve lift and size, that the flow area created by valve lift may be limited by the minimum flow area in either the valve throat or in the

port area. This being the case, any increase in valve lift may only yield an incremental increase in flow capacity, but it does ensure that a maximum effective flow area is available longer. Asmus [3] states that this can have an effect on the engines volumetric efficiency during the intake stroke at high speeds; it depends on the intake valve flow capacity as the piston approaches bottom dead center and as the cylinder pressure rises from its depressed state early in the intake stroke.

Constrained by cylinder head geometry, engines are generally designed with the maximum combined valve sizes. Stroke-bore ratio is one of the principle factors in determining the total valve area in relation to swept volume. The volume of exhaust that must be evacuated out of the cylinder is approximately 2.75 times the volume of fresh charge that flows into the cylinder via the intake valve [3].

Asmus [3] concludes that the intake valve closing event is the single most significant determinant of the balance between low-speed and high speed volumetric efficiency and, therefore must be established on the basis of desired engine performance characteristics.

2.2 EXPERIMENTAL ANALYSIS OF THE GAS EXCHANGE PROCESS

It is expensive and requires a substantial amount of time to design and create new engine components for testing. Simple modifications can be made to critical pieces of an engine to provide an idea of improvements that can be gained in the design. Things such as camshaft staging and the rounding of the corners on intake components can provide direction on how to improve the design and performance of an engine.

There are several well explored and well documented methods available to provide experimental analysis of the gas exchange process of an engine. Two key

experiments to determine intake flow characteristics can be performed on a steady state flow bench; the measurement of discharge and flow coefficients and the calculation of the internal flow losses within the intake system.

Engine performance is often measured by means of cylinder pressure data. Cylinder pressure is recorded by means of an in-cylinder pressure transducer and a shaft encoder during normal engine operation. Cylinder pressure data represented as a function of cylinder volume allows for the calculation of work transfer between the gas and the piston. Many engine performance parameters can be derived from cylinder pressure data such as mean effective pressure, heat release rate, mass fraction burned, estimated pressure drop across the ports, among others.

Much of the analysis performed in this work is based on measurements obtained through steady state flow bench testing and the evaluation of the pressure drop across the port and valve as well as the calculation of mean effective pressure from collected cylinder pressure data. In light of this, much effort has been made to understand the appropriate steps required to obtain accurate results in both steady state flow bench testing and in the collection of in-cylinder pressure data.

2.2.1 Steady State Flow Bench Testing. Steady state flow testing is a very useful tool when attempting to analyze an engine's port and valve design. The fundamental idea is to pull air through a cylinder head and a mock cylinder, at a steady state and measure pressure drops across the system. This idea can be extended to other intake system components. Basic laws of fluid mechanics can then be implemented to determine such things as pressure loss coefficients, fluid velocities, and flow rates, which will be defined in greater detail in a subsequent section.

Frictional losses in the intake system including the intake manifold and intake port can result in significant pressure drop at high load conditions which has an effect on the overall work required to induct fresh charge. Improving intake manifold and intake port design can reduce those pumping losses and provide an increase in fuel efficiency. This can be analyzed on the steady state flow bench by calculating pressure loss coefficients which are a direct function of the pressure drop across the reference area, i.e. the valve.

A requirement of the steady state flow condition is that flow is fully turbulent so that the loss of velocity head is independent of the pressure drop or flow rate. The use of a Reynolds number is a key parameter in designing fluids experiments since non-dimensional parameters of fluids are similar as long as the Reynolds number is the same. Because discharge and flow coefficients are a measured at a particular point within the intake system, the Reynolds number must be determined at the appropriate reference area (i.e., valve curtain area or port area depending on the calculation being performed). Xu [4] warned that in steady flow tests, when the Reynolds number or pressure drop increase, errors in the measured static flow coefficient, due to the assumption of incompressible flow, also increase.

Steady state flow testing is beneficial when comparing engine heads with similar geometries under the same conditions. However, it is limited by not being able to compare different engine configurations and does not fully grasp the same flow dynamics as normal engine testing.

2.2.1.1 Flow and discharge coefficients. The purpose of the intake assembly is to allow an engine to have a high volumetric efficiency to achieve optimal power and torque. In order to accurately calculate volumetric efficiency for an engine, a mass flow rate term must be known. The flow across a valve can be modeled using isentropic compressible flow theory [2] through an orifice of the same cross sectional area as the valve curtain area or minimum port area, represented above in Figure 2.1. The flow through the port and valve assembly is by no means an isentropic flow. Present is a substantial amount of flow friction due to surface roughness and flow separation due to sharp corners. A term must be introduced to account for the ratio of actual mass flow rate to the theoretical mass flow rate.

Flow and discharge coefficients are calculated as a ratio of measured mass flow rate to an isentropic compressible flow rate through a reference flow area in the valve or port assembly. Xu [4] writes that depending on the reference area chosen, the ratio can be calculated as a flow coefficient or a discharge coefficient. The discharge coefficient refers to the flow rate referenced to the gap between the valve edges and the valve seats. The flow coefficient refers to the corresponding flow area in the port, either the minimum flow area in the port or the valve inner seat area, in which the valve stem blocking effect can be included or neglected.

Xu [4] goes on to cite some distinct differences between the use of a discharge coefficient compared to that of a flow coefficient. The use of a discharge coefficient is better suited to lower valve lifts, particularly when the gap between the valve and seat edges is small. The use of a flow coefficient is suitable for high valve lifts when the port

area becomes the largest restriction. Xu [4] warns that due to the scaling of flow coefficients, they are not suited for lower valve lifts where the flow capacity is small.

Lumley [5] writes that it is possible to improve the value of a discharge coefficient. By improving the inlet flow conditions, such as rounding sharp corners, improving valve location in the cylinder, or modifying a poorly designed inlet port it is possible to reduce the effects of flow friction and flow separation. Lumley [5] claims that just by porting the engine head, i.e. reshaping the port by use of file or grinder, an improvement in discharge coefficient from 0.6 to nearly 0.7 can be seen.

2.2.1.2 Internal flow loss in the intake system. Another way of determining the performance of an intake system is by looking at the flow losses from internal fluid flows. There are several phenomena that can have an effect on the internal flow; wall friction, pipe bends, obstructions such as the carburetor or the throttle, intake manifold heating and high residual fraction. An intake system can be analyzed using minor losses, i.e. losses due to bends or obstructions like valves. The pressure drop across a component that has a loss coefficient equal to one is equal to the dynamic pressure, $\rho V^2/2$ [6].

By using Euler's equation for compressible flows along a streamline, shown in vector form in Equation 2.1 and adding a term for viscous pressure losses, viscous flow through an internal passage can be analyzed. This loss term is expressed as a product of the pressure-loss coefficient and the dynamic velocity head [6]. By making certain assumptions, such as incompressible and irrotational flow, Euler's equation can be rearranged to determine pressure loss terms by knowing several parameters: gas constant,

ratio of specific heats, ambient temperature and pressure, pressure ratio, geometric flow area, and mass flow rate.

$$\rho \mathbf{g} - \nabla p = \rho[\frac{\partial \mathbf{v}}{\partial t} + (\mathbf{v} * \nabla)\mathbf{v}] \tag{2.1}$$

Measured loss coefficients can be used to predict overall system performance and calculate the percentage losses in the system due to each component. By calculating losses in this manner, certain sections of the inlet system that have high flow losses can be isolated. Flow losses can also be used to estimate overall system gains from reductions in component losses. Each assembly subsystem (i.e. air cleaner, carburetor, manifold and head [2]) can be subdivided further into component losses. For example, when analyzing the head, the subsystem can be divided into port, valve stem, and valve head losses. This allows for a more exact identification of the flow restrictions.

2.2.2 Engine Performance Measurements. Other engine parameters are important to obtaining good experimental results. The use of an absolute pressure transducer in the intake manifold, for example, is helpful when attempting to analyze flow characteristics within the intake system. The use of a dynamometer capable of determining the load on an engine is important for comparing different operating set points and obtaining a value of work at the output shaft. Temperature measurements should be taken at certain points throughout the engine, such as the intake air temperature, oil temperature, and exhaust temperature of each cylinder. Though these measurements are important, much of these are fairly straight forward and not as critical to this work as the acquisition of accurate pressure data.

2.2.2.1 Collection of pressure data. Piezoelectric pressure transducers, while normally used in collection of cylinder data because of their accuracy, size and thermal characteristics, require pressure referencing because they only measure a dynamic pressure. Piezoelectric transducers contain a quartz crystal exposed to cylinder pressure through a diaphragm. As the pressure increases, the crystal is compressed and emits a charge. The charge is then amplified and turned into a voltage via the charge amplifier, which can then be converted into a pressure value, using a scaling factor based on transducer sensitivity. It is important to understand that dynamic pressure is a measure of the difference in stagnation pressure from static pressure and is not tied to absolute or gauge pressure in any way. In order to properly account for this, a pressure referencing or 'pegging' technique must be employed.

Improper pressure referencing will cause errors in such parameters as: compression and expansion polytropic indices, heat release energy and heat release rate, mass fraction burned and resultant burn angles, estimated charge temperature, estimated cylinder charge mass, log pressure versus log volume plots, peak cycle pressure, and estimated pressure drop across ports [13].

There are several well examined methods available to reference pressure. Brunt and Pond [13] discuss each method. All referencing methods have advantages, disadvantages, and an associated level of error. Some of these methods include: pegging cylinder pressure to inlet manifold pressure near intake BDC using absolute inlet manifold pressure transducer(s), pegging to exhaust manifold pressure near exhaust TDC using exhaust manifold absolute pressure transducer(s), setting the pressure to an estimate of the pressure during part of the engine cycle, or using a numerical referencing

technique based on complying with an assumed polytropic index or rate of change of index during compression. These pressure referencing methods, along with others, are thoroughly examined in a paper by Randolf [14].

Pressure referencing, based on inlet manifold pressure, provides simplicity at the cost of added experimental expense in the form of additional instrumentation, data acquisition requirements, and component machining. Brunt and Pond [13] discuss inlet manifold pressure referencing which is carried out by determining the manifold pressure at BDC of the induction stroke via an absolute pressure transducer. The average pressure values of several crank angle degrees on either side of this location are taken to reduce the sensitivity to noise. The entire cylinder pressure curve is then shifted so that the cylinder pressure at BDC is equal to the intake manifold pressure at BDC. According to Brunt and Pond [13], bottom dead center is chosen because the piston motion is relatively slow around this point and the pressure drop across the valves should be at a minimum. Flow momentum at high speeds can present issues with the accuracy of this method.

Regardless of the type or accuracy of the in-cylinder pressure transducer used, the ability to understand and reduce measurement noise is critical. There are several different types of noise that can be introduced to a data acquisition system, e.g. statistical noise, electrical noise, and mechanical noise. Lancaster et al. [15] discuss the importance of understanding statistical and cyclic variations in pressure data between cycles. Lancaster [15] states that for any given crank angle the average of N measurements is a more reliable estimator than any individual cycle measurement. This arises from the fact that the variance of the average diminishes with the number of cycles used to compute it. Lancaster et al. [15] make another argument for averaging test data; stating that the

engine, itself, is an averaging device responding to mean values of fuel and air flow, by generating mean indicated power. Therefore, it is appropriate to use the mean of many cycles when calculating quantities that are compared with engine measurements. The number of cycles needed to obtain an accurate average should be determined by the cyclic variability of the engine. If the cyclic variability of the engine is high, then a larger number of cycles will be required to obtain a reasonable average.

2.2.2.2 Measurement of pumping work by means of cylinder pressure. By focusing on the pumping loop of a cylinder pressure versus cylinder volume diagram, the amount of work transfer between the piston and cylinder gases can be determined during the intake and exhaust strokes. Reducing this work transfer will reduce the pumping losses to the system and increase the overall efficiency of the engine. The conventional definition of pumping work is depicted in Figure 2.5; it is the sum of the shaded area A and the shaded area B normalized by the displacement volume of the engine. Any change in valve geometry, lift characteristics, or timing will manifest itself in these curves by altering the shape.

A decrease in the pumping work of an engine will ultimately result in improved fuel efficiency by reducing flow friction and eliminating parasitic losses to the engine. A term used in several studies, such as the one conducted by Sherman and Blumberg [7], is a term called specific fuel consumption (sfc) to quantify engine performance. Specific fuel consumption, the fuel flow rate per unit power output, is a more useful parameter than a measurement mass flow rate per unit time. It measures how efficiently an engine is using the fuel supplied to produce work [5], where $\dot{m}_f$ is the mass flow rate of fuel and

P is the power produced by the engine (which can be either represented as brake or indicated power depending on the type of analysis performed):

$$sfc = \frac{\dot{m}_f}{P} \tag{2.2}$$

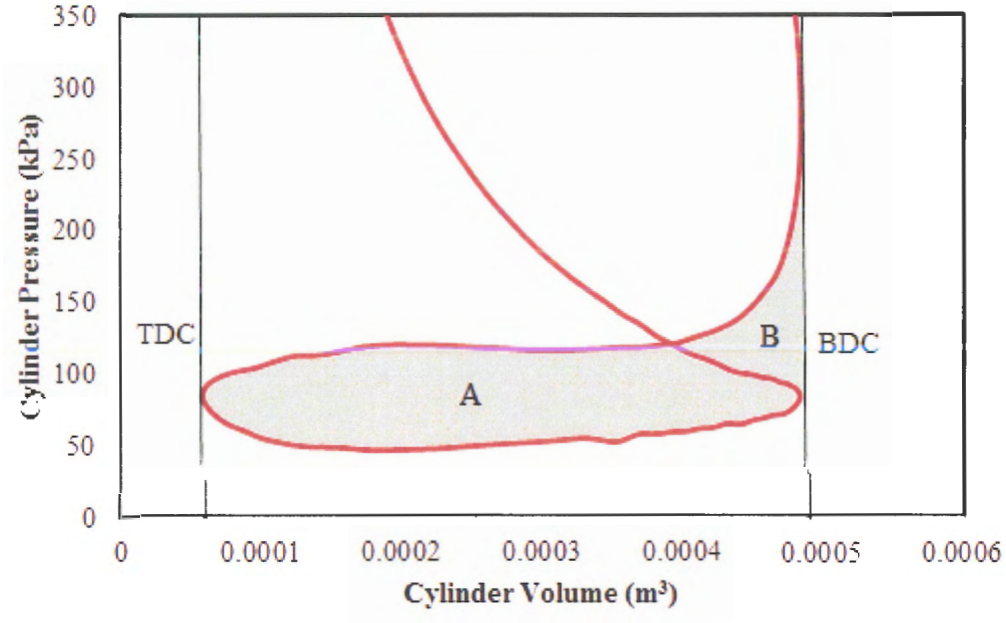

Figure 2.5: Depiction of pumping work for the test engine

Again, any decrease in the pumping losses, whether it be an improvement in intake flow loss or a beneficial change in valve timing events, should increase the overall power output of the engine decreasing the value of sfc, which is desirable. For example, assume brake specific fuel consumption (bsfc) is being analyzed. Brake specific fuel consumption is a function of brake power (P_b) that can be defined in terms of brake mean effective pressure (bmep). This bmep term is dependent on the indicated mean effective pressure (imep), the losses due to pumping mean effective pressure (pmep), and the losses due to frictional mean effective pressure (fmep). Any increase in imep or decrease

in pmep or fmep will result in an overall increase of bmep, which leads to a decrease in bsfc.

There are several technologies available to reduce the pumping work of an engine; variable valve timing allows an engine to change valve timings dynamically to adjust for a change in operating conditions. There is the option of fresh charge dilution, which can be added in the form of exhaust gas recirculation (EGR) or an excess of fresh air (lean operation). Cylinder deactivation is also an option on automotive engines; this is a process whereby certain cylinders are rendered inactive until the operator requires more power or torque [8]. However, these are very expensive additions to small, economically priced engines. Therefore, when considering a single camshaft engine the process of choosing appropriate valve timing events is a balancing process that requires the tradeoff of high speed power at the cost of low speed torque.

2.3 MODELING OF THE GAS EXCHANGE PROCESS

Computational techniques have been used intensively to simulate the different phenomena that occur in internal combustion engines [9]. These techniques generally provide accurate results of engine performance and assessments of the effects of various operational and design parameters. For example, it is both costly and time consuming to cut a new camshaft or stage a camshaft to test the timing of a desirable valve event. Therefore, an engine simulation is a helpful tool when analyzing this type of design condition. Heywood [2] states that models can be categorized as either thermodynamic or fluid dynamic in nature. This depends on which equations give the model its predominant structure. Heywood [2] warns that any engine model must balance complexity across its sub models and that a model is no more accurate than its weakest

link. Accordingly, critical phenomena should be described at comparable levels of sophistication.

2.3.1 Thermodynamic Formulation. For most energy based simulations a First Law energy balance coupled with an ideal gas assumption is used to describe the behaviors of an engine. Sherman and Blumberg [7] developed an engine model with the goal of describing the analysis of the induction and exhaust processes of a spark ignition engine. The completed model predicts cylinder mass, cylinder pressure, cylinder temperature, and flow rate during the exhaust, intake and valve overlap regions of engine operation. The model developed by Sherman and Blumberg [7] allows for the calculation of pumping losses and valve throttling as a function of operating parameters.

Poulos and Heywood [10] discuss the basic framework of an engine cycle simulation. There are four continuous processes that take place in a four stroke internal combustion engine: compression, combustion (including expansion), exhaust, and induction. The thermodynamic system consists of the instantaneous contents of a single cylinder of an engine. Poulos and Heywood [10] write that the system is generally open to the transfer of mass, enthalpy, and energy in the form of work and heat. Throughout the simulation, the cylinder is treated as a variable volume plenum, spatially uniform in pressure.

Each process requires special assumptions to be made in order to build a functional model. According to Poulos and Heywood [10], the composition within the cylinder for the intake, compression, and expansion strokes are assumed to be homogenous non-reacting ideal gases. The charge during the intake and compression stroke is a mixture of air, fuel vapor, and residual gas remaining from the previous cycle.

Poulos and Heywood [10] discuss a two zone combustion model in which the cylinder is divided into two zones during the combustion process: burned and unburned. Each zone is assumed to be uniform in temperature and composition.

It has been shown experimentally by Woshni [11] that the primary method of heat transfer within a spark ignition engine is from convection to the combustion chamber walls due to turbulent flows. Sherman and Blumberg [7] describe the heat transfer coefficient as a relationship between the Nusselt number, N_u, and the Reynolds number, R_e, for turbulent flows in a pipe.

2.3.2 Fluid Dynamic Model. To predict flow through the manifolds and valves a fluid dynamic based model is required. Fluid dynamic based models come in several forms. Heywood [2] discusses three different types: quasi-steady flow models, filling and emptying methods, and gas dynamic models. In general, most engine models use a quasi-steady flow model due to its ability to calculate mass flow rates without extensive calculation. Heywood [2] states that the drawback to this form is its inability to predict variation in volumetric efficiency with engine speed due to some of the phenomena which govern the change being omitted.

In order to properly account for the flow through the intake system, certain parameters must be accounted for. The intake system geometry can be modeled using pipe diameters and lengths. The flow restrictions, due to valve characteristics, can be accounted for by using valve lift profile with respect to crank angle in conjunction with the valve geometry. This allows for the calculation of the change in valve curtain area at each crank angle degree.

2.3.3 Application of Engine Simulations. Engine simulations can be used to predict many performance parameters. The cylinder pressure and mass flow rates during the gas exchange process are of particular interest during this study. Sherman and Blumberg [7] use their model to compute mass flow rates versus crank angle for standard engine valve timings. The model is a combination of a thermodynamic simulation and an induction/exhaust flow model which provides values of pumping and throttling loses. Brake specific fuel consumption (bsfc) is used to quantify improvements made to the pumping loop. Sherman and Blumberg [7] use the model to predict the effects of altering specific valve timings. Exhaust valve closing event is retarded and advanced from the standard case. It is found that a change in this valve event corresponds to a change in residual fraction. When the valve overlap is advanced, the predominant effect on residual gas fraction is reverse flow. When the overlap is retarded substantially, the predominant effect is due to trapped exhaust gases in the cylinder.

Sherman and Blumberg [7] also used their thermodynamic model to predict the timing effects of intake valve closing. The approach used was to adjust intake valve closing, with respect to a conventional valve timing baseline and obtain the calculated load and compute the resulting fuel consumption and emissions. It is shown that an early IVC event correlates to an increase in bsfc with an increase of load when compared to a standard IVC timing. However, for a low speed and low load set point an early IVC can drastically decrease the engine losses due to backflow.

Ham and Park [12] expand upon the quasi-steady thermodynamic model developed by Poulos and Heywood to improve the prediction accuracy. This was done to model the flow in the intake manifold as a one-dimensional unsteady compressible flow.

The model was validated using volumetric efficiency versus engine speed as a metric of comparison. The experimental results were compared to a 1 dimensional model as well as a zero dimensional model. It was determined that the results matched reasonably well between the experimental data and the 1-D model.

Only the intake valve effects are considered in the study conducted by Ham and Park [12]. Intake valve events, which include intake valve closing time, intake valve opening time, maximum intake valve lift time, maximum intake valve lift, and a combination of all of the above, are considered in the study. Ham and Park [12] conclude that the best way to improve volumetric efficiency is to change intake valve closing time. While intake valve opening has a small effect on volumetric efficiency, it can be an important factor in combustion stability due to residual gas fraction.

He et al. [9] find that engine efficiency increases with earlier EVO and EVC. For example, in their experiments, as the exhaust valve timing is advanced by 10°CA, the engine efficiency increases from 0.3673 to 0.3695 at the engine speed of 8000RPM (i.e. a relative increase of 0.6%). He et al. [9] go on to discuss that the exhaust valve timing has a great influence on the engine work process, especially the gas exchange process. With the earlier EVO, more combustion products are exhausted during the expansion stroke, and the cylinder pressure at the exhaust stroke decreases. Therefore, as the exhaust valve timing is advanced, the mean pressure loss for gas exchange decreases and the engine efficiency increases.

Within the context of this work a desired engine simulation must allow for the input of the camshaft profile and the subsequent valve event timings. Thus it must also allow for the alteration of these valve events to discern the effects of various timings. A

reasonable flow model is required to predict improvements in mass flow rate through the engine so a comparison of experimental and analytical results can be made. Ideally the model will take account of the engine's geometry; the manifold, valve, and cylinder dimensions are critical to the engine's performance characteristics.

In addition to a fluid dynamic model, an accurate thermodynamic model is also important. Accounting for the thermodynamic characteristics of the engine is important in order to determine the power gain or loss with respect to altering valve events. An engine simulation model developed by W.C. Reynolds of Stanford University and expanded in collaboration with Lumley [5], discussed in detail in a subsequent section, cover all of these requirements.

2.4 SMALL ENGINE DESIGN

The small engine market is overwhelmingly dominated by single cylinder and V-Twin designs. Most of these engines are air-cooled by utilizing a forced air fan design driven by the flywheel. They generally have simple lubrication systems using a small oil pump driven by the crankshaft. These engines normally have low cost carburetors and fixed timing ignition systems using a magneto located on the fly wheel. As a result, manufacturers have to select an Air Fuel Ratio (A/F) and ignition timing to ensure that the engine remains within safe operating conditions [16].

Novel engine management methods are generally complex and require additional components. Smither et al. [16] state that incorporating these systems require complex wiring harnesses and multiple sensors diversely located around the engine; leading to costly and environmentally vulnerable systems. These methods increase the manufacturing cost and decrease the robustness of an engine. Another cost associated

with incorporating these novel systems is in the training of technicians to appropriately identify and repair malfunctioning parts.

Small engine manufacturing is a cost driven market. In most cases, cost trumps performance; for this reason the amount of capital funneled into a small engine manufacturer's research and development program is limited compared to that of automotive engine development programs. Many manufactures use a set of design guidelines that dictate the specifications of an engine, based on their previous design, rather than spending time and effort modifying the design to increase the performance, while maintaining the same price point. There is a void to be filled by providing a set of design protocols that deliver guidance for small engine designers to follow when improving a current engine family or creating a new line. The protocols should be relatively simple to understand and use. They should only use basic engine data acquisition equipment that is generally available to all engine manufactures. It is also important to provide an accurate model that can be used with confidence to predict the performance of certain engine design parameters.

3. EXPERIMENTAL FACILITY

3.1 STEADY STATE FLOW BENCH AND TESTING PROCEDURE

3.1.1 Steady Sate Flow Bench. A steady state flow bench was constructed to aid in the experimentation of internal combustion engine intake systems. The flow bench, depicted in Figure 3.1, consists of several vital components and pieces of instrumentation used to measure the flow characteristics of various intake components.

The instrument stand on the left side of Figure 3.1 provides a mounting point for several pieces of instrumentation. These include ambient (room) temperature and pressure sensors, as well as an ambient humidity sensor. The humidity and temperature readings are used to calculate the humidity correction factor required for volumetric flow rate computations.

The test component is mounted to a clear Pyrex cylinder which enables visual observation of the air flow. In the case of the engine head, a micrometer is used to position the valve and to experimentally measure valve lift. A bell-shaped inlet guide is attached to the intake port of the head with the purpose of guiding the flow smoothly into the port and eliminating flow separation at the inlet.

The remaining plumbing and instrumentation are located below the table. This includes a large settling tank where another pressure transducer measures the valve pressure drop compared to ambient pressure. Next, the Laminar Flow Element (LFE) is used to acquire air flow data for calculation of the discharge and flow coefficients. The measuring points for the LFE reference pressure, temperature, and pressure drop are located in close proximity to the unit to maximize the accuracy of the collected data.

Finally, the flow is pulled through the system by means of a liquid ring vacuum pump, seen on the far right of Figure 3.1 in blue. The flow rate can be adjusted based on the setting of a relief valve near the vacuum pump. The more open the relief valve is the smaller the pressure drop across the intake component, conversely, if the relief valve is closed then vacuum pump is pulling the air strictly through the intake component mounted on the flow bench.

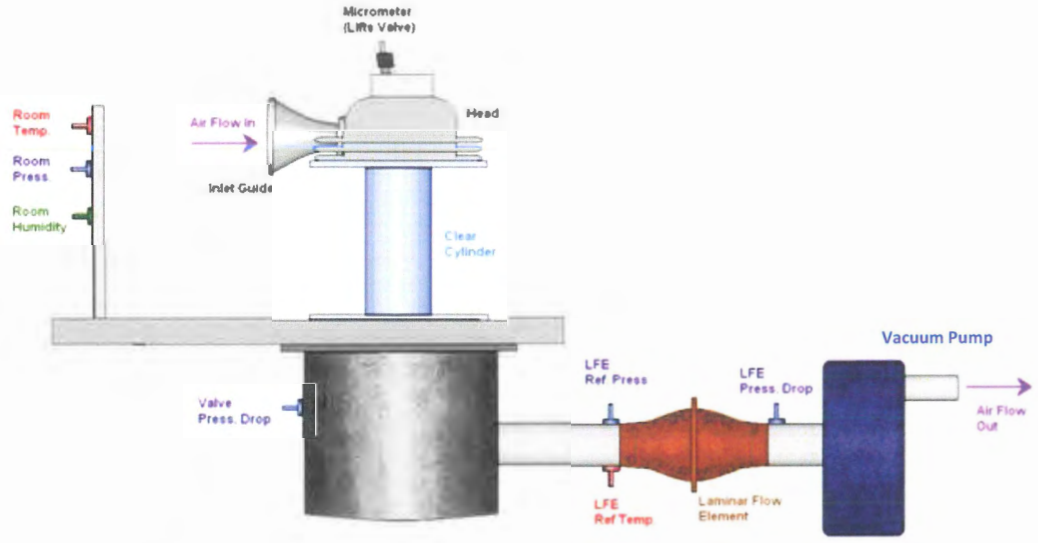

Figure 3.1: Flow bench diagram with all instrumentation included

The front panel instrumentation is shown in Figure 3.2. The panel consists of a type K thermocouple used to measure ambient temperature (accurate to within $\pm$ 0.75% of the full scale), which is in turn, used to obtain an accurate air density measurement. An Omega PX209 solid state absolute pressure sensor is used to make an accurate ambient pressure measurement ($\pm$ 0.25% full scale) and provide a reference pressure to a Druck LPX 1000 series differential pressure sensor (accurate to $\pm$ 0.5% full scale). The

Druck measures the pressure differential between two points, the ambient pressure and the surge tank, for example.

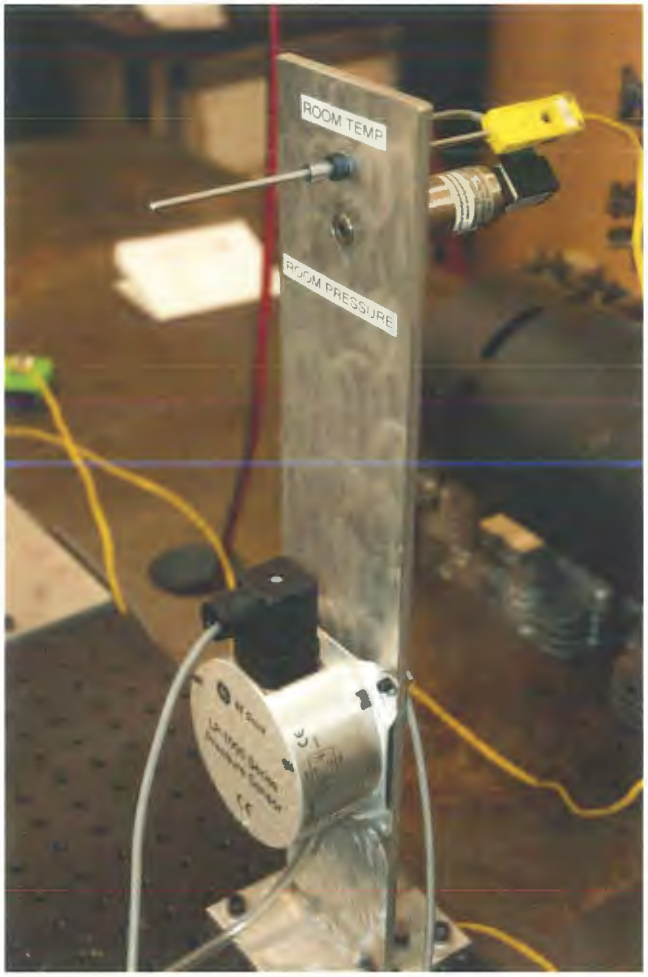

Figure 3.2: Front pannel instrumentation for steady state flow bench setup

Figure 3.3 depicts the flow bench with engine head mounted to the Pyrex cylinder, along with valve positioning fixture. The Pyrex cylinder has the same dimensions as the test engine's cylinder bore. Also included in this picture are the digital displays for valve pressure drop, ambient pressure, and pressure readings across the laminar flow element. The computer is used for data acquisition and reduction.

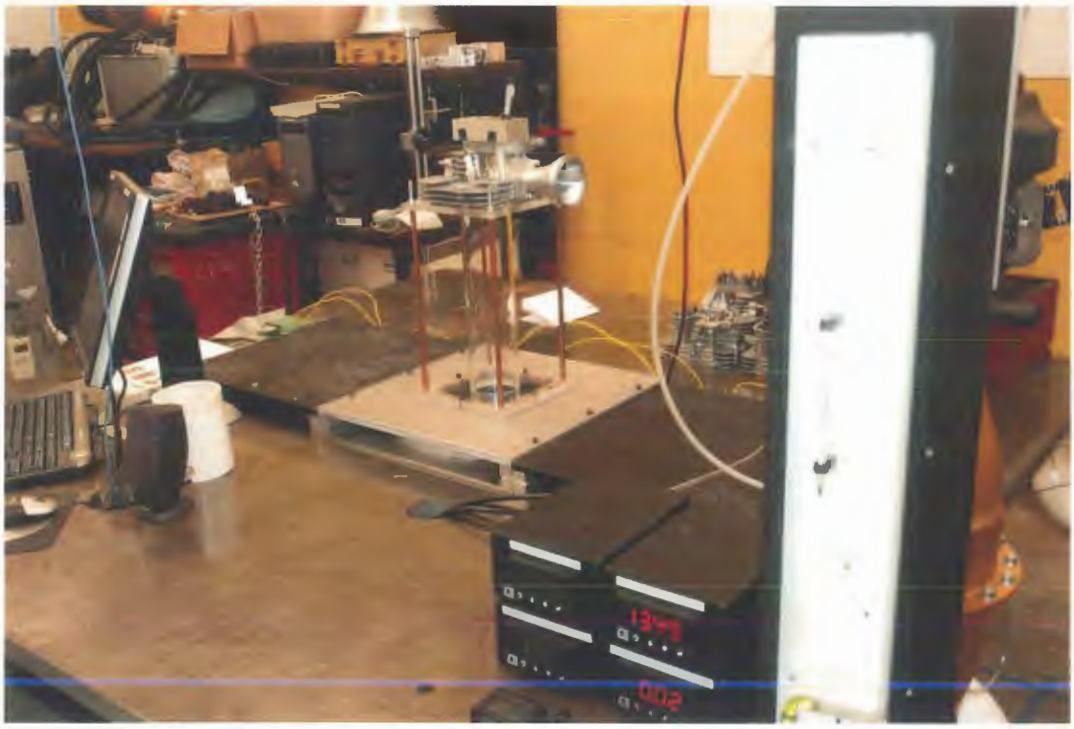

Figure 3.3: Top side of the flow bench

The cylinder head setup is shown below in Figure 3.4. The head is bolted down to a plexiglass top that is connected directly to the Pyrex glass cylinder. For the cylinder heads, it is critical that tests are run with the sparkplug in its proper place to get an accurate flow measurement. A rubber O-ring provides an interface and an air-tight seal between the glass and the cylinder head. The bell-mouth can be seen attached to the intake port on the head. This allows for a smooth transition between the intake port area and the ambient air. Attached to the top of the head is an aluminum block that houses the micrometer used to adjust the lift of the intake valve. The micrometer allows the valve to be held at a constant lift which fixes the cross sectional flow area available to the through the head. Other intake components can be attached to the plexiglass top as well.

Figure 3.4: Cylinder head with bell-mouth and valve control mechanism attached

The settling tank in Figure 3.5 is used as a damping mechanism to reduce the pressure fluctuations to the downstream laminar flow element in order to allow for a more consistent flow rate measurement. A fitting can be seen in the middle of the tank that provides the Druck pressure transducer on the front panel the ability to sample the pressure in the settling tank and provide a comparison to the ambient pressure (i.e. differential pressure across the intake component). This vertical distance is important to take note of when performing flow loss calculations. The flow of air enters from the top through the Pyrex glass cylinder and exits near the bottom at the right side of the tank. When performing fluid velocity calculations, based on the volumetric flow rate measurement of the LFE, the area expansion between the Pyrex glass cylinder and the settling tank must be appropriately accounted for.

Figure 3.5: Settling tank fixture

Once the flow progresses past the settling tank, it enters the LFE, which can be seen in Figure 3.6. This Meriam Z50MC2-4 Laminar Flow Element can handle up to 12.06 cubic meters of air per minute. Its inlet and exit are 101.6 millimeters in diameter. The LFE determines the actual volumetric flow rate of air through the system by inducing laminar flow through a capillary to produce a differential pressure. To obtain the volumetric flow rate, the differential pressure across the flow element is measured using an absolute pressure transducer and a second Druck differential pressure sensor. The inlet air temperature is measured via a type K thermocouple and the relative humidity is measured by a Testo Term 610 hand held temperature and humidity sensor (accurate to within $\pm$ 2% FS). Using the calibration table associated with the particular LFE as well as correction factors for humidity, viscosity, and temperature a flow rate can be

calculated. The accuracy of the measurement gathered from the LFE, and furthermore the accuracy of the data used to calculate flow characteristics of the steady state flow bench tests, is dependent on the accuracy of the Omega absolute pressure transducer, the Druck differential pressure transducer, the temperature reading acquired from the type K thermocouple, and the humidity reading.

Figure 3.6: Meriam laminar flow element and associated instrumentation

The flow then proceeds to the liquid ring vacuum pump shown below in Figure 3.7. The pump requires the use of an electric motor to power the impeller which creates the suction. The water is pushed to the outside of the impeller creating a seal and pulling air through the system. A head of water is supplied to the pump from the large holding

tank to the left of the stand. A cooling loop pushes water over a heat exchanger in order to cool the pump water.

Figure 3.7: Liquid ring vacuum pump setup

The relief valve that is used to control the flow of air is shown in Figure 3.8. The configuration on the left shows the valve fully open and the configuration on the right dipicts the valve fully closed. The degree to which the valve is closed is used to control the pressure drop across the intake component. The fully open valve correlates to a minimal flow through the intake system, due to the pump pulling air through the relief

valve. When the valve is completely closed the pump pulls all the air through the intake system. This correlates to the the largest pressure drop the system can create for a given set up.

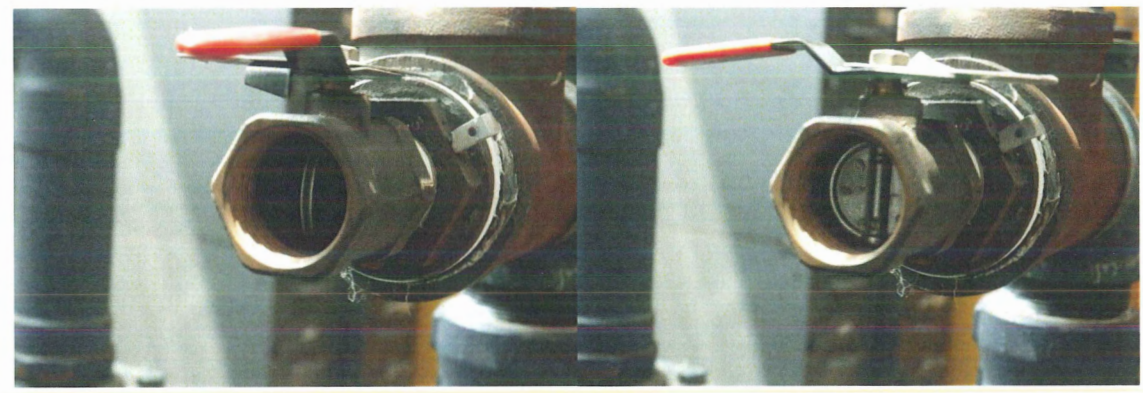

Figure 3.8: Vacuum pump relief valve used to control pressure drop

3.1.2 Steady State Flow Bench Testing Procedure. The component that is to be tested is attached securely to the top of the plexiglass plate atop the Pyrex cylinder. The instrumentation is turned on to allow time to warm up; the differential pressure readouts are zeroed. This will show that there is no pressure drop across the system while the setup is static. The cooling loop for the vacuum pump is turned on and allowed to reach its operating pressure (50 psi). The liquid ring vacuum pump is the turned on and allowed to run with the relief valve open for 10 minutes to ensure steady state operating conditions.

Once the instrumentation and the vacuum pump are ready, the data acquisition software is opened and data is ready to be collected. The relief valve on the vacuum pump is adjusted to reach the desired pressure drop. Xu [4] states that it is widely adopted for steady state flow tests to be carried out under conditions of a constant

pressure drop of 2.4 or 5.0 kPa. Larger pressure drops, up to 16.9 kPa, have been used in studies by Ford. The flow and discharge coefficient testing used a pressure drop of 1.3 kPa, 3.1 kPa and 5.0 kPa respectively to allow for a large range of realistic flow conditions with regards to the size of the test engine. The pressure loss coefficient tests were run at a pressure drop of 1.3 kPa, 2.5 kPa, and 5.0 kPa respectively. Data was collected to for two minutes and averaged to reduce the sensitivity to noise and transients in the system.

3.1.3 Steady State Flow Bench Data Reduction. A National Instruments data acquisition board is utilized to collect and compile the majority of the experimental data. This process is controlled by a LabVIEW program written for this experiment. The data collected by the DAQ board and written to a text file includes: ambient temperature and pressure, LFE ambient temperature and pressure, LFE differential pressure, and differential pressure across the valve.

A program written in MATLAB imports the text file created by the LabVIEW code. It then calculates several values based on the inputs from the instrumenation. Once completed it outupts a Microsoft Excel file that contains all relavent parameters such as: volumetric flow rate, mass flow rate, Reynolds numbers for the flow through the port, valve and cylinder, as well as the Mach numbers for the flow through the valve and port. The file also contains the differential pressure values between the ambient and the settling tank, the differential pressure across the LFE, the ambient pressure, and ambient temperature.

3.2 ENGINE STAND TESTING AND PROCEDURE

3.2.1 The Engine Stand. Within the context of this investigation the test engine is an air cooled 850cc, four stroke, two cylinder, V-twin engine with a single camshaft. The engine is carbureted and uses a single fixed spark timing to initiate the combustion process. Additional engine parameters can be seen in Table 3.1.

Table 3.1: Test Engine Specifications

Cylinders	2
Displacement (cm^3)	852.0
Bore (mm)	84.5
Stroke (mm)	76.0
Connecting Rod Length (mm)	122.0
Compression Ratio	8.2

3.2.2 Engine Instrumentation. The test engine is outfitted with two Kistler 6061 B piezoelectric pressure transducers (one for each cylinder and each with an accuracy of $\pm$ 0.5% of full scale) in conjunction with two Kistler Type 5010 charge amplifiers (one for each pressure transducer). These particular cylinder pressure transducers are liquid cooled to avoid thermal shock from the extreme temperature changes experienced inside a combustion chamber. Also used, are two Motorola MPX 4115A absolute pressure transducers (accurate to within $\pm$ 1.5% of the full scale voltage) to measure the inlet absolute pressure of both manifolds directly above the intake valve. All pressure data is recorded by a data acquisition system with respect to the crank angle degrees of the engine; sampled by a BEI Optical Shaft Encoder in 0.5 crank angle increments.

The engine is connected by a vertical driveshaft to an electric clutch. When the clutch is engaged it couples the engine to a Land and Sea water-brake dynamometer. This allows for the engine to be loaded by applying a hydrodynamic pressure to the internal mechanism of the dynamometer. The software associated with dynamometer is loaded on a computer in the engine control side of the lab and allows for full control of engine speed and load. The software allows the measurement of certain engine parameters such as: engine speed, torque, and power, along with various temperatures which are taken by means of type K thermocouples. The temperature measurements include intake temperature measured in the air filter, intake manifold temperature measured just above the intake valves, cylinder wall temperature, exhaust gas temperature for both exhaust manifolds, and the oil sump temperature. A Meriam Z50MC2-2 laminar flow element is fitted upstream of the engine intake to measure the air flow rate of the engine under different operating conditions. Again, the accuracy of the air flow measurements are a function of the accuracy of the absolute pressure transducer, differential pressure transducer, type k thermocouple, and relative humidity reading. The engine setup along with the associated instrumentation is shown below in Figure 3.9.

3.2.3 Engine Testing Procedure. For the purposes of collecting cylinder pressure data, a Cycle B Six-Mode test procedure as discussed in SAE J1088 and Appendix B to Subpart E of Part 89 of the Code of Federal Regulations was used. This testing regime requires six different engine set points, five at 100% speed and varying load from 100% to 10% and one case performed at an idle condition (no load). The full

speed set points were run at an engine speed of 3060 RPM and the idle case was conducted at 1550 RPM. The testing procedure is given below in Table 3.2.

Figure 3.9: Engine test stand and instrumentation

Table 3.2: Cycle B Six-Mode test procedure

Mode	1	2	3	4	5	6
Rated Speed (RPM)	3060	3060	3060	3060	3060	1550
Speed Setting (% Rated)	100	100	100	100	100	Idle
Load Setting (% Rated)	100	75	50	25	10	0
Weighting Factors (%)	9	20	29	30	7	5

This test procedure is widely accepted due to its accuracy of measuring different engine performance data. It also allows for a direct comparison to the data set collected by the engine manufacturer with the same engine.

3.2.4 Engine Data Reduction. A code was developed in MATLAB to appropriately scale and correct the pressure data obtained from engine tests. The pressure referencing code reads a text file that contains all the pertinent data for each cycle of a test and stores it as a vector. After the vector is stored, the code breaks up the data into the appropriate number of cycles (generally tests were recorded at 300 or 600 cycles). Next, bottom dead center of the induction stroke is located for each cylinder and the intake manifold pressure is averaged over several points on either side. The difference in magnitude between the unreferenced cylinder pressure and MAP pressure is then added to the value of cylinder pressure at every crank angle of the cycle data. Finally, the cycle data for the cylinder pressure and manifold pressure is averaged over every crank angle degree to determine the 300 cycle average pressure data; this helps to wash out any errors or faulty cycles. The MATLAB code specific to this engine can be seen in Appendix A. A secondary code was written to accommodate different engine types. The corrected cylinder data can then be saved to text files and used as inputs to other codes.

Below, in Figure 3.10 and Figure 3.11 an example of the pressure referencing code is depicted. This shows the cylinder pressure curve being shifted from its raw pressure value to an absolute referenced value.

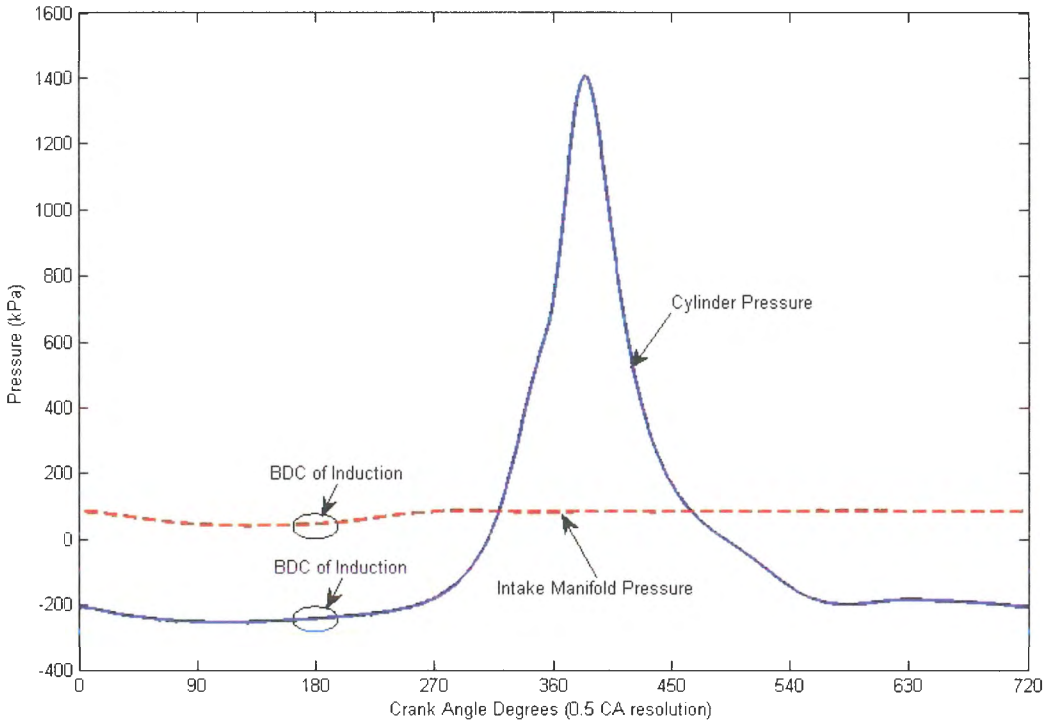

Figure 3.10: Intake manifold pressure and uncorrected cylinder pressure

Notice, in Figure 3.10, that at BDC of the induction stroke the cylinder pressure value is -200 kPa and the manifold pressure is nearly 80 kPa. Note that on an absolute scale 0 kPa represents a perfect vacuum, hence the need for pressure referencing.

Once the cylinder pressure has been referenced, it can be seen in Figure 3.11 that the pressure of the manifold matches the pressure of the cylinder at BDC. Once the pressure has been corrected, it can be utilized in heat release rate and MEP studies.

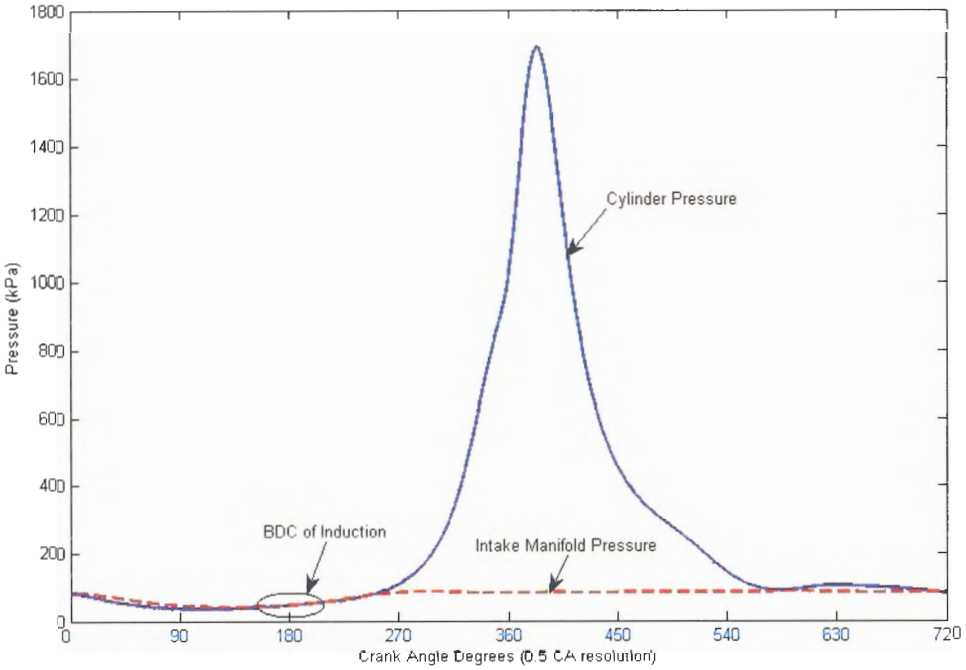

Figure 3.11: Intake manifold and properly referenced cylinder pressure

3.3 EXPERIMENTAL ERROR ANALYSIS

An uncertainty analysis was performed on the experimental instrumentation to determine the range of error that can be expected with the measurements. The error analysis was based on the sequential perturbation laid out by Figliola and Beasley [17].

The steady state flow bench and the engine stand both make use of a laminar flow element to measure the air flow through each system. Both laminar flow elements are equipped with the same set of instrumentation as discussed previously. To perform the analysis an arbitrary fixed operating point was selected for the LFE and a result, $R_{o,}$ was calculated, where $R_o=f(x_1, x_2, x_3, x_4)$, based on the measurements of the independent variables: differential pressure, ambient pressure, temperature, and air density (x_1, x_2, x_3, and x_4 respectively). The equation used to calculate the rate of airflow through the LFE

is shown in Equation 3.1, where B and C are constants specifically related to each individual LFE, DP is the differential pressure across the LFE measured by the Druck Transducer, P_f is the absolute pressure measured at the LFE, P_{std} is the ambient absolute pressure, T_f is the temperature of the flowing air at the LFE, T_{std} is the ambient air temperature, and the value of the ratio of ρ_{wet}/ρ_{dry} is taken from a table associated with the LFE based on a temperature and a relative humidity reading.

$$\text{Volumetric Flow Rate} = [B(DP) + C(DP)^2]\left(\frac{P_f}{P_{std}}\right)\left(\frac{T_{std}}{T_f}\right)\left(\frac{\rho_{wet}}{\rho_{dry}}\right) \quad (3.1)$$

This calculation was repeated by individually adding the uncertainty, u_{xi}, of each independent variable as seen in Equation 3.2 through Equation 3.5. For this calculation there are four independent variables (x_1, x_2, x_3, and x_4) that have an effect on the calculation of the flow measurement.

$$R_1^+ = f(x_1 + u_{x1}, x_2, x_3, x_4) \quad (3.2)$$

$$R_2^+ = f(x_1, x_2 + u_{x2}, x_3, x_4) \quad (3.3)$$

$$R_3^+ = f(x_1, x_2, x_3 + u_{x3}, x_4) \quad (3.4)$$

$$R_4^+ = f(x_1, x_2, x_3, x_4 + u_{x4}) \quad (3.5)$$

This calculation was repeated again by decreasing the independent variables by their respective uncertainties (i.e. x_1-u_{x1}), to estimate the lower error range of operation. The differences between the fixed operating point and both the positive uncertainty and negative uncertainty can be calculated, represented by Equation 3.6 and Equation 3.7 respectively.

$$\delta R_i^+ = R_i^+ - R_o \quad (3.6)$$

$$\delta R_i^- = R_i^- - R_o \quad (3.7)$$

Finally, the approximation of the uncertainty contribution from each variable can be evaluated by Equation 3.8 and the uncertainty result can be calculated by Equation 3.9,

$$\delta R_i = \frac{|\delta R_i^+| + |\delta R_i^-|}{2} \tag{3.8}$$

$$u_R = \pm \left[\sum_{i=1}^{L} (\delta R_i)^2 \right]^{1/2} \tag{3.9}$$

By using the uncertainites associated with each piece of insturmentation, the range of error that can be expected in the flow measurement of both the steady state flow bench and engine testing statnd is calculated to be $\pm$ 0.0164 m^3/min of air.

Similar analysis can be performed on the pressure data for the engine test stand. However, the error associated with this instrumentation is small when compared to the overall cyclic variability of the engine. Engine stand pressure data was recorded in 300 cycle tests, the average pressure of those 300 cycles was calculated and reported. A more useful value to determine the expected range error in the pressure data is the use of a coefficient of variation (COV) of indicated mean effective pressure (imep). It is calculated as the standard deviation of the imep divided by the mean imep and is usually expressed as a percent [2], shown in Equation 3.10.

$$\mathrm{COV_{imep}} = \left(\frac{\sigma_{\mathrm{imep}}}{\mathrm{imep}} \right) 100 \tag{3.10}$$

Engine reliablity generally becomes a concern when the value of COV exceeds 10 percent [2]. For the test engine operating points the value of COV ranges from 6-8 percent depending on the mode.

4. INITIAL DESIGN CONSIDERATIONS

4.1 FOCUS ON DESIGN CONCERNS

There are several areas of the intake system design that require specific focus to obtain a better understanding of the gas exchange process. As discussed earlier, these concerns are port geometry, valve geometry, valve event timings, intake manifold design, and cylinder to cylinder communication.

4.1.1. Stock Head Comparison. The cylinder heads of the test engine each have a slightly different design. A distinct difference can be seen in Figure 4.1, which is the intake port resides on opposite sides of the head for cylinder 1 compared to cylinder 2. Another important consideration is the length of the intake ports. The intake port for cylinder 2 is 35 mm longer than that of cylinder 1.

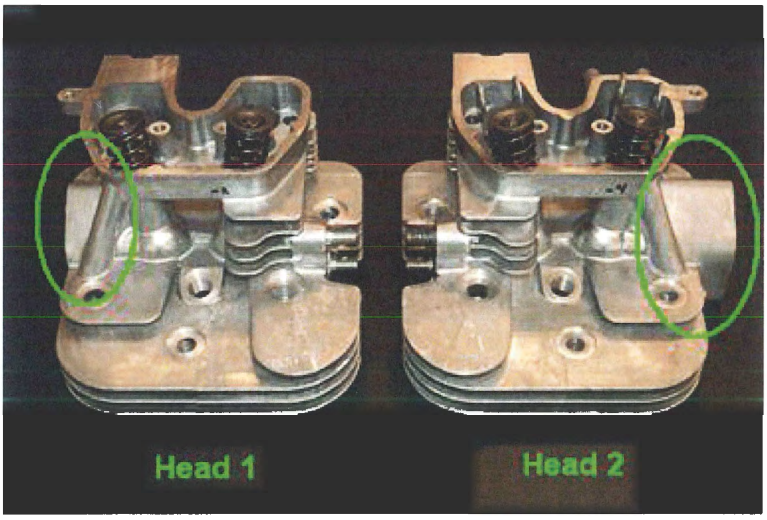

Figure 4.1: Visual comparison of the test engine's cylinder heads

4.1.2 The Stock Port Design and Proposed Modifications. Due to the simplicity of the manufacturing process used to build these small engines, the stock intake ports of the cylinder heads are designed with a sharp 90 degree corner between the port and the valve head. Internal fluid flow is subject to sizable head loss when exposed to pipe bends. Young [18] states that the losses are due to the separated region of flow near the inside of the bend and the swirling of secondary flow that occurs is because of the imbalance of centripetal forces as a result of the curvature of the pipe centerline.

In place of a sharp corner, a fillet radius is proposed to allow for a better transition between horizontal and vertical flow. Rounding the port angle should help the flow process and increase the volumetric efficiency of the engine. The performance of the stock and modified engine heads are examined using CFD modeling, steady state flow bench testing, and engine stand testing.

A second intake design concern is the restriction that occurs in the port before the bend. After a certain valve lift the port is the smallest cross sectional area downstream of the carburetor. Once the flow makes it through the port area and into the throat, which has a larger cross sectional area than the port, it experiences a sudden expansion in combination with the 90 degree bend. This expansion adds another form of flow loss to the intake system. Above approximately two-thirds valve lift, the valve curtain area becomes larger than the port cross sectional area. An increase in port diameter should allow for a higher maximum mass flow rate and reduce losses due to the sudden expansion between the port and throat.

4.1.3 Experimental Valve Characteristics. The poppet valves on the test engine are controlled by a single camshaft, which is used to operate both sets of valves in each cylinder. Table 4.1 displays further information on the intake valve geometry.

Table 4.1: Critical valve geometry properties

Parameter	Symbol	Value
Valve Head Diameter	D_V	34.60 mm
Valve Inner Seat Diameter	D_S	32.80 mm
Throat Diameter	D_T	31.50 mm
Valve Lift	L_V	up to 8.254 mm
Valve Seat Angle	φ	45.25 deg

Initial deductions about improper valve sizing are hard to make prior to testing; a quick rule of thumb from Heywood [2] is that the intake valve head diameter is approximately 44% of the cylinder bore and the maximum lift is 12% of cylinder bore. A comparison shows that for the test engine, the valve head diameter is closer to 41% of the cylinder bore and the ratio of maximum valve lift to engine bore is only 9.7%. Heywood [9] also states that, at maximum valve lift, typical values of L_V/D_V are 0.25. This is slightly higher than what is observed on the test engine. As the engine does not meet certain "rules of thumb" an initial assumption would be to increase valve diameter slightly and valve lift accordingly.

Valve event timings are critically important to controlling the amount of charge inducted and exhausted per cycle. Figure 4.2 shows the breakdown of a typical camshaft profile for an engine. Imposed on the plot are the different sections of the profile.

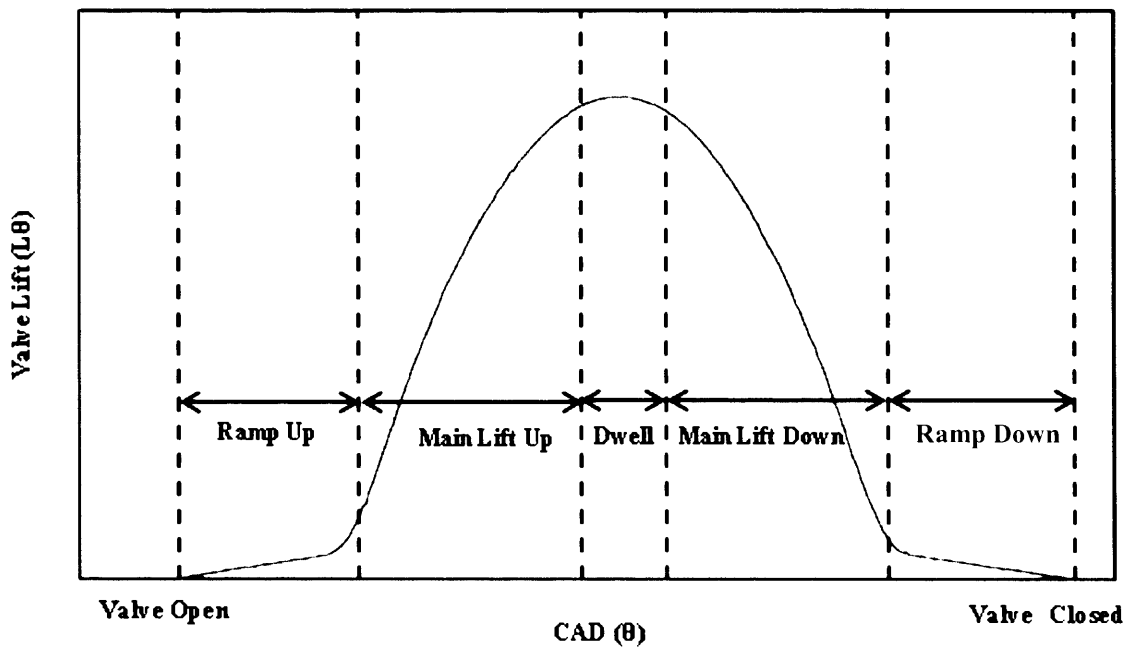

Figure 4.2: Typical valve lift profile with lift sections depicted

There are five main sections of a valve lift profile: ramp up, main lift up, dwell, main lift down, and ramp down. The ramp up period begins the valve opening process, starting with the initial cracking of the valve. This process does not create any discernible valve lift and is generally not considered when picking specified valve lift timings. Heywood [2] states that SAE defines valve opening and closing positions of mechanical lifters to be 0.15 mm plus the specified lash. Main lift up dictates how fast and to what height the valve opens. Dwell accounts for the time that the valve stays around its maximum lift point. Main lift down, similar to main lift up, dictates how fast the valve closes. Ramp down is the final valve closing event; it is a slow draw down to the closing and is generally disregarded due to the valve opening and closing assumption stated above.

The valve lift profiles for the test engine are shown in Figure 4.3. The valve profiles are offset due to the phasing set of the cylinders. The positions of the cylinders are 90 degrees out of phase and the processes of each cylinder are 270 degrees out of phase. It should be noted that the geometry of the intake and exhaust valve differ. The diameter for the head of the exhaust valve is smaller than that of the intake valve; also, the lift for the exhaust valve is higher than the lift of the intake valve. A reason for this difference is the fact that the pressure in the cylinder during the exhaust stroke is higher than the pressure during the intake stroke. That is, exhaust is forced out of the cylinder with the assistance of a larger pressure gradient due to an ascending piston then when intake charge is pulled in.

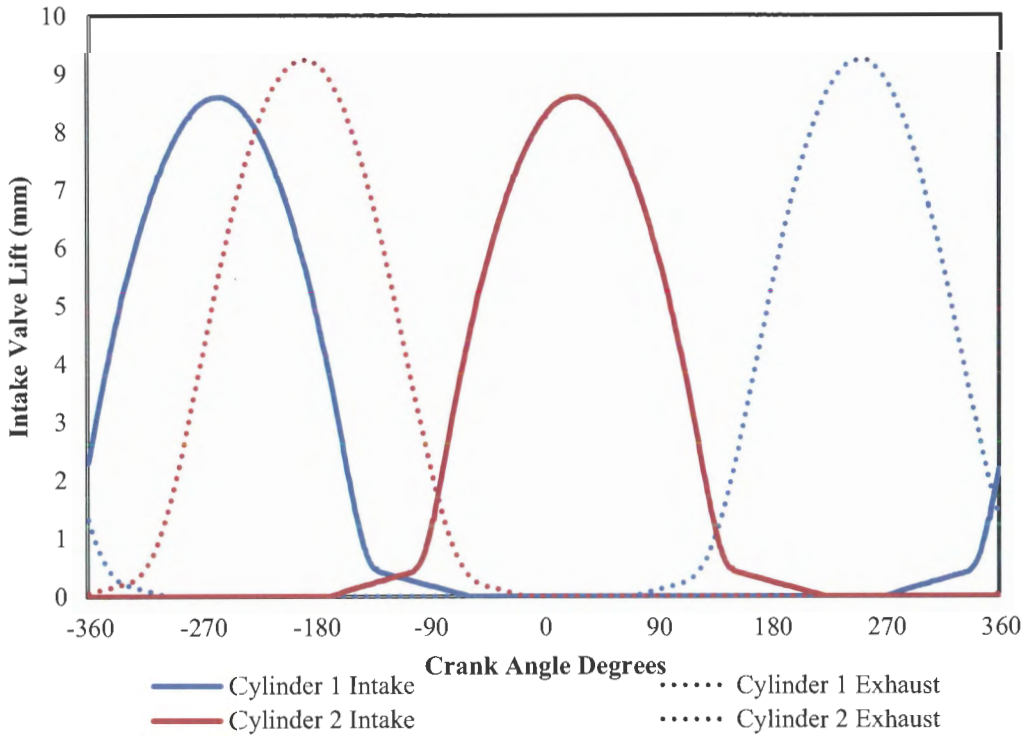

Figure 4.3: Intake and exhaust valve lift profile for both cylinders of test engine

The intake valve for each cylinder is plotted as a solid line in its respective color (blue for cylinder 1 and red for cylinder 2). The exhaust valve for each cylinder is plotted as a dotted line for its respective color. It can be seen that there is an overlap of the intake valve and exhaust valve event for each cylinder. There is an overlap between the end of the intake valve event of cylinder 1 and the beginning of the intake valve event of cylinder 2. Similar behavior is seen in the exhaust valve profile for both cylinder 1 and cylinder 2. Table 3.2 gives the stock valve timings for the test engine.

Table 4.2: Test engine valve event timings

Valve Event	Valve Timing
EVO	135° ATDC of Expansion
EVC	7° ABDC of Induction
IVO	7° BTDC of Exhaust
IVC	39° ABDC of Compression

Following the SAE guideline mentioned by Heywood [9] the overlap of the intake valves becomes negligible. For a carbureted engine, any cylinder communication through the intake manifold must occur prior to the carburetor in the plenum. For a fuel injected engine, many manifolds split later in the intake system causing the cylinders to contend for air flow. However, if the valve overlap time between the intake valves is short and the valve lifts during this time period are less than the lifts required to assume the valve open (or closed), the cylinders should not be competing for intake air flow which should have a negligible effect on cylinder-to- cylinder performance. However, under heavily throttled conditions the filling process of one manifold could occur while another is inducting fresh charge. Although, at throttled set points the mass flow rate of

air required by the engine is much less than those at the high load conditions and therefore the intake assembly should have the capacity to handle both manifolds.

4.2 CYLINDER DISCREPANCIES

4.2.1 Test Engine Cylinder Setup. As discussed in Section 3.2, the experimental engine is a two cylinder V-Twin engine. The cylinders are offset 90 degrees from each other. The four processes of each cylinder, i.e. compression, expansion, exhaust and induction are phased 270 degrees apart. The full pressure versus crank angle diagram is shown in Figure 4.4. The pressure variations due to the four processes of each cylinder can be seen. It should be noted that the peak pressure of cylinder 1 is approximately 300 kPa lower than that of cylinder 2. This is important in that it speaks to an imbalance between the two cylinders, which is undesirable to the overall performance of the engine. It can also be seen by examining Figure 4.4 that there is a substantial amount of time where the engine is running under its own inertia, i.e. there is no power being produced by either cylinder.

In Figure 4.5, a process diagram is shown. The process diagram depicts the pressure, piston position, and process duration for each cylinder. The position of the crankshaft is shown on the x-axis with respect to crank angle degrees. Zero crank angle degrees represents top dead center of the compression stroke for cylinder 1(top dead center location for cylinder 2 occurs at 270 degrees). The pressure within the cylinder can be seen on the right y-axis and the distinction between the cylinder processes can be seen on the left y-axis.

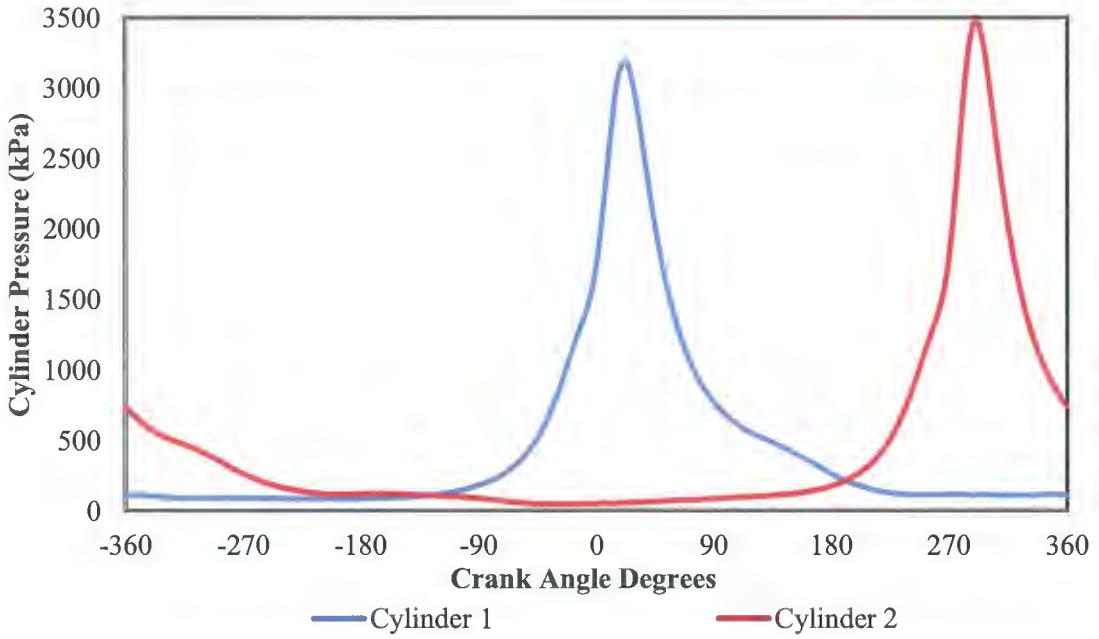

Figure 4.4: Cylinder pressure versus crank angle degrees for cylinder 1 and cylinder 2

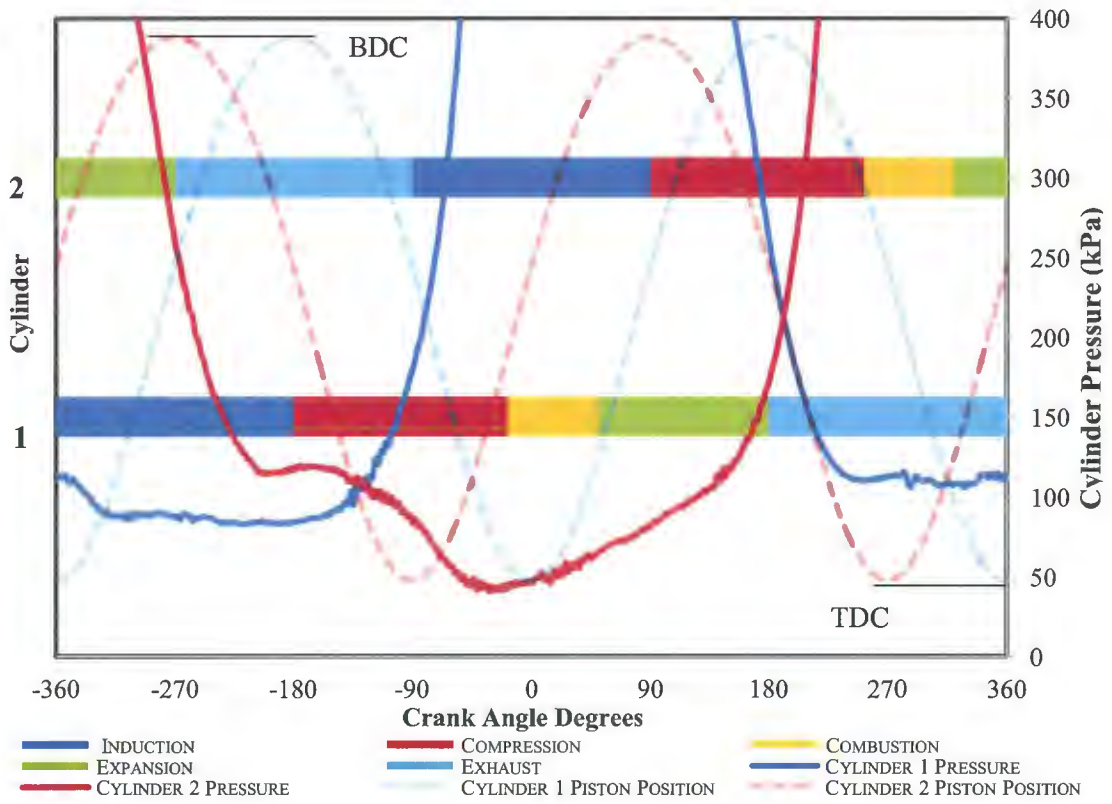

Figure 4.5: Cylinder process diagram for the test engine

The solid lines in Figure 4.5 represent the pressure for each cylinder; blue for cylinder 1 and red for cylinder 2. The cylinder pressure is resolved to show the bottom 400 kPa which results in a better depiction of the gas exchange process. The dashed lines show the motion of the piston, for each cylinder in its respective color, as well as a notation for top dead center and bottom dead center. The solid horizontal bars describe the process duration for each cylinder; cylinder 1 is represented by the bottom horizontal bar and cylinder 2 is represented by the top horizontal bar.

The purpose for this graph is to assist in describing a second means by which the two cylinders can communicate via the crankshaft. For small engines, the space within the crankcase is generally limited. Thus, the connecting rods often share the same journal bearing. Therefore, the power delivered through each connecting rod is transmitted through the shared journal to the crankshaft. This means the processes of one cylinder can directly affect the other. For the process diagram in Figure 4.5 one can compare the processes in cylinder 1 with respect to the processes in cylinder 2. That being said, it can be seen that while cylinder 1 is going through its induction stroke, cylinder 2 is proceeding through its expansion stroke and into its exhaust stroke. Conversely, while cylinder 2 is undergoing its induction process, cylinder 1 is going through its compression, combustion, and beginning of the expansion stroke. These processes and their effects on engine performance will be expounded upon later.

4.2.2 Cylinder Pressure versus Cylinder Volume Diagrams. One of the best tools available to depict cylinder pressure performance is the cylinder pressure versus cylinder volume (P-V) diagram. These plots are a representation of the pressure in the cylinder with respect to cylinder volume; they are useful in the calculation of mean

exchange process. Many of the guidelines and concerns touched upon in this chapter will be discussed in greater detail throughout the subsequent sections in how they apply to the test engine in particular. Some of these can be used in preliminary sizing of critical engine components. They can also be used to analyze the design parameters of current production engines to provide insight on improving future engine design within a similar size class.

5. COMPUTATIONAL FLUID DYNAMICS AND INITIAL FLOW TESTING

5.1 COMPUTATIONAL FLUID DYNAMICS

5.1.1 Motivation. Computational fluid dynamics provides a very useful tool when attempting to model flow regimes through a pipe or restriction. After defining the geometry of the specimen, the volume can be divided into a discrete mesh. The physical properties of the model can be defined; including factors such as boundary conditions, initial conditions, equations of motion, and fluid properties.

The CFD presented in this work was completed by Cary et al. [18]. A baseline model was developed for the test engine head to provide a metric by which to measure any improvements. A geometrical mesh was created to match the exact dimensions of the test engine's stock cylinder head. Once a performance baseline is obtained, areas of improvement can be deduced and alterations can be made to the geometry of the model. Performance gains can be quantified by comparing the improved model to the stock model.

That being said, the purpose of the CFD model for this work is not to capture the exact physics of the fluid flow between the intake port and the cylinder. It is performed to provide incentive to experimentally explore the ability to improve intake flow conditions and provide initial justification for those improvements.

5.1.2 Computational Fluid Dynamic Model. The geometry of the model was made to represent the exact dimensions of the test engine's cylinder and cylinder head configuration, including the port geometry and the valve. For the intake boundary conditions an atmospheric representation is made. A large globe attached to the cylinder

configuration was subject to a uniform atmospheric pressure in order to supply the fluid for the flow analysis. Figure 5.1 displays a cross section of the experimental mesh. The hemispherical globe (which provides a means to apply a pressure drop to the system) and valve configuration can be seen.

Figure 5.1: Cross-section of the three-dimensional mesh featuring the valve at full lift

For the CFD a k-ε turbulence model with a no slip wall boundary condition was used in the program Fluent. At the inlet, an ambient pressure condition was applied. Similarly, at the open exit of the cylinder a far-field pressure boundary condition was specified. The far-field pressure is less than the ambient pressure at the inlet, simulating a pressure drop across the system, driving the flow.

Mass flow rates for both the experimental (collected on the steady state flow bench for the stock engine heads) and simulated data sets were compared in order to

validate the CFD results. It can be seen in Table 5.1 that the differences between the experimental and simulated results are roughly 8% or less for the base engine head design. When considering this difference, it must be emphasized that no tuning was done to the fluid dynamic model. That is, once the model was developed the tests were run without altering parameters thereby eliminating attempts to make the data agree more concisely. The port geometry was used to develop a three-dimensional mesh at a fixed valve lift, and a pressure drop was applied between the inlet and outlet. Hence, the agreement of the mass flow rate is quite good.

Table 5.1: Mass flow rate comparison for the validation of the CFD simulation.

Validation of CFD Model for Engine Head Flow Tests			
Valve ΔP (kPa)	Exp. Mass Flow Rate (kg/s)	Sim. Mass Flow Rate (kg/s)	Difference (%)
2.50	0.030	0.032	8.25
3.00	0.032	0.035	8.16
5.00	0.042	0.045	7.27

From the CFD results, 2-D and 3-D plots of pressure contours and streamlines were generated to give a better visualization of fluid flow. After review of the 2-D cross-sections of the CFD model, a significant flow separation occurs in the intake system. The sharp corner formed at the interface of the horizontal portion of the intake port and the vertical passage containing the valve creates a recirculation region on the downstream side of the corner. A recirculation zone manifests itself when a fluid flow experiences a rapid bend and cannot stay attached to the internal surface of a pipe. This is depicted by a region of low pressure and no net mass flow. This recirculation causes the fluid to stagnate and blocks the airflow around the near side of the valve, as shown in Figure 5.2 below, which depicts the flow at a valve pressure drop of 3.0 kPa. It can also be seen that

the vast majority of the airflow into the combustion chamber is around the far side of the intake port area. The pressure contours shown in Figure 5.2 are measured in Pascals.

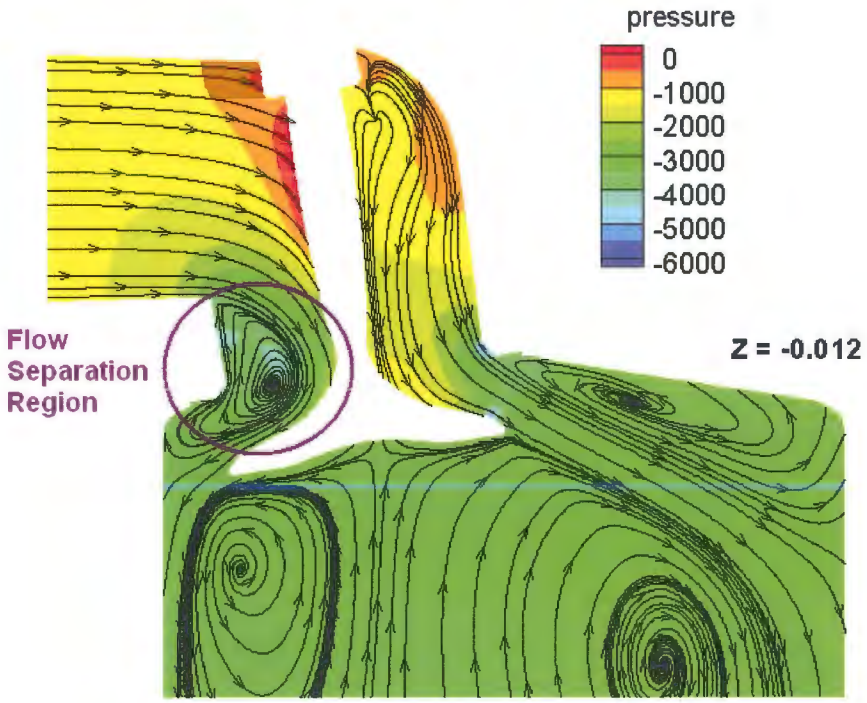

Figure 5.2: Pressure contours and streamlines of airflow through base head intake port

For internal flows, an area of flow separation correlates to an increase in flow loss in the system. By decreasing the flow separation region an increase in mass flow rate through the system should be realized. This will improve the overall operating efficiency, particularly at high end operating conditions.

A 7mm fillet radius was added to the CFD mesh to reduce the severity of the transition between horizontal and vertical flow in the stock port. This modification can be seen in the screenshot of the CFD internal geometry depicted below in Figure 5.3.

Figure 5.3: Modified head internal geometry used in CFD simulation

Another streamline graphic was generated for the modified head in the same plane and valve pressure drop as Figure 5.2 and is given in Figure 5.4, below. When compared to Figure 5.2, the flow separation and recirculation region has been largely eliminated with significant flow now occurring on the near side of the valve. This increases the effective flow area available to engine during the induction stroke. An area of high pressure can be seen at the corner of the port, forcing the flow to adhere to the port surface. Essentially, what this means is that the engine has to provide less work (or energy) to induct the same amount of intake charge as what was observed in Figure 5.2. Or, for the same amount of work, it can induct far more intake charge. This improves the overall operational efficiency of the engine particularly at high speed-high load (wide open throttle) conditions.

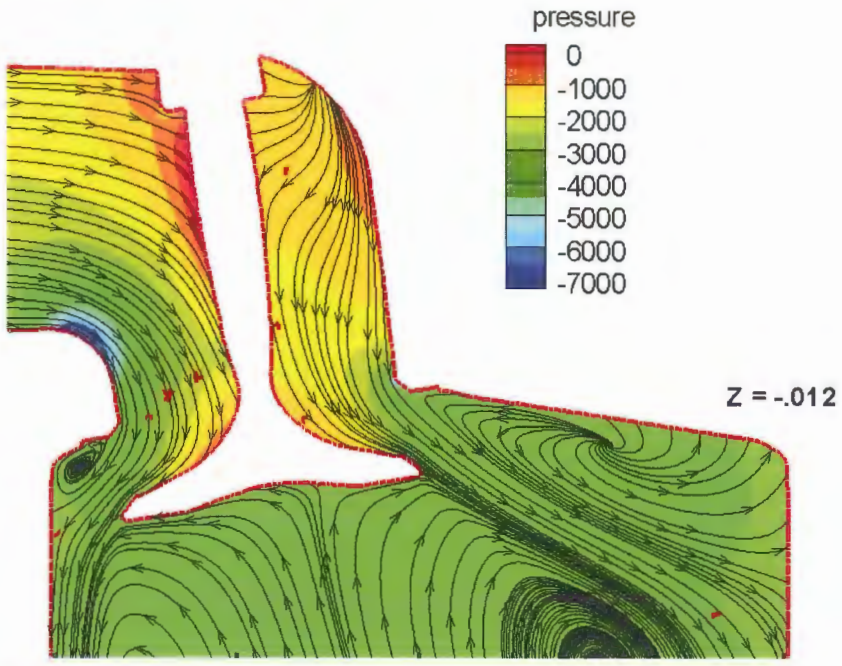

Figure 5.4: Airflow streamlines through engine head modified with 7mm radius

These results are quantified in Table 5.2, which compares key parameters including flow and discharge coefficients for the base and modified heads as determined from the CFD simulations. Again, the key to optimizing flow and discharge coefficients is to allow the value to approach 1. The closer the coefficient is to 1, the closer the flow regime is to an isentropic flow.

Equation 5.1 and Equation 5.2 represent the equations used to calculate the discharge coefficient and flow coefficient respectively. Equation 5.3 represents the ideal velocity head used in the calculation of Equation 5.1 and Equation 5.2,

$$C_d = \frac{Q}{A_v V_o} \tag{5.1}$$

$$C_f = \frac{Q}{A_p V_o} \tag{5.2}$$

$$V_o = \sqrt{\frac{2\Delta P_v}{\rho}} \tag{5.3}$$

where Q is the volumetric flow rate measured by the LFE, A_v is the valve curtain area which is a function of the valve head diameter and the valve lift, A_p is the minimum port area as seen in Figure 2.1, ΔP_v is the measured pressure drop across the valve, and ρ is the ambient air density.

Table 5.2: CFD comparison of base and modified heads for key performance parameters

Improvement Quantifications of Modified Head			
	Base Head	Modified Head	% Increase (%)
Mass Flow (kg/s)	0.035	0.044	24.6
Volume Flow (m^3/s)	0.029	0.036	24.6
Cd	0.460	0.574	24.6
Cf	0.678	0.845	24.6

Comparing the stock simulated and the modified simulated heads shows an improvement of 24.6% for the flow parameters listed. This improvement predicted by the CFD model points to modifications being needed in the port area of the experimental engine head. A few important conclusions can be drawn. First, the simulation provides good visualization of fluid flow through the intake port and into the cylinder. It is also effective at identifying inefficiencies and places where improvements to the design can be made.

5.2 STEADY STATE TESTING FOR FLOW AND DISCHARGE COEFFICIENTS

5.2.1 Flow Bench Testing. The methodology used for flow bench testing is discussed in Section 3.1.2 under Steady State Testing Procedure. Steady state flow tests were conducted at different pressure drops and varying valve lifts to observe the losses

due to the valve head and port area respectively. As discharge coefficients represent the restriction due to the valve curtain area, it is an important determinant of low valve lift engine flow operation. The flow coefficient represents the flow restrictions due to the port and becomes a key factor when the area of the valve curtain is greater than the port area.

5.2.2 Experimental Error Range of Flow Bench Testing. In order to have confidence in the experimental results, it is important to understand how repeatable the steady state flow tests are. This test is beneficial in that it shows the range of experimental error that should be expected using the current testing methodology. Figure 5.5 shows the repeatability results obtained by running eight sets of tests; varying valve lifts up and down. The plot shows the upper extreme and lower extreme limits of the results obtained during testing, as well as the mean coefficient value. The coefficient is plotted against the ratio of valve lift to valve diameter.

The upper and lower bounds represent the highest and lowest values of C_f and C_d obtained for each set point during the test. For appreciable valve lifts, the difference between the C,average and C,upper bounds and C,average and C,lower bounds is approximately 3%. For a low valve lift, the difference for the discharge coefficient is approximately 6.5% between the average and the upper bounds and the average and lower bounds. With a low range of experimental repeatability tests taken on the same flow bench operating under the same testing methodology are comparable. However, care must be taken when comparing results between different steady state flow benches and different engine geometries as there is no standardized way to conduct tests.

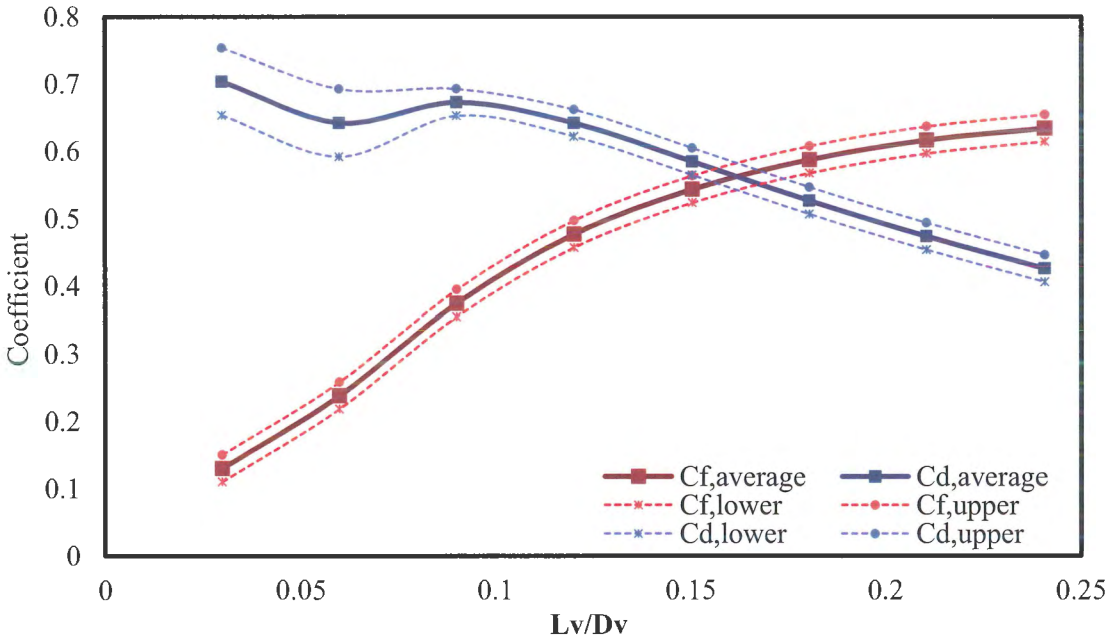

Figure 5.5: Repeatability testing results for flow and discharge coefficients

5.2.3 Results for Flow and Discharge Coefficient Tests. The discharge coefficient decreases with valve lift due to its dependence on the flow orifice area around the valve and valve seat. At low valve lifts, the valve curtain area is the limiting factor in flow rate which causes the discharge coefficient to be highest at this point. At high lift, flow separation at the valve and port edges reduces the effective flow area and hence reduces the value of C_d.

The value of the flow coefficient increases with valve lift as it uses the port geometry as the referenced flow area which only becomes the limiting factor when it is exceeded by the valve curtain area. The flow and discharge coefficients for varying pressure drops are plotted against normalized valve lift in Figure 5.6 below.

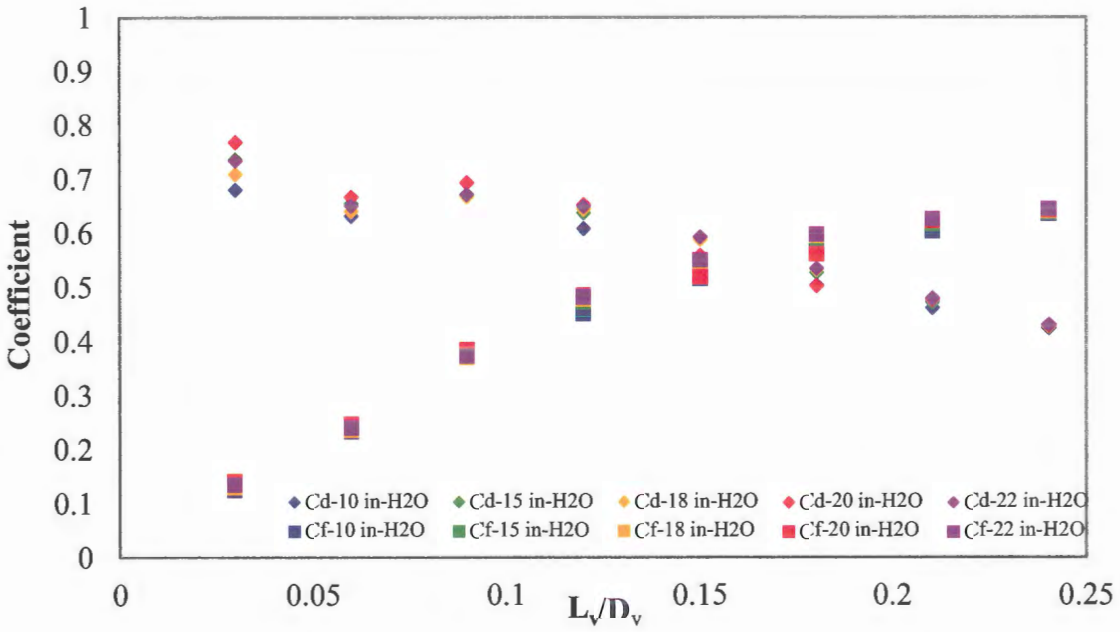

Figure 5.6: Flow and discharge coefficients for varying pressure drops and valve lifts

Flow and discharge coefficients are relatively insensitive to pressure drop above an appreciable valve lift. However, for a small L_v/D_v, the discharge coefficient can vary up to 0.12. A comparison of the flow and discharge coefficients between the two cylinder heads at a fixed pressure drop can be seen in Figure 5.7, below.

Based on these results, it can be seen that head 1 produced slightly higher discharge and flow coefficients at every valve lift investigated in the test procedure. This is most likely due to the slightly shorter runner length of cylinder head 1 compared to cylinder head 2, shown in Figure 4.1.

The cylinder heads were modified as discussed in Section 4.1.1. The 90 degree angle was filed down to a 7mm radius. Figure 5.8 presents the results of the flow and discharge coefficient tests for the stock head compared to the modified head. The results

are presented at a single pressure drop. As shown in Figure 5.2, C_f and C_d are not a strong function of pressure drop.

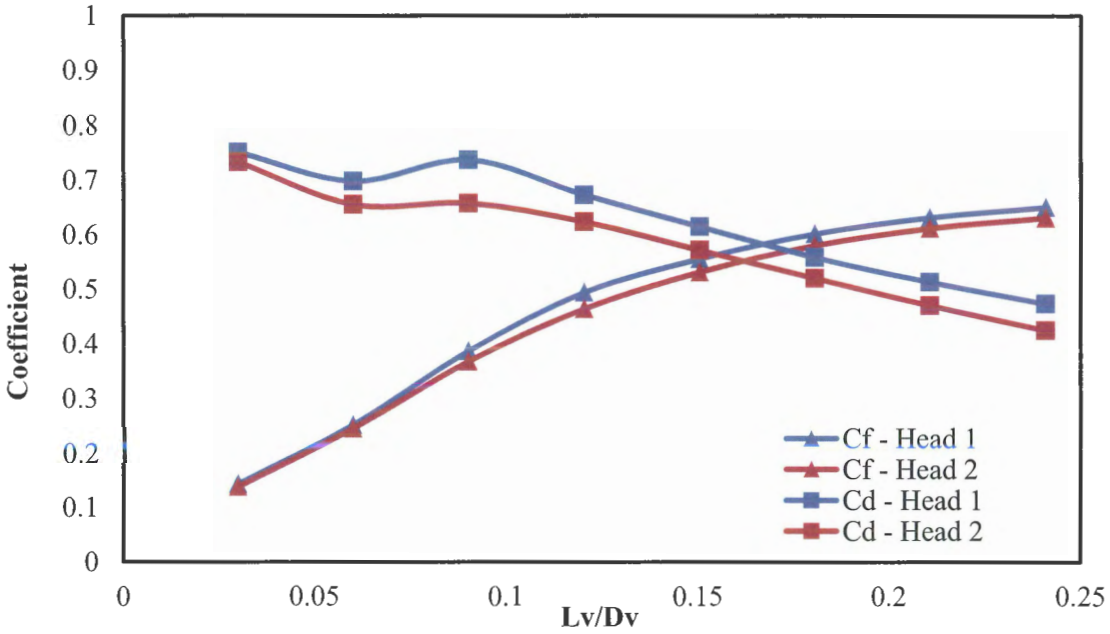

Figure 5.7: A comparison of flow and discharge coefficients for head 1 and head 2

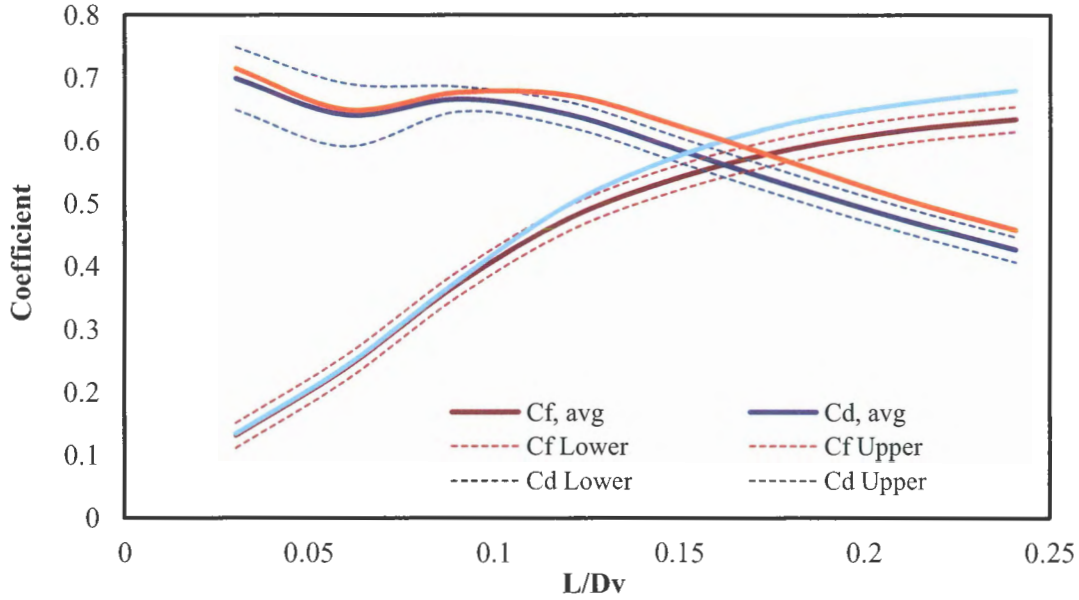

Figure 5.8: Flow and discharge coefficients for stock head compared to modified head

There is a coefficient improvement for the modified head over the stock head for almost all lift values. A very minimal improvement of both flow and discharge coefficients is seen for low valve lifts. This is due to the fact that at low valve lifts there is not enough flow area to see an appreciable change in flow characteristics. Also, flow separation at the corner of the port is smaller at lower flow rates. Once the valve lift reaches a certain point both the flow and discharge coefficient curves for the modified heads begin to deviate away from the stock curve. Recall in Section 2.2.3 that the use of a flow coefficient is better suited for high valve lifts where the port becomes the restriction. The improvement of flow coefficients come at higher valve lifts.

Once the valve reaches an appreciable lift, the discharge coefficients and flow coefficients for the modified heads rise to be well outside of the experimental error. This correlates to an improvement in mass flow rate of 9.98% as collected on the steady state flow bench.

5.2.4 Integrated Flow Coefficient and Mach Index. Integrated flow coefficient shown in Equation 5.4 is the value obtained when the flow coefficient is averaged over the time between intake valve open (IVO) and intake valve closed (IVC). The total intake flow quantity is dependent of camshaft profile and valve open duration [4]. It is useful in determining overall port efficiency over the entire range of valve lifts and is a good value to use in the comparison of different head designs. The Ricardo mean flow coefficient [4] equation was used along with Simpson's Rule to complete these calculations. The Simpson's Rule expansion of the Ricardo equation can be seen below. Where θ_1 is the crank angle of intake valve opening and θ_2 is the crank angle of intake valve closing. The value $C_f(\theta)$ is calculated as the flow coefficient at a particular crank

angle between IVO and IVC. That is, $C_f(\theta_b)$ is the flow coefficient of the current crank angle position while $C_f(\theta_a)$ is the flow coefficient of the previous crank angle position.

$$\bar{C}_f = \frac{\int_{\theta_1}^{\theta_2} C_f d\theta}{\theta_2 - \theta_1} = \frac{\sum \frac{\theta_b - \theta_a}{6}\left[C_f(\theta_a) + 4C_f\left(\frac{\theta_a + \theta_b}{2}\right) + C_f(\theta_b)\right]}{\theta_2 - \theta_1} \tag{5.4}$$

Mach index, Z, can be defined as the ratio of the velocity through the effective valve area to the speed of sound of air and helps quantify the restriction of the port at a specified engine speed. It correlates well to the mean Mach number at the inlet valve's smallest area. The equation development to calculate this value can be seen below in Equation 5.5 through Equation 5.9.

The mean effective flow velocity can be determined by the isentropic rate at which the piston can pull air into the cylinder divided by the quantity of the port area (the flow restriction) multiplied by the integrated flow coefficient to better represent real flow conditions. The rate at which the piston can displace air is a product of the surface area of the piston, Equation 5.5, and the mean piston speed, Equation 5.6. Where B is the cylinder bore, L is the engine stroke, and N is the rotational speed of the crankshaft.

$$A_p = \frac{\pi}{4}B^2 \tag{5.5}$$

$$\bar{S}_p = 2LN \tag{5.6}$$

The flow restriction can be defined as the product of the integrated flow coefficient, $\bar{C}_f$, and the port area, A_p, so the flow velocity into the cylinder can be defined by Equation 5.7.

$$V_c = \frac{\pi B^2 LN}{2\bar{C}_f A_p} \tag{5.7}$$

The speed of sound for an ideal gas undergoing an isentropic process is defined as Equation 5.8 where γ is the ratio of specific heats, R is the gas constant and T is the absolute temperature of the fluid.

$$c = \sqrt{\gamma RT} \tag{5.8}$$

Then by dividing Equation 5.7 by Equation 5.8 the Mach index can be calculated, Equation 5.9.

$$Z = \frac{\pi B^2 LN / \bar{C}_f A_p}{\sqrt{\gamma RT}} \tag{5.9}$$

Some assumptions are made when developing Equation 5.9. First, the calculation of the piston surface area assumes that the piston has a flat top. Second, the equation is assuming an isentropic flow modified by a flow coefficient. Lastly an ideal gas assumption is being made of the working fluid.

As a general rule, Mach index is considered at the highest engine speed design point in which a value below 0.5 is preferred. Typically, an engine's volumetric efficiency will drop considerably for Mach index greater than 0.5, due to inlet flow choking [2]. A method to combat the effect of high Mach index is to increase the size of the intake valves.

Integrated flow coefficients and Mach indices are shown below in Table 5.3 for a comparison between head 1 and head 2. As shown, all of the Mach indices are in the range of 0.81 to 0.87. These results indicate that the restriction is high and the flow through the intake port may be heavily restricted during a portion of the intake process.

Table 5.3: Integrated C_f and Mach indices at three different valve pressure drops

Integrated Flow Coefficient and Mach Index						
	Head 1			Head 2		
Valve ΔP (kPa)	2.5	3.0	5.0	2.5	3.0	5.0
Integrated Cf	0.306	0.306	0.302	0.312	0.292	0.292
Z (Mach Index)	0.828	0.829	0.839	0.814	0.867	0.868

The results from the flow tests are quantified in Table 5.4 and include the integrated flow coefficient and Mach index values. Only values at 3.0 kPa pressure drop are reported due to similarities of data at different pressure drops. The values returned for the integrated flow coefficient and Mach index are averaged over the entire valve profile, while the other values are specific to a valve lift of 8.25mm (or full valve lift for the test engine's stock camshaft).

Table 5.4: Experimental comparison of key parameters for base and modified heads

Improvement Quantifications of Modified Head			
	Base Head	Modified Head	Increase (%)
Mass Flow (kg/s)	0.032	0.035	7.71
Volume Flow (m^3/s)	0.027	0.029	7.71
Cd	0.428	0.462	7.77
Cf	0.631	0.680	7.77
Integrated Cf	0.292	0.330	13.01
Z (Mach Index)	0.867	0.768	-11.42

By eliminating the sharp corner in the port, as shown in Figure 5.3, an improvement in flow through the engine head at both high and low pressure differentials can be seen in both the simulated and the experimentally modified head. The integrated flow coefficient and Mach index given in Table 5.4, show the improvement which should

be expected in engine performance as the effect is integrated over the valve lift profile as opposed to a fixed lift.

Overall, the CFD analysis provides a reasonable preliminary test when attempting to initially understand the intake flow phenomena. The flow and discharge coefficient tests offer a means by which the flow losses can be experimentally quantified. Also, improvements in design can be realized by running the same test for modified components as seen throughout this section. Again, modifying the stock intake port with a 7mm radius shows an improvement of almost 8% in flow and discharge coefficients.

6. STEADY STATE PRESSURE LOSS COEFFICIENT

6.1 PRESSURE LOSS COEFFICIENT FORMULATION AND PROCEDURE

An alternative measure of system performance, by means of basic fluid mechanics, can be used to understand the flow loss through separate components in an intake system. This provides a method to better determine where a flow restriction occurs. Loss coefficients are directly related to fluid pressure drop and to a good approximation, are additive for components in a system. This technique of measuring pressure loss can better differentiate between components with high flow loss coefficients. Overall system improvements from reducing component loss can be estimated.

Similar to the series of tests used to determine flow and discharge coefficients, the pressure loss tests are again conducted on a steady state flow bench. Pressure loss coefficients can also be used to determine the flow losses due to the port and the valve. However, unlike flow and discharge coefficients, pressure loss measurements can further measure the restrictions due to other intake components, such as the manifold and the carburetor. A steady state testing methodology, as described in Chapter 3, was used and the specifics of the particular pressure loss tests will be discussed in greater detail in a later section.

6.1.1 Fluid Dynamic Formulation. In order to properly perform the analysis, it is important to understand what assumptions are being made of the equations governing the flow. For this set of experiments the basic problem being examined is the pressure drop across the different components of the test engine (air filter, carburetor, intake

manifold and cylinder head). The pressure drop across an intake component speaks to a restriction in flow through that particular component. The overall goal is to reduce the pressure drop across the intake system to improve the flow conditions. The working fluid for these tests will consist strictly of air. Several assumptions such as the ideal gas law, steady state flow, inviscid flow, and incompressible flow will be used and discussed throughout the development of the equations. The formulation developed follows closely with that of Young [6] and other fluid mechanics texts.

The Eulerian method can be used to solve these fluid mechanic based problems. The motion of the fluid can be described by defining parameters such as pressure, density, and velocity as functions of both time and space. This method helps to determine the flow properties at fixed points in space as the fluid progresses past these points.

By using the Eulerian method, the velocity field can be described by specifying the velocity (**V**) at all points and all times within the flow field of interest [6]. This can be expressed in three dimensions in Cartesian coordinates as

$$\mathbf{V} = u\mathbf{i} + v\mathbf{j} + w\mathbf{k} \tag{6.1}$$

where it can be said that the components u, v, and w are the velocity in the x, y, and z directions respectively and **i**, **j**, and **k** are their respective unit vectors.

Thus, by knowing the derivative of the velocity vector, the acceleration vector can be determined. By the use of the chain rule on Equation 6.1,

$$\mathbf{a}(t) = \frac{d\mathbf{V}}{dt} + \frac{\partial \mathbf{V}}{\partial x}\frac{dx}{dt} + \frac{\partial \mathbf{V}}{\partial y}\frac{dy}{dt} + \frac{\partial \mathbf{V}}{\partial z}\frac{dz}{dt} \tag{6.2}$$

and replacing dx/dt, dy/dt, and dz/dt with u,v, and w the acceleration term then becomes,

$$\mathbf{a}(t) = \frac{\partial \mathbf{V}}{\partial t} + u\frac{\partial \mathbf{V}}{\partial x} + v\frac{\partial \mathbf{V}}{\partial y} + w\frac{\partial \mathbf{V}}{\partial z} \tag{6.3}$$

and in component form Equation 6.3 can then be expanded as

$$a_x = \frac{\partial u}{\partial t} + u\frac{\partial u}{\partial x} + v\frac{\partial u}{\partial y} + w\frac{\partial u}{\partial z} \tag{6.4a}$$

$$a_y = \frac{\partial v}{\partial t} + u\frac{\partial v}{\partial x} + v\frac{\partial v}{\partial y} + w\frac{\partial v}{\partial z} \tag{6.4b}$$

$$a_z = \frac{\partial w}{\partial t} + u\frac{\partial w}{\partial x} + v\frac{\partial w}{\partial y} + w\frac{\partial w}{\partial z} \tag{6.4c}$$

By observing Newton's second law of motion applied to the mass of a fluid particle, Equation 6.5 can be written,

$$\delta\mathbf{F} = \delta m\mathbf{a} \tag{6.5}$$

and then expanded to reveal the x, y, and z components such that

$$\delta F_x = \delta m a_x \tag{6.6a}$$

$$\delta F_y = \delta m a_y \tag{6.6b}$$

$$\delta F_z = \delta m a_z \tag{6.6c}$$

where the mass term, δm can be defined as a function of the fluid density, ρ,

$$\delta m = \rho \delta x \delta y \delta z \tag{6.7}$$

The force term as expressed in the second law, Equation 6.5, is made up of two different forces. Both surface forces, $\delta\mathbf{F}_s$, and body forces, $\delta\mathbf{F}_b$, are present. The surface forces can be separated into a term representing the normal force, σ, and the shearing forces, τ. By summing surface forces on the particle surface in three dimensions, the component form of $\delta\mathbf{F}_{surface}$, due to the surface forces, then becomes

$$\delta F_{surface,x} = \left(\frac{\partial \sigma_{xx}}{\partial x} + \frac{\partial \tau_{yx}}{\partial y} + \frac{\partial \tau_{zx}}{\partial z}\right)\delta x \delta y \delta z \tag{6.8a}$$

$$\delta F_{surface,y} = \left(\frac{\partial \tau_{xy}}{\partial x} + \frac{\partial \sigma_{yy}}{\partial y} + \frac{\partial \tau_{zy}}{\partial z}\right)\delta x \delta y \delta z \tag{6.8b}$$

$$\delta F_{surface,z} = \left(\frac{\partial \tau_{xz}}{\partial x} + \frac{\partial \tau_{yz}}{\partial y} + \frac{\partial \sigma_{zz}}{\partial z}\right)\delta x \delta y \delta z \tag{6.8c}$$

While the surface forces account for the normal stress in each respective direction and the shear stress in each respective adjacent direction, the body forces are accounted for by the acceleration due to gravity, g. Thus, in component form the body forces, $\delta \mathbf{F}_{body}$, become

$$\delta F_{body,x} = \delta m g_x \tag{6.9a}$$

$$\delta F_{body,y} = \delta m g_y \tag{6.9b}$$

$$\delta F_{body,z} = \delta m g_z \tag{6.9c}$$

then, the total force that the body experiences is the sum of the surfaces forces and the body forces,

$$\delta \mathbf{F} = \delta \mathbf{F}_{surface} + \delta \mathbf{F}_{body} \tag{6.10}$$

thus, by using the component form of acceleration from Equation set 6.4, the definition of mass from Equation 6.7, the component form of the surface force from Equation set 6.8, the component form of the body forces in Equation set 6.9, and the relationship shown in Equation 6.10 gives

$$\rho g_x + \frac{\partial \sigma_{xx}}{\partial x} + \frac{\partial \tau_{yx}}{\partial y} + \frac{\partial \tau_{zx}}{\partial z} = \rho\left(\frac{\partial u}{\partial t} + u\frac{\partial u}{\partial x} + v\frac{\partial u}{\partial y} + w\frac{\partial u}{\partial z}\right) \tag{6.11a}$$

$$\rho g_y + \frac{\partial \tau_{xy}}{\partial x} + \frac{\partial \sigma_{yy}}{\partial y} + \frac{\partial \tau_{zy}}{\partial z} = \rho\left(\frac{\partial v}{\partial t} + u\frac{\partial v}{\partial x} + v\frac{\partial v}{\partial y} + w\frac{\partial v}{\partial z}\right) \tag{6.11b}$$

$$\rho g_z + \frac{\partial \tau_{xz}}{\partial x} + \frac{\partial \tau_{yz}}{\partial y} + \frac{\partial \sigma_{zz}}{\partial z} = \rho\left(\frac{\partial w}{\partial t} + u\frac{\partial w}{\partial x} + v\frac{\partial w}{\partial y} + w\frac{\partial w}{\partial z}\right) \tag{6.11c}$$

The component equations from Equations 6.11a, 6.11b, and 6.11c are the general differential equations of motion for a fluid. From this point there are more unknowns then equations. So, in order to acquire a solution to these equations further assumptions must be made.

For these experiments the flow of air through a test configuration is driven by a pressure gradient (or suction) created by the vacuum pump on the steady state flow bench. This pressure differential causes the air to accelerate to a steady state flow velocity as well as overcome viscous losses in the passage. The majority of viscous losses are accounted for by skin friction between the air and the passage surface, or by flow separation caused by inconsistencies in the fluid's velocity profile (i.e. a corner or change in cross sectional area). Initially these losses are neglected to simplify the development of the equations. They are accounted for in the end by introducing a viscous pressure loss term. This pressure loss term is used to modify the flow from the assumed ideal case, similar to the way a discharge coefficient modifies isentropic flow.

Returning to the equations of motion, the shearing terms (i.e. τ_{xy}, τ_{xz}, τ_{yx}, etc…) arise from the viscosity of the fluid. It is know that for air the viscosity term is small, and therefore it seems reasonable to assume that under some circumstances the effects of viscosity can be neglected (and thus the shearing stress) [6]. Furthermore, when the shearing forces are neglected, the normal force is no longer dependent on direction, thus the pressure, P, can be related to the normal forces in each of the respective planes

$$-P = \sigma_{xx} = \sigma_{yy} = \sigma_{zz} \tag{6.12}$$

Then, by using the inviscid assumption (viscosity is zero) Euler's equations of motion can be obtained. Again, because the idea is not to model the exact characteristics

of the flow these assumptions are made to reduce the complexity of the end equations. Since the parameters are being obtained through experimental measurements they already account for viscous effects. Thus, a term will be added in the end that helps account for those losses. Simplifying Equation set 6.11 by removing the shearing terms and substituting in Equation 6.12, Euler's equations of motion can be written as

$$\rho g_x - \frac{\partial P}{\partial x} = \rho\left(\frac{\partial u}{\partial t} + u\frac{\partial u}{\partial x} + v\frac{\partial u}{\partial y} + w\frac{\partial u}{\partial z}\right) \tag{6.13a}$$

$$\rho g_y - \frac{\partial P}{\partial y} = \rho\left(\frac{\partial v}{\partial t} + u\frac{\partial v}{\partial x} + v\frac{\partial v}{\partial y} + w\frac{\partial v}{\partial z}\right) \tag{6.13b}$$

$$\rho g_z - \frac{\partial P}{\partial z} = \rho\left(\frac{\partial w}{\partial t} + u\frac{\partial w}{\partial x} + v\frac{\partial w}{\partial y} + w\frac{\partial w}{\partial z}\right) \tag{6.13c}$$

Because of the nonlinear velocity terms that arise in the convective acceleration portion of Equation set 6.13 Euler's equations are nonlinear, partial differential equations for which there is no general method of solving. However, it can be simplified further by making a couple more general assumptions. First, by expressing Equation set 6.13 in vector form

$$\rho\mathbf{g} - \nabla P = \rho\left[\frac{\partial \mathbf{V}}{\partial t} + (\mathbf{V}\cdot\nabla)\mathbf{V}\right] \tag{6.14}$$

and making an assumption of steady state flow, that is the velocity field at a point is not changing with respect to time (dV/dt is zero), Euler's equation becomes

$$\rho\mathbf{g} - \nabla P = \rho[(\mathbf{V}\cdot\nabla)\mathbf{V}] \tag{6.15}$$

Furthermore, if Equation 6.15 is integrated along a streamline that has a coordinate system with a vertical z axis, so that the up direction is positive, the gravity vector can be expressed as

$$\mathbf{g} = -g\nabla z \tag{6.16}$$

then a vector identity can be employed to expand the convective term in Equation 6.15, that is

$$(\mathbf{V}\cdot\boldsymbol{\nabla})\mathbf{V}=\frac{1}{2}\boldsymbol{\nabla}(\mathbf{V}\cdot\mathbf{V})-\mathbf{V}\times(\boldsymbol{\nabla}\times\mathbf{V}) \tag{6.17}$$

and substituting Equation 6.17 into Equation 6.15 yields

$$-\rho g\boldsymbol{\nabla}z-\boldsymbol{\nabla}P=\frac{\rho}{2}\boldsymbol{\nabla}(\mathbf{V}\cdot\mathbf{V})-\rho[\mathbf{V}\times(\boldsymbol{\nabla}\times\mathbf{V})] \tag{6.18}$$

and through rearranging key terms can be expressed as

$$\frac{1}{2}\boldsymbol{\nabla}(V^2)+g\boldsymbol{\nabla}z+\frac{\boldsymbol{\nabla}P}{\rho}=[\mathbf{V}\times(\boldsymbol{\nabla}\times\mathbf{V})] \tag{6.19}$$

By maintaining the path along the streamline and taking the dot product of each term in Equation 6.19 by the differential length d**s** it becomes

$$\frac{1}{2}\boldsymbol{\nabla}(V^2)\cdot d\mathbf{s}+g\boldsymbol{\nabla}z\cdot d\mathbf{s}+\frac{\boldsymbol{\nabla}P}{\rho}\cdot d\mathbf{s}=[\mathbf{V}\times(\boldsymbol{\nabla}\times\mathbf{V})]\cdot d\mathbf{s} \tag{6.20}$$

and while the differential length is parallel to the velocity vector, the term $\mathbf{V}\times(\boldsymbol{\nabla}\times\mathbf{V})$ is perpendicular to **V** and therefore, is equal to zero. For this investigation, to a reasonable accuracy, only one dimensional flow is considered under steady state conditions (i.e. $\nabla P\cdot ds=\left(\frac{\partial P}{\partial x}\right)dx+\left(\frac{\partial P}{\partial y}\right)dy+\left(\frac{\partial P}{\partial z}\right)dz=dP$). That said, unsteady terms are assumed to be zero, that is, only convective terms are considered. Equation 6.20 can be reduced to

$$\frac{1}{2}d(V^2)+gdz+\frac{dP}{\rho}=0 \tag{6.21}$$

Equation 6.21 states that for inviscid, irrotational, steady flow the change in terms V, z and P occur along a streamline. Thus Equation 6.21 can be integrated to yield

$$\int\frac{dP}{\rho}+\frac{1}{2}(V^2)+gz=0 \tag{6.22}$$

Equation 6.22 shows that the sum of the pressure, P, dynamic velocity head, $V^2/2$, and the potential energy is constant. For example, any change in pressure must be compensated for by a change in velocity, a change in potential energy, or both. Thus, a solution to Euler's equation is obtained and can be written as

$$\frac{P}{\rho} + \frac{V^2}{2} + gz = \text{constant} \tag{6.23}$$

Equation 6.23 then becomes Bernoulli's equation. It is often times acceptable to write Equation 6.23 between two points on the same streamline [6]. For these experiments point 1 is considered to be the ambient conditions just outside of the entrance plane of the component or system being tested. Point 2 is considered at the exit plane of the component or system being tested. Considered Figure 2.1 presented earlier; assume, for example, that the air filter is the component to be analyzed. The conditions of point 1 would be the ambient conditions somewhere near the entrance plane of the air filter. Point 2 would be located at the exit plane of the hose just as the transition between the hose and the plenum occurs. So, writing Equation 6.23 between two points yields

$$\frac{P_1}{\rho} + \frac{V_1^2}{2} + gz_1 = \frac{P_2}{\rho} + \frac{V_2^2}{2} + gz_2 \tag{6.24}$$

Again, an assumption of incompressible flow is being employed so the density of air is taken to be the equivalent at all points in the flow. For this part the change in elevation between point one and point two (i.e. Δz) is considered small and the effects due to gravity will be neglected. However, it will be accounted for in a later set of calculations. Equation 6.24 can then be rewritten as

$$\frac{P_1}{\rho} + \frac{V_1^2}{2} = \frac{P_2}{\rho} + \frac{V_2^2}{2} \tag{6.25}$$

Since the working fluid throughout this experiment is air and assuming heat transfer between the fluid and the internal walls of the components is negligible, it is known that enthalpy, h, can be defined as

$$dh = \frac{dP}{\rho} \quad \text{and} \quad h = \frac{P}{\rho} \tag{6.26}$$

furthermore, using the assumption of an ideal gas,

$$P = \rho RT \tag{6.27}$$

the equation of enthalpy, Equation 6.26, can then be written in terms of the ratios of specific heats

$$h = c_p T = \frac{c_p}{R}\frac{P}{\rho} = \frac{\gamma}{\gamma - 1}\frac{P}{\rho} \tag{6.28}$$

At this point a viscous pressure loss term is introduced to account for the losses due to the viscous effects of the flow and the flow separation due to the geometry of the component. Earlier these effects were neglected to simplify the equations and are now being introduced in a different form. The viscous pressure loss term can be defined by relating the dynamic velocity head at point 1 to the dynamic velocity head at point 2. This loss term is expressed as a product of the pressure loss coefficient and the dynamic velocity head

$$\Delta P_{\text{loss } 1-2} = K_{L\,1-2}\left(\frac{1}{2}\rho V_2^2\right) \tag{6.29}$$

where the loss coefficient, $K_{L1\text{-}2}$, is the loss associated with moving the fluid from point 1 to point 2 (taken to be the losses associated with viscous effects and flow separation). A system in which the dynamic velocity head at point 1 is equivalent to the dynamic velocity head at point 2 would have a loss coefficient equal to 1 (i.e. the effects due to

viscous losses and flow separation would be zero). Therefore, rewriting Equation 6.25 in terms of Equation 6.28 and Equation 6.29 yields

$$\frac{\gamma}{\gamma-1}\frac{P_1}{\rho}=\frac{\gamma}{\gamma-1}\frac{P_2}{\rho}+\frac{V_2^2}{2}+\frac{\Delta P_{loss\ 1-2}}{\rho} \tag{6.30}$$

This is true under the assumption that the losses associated with accelerating the fluid from zero velocity at point 1 to the inlet of the component are negligible so that $K_{L1\text{-}2}$ equals the total loss for the passage. The loss coefficients express the loss throughout the passage. Then, by applying the ideal gas law, Equation 6.27, and the continuity equation

$$\rho A_1 V_1 = \rho A_2 V_2 \tag{6.31}$$

Equation 6.30 can be rearranged to determine pressure loss terms by knowing several parameters: gas constant, ratio of specific heats, ambient temperature and pressure, pressure ratio, geometric flow area, and mass flow rate

$$2\frac{\gamma}{\gamma-1}\frac{P_1}{RT_1}A_2^2\left(\frac{P_2}{P_1}\right)^{2/\gamma}\left[1-\left(\frac{P_2}{P_1}\right)^{\gamma-1/\gamma}\right]=\dot{m}^2[1+K_{L1-2}] \tag{6.32}$$

Since the pressure and temperature taken at point 1 is assumed to be stagnant, there is a term associated with an energy change from static to kinetic energy going from point 1 to point 2. This manifests itself on the right hand side of the equality and is added to the loss coefficient term.

The key advantage to the use of pressure loss coefficients is that the loss coefficients for a fixed fluid velocity are directly proportional to fluid pressure drop and to a good approximation, are additive for components of a system.

6.1.2 Accounting for Major and Minor Losses in Steady State Flow Testing.

Because of the location at which the differential pressure reading is taken on the steady state flow bench, losses must be accounted for when attempting to obtain the pressure at the intake valve. Figure 6.1 depicts the different flow areas and measurement locations that are accounted for in the system. The differential pressure between the ambient conditions and the surge tank (below the glass cylinder) is recorded. Between these two points are five different changes in area and one meter of vertical elevation. The changes in cross sectional area are between the surge tank and glass cylinder, glass cylinder and the valve, the valve and port area, and the port area and the ambient.

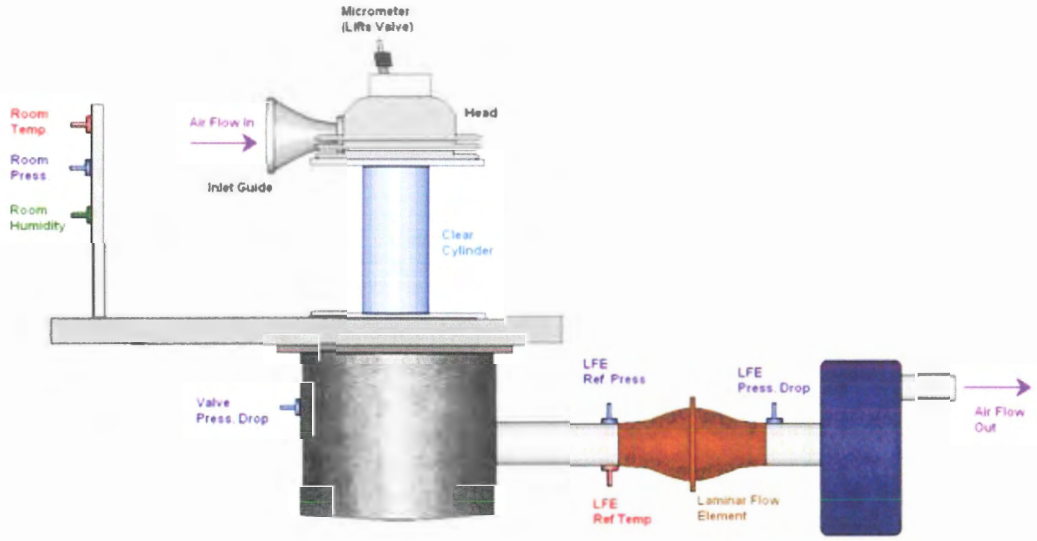

Figure 6.1: Depiction of the steady state flow bench

The energy equation, Equation 6.33, is used to determine the unknown pressure at the points in between the ambient room conditions and the conditions in the surge tank. The laminar flow element is responsible for measuring the volumetric flow rate of the

working fluid through the system. By knowing the density of the working fluid and the cross sectional areas of the components, a fluid velocity term can be found for each point in the system.

$$\frac{P_1}{\rho} + \frac{V_1^2}{2} + gz_1 = \frac{P_2}{\rho} + \frac{V_2^2}{2} + gz_2 + h_L \tag{6.33}$$

A new term is introduced that accounts for the head loss in the system. The head loss, h_L, is made up of two separate terms. The major head loss, h_{Lmajor}, accounts for the loss due to viscous effects in a straight pipe and the minor head loss, h_{Lminor}, accounts the loss due to various components throughout the system.

$$h_L = h_{Lmajor} + h_{Lminor} \tag{6.34}$$

When calculating the pressure differential between the surge tank and the ambient conditions, losses due to the viscous effects must be considered. The Darcy-Weisbach equation is used to account for the friction between the fluid and the glass cylinder. The Darcy-Weisbach equation is valid for both horizontal and vertical flow. It is used under the circumstance of steady, fully developed, incompressible pipe flow.

The major head loss is a function of the friction factor (f), pipe length (l), pipe diameter (D), fluid velocity (v), and the acceleration due to gravity (g). A Moody chart is used to determine the friction factor (f) based on a Reynolds number ($Re = \rho vD/\mu$) of the flow and an assumption of the material roughness (ε/D). The glass cylinder was assumed to be smooth. For the Reynolds numbers encountered throughout these experiments the surface roughness is not a major factor (for values of 0 to 0.0002 the overall effects on friction factors are small). The friction factors used for these calculations ranged from 0.0215 to 0.0250 depending on the Reynolds number of the flow.

Minor losses occur in system components such as: valves, pipe bends, and pipe expansions and contractions. A useful way to relate this data is to specify a loss coefficient, K_L. Each type of component geometry has an associated loss coefficient that is determined by experimental data. Loss coefficients for both sudden expansions and sudden contractions are a function of area ratio. Based on the empirical correlation of the area ratio to the loss coefficient for sudden expansions the coefficient used for the expansion from the glass cylinder to the surge tank was 0.91. The loss coefficient associated with the expansion from the valve cross sectional area and the glass cylinder was taken as 0.68.

So, in effect, the pressure change is attributed to the elevation change, the head loss associated with the frictional effects, and the flow loss due to sudden changes in flow area or direction. By using these correlations the pressure at the various flow areas can be determined.

6.1.3 Pressure Loss Testing Procedure. There were three tests run for each component and combination of components. The first test was run with the relief valve on the vacuum pump open (RVO), which correlates to a minimal flow though the actual flow bench (1.2 kPa). The second test was run with a valve pressure drop of 2.5 kPa and the third test was run with a valve pressure drop of 5.0 kPa.

This methodology was used to better simulate different engine conditions, i.e. closed throttle, partial throttle and a wide open throttle case. Each component underwent all three tests on an individual basis, without the addition of other intake components. Next, an additive procedure was used in which the air filter system underwent the three flow tests. Next, the carburetor was added to the air filter and the three set points were

run again. Then, the manifold was added to the air filter and carburetor and tested. Lastly, the head was attached to the flow bench and the intake system bolted to the head. The head was tested at a maximum valve lift to predict a 'best case' scenario for flow conditions through the head. This maximum valve lift case allows for a maximum flow area through the intake valve and limits restrictions. The entrance and exit areas of each component are represented in Figure 6.2.

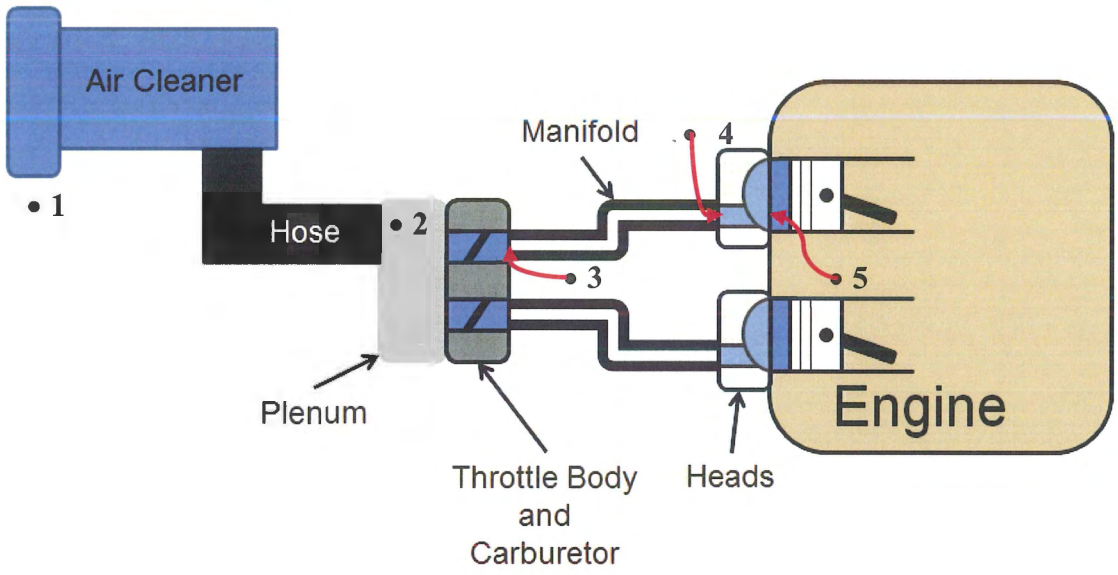

Figure 6.2: Critical areas of pressure loss testing

Measured loss coefficients can be used to predict overall system performance and calculate the contribution to the total losses in the system due to each component. By calculating losses in this manner, they can pin-point certain sections of the inlet system that have high losses. They can also be used to estimate overall system gains from reductions in component losses. Each assembly subsystem (i.e. air cleaner, carburetor,

manifold and head) can be subdivided further into component losses. For example, when analyzing the head, the subsystem can be divided into port area, valve stem, and valve head losses.

In a real intake system, the exit flow velocity of the air filter system will be the intake flow velocity of the carburetor subsystem (if present). Likewise, the exit flow velocity of the carburetor will be the intake flow of the manifold. Because the system is very sensitive to inlet and boundary conditions, it is, therefore, important to maintain this order when conducting the tests. That is: air filter, carburetor, manifold, and head. The procedure was run in reverse in order to verify this reasoning. The comparison between the two tests yielded different results, showing the greatest losses in different components and the pressure loss coefficients for the two tests were not similar. The pressure loss coefficient due to the head decreased by approximately 63%, the loss coefficient of the manifold decreased by approximately 5%, the loss coefficient of the carburetor increased by approximately 50%, and the pressure loss coefficient of the air filter decreased by 35%.

The results were obtained by using an expanded version of Equation 6.32 to include all loss terms for the system.

$$\frac{\gamma}{\gamma-1}\left[\frac{P_1}{\rho_1}-\frac{P_5}{\rho_5}\right]=\frac{V_5^2}{2}\left[\left(\frac{\rho_5}{\rho_2}\right)^2\left(\frac{A_5}{A_2}\right)^2 K_{1-2}+\left(\frac{\rho_5}{\rho_3}\right)^2\left(\frac{A_5}{A_3}\right)^2 K_{2-3}+\left(\frac{\rho_5}{\rho_4}\right)^2\left(\frac{A_5}{A_4}\right)^2 K_{3-4}+K_{4-5}\right] \quad (6.35)$$

And through using isentropic relations between pressure and density, Equation 6.37 can further be simplified to:

$$2\frac{\gamma}{\gamma-1}\frac{P_1^2}{RT_1}A_5^2\left(\frac{P_5}{P_1}\right)^{\frac{2}{\gamma}}\left[1-\left(\frac{P_4}{P_1}\right)^{\frac{\gamma-1}{\gamma}}\right]=\dot{m}^2\left(1+K_{sys}\right) \quad (6.36)$$

where

$$K_{sys} = K'_{1-2} + K'_{2-3} + K'_{3-4} + K'_{4-5} \tag{6.37}$$

and

$$K'_{1-2} = \text{equivalent losses for subsytem 1} = \left(\frac{P_5/P_1}{P_2/P_1}\right)^{\frac{2}{\gamma}} \left(\frac{A_5}{A_2}\right)^2 K_{1-2} \tag{6.38a}$$

$$K'_{2-3} = \text{equivalent losses for subsytem 2} = \left(\frac{P_5/P_1}{P_3/P_1}\right)^{\frac{2}{\gamma}} \left(\frac{A_5}{A_3}\right)^2 K_{2-3} \tag{6.38b}$$

$$K'_{3-4} = \text{equivalent losses for subsytem 3} = \left(\frac{P_5/P_1}{P_4/P_1}\right)^{\frac{2}{\gamma}} \left(\frac{A_5}{A_4}\right)^2 K_{3-4} \tag{6.38c}$$

$$K'_{4-5} = \text{equivalent losses for subsytem 4} = K_{4-5} \tag{6.38d}$$

The system losses can be expressed as the sum of the equivalent subsystem losses which are calculated from experimentally determined subsystem losses, obtained from flow bench testing, multiplied by pressure and area ratio factors.

6.2 PRESSURE LOSS COEFFICIENT RESULTS

The above pressure loss testing methodology was applied to the stock and modified head of the test engine. The results are provided below and discussed beginning with the experimental results obtained from the steady state flow testing, in Table 6.1.

Table 6.1: Typical experimental results from pressure loss flow testing

		Pressure for each Component			Flow Area (m^2)	Mass Flow Rate (kg/s)		
		1.2 kPa	2.5 kPa	5.0 kPa		1.2 kPa	2.5 kPa	5.0 kPa
Ambient	**P1**	97.70	97.53	97.67				
Air Filter	**P2**	79.18	73.68	62.24	0.00322	0.0270	0.0609	0.0822
Carburetor	**P3**	78.37	72.18	60.08	0.00053	0.0170	0.0255	0.0363
Manifold	**P4**	75.91	65.67	47.74	0.00078	0.0163	0.0249	0.0356
Head	**P5**	75.08	63.10	42.74	0.00080	0.0121	0.0156	0.0192

In Table 6.1, the intake pressure, flow area and mass flow rate, are provided for each system component. This data represents the flow conditions at a full operational valve lift (8.25 mm). The pressure values for each component represent the pressure at the cross sectional area of the exit.

It is important within context of this testing to maintain turbulent flow throughout the intake system. Table 6.2 expresses the calculated Reynolds numbers for each component at the three respective pressure drops.

Table 6.2: Reynolds numbers for each component from the experimental data

		Reynolds Number		
		1.2 kPa	2.5 kPa	5.0 kPa
Air Filter	N_{R1}	29,624	66,819	90,273
Carburetor	N_{R2}	45,948	68,914	97,951
Manifold	N_{R3}	36,395	55,499	79,340
Head	N_{R4}	26,497	34,257	42,293

It can be seen in Table 6.2 that the flow regimes through each component are fully turbulent. This allows for the data to be compared at fluid dynamically similar states.

Analyzing the results show that the largest losses are realized in the carburetor and the head. Both of these systems have the largest restrictions, so intuitively, the pressure drop across them should be relatively large. Below can be seen the results of the tests. First, Table 6.3 shows the results of the additive procedure in which the air filter subsystem was tested first, followed by sequentially adding the carburetor, manifold, and finally the head.

Table 6.3: Pressure loss coefficient results for the additive testing procedure

	PER COMPONENT			SYSTEM			% PER COMPONENT		
	1.2 kPa	2.5 kPa	5.0 kPa	1.2 kPa	2.5 kPa	5.0 kPa	1.2 kPa	2.5 kPa	5.0 kPa
Air Filter									
K'_{1-2}	0.01587	0.00723	0.00681	0.01587	0.00723	0.00681	**4.751**	**2.871**	**3.286**
Carburetor									
K'_{2-3}	0.07228	0.06273	0.05448	0.08815	0.06996	0.06129	**21.640**	**24.915**	**26.302**
Manifold									
K'_{3-4}	0.07706	0.06629	0.05761	0.16521	0.13624	0.11889	**23.072**	**26.329**	**27.813**
Head									
K'_{4-5}	0.16880	0.11553	0.08823	0.33401	0.25177	0.20713	**50.537**	**45.886**	**42.599**

The last three columns to the right in Table 6.3 are plotted in Figure 6.3 to better depict the contribution of each component. It can be seen that the head accounts for the largest pressure loss in the system. This is a contribution of the flow restriction due to the port, valve stem, and valve head. The carburetor and intake manifold each make up a considerable portion of the total intake system loss. The flow losses due to the air filter system are almost negligible, since it is designed to have enough capacity to feed two cylinders.

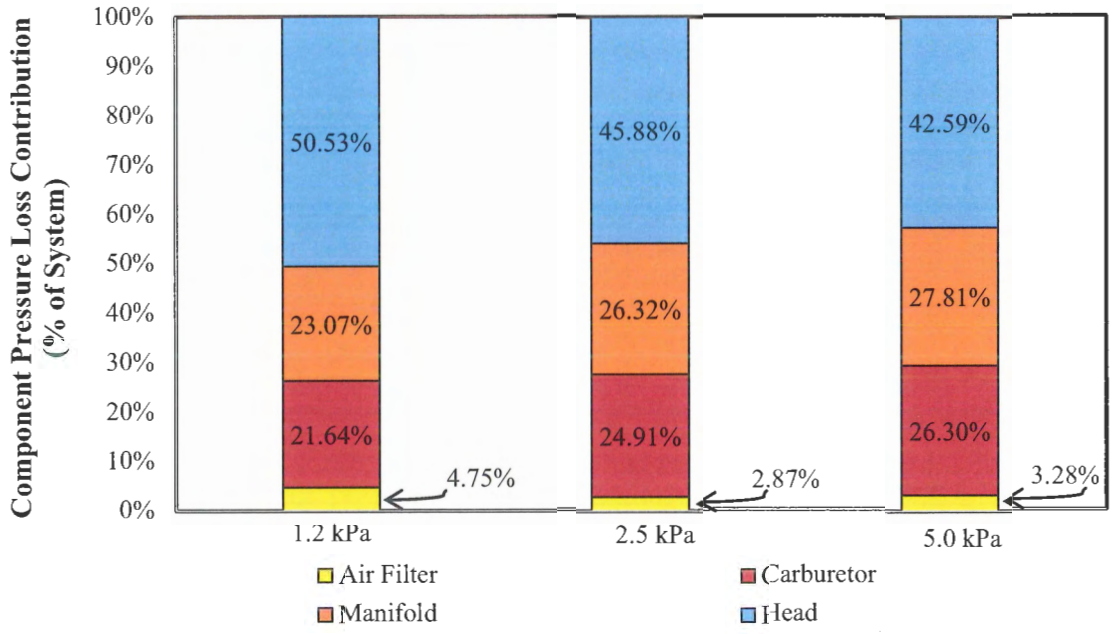

Figure 6.3: Component pressure loss contribution for the additive testing procedure

For an increasing pressure drop, the contribution of the system's pressure loss due to the head reduces and the losses due to both the intake manifold and the carburetor increase. This can be attributed to the flow conditions in each component. As the velocity of the fluid increases, the viscous losses due to skin friction increase for the carburetor and manifold. However, the pressure loss coefficient in the head decreases due to the reduction in flow separation.

After determining that the head is the largest contributor to flow loss, Figure 6.3, it was separated into its three subsystem components. Those are the port area, valve stem, and valve head. An additive test was conducted starting with the head with no valve to verify the losses due to the port. Then, the tests were run with just the valve stem, disregarding the valve head. Lastly, the whole valve assembly was used in order to observe the losses due to the valve head. The valve was held at a specific lift such that the

valve curtain area was equivalent to the cross sectional port area. Below, the results of these tests are seen in Figure 6.4 for the stock head and Figure 6.5 for the modified head with a rounded port corner.

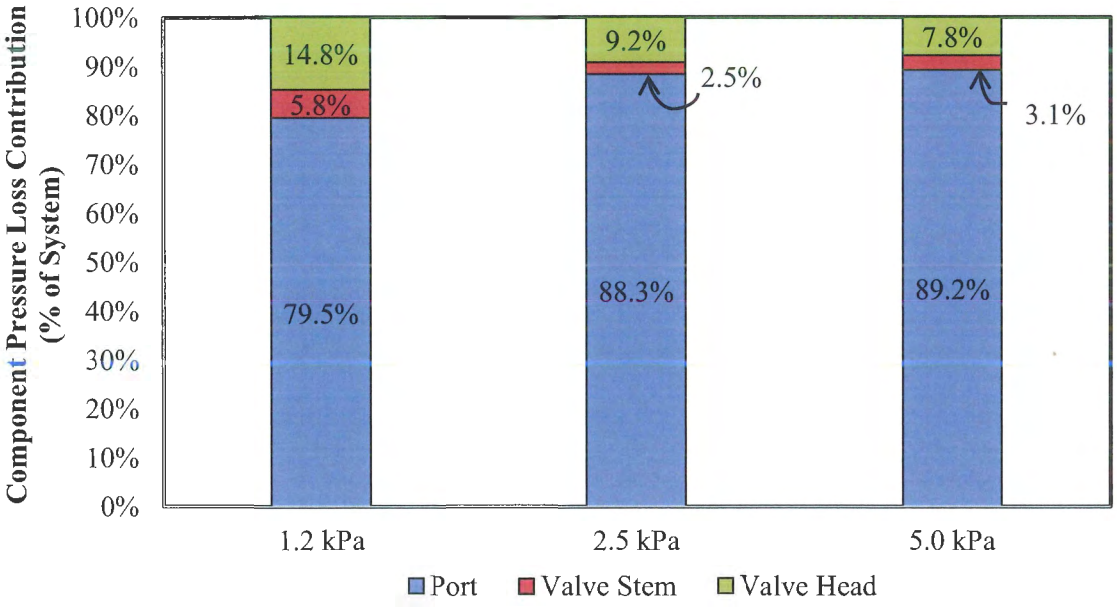

Figure 6.4: Stock cylinder head subsystem pressure loss contribution

The stock head pressure loss distribution shows that the port makes up the vast majority of flow loss in the system, 75% to 90% depending on the pressure drop. The loss due to the valve stem is negligible because it accounts for such a small area. The loss due to the valve head accounts for approximately 8-9% in medium to high flow cases. Keep in mind that these results are for a valve curtain area equal to the port cross sectional area. The loss due to the valve head will increase with lower valve lifts as it becomes the largest restriction in the system.

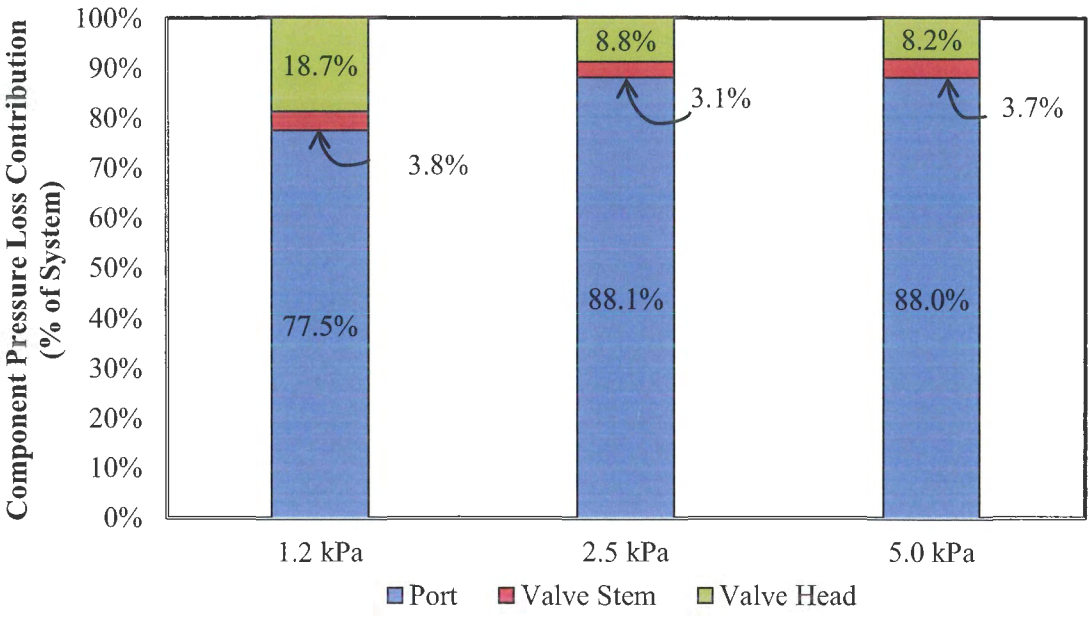

Figure 6.5: Modified cylinder head subsystem pressure loss contribution

The distribution between the stock and modified heads are similar in that the port makes up the majority of the loss contribution. The loss due to the valve stem at low flow rate increases, while the loss due to the valve head decreases. The loss due to the valve head under all conditions remains fairly constant around 8-9%. However, while the distribution of pressure loss does not change drastically, the pressure loss values between the tests differ. Below, in Table 6.4, the pressure loss values to each component can be seen and a comparison is made between the stock and modified heads.

Table 6.4: Pressure loss coefficient results for stock and modified heads

	Pressure Loss Coefficient		
Set Point	**1.2 kPa**	**2.5 kPa**	**5.0 kPa**
Stock	0.74	0.59	0.55
Modified	0.64	0.54	0.51
% Decrease	13.32	7.34	7.36

An improvement in pressure loss coefficient is seen for the modified head compared to the stock head for all pressure drops. For a pressure differential of 1.2 kPa an improvement of 13.32% is seen and an improvement of approximately 7.35% is observed for the pressure drop of both 2.5 and 5.0 kPa. The improvement seen at the low pressure drop is due to a decrease in flow separation being more prominent at this set point.

These steady state flow tests point to the head and more specifically, the port as being the largest contributor to flow loss in the system. This provides the engine designer with an area of improvement that can be used to modify an aspect of the design. That is, improvement in port flow area and removal of the sharp corner in the transition between the port and the throat.

The last two chapters have discussed different types of steady state flow tests that can be used to quantify the performance of an engine's intake system. A steady state flow bench can be a very powerful tool. It does, however, have some limitations. For example, it cannot capture the true dynamics of a working engine. The variable flow area created by the lift of the valve coupled with the motion of the piston creates large pressure fluctuations during normal engine operation. For this reason engine operation is actually a very dynamic process. It is, therefore, important to provide engine testing analysis along with the steady state flow bench analysis to obtain a more realistic view of the improvements that can be gained. Because of the variation of flow area, flow rates, and pressure differentials the improvements observed on the steady state flow bench may not completely manifest themselves during normal engine operation.

7. BASELINE ENGINE TESTING

7.1 BASELINE PRESSURE DATA

Up to this point, all experimental tests have been conducted under steady state flow conditions. While this provides a powerful tool by which to analyze the performance of intake components, it does not capture the dynamic effects of actual engine operation. The variation of valve lift and piston motion experienced under real engine testing is anything but steady. Various parameters can be captured during engine testing and performance characteristics can be determined.

Cylinder and manifold pressure data was collected using the experimental set up and testing methodology discussed in Chapter 3. The pressures from both cylinders, as well as the pressures from both manifolds, are displayed and the trends are discussed in the following sections. The pressures of the cylinder and manifold are compared between the two cylinders, as well as a comparison of the same cylinder under different operating modes for the stock engine setup.

7.1.1 Trends in Cylinder Pressure Data with Respect to Crank Angle. For this analysis, the recorded cylinder pressure data is displayed as a function of crank angle degrees (CAD). The data from both cylinders are shifted to a top dead center mark (of the compression stroke) of 360 degrees to allow for better comparisons. For Figure 7.1 the cylinder pressure is displayed on the left y-axis, intake manifold pressure is displayed on the right y-axis, and the crank angle measurement is displayed on the x-axis ranging from 0 to 720 degrees (representing four strokes or two complete cycles).

In comparing the two cylinders, it can be seen that the pressure begins to deviate during the compression stroke, before ignition of the fuel and air mixture. After the combustion process initiates, it can be observed in Figure 7.1 that the peak cylinder pressure for cylinder 2 is 800 kPa higher than the peak cylinder pressure of cylinder 1. This trend remains present for all modes at lower magnitudes. The figures comparing the other four high speed modes can be found in Appendix A. For mode 6 (idle condition), Figure 7.2, the shape of the pressure curves differ significantly. Generally, the peak pressure in each cylinder will affect its overall power output.

A second trend is that the pressure for intake manifold 2 is a few kPa lower than the pressure for intake manifold 1 around peak piston speed (90 degrees before BDC of the intake stroke) and leading up to the IVC event. The pressure in manifold 2 stays below the pressure in manifold 1, but both cylinders reach the same pressure after the IVC event as manifold 2 takes marginally longer to fill. Each manifold experiences different dynamic effects during manifold filling (the time between IVC and IVO).

The variations between the pressure for cylinder 1 and cylinder 2 and the pressure of intake manifold 1 and intake manifold 2 speaks to a variation in the dynamic effects between the cylinders of the engine. That is, each cylinder experiences different charge density which plays a role in determining the amount of air and fuel introduced to each cylinder. With the amount of charge differing in each cylinder the energy characteristics of each cylinder will change, and thus, the overall output of each cylinder and ultimately the engine.

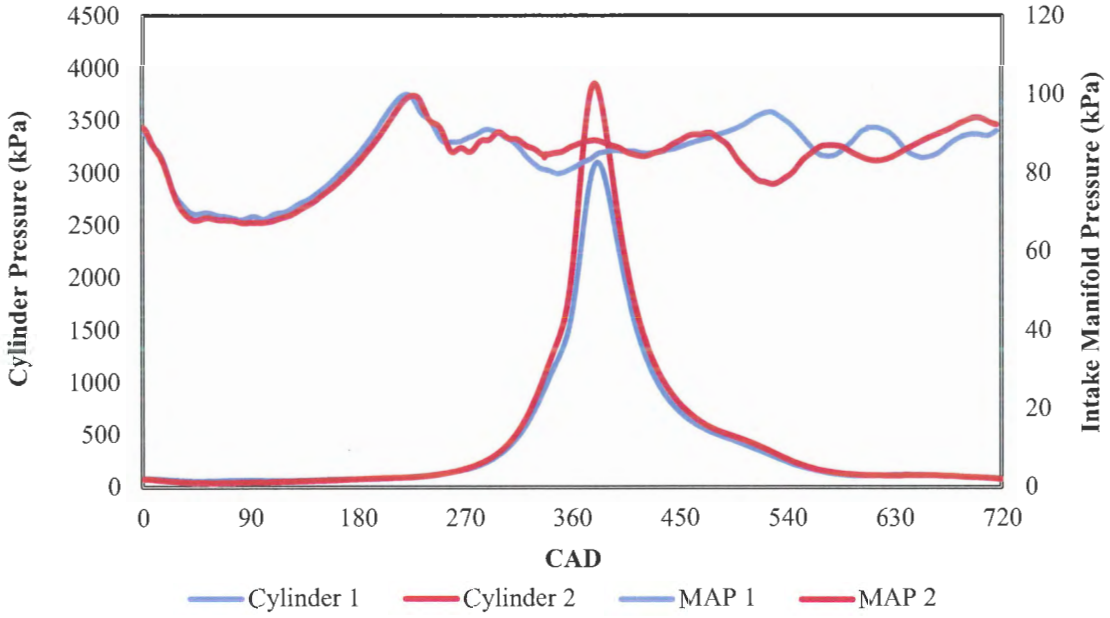

Figure 7.1: Cylinder and intake manifold pressure comparison for mode 1 operation

The idle condition of the test engine can be observed in Figure 7.2. The exhaust and intake pressure match well between the two cylinders. The peak pressure and the pressure during the expansion process are much lower for cylinder 1 than for that of cylinder 2. The pressure in both manifolds match well for the beginning of the induction stroke. However, unlike the first five modes, intake manifold 1 pressure is lower than intake manifold 2 during the end of the induction stroke and throughout the manifold filling process. For the idle condition, the manifold filling is slow and the pressure does not fully recover before the next cycle. This can be observed by the quick pressure rise in the manifold, close to TDC of the exhaust stroke, after an almost linear draw up. This sudden rise in intake manifold pressure is due to the intake valve opening event, where the pressure in the cylinder is greater than that of the manifold. This creates a vacuum between the intake manifold, the cylinder, and ultimately the exhaust manifold. This

pressure differential between the manifolds and cylinder causes exhaust gas residuals (exhaust gases remaining from the exhaust stroke) to dilute the fresh charge that is waiting in the intake manifold. Recall that the intake valve opens before and the exhaust valve closes after TDC of the exhaust stroke (this is the valve overlap period).

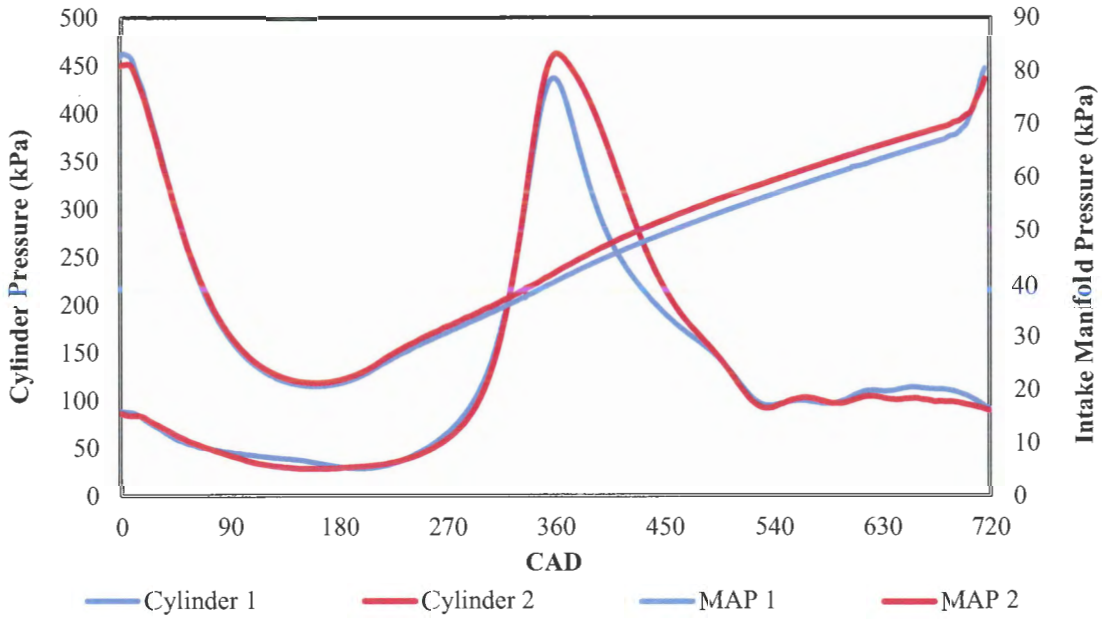

Figure 7.2: Cylinder and intake manifold pressure comparison for mode 6 operation

A comparison of all six modes for cylinder 1 can be seen in Figure 7.3, which depicts an overall view of the cylinder pressure. The variation in the peak pressure between the six modes becomes apparent when compared to one another. The cylinder pressure decreases drastically with a decrease in load, resulting in a lower engine power output (i.e. the effects of throttling).

The gas exchange process is shown with greater detail in Figure 7.4. The reduction in the intake pressure with respect to mode due to throttling can be noticed; as

the engine load is decreased the engine becomes more throttled, increasing the pressure drop in the cylinder. The difference in expansion pressure can also be seen, as well as the effectiveness of the blowdown process. The cylinder pressure decreases with the mode for the expansion process due to lower peak pressures in the cylinder during the combustion event. The effectiveness of the blowdown process has an influence on the amount of work the piston has to exert in order to expel the burned cylinder gases during the exhaust stoke. The exhaust pressure for mode 1 is higher than that for the subsequent modes. However, the exhaust pressures for mode 2 through mode 6 are very similar. The cylinder pressure for all modes approach the same pressure during the time of the valve overlap period; that is the time between when intake valve opens and the exhaust valve closes.

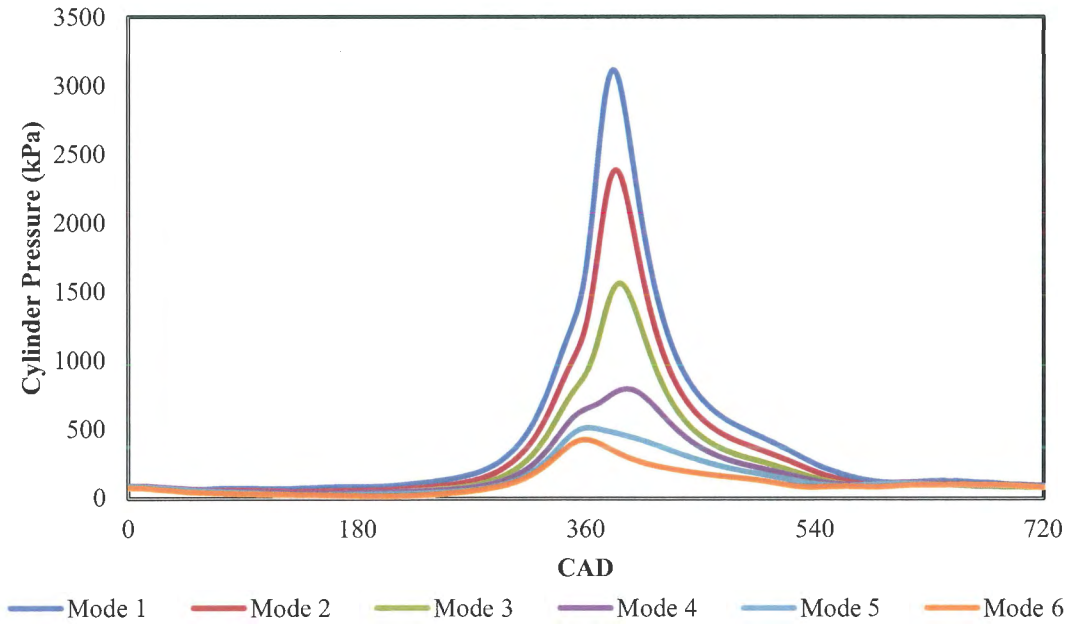

Figure 7.3: Compilation of cylinder pressure for all 6 modes of cylinder 1

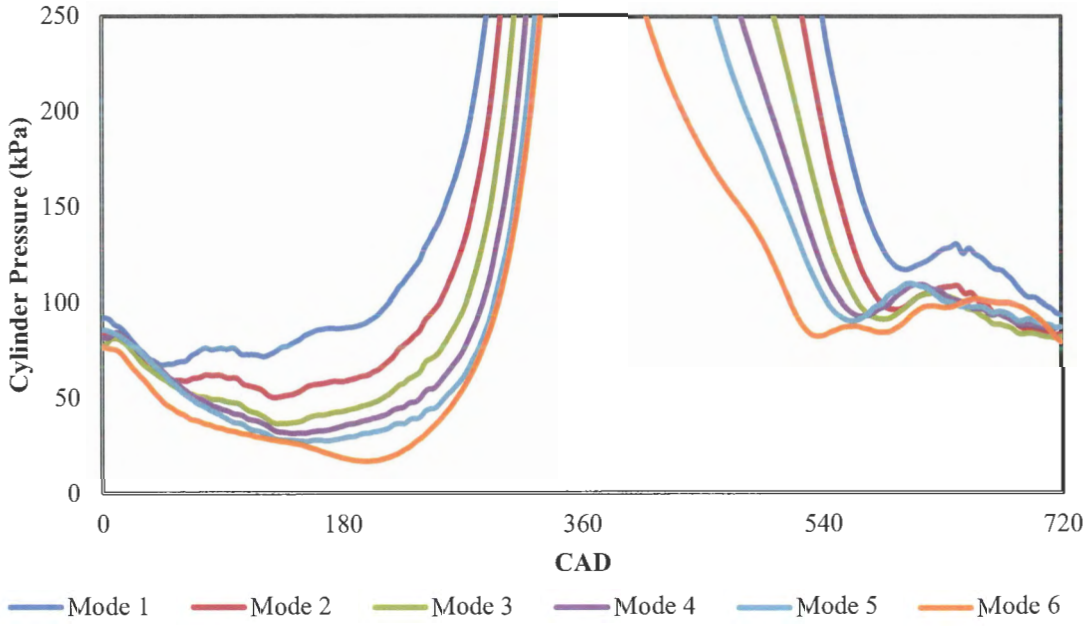

Figure 7.4: Gas exchange processes for all 6 modes of cylinder 1

The pressure of intake manifold 1 can be seen in Figure 7.5 for all six modes. A similar effect to that of the cylinder pressure can be observed at top dead center of the intake stroke (720°), that is the manifold pressures of the first 5 modes converge to the same value. This is presented to reinforce the fact that the load placed on an engine causes a great change to the intake dynamics that are experienced. The effect of throttling can be seen in the reduction of intake manifold pressure during the intake stroke. The effect of engine load on manifold filling can also be observed. For low load set points, the manifold takes longer to fill even while running at the same speed set points. The pressure variations in the manifold are present for modes 1 and 2, after that the fluctuations become minimal. The amplitude of the pressure fluctuations are a function of both engine speed and engine load.

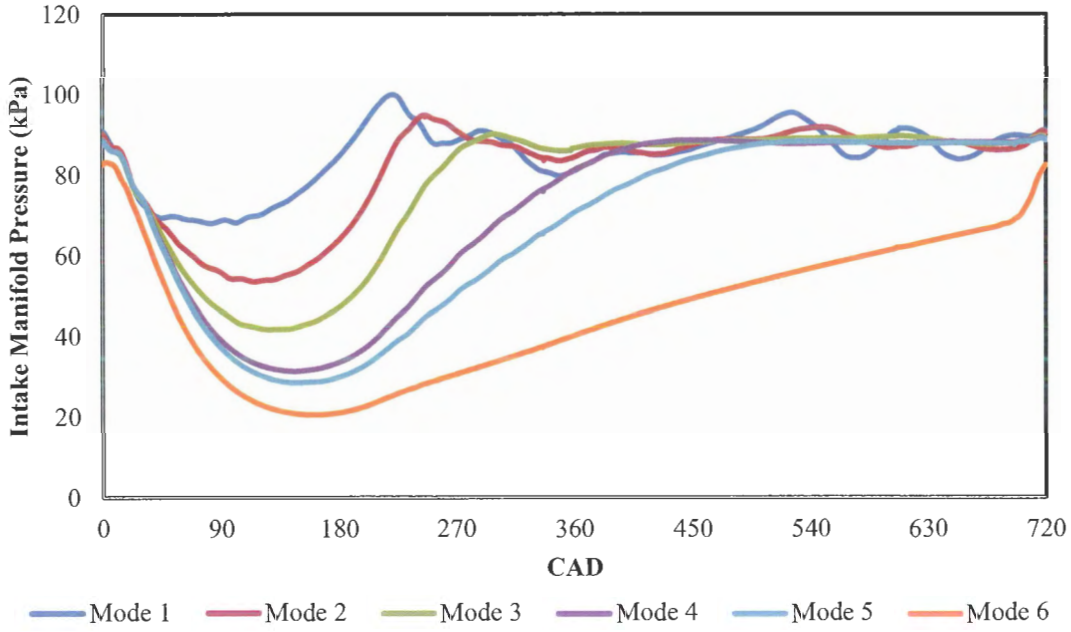

Figure 7.5: Compilation of manifold pressure for all 6 modes of cylinder 1

Some points about the different manifold dynamics between operating modes can be made. Again, the manifold filling dynamics differ between mode 1 and mode 2; the pressure variations of mode 2 are much less than those of mode 1. A pressure rise in manifold 1 can be seen at TDC of the induction stroke to match the first four modes; cylinder 2 does not realize the same effect. Similar to the other high speed set points, this pressure increase represents a back flow out of the cylinder and into the intake manifold during the valve overlap period.

The same series of figures can be seen below for the processes of cylinder 2. Figure 7.6 provides a look at the cylinder pressure of all six modes for cylinder 2 of the test engine, while Figure 7.7 depicts the gas exchange processes. The intake manifold pressures can be observed in Figure 7.8 for the six mode test procedure.

The trends in peak pressure for cylinder 2 remain similar to that of cylinder 1 with the exception of having a higher peak pressure, as can be observed in Figure 7.6 in a comparison of mode 1. Another difference occurs in the gas exchange process which can be seen in Figure 7.7. For cylinder 2, the pressure dips lower than that of cylinder 1 during the intake stroke and at the end of the expansion stroke (particularly for mode 1 and mode 2), close to the occurrence of peak piston speed. The trend in the pressure during the expansion process remains similar between the two cylinders, as well as the effectiveness of the blowdown process. A similar pressure rise is seen in both cylinders during the middle of the exhaust stroke. This correlates to the piston being required to exert additional work to expel the exhaust gases. The variation in exhaust pressure between modes in cylinder 2 is slightly greater than the variations experienced by cylinder 1.

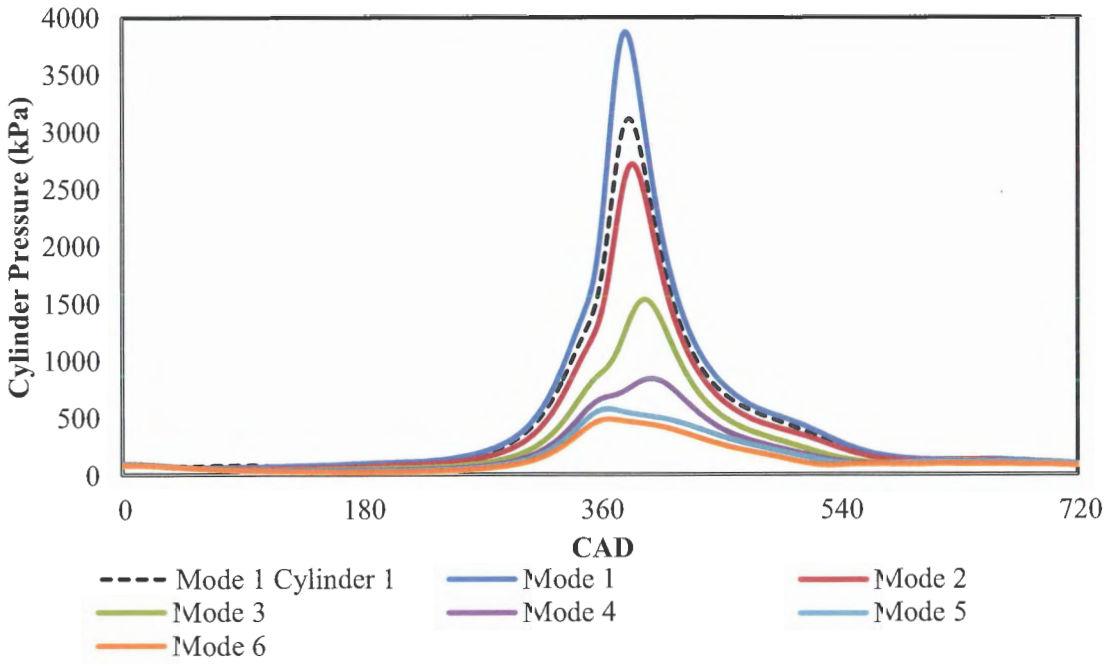

Figure 7.6: Compilation of cylinder pressure for all 6 modes of cylinder 2

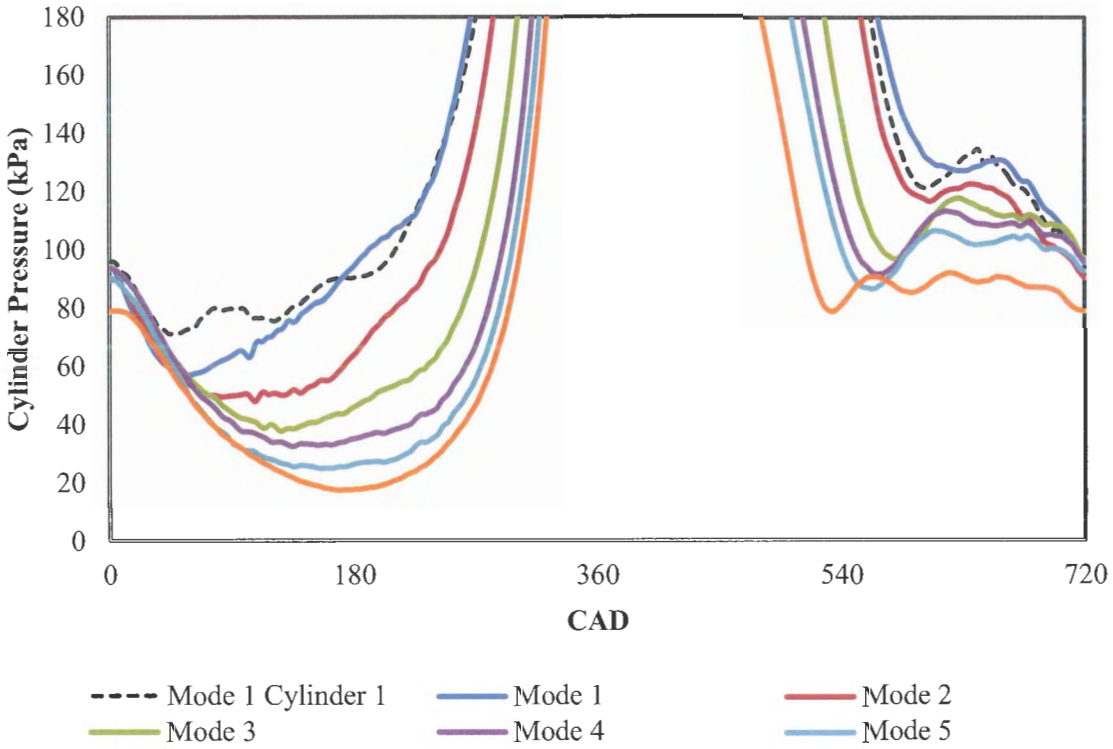

Figure 7.7: Gas exchange processes for all 6 modes of cylinder 2

The compilation of manifold 2 pressures can be seen in Figure 7.8 for all six modes. Manifold 2 undergoes similar trends as that of manifold 1; the effect of throttling can be seen as the minimum intake pressure decreases with mode and the time the manifold takes to fill increases with mode as air flow into the intake manifold becomes more restricted. It can be seen in the intake manifold of cylinder 2, similar to the intake manifold of cylinder 1, that the intake pressure at mode 6 operation never fully recovers to ambient conditions as the previous 5 modes do. By improving flow conditions within the engine, the pressure drop in the intake manifolds would ideally be reduced. Thus, energy required by the engine to induct fresh charge would be reduced.

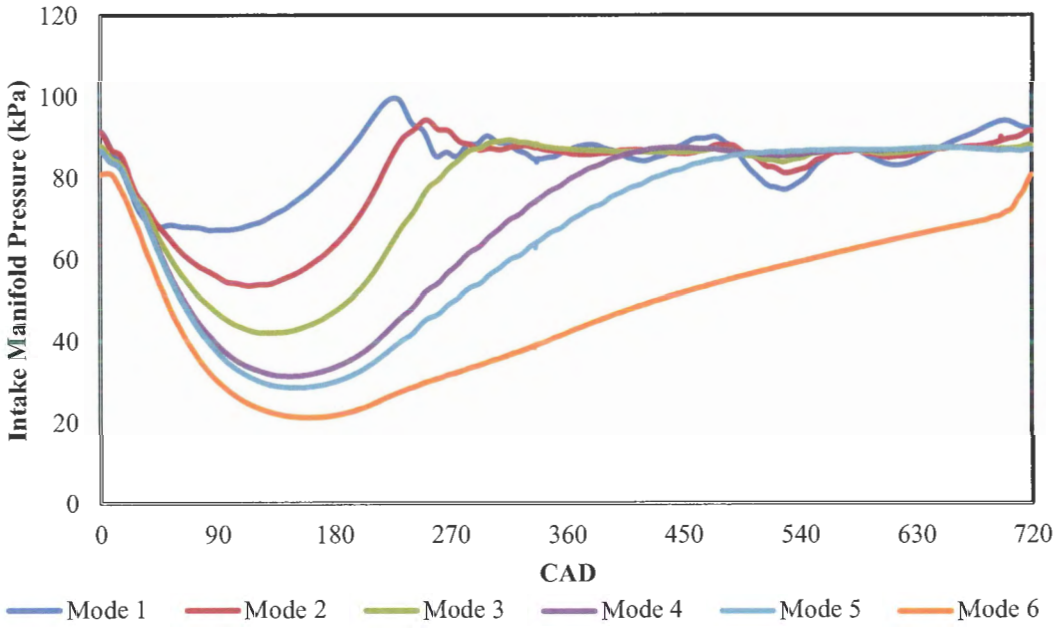

Figure 7.8: Compilation of intake manifold pressure for all 6 modes of cylinder 2

7.1.2 Trends in Cylinder Pressure Data with Respect to Cylinder Volume.

A common way of calculating engine performance parameters, such as mean effective pressure (mep), is through the use of cylinder pressure as a function of cylinder volume. The pumping loops for both cylinder 1 and cylinder 2 are shown below for all six modes, as well as a motored test which was collected by means of a motoring dynamometer used in a parallel study by Singh et al. [19]. Both cylinders are overlaid on the same plot so the discrepancies can be seen.

It can be observed in Figure 7.9, mode 1, that the pressures in both cylinders are very similar at bottom dead center of the induction stroke. But as discussed earlier, the pressure in manifold 2 is slightly lower than that of manifold 1 at BDC; this is evident on the plots of pressure versus volume. The pressures in both cylinders match reasonably well during the expansion stroke even with the difference in peak cylinder pressure being

evident. As previously described, the pressure during the compression and exhaust strokes do differ between the two cylinders.

Both cylinders experience a decrease in pressure towards the end of the exhaust stroke as the intake valve opens, particularly for modes 1 and 2. The pressure differential between the intake manifold and cylinder has the effect of minimizing the amount of exhaust gas residuals, preventing them from diluting the fresh cylinder charge.

The effects of intake valve closing cannot easily be seen on a pressure-volume trace due to the fact that back flow out of the cylinder into the intake manifold is the key loss for this particular event. Turning focus to the exhaust valve opening event it can be noted again that both cylinders are very similar during the blowdown process. The purpose of the exhaust valve open timing is to allow the blowdown process to assist in equalizing cylinder pressure and exhaust manifold pressure before bottom dead center of the expansion stroke. If the cylinder pressure is much above exhaust manifold pressure the piston has to provide additional work to expel the burned cylinder gases, causing an increase in pumping work. During mode 1 operation, Figure 7.9, the cylinder pressure around bottom dead center of the expansion stroke is well above exhaust pressure for both cylinders. A similar effect is seen during mode 2, Figure 7.10; however, to a lesser degree. An improvement is seen for mode 3, mode 4, and mode 5 (Figure 7.11, 7.12, and 7.13), for the high speed operating conditions, where the cylinder pressure dips to the exhaust pressure around bottom dead center. There is, however, a slight pressure bulge a quarter of the way through the exhaust stroke for these low load modes. Under mode 6 operation, Figure 7.14, the cylinder pressure dips below the exhaust manifold pressure

before bottom dead center of the expansion stroke and experiences a pressure rise after the piston begins the exhaust stroke.

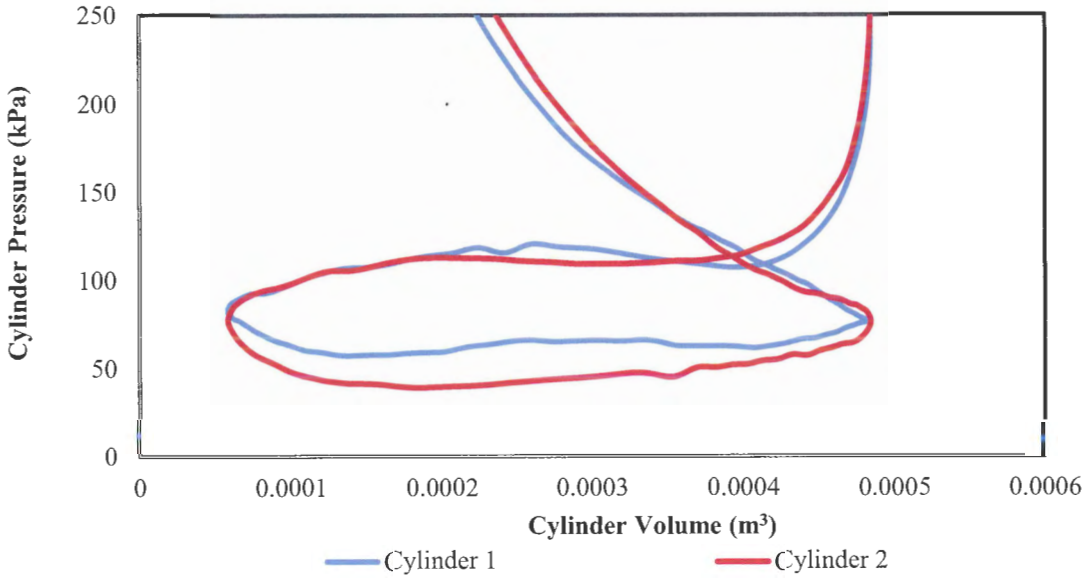

Figure 7.9: Mode 1 pumping loop for cylinder 1 and cylinder 2

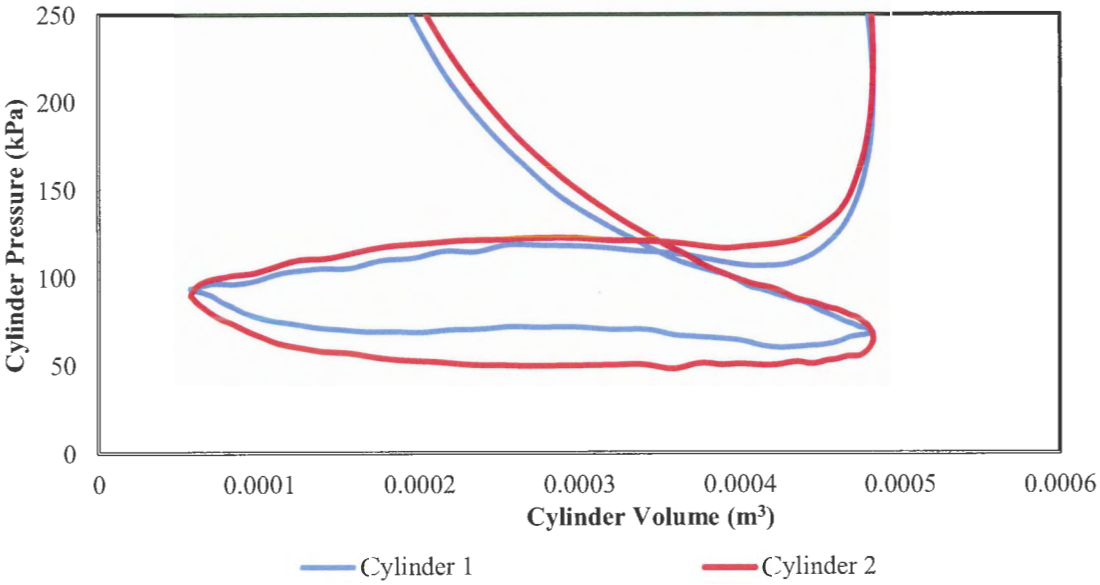

Figure 7.10: Mode 2 pumping loop for cylinder 1 and cylinder 2

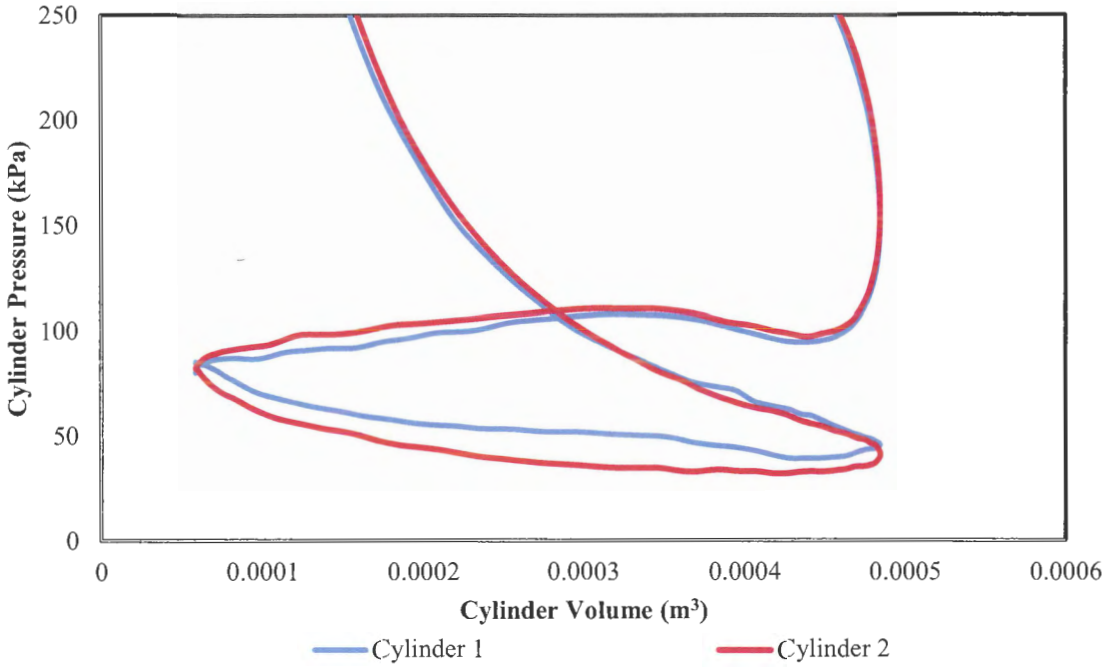

Figure 7.11: Mode 3 pumping loop for cylinder 1 and cylinder 2

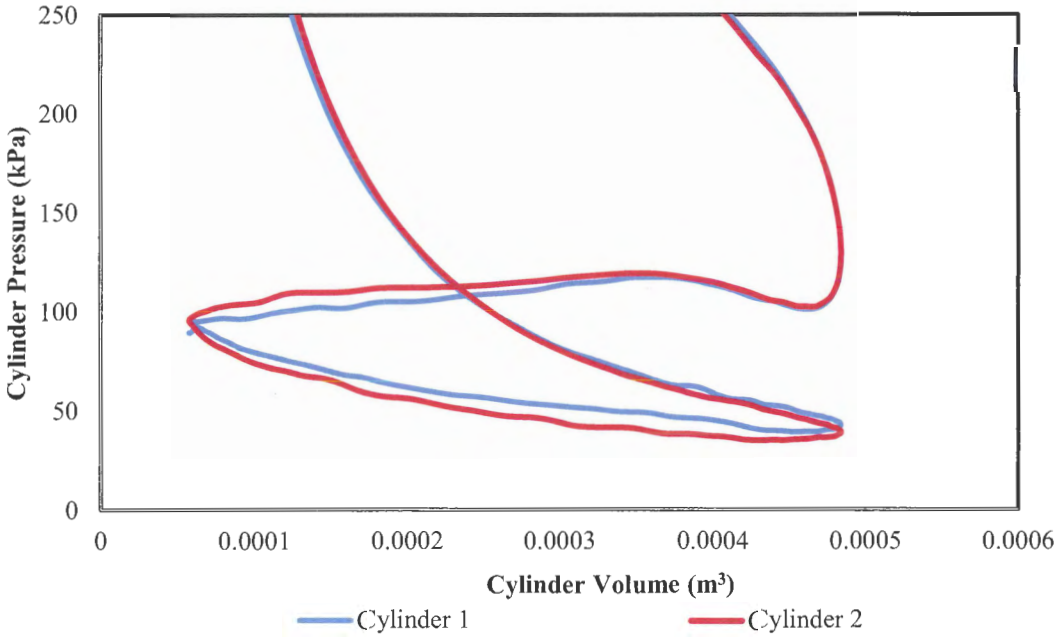

Figure 7.12: Mode 4 pumping loop for cylinder 1 and cylinder 2

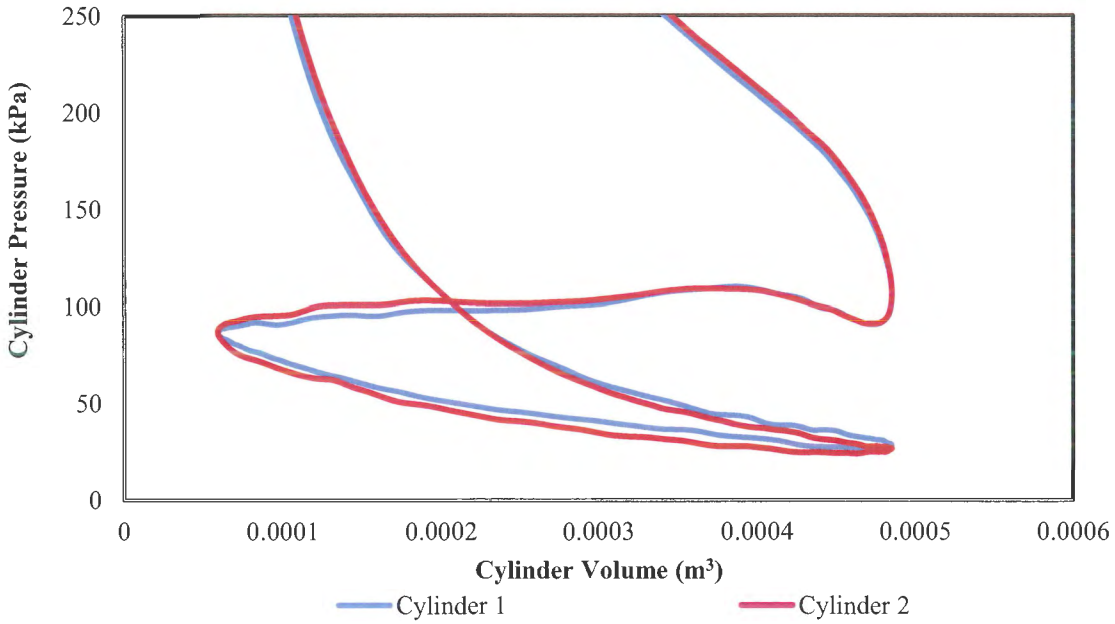

Figure 7.13: Mode 5 pumping loop for cylinder 1 and cylinder 2

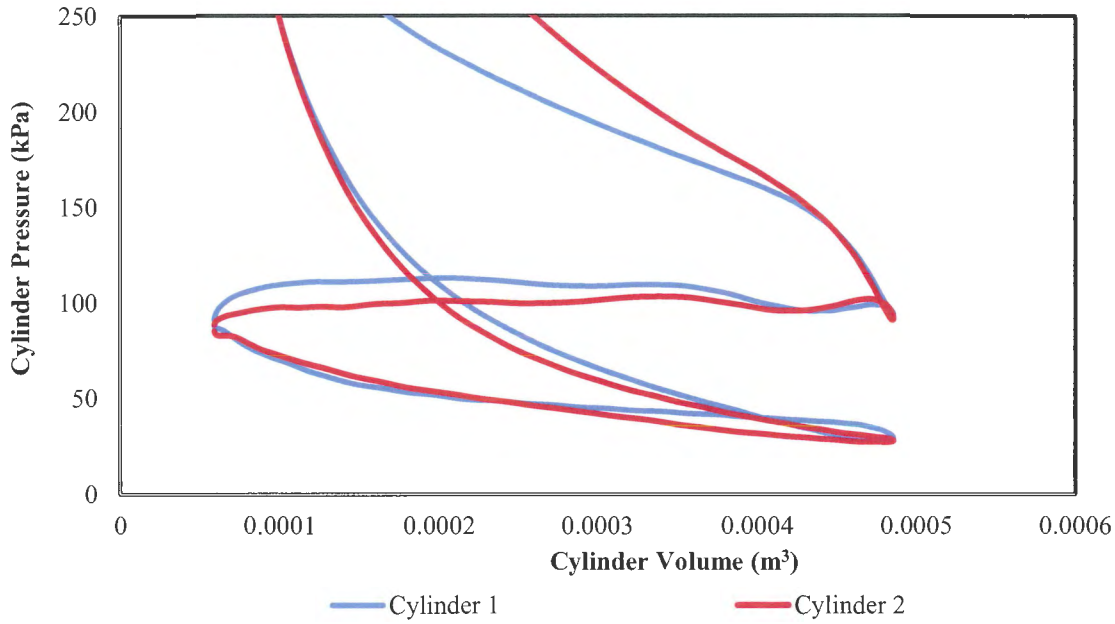

Figure 7.14: Mode 6 pumping loop for cylinder 1 and cylinder 2

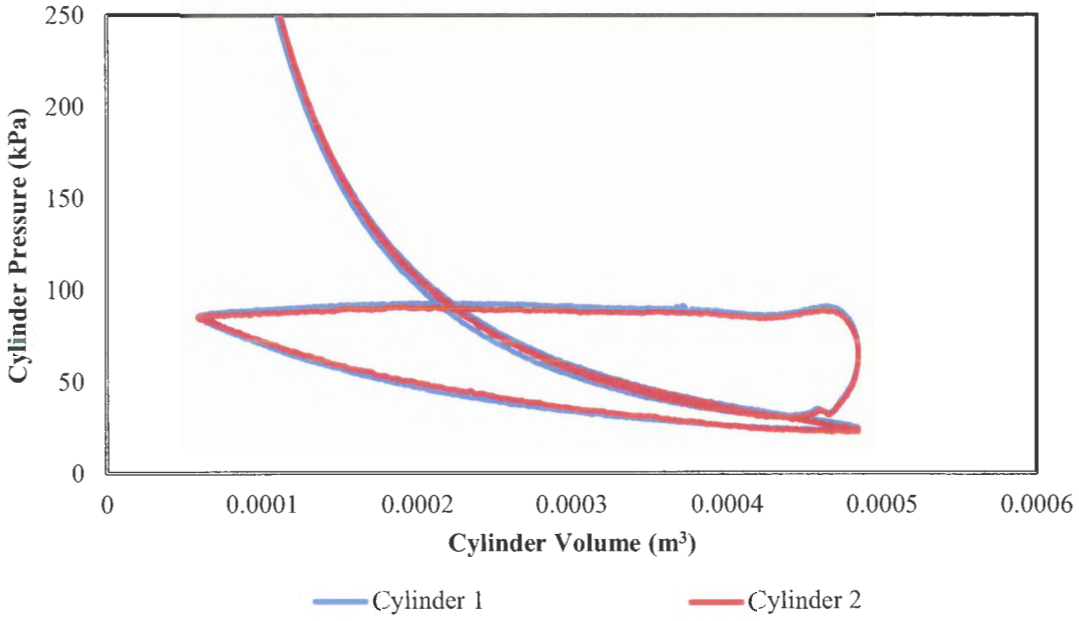

Figure 7.15: Motored pumping loop for cylinder 1 and cylinder 2

The pressure for cylinder 2 during the induction stroke dips below that of cylinder 1 for modes 1 through 5 (high speed engine operation). Since the cylinders, valve timings, and valve lifts are identical, the pumping loops should be similar as seen in the motored engine test case, Figure 7.15. However, a large difference can be seen in the pressure during the intake stroke of cylinder 2 compared to that of cylinder 1, particularly for modes 1,2, 3, and 4. The intake pressures are more similar between the two cylinders for mode 5 and mode 6. Again, the pressures in both cylinders agree very well for the motored engine data. Since this discrepancy occurs only for fired and high speed tests, it seems to point to the phasing of the cylinders and the differences between the two intake manifolds as the primary sources of inconsistency between the pumping loops.

7.2 MEAN EFFECTIVE PRESSURE ANALYSIS

Pressure data for the gas in the cylinder over the operating cycle of the engine can be used to calculate the work transfer from the gas to the piston [10]. The indicated work is calculated as the integral of the cylinder pressure with respect to cylinder volume to give the enclosed volume of a P-V diagram. The term is normalized by cylinder displacement volume and represented as a mean effective pressure (mep), expressed in kPa. This allows for the comparison of mean effective pressures across a variety of engines. The mean effective pressure is calculated as shown in Equation 7.1:

$$\text{mep} = \frac{1}{V_d} \int P_{cylinder} dV \tag{7.1}$$

where the bounds of integration are the dependent on the definition being used.

The mean effective pressure term can be tied to several different measures. There is the brake mean effective pressure, bmep, which is a function of the total work output of the engine as recorded by the dynamometer. The indicated mean effective pressure, imep, is used to calculate the work transfer between the cylinder gases and the piston and does not include the frictional effects that are associated with bmep. The pumping mean effective pressure is used to measure the work required to exhaust the burned charge from the previous cycle and induct the fresh charge of the current cycle. Lastly, frictional mean effective pressure, fmep, accounts for the frictional losses of the engine and is usually defined by the difference of bmep and imep.

There are two common definitions used when presenting imep values. The first is the gross indicated mean effective pressure; this is the work delivered to the piston over the compression and expansion strokes. The second definition is the net indicated mean effective pressure; this is the work delivered to the piston over all four strokes of the

engine cycle. Another way to consider net imep is by the addition of pumping mean effective pressure to gross indicated mean effective pressure.

Pumping mean effective pressure is the work delivered to the piston over the exhaust and induction strokes of an engine. Due to the pressure during the exhaust stoke being higher than the pressure during the intake stroke, the pumping work is calculated as a negative number indicating that the piston is providing work to the cylinder gases (this is considered a loss to the engine). The deeper the pressure dip during the intake stroke or greater the pressure bulge during the exhaust stoke, then the larger will be the enclosed area of the pumping loop and more work will be required of the engine. This creation of work relates to an increase of fuel consumption and a decrease in operating efficiency. In Figure 7.16 below, can be seen a culmination of the calculated pumping work for all six modes for both cylinders during a full six mode baseline test.

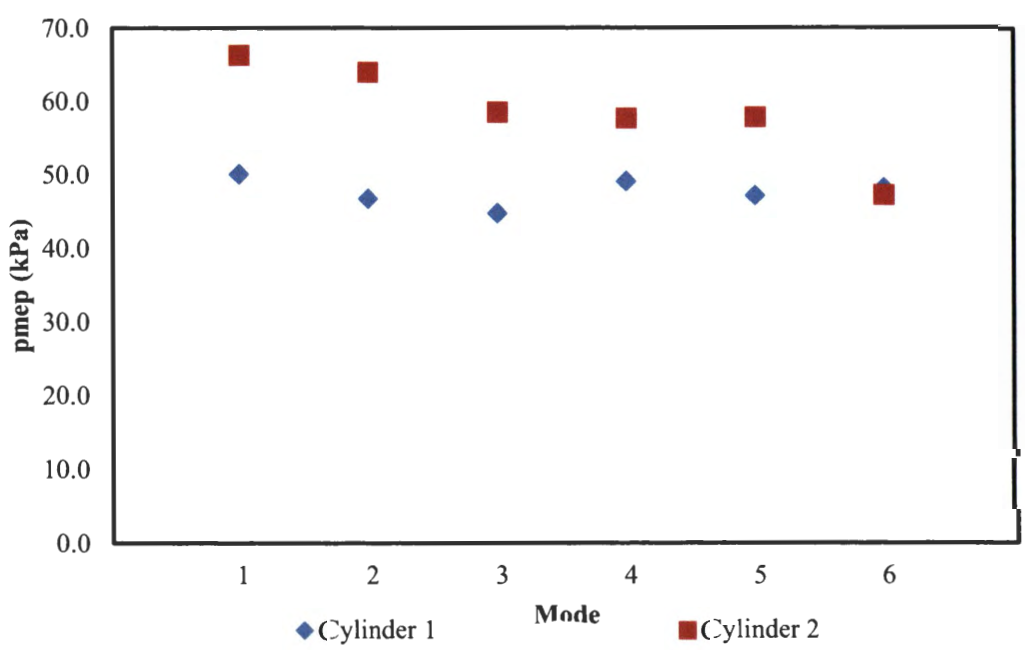

Figure 7.16: Pumping work values for cylinder 1 and cylinder 2; modes 1-6

The results displayed above are typical for the test engine. The pumping work of cylinder 2 is generally much larger in magnitude for mode 1 through mode 5 than that of cylinder 1. For both cylinders, the pumping work of mode 6 is very similar in magnitude; however, they differ slightly in the shape of the pressure trace.

Table 7.1 contains the calculated pumping, gross indicated, and net indicated mean effective pressures for two data sets. The gross indicated work is larger for cylinder 2 than cylinder 1, which is an artifact of the difference in peak pressure between the two cylinders. The net indicated mean effective pressure, highlighted in yellow, is summation of the work done between the piston and the cylinder gases for all four strokes. By either reducing pmep or increasing gross imep, the overall work output of the engine can be increased.

Table 7.1: Mode 1 mean effective pressures for both cylinders of two data sets

	Mean Effective Pressure (kPa)					
TEST	**$PMEP_1$**	**$PMEP_2$**	**$IMEP_{g1}$**	**$IMEP_{g2}$**	**$IMEP_{n1}$**	**$IMEP_{n2}$**
1	50.2	66.3	670.2	710.3	620.0	644.0
2	51.2	66.9	690.8	723.5	639.6	656.6

7.3 CRANKSHAFT ACCELERATION

As discussed in section 4, the connecting rods of small V-Twin engines generally share the same journal bearing on the engine's crankshaft. This provides a point where the two cylinders can have a direct effect on one another, thereby altering the performance of one cylinder with respect to the other. The purpose of this test is to find out the time it takes for each cylinder to complete its induction stroke, in the expectation

that it provide some insight on why the pumping loops of the two cylinders are so dramatically different at high load set points.

In order to perform this reduction, engine data was taken both with respect to time and with respect to crank angle degrees. An internal clock on the data acquisition system was used to collect the time series data. A trigger was used to ensure the simultaneous collection of both sets of data to allow for direct comparison between the two methods. This process allows for the evaluation of crank angle degrees with respect to time in order to determine the speed at which the engine goes through each process.

Due to the phasing of the two cylinders, the time it takes for each to complete its respective induction stroke differs. The process of one cylinder with respect to the other, therefore, must be considered. The time for each cylinder to complete its induction stroke (TDC-BDC) can be observed below in Table 7.2. The time difference between the two cylinders becomes negligible after mode 4, thus the comparisons are not included. For mode 1, cylinder 2 completes its induction stroke 0.13 ms quicker than cylinder 1 . This can affect the pressure drop across the valve and increase the amount of fresh charge pulled into the cylinder (i.e. an increase in charge density). Ultimately, this difference in charge density will have an effect on the energy output of each cylinder.

Table 7.2: Time of induction process of both cylinders

	Time of Induction Process (ms)				
	Cylinder 1		Cylinder 2		
	time	dθ/dt	time	dθ/dt	Δt
Mode 1	5.39	33.40	5.26	34.22	0.13
Mode 2	5.38	33.46	5.26	34.22	0.12
Mode 3	5.37	33.52	5.07	35.50	0.30
Mode 4	5.29	34.03	5.25	34.29	0.04

Specifically, the concern is the particular processes that each cylinder is experiencing with respect to the other. Refer to Figure 4.4 to visually supplement the description of cylinder phasing. The idea being that cylinder 1 is assisting cylinder 2 during its induction stroke due to the fact that cylinder 1 is undergoing its compression, combustion, and expansion processes. However, while cylinder 1 is undergoing its induction process, cylinder 2 is completing the expansion stroke and beginning the exhaust stroke. That is, for the induction stroke of cylinder 1 the piston is, naturally, descending while cylinder 2 is also descending through its expansion stroke and begins to ascend into the exhaust stroke (both of these processes provide no energy to the piston and crankshaft assembly). Simply put, the piston in cylinder 1 is moving in the same direction as the piston in cylinder 2 for the majority of the induction stroke with no energy being added to the system. However, the induction process of cylinder 2 is different. While piston 2 is descending during the induction stroke, piston 1 is returning to TDC of the compression stroke, initiating combustion, and proceeding into the expansion process. The piston travel of cylinder 1 and cylinder 2 are in opposite directions during the induction stroke of cylinder 2. Cylinder 1 also has the added energy of combustion to help assist the rotation of the crankshaft.

7.4 COMPARISON OF THE STOCK AND MODIFIED HEADS FOR BASELINE PRESSURE TESTING

The modified heads, as discussed in Chapter 5 and Chapter 6 were installed on the test engine and a 6-Mode baseline test was conducted. It was predicted by both sets of steady state flow bench tests that there should be an improvement in mass flow rate of air for the modified heads. Table 7.3 depicts the results from the modified head baseline engine tests.

Table 7.3: Test engine air mass flow rate comparison of stock and modified heads

	Engine Air Mass Flow Rate (kg/s)					
Mode	1	2	3	4	5	6
Modified Heads	0.0205	0.0169	0.0133	0.0103	0.0085	0.0042
Stock Heads	0.0204	0.0168	0.0131	0.0098	0.0081	0.0040
% Increase	0.5%	0.6%	1.5%	4.9%	4.1%	4.8%

However, it can be seen that the engine does not see any appreciable mass flow rate increase for the high speed and high load set points. Not until mode 4 operation does the flow rate of intake air increase enough to be noticeable. This fortifies the closing statements of Chapter 6 in that the steady state flow bench cannot truly capture the dynamic characteristics of the engine. The lack of improvement in air flow points to the timing of intake valves as a key dynamic restriction in the intake system. That is, the timing of the valves does not allow the flow improvements made to the port to manifest itself under normal engine operation. Optimizing the timing of the intake valves should allow the improvements made to the port to be more effectively utilized.

8. STAGING OF THE TEST ENGINE'S CAMSHAFT

8.1 CAMSHAFT STAGING

By staging the camshaft, insight can be gained on the effects of various valve timings on engine operation. As discussed earlier, the ideal valve events differ between operating modes. That is, the ideal valve timings for a high speed full load set point are different than the ideal valve timings for a low speed low load set point. The small engines market is made up almost entirely of fixed valve timing engines. Therefore, the selection of those valve timings is vitally important to efficient engine operation at critical set points.

For these tests the camshaft will be staged incrementally four different ways. The order in which the tests are conducted is as follows: 10 crank angle degrees advanced, 5 crank angle degrees advanced, 5 crank angle degrees retarded, and 10 crank angle degrees retarded. These four tests will be compared to the stock 6-Mode baseline data discussed in Chapter 7.

8.1.1 Camshaft Staging Experimental Procedure. The test engine uses a single camshaft with fixed valve timings. There are four lobes (two intake valves and two exhaust valves) used to move the push rods which in turn control the valves. In order to test alternate valve timing events the cam must be staged, that is all valve timings must be advanced or retarded the same amount to experiment with a single timing. This can obscure the results slightly since all four valve events are moving, but by zeroing in on the area around the specific events some deductions can be made. Since cutting new

camshafts for experimental purposes is costly and tedious, staging is a relatively quick way to determine if any improvements can be achieved.

In order to stage the camshaft the engine case must be separated. This was achieved by disassembling the test stand setup described in Chapter 3 of this work. Once the engine was separated from the dynamometer apparatus and the case was split, the push rods were removed and the camshaft was staged. The internal components of the test engine can be seen in Figure 8.1. The camshaft is operated by a large gear that rotates by synchronizing with the crankshaft of the engine. The camshaft gear has twice the number of teeth as that of the crankshaft gear and therefore, makes one rotation for every two rotations the crankshaft makes.

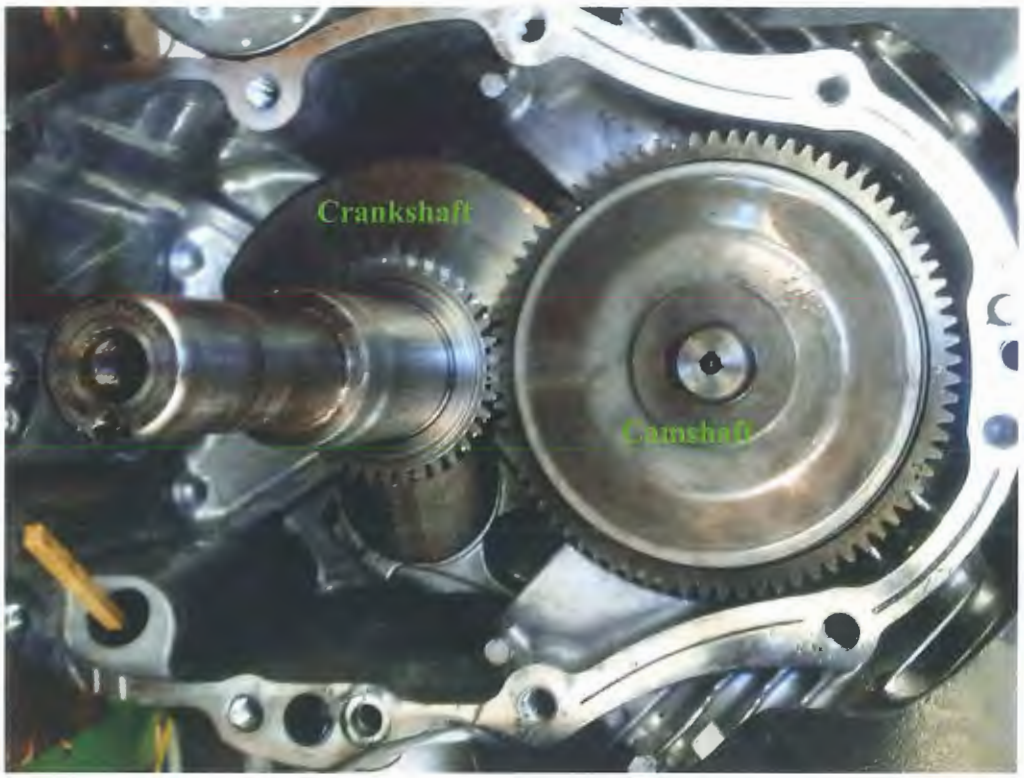

Figure 8.1: Internal configuration of the test engine

A punch mark located on a tooth of the crankshaft gear syncs up with a punch mark located between two gear teeth on the camshaft. When these two punch marks are at the same location it signifies the stock camshaft setting. The camshaft was removed and rotated counter clockwise the appropriate distance, with respect to the punch mark on the crankshaft, to advance the timing and rotated clockwise the appropriate distance to retard the timing. Another way to conceptualize this is when the camshaft is advanced the valve timings are occurring earlier than those of the stock setting when the camshaft is advanced the valve events are occurring later than the stock timings.

The engine stand was reassembled including all appropriate instrumentation. Several 6-Mode tests were conducted for each camshaft location to ensure the data acquisition system was working properly after being reassembled.

8.2 EXPERIMENTAL RESULTS AND ANALYSIS

As mentioned in the previous section, a 6-Mode testing procedure was used to collect the data for this set of experiments. The data in this section will be discussed in a similar way to that of the baseline data where particular trends will be emphasized.

8.2.1 Comparison of Cylinder Pressure Trends for the Staged Camshaft.

Below are a series of figures comparing the pressure of each cylinder and each operating mode to each camshaft staging test. First, cylinder pressure plotted as a function of cylinder volume will be presented, beginning with all six modes from cylinder 1.

In Figure 8.2 can be seen the results from the four camshaft staging tests and the stock baseline data for cylinder 1 mode 1. The effects of the exhaust valve opening event can be immediately seen. By advancing the valve timing, it is occurring earlier in the expansion process further away from the start of the exhaust stroke. This allows more

time for the cylinder pressure to equalize with the pressure of the exhaust manifold. By doing this, the piston is required to exert less energy during the exhaust stroke because it no longer has to overcome a pressure differential between the cylinder and the exhaust manifold. However, by opening the exhaust valve earlier, the thermal efficiency of the engine decreases drastically, as it has an effect on the expansion ratio. Losses due to thermal efficiency have a direct impact on imep and torque. Asmus [3] states that the rate at which efficiency is lost to early EVO is in the range of 0.12% per degree. Advancing this timing too far, while improving the pumping work of the engine, is not desirable when designing for overall engine efficiency. The loss in thermal efficiency due to early EVO was observed to be 0.10% per degree for the stock timing and closer to 0.13% per degree for the advanced timing.

Conversely, retarding the valve timing (i.e. moving it further into the expansion stroke and closer to the beginning of the exhaust stroke) keeps the pressure in the cylinder much higher than that of the exhaust manifold, drastically increasing the amount of work the engine has to provide to exhaust the cylinder gases. However, the in-cylinder temperatures stay high and the thermal efficiency of the operating point increases.

The effects due to the exhaust valve closing event are not evident in the first two modes of cylinder 1 operation. This was an unexpected result, as retarding the timing of EVC moves the event closer to TDC of induction. This normally causes a rise in cylinder pressure around the end of the exhaust stroke. Asmus [3] writes that during idle EVC regulates the quantity of exhaust allowed to flow back into the combustion chamber through the exhaust valve under influence of the intake manifold vacuum. Asmus [3] goes on to state that at wide open throttle and high engine speeds it regulates how much

gas can escape. A more retarded EVC favors high speed power at the expense of low speed torque and idle stability.

No conclusions can be drawn with respect to the overlap of IVO and EVC for cylinder 1 as it remains constant throughout the tests. However, the effects of IVO can be seen in the test where the camshaft is staged 10 crank angle degrees retarded. By retarding this particular event it is being moved closer to TDC of the exhaust stroke. This allows less time for the equalization of intake manifold pressure and cylinder pressure. Therefore, by the time the intake valve reaches an appreciable lift, the piston is descending towards BDC of the induction stroke. This causes an excess pressure drop across the valve and into the cylinder increasing the pumping work slightly. Advancing this event does, however, reduce the amount of exhaust gas residuals allowed to dilute the fresh charge in the intake manifold. As is the case with the EVO event, IVO becomes a balance of minimizing exhaust gas residuals and minimizing the pressure drop between the intake manifold and cylinder.

Keep in mind that by shifting the valve events, the cross sectional flow area of the valve created by the lift changes with respect to piston speed. This can have a positive effect on in cylinder charge density if the flow area is larger at a higher piston speed. It can have an adverse effect if the flow area remains small during the portion of high piston speed.

The effects of intake valve closing cannot be readily seen on the plots of cylinder pressure versus cylinder volume. The key to this timing is, at high speeds, to increase the time allowed for the ram effect to take place. As mentioned, this event occurs well into the compression stroke (where the piston is ascending towards TDC). The ram effect

takes advantage of the inertial effects of the intake gas caused by the limited flow area of the valve and the high speed of the piston. The effects of this valve event are better seen through the description of mass flow rate of air.

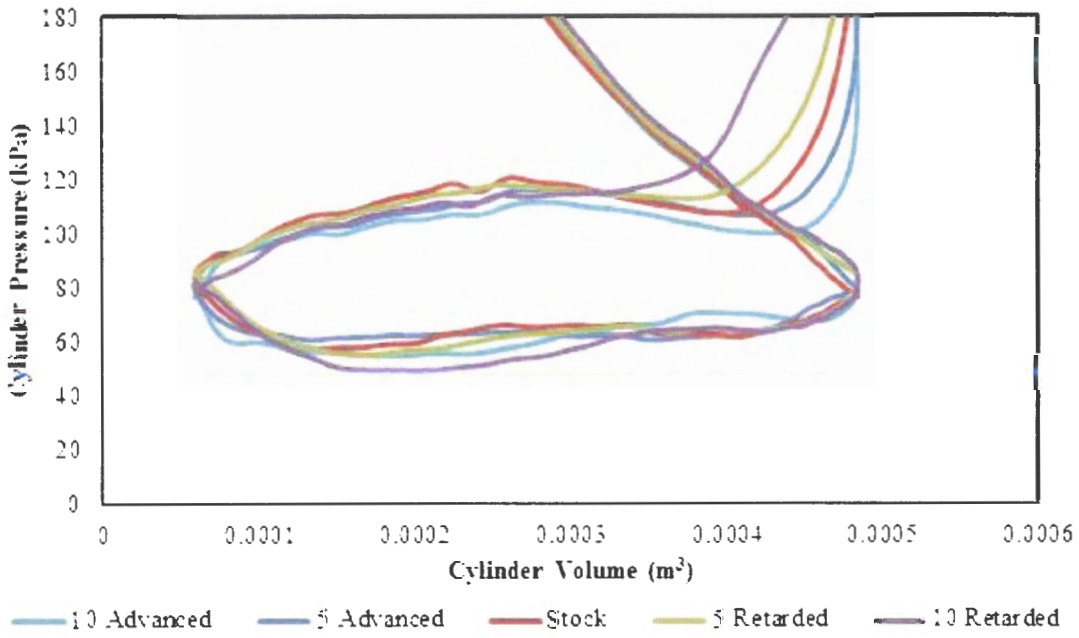

Figure 8.2: Cylinder 1 mode 1 pressure versus volume for all camshaft staging tests

The general trends remain fairly consistent throughout the testing. For cylinder 1 mode 2, (Figure 8.3) the alteration of EVO still has the same effect on the pressure within the cylinder. That is for a more advanced timing the pressure in the cylinder reduces close to that of the exhaust manifold pressure. When the valve is retarded the cylinder pressure still remains high into the exhaust stroke. Similar trends are seen in the shape of the pressure curve at the beginning of the induction stroke due to the intake valve opening event.

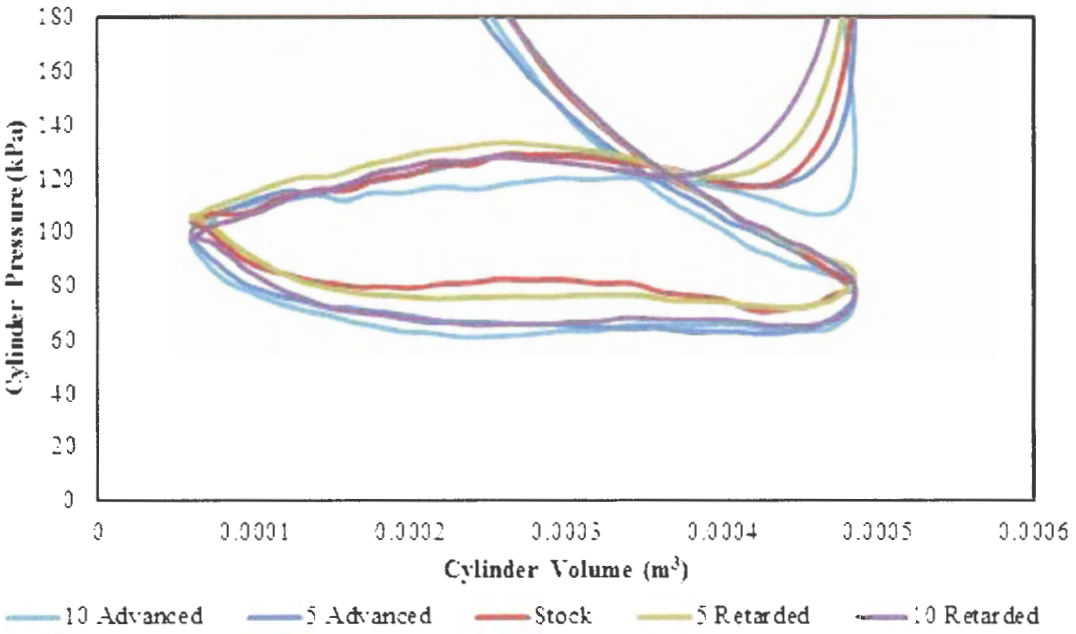

Figure 8.3: Cylinder 1 mode 2 pressure versus volume for all camshaft staging tests

It can be seen in Figure 8.4, Figure 8.5 and Figure 8.6 (representing mode 3, mode 4, and mode 5 respectively) that the cylinder pressure for the 10 crank angle degrees advanced test is much lower than the other four tests during the blow down process. Other valve events also play a role in this decrease in cylinder pressure. The amount of charge entering the cylinder is reduced and therefore, the amount of power the engine is capable of producing is reduced.

The effects due to the EVC event can be realized for the lower load set points in cylinder 1. When comparing the 10 crank angle degrees and 5 crank angle degrees advanced pressure traces to the other three, the cylinder pressure stays higher at the end of the exhaust stroke for the advanced set points than for the stock and retarded set points. This trend is apparent in mode 3, mode 4, and mode 5 operation. The effects of IVO can be seen in the shape of the pressure traces during the beginning of the induction

stroke, that is, the pressure for the 10 crank angle degrees advanced trace stays higher and has a slower draw down than the trace for 10 crank angle degrees retarded.

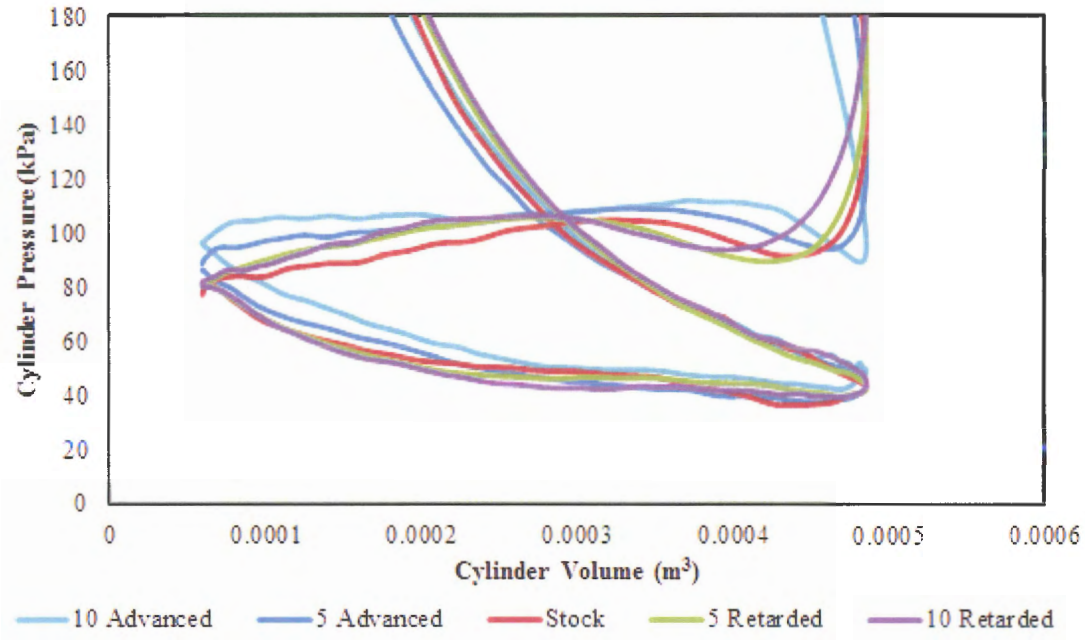

Figure 8.4: Cylinder 1 mode 3 pressure versus volume for all camshaft staging tests

As can be seen in for mode 4 and mode 5 operation, (Figure 8.5 and Figure 8.6 respectively) the staging effects of EVO on the pumping work at these low load set points becomes minimal; even at stock operation the cylinder pressure has time to equalize with the exhaust pressure. This is due to the overall peak pressure of these operating points being much less than those of the higher load set points. A large variation of pressure can be seen during the compression stroke.

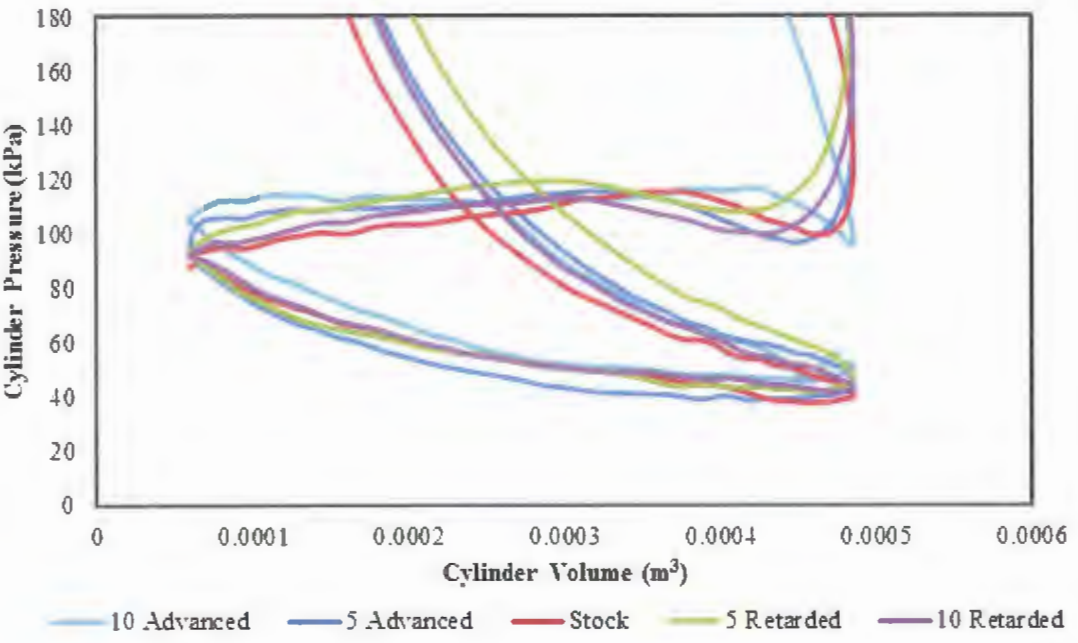

Figure 8.5: Cylinder 1 mode 4 pressure versus volume for all camshaft staging tests

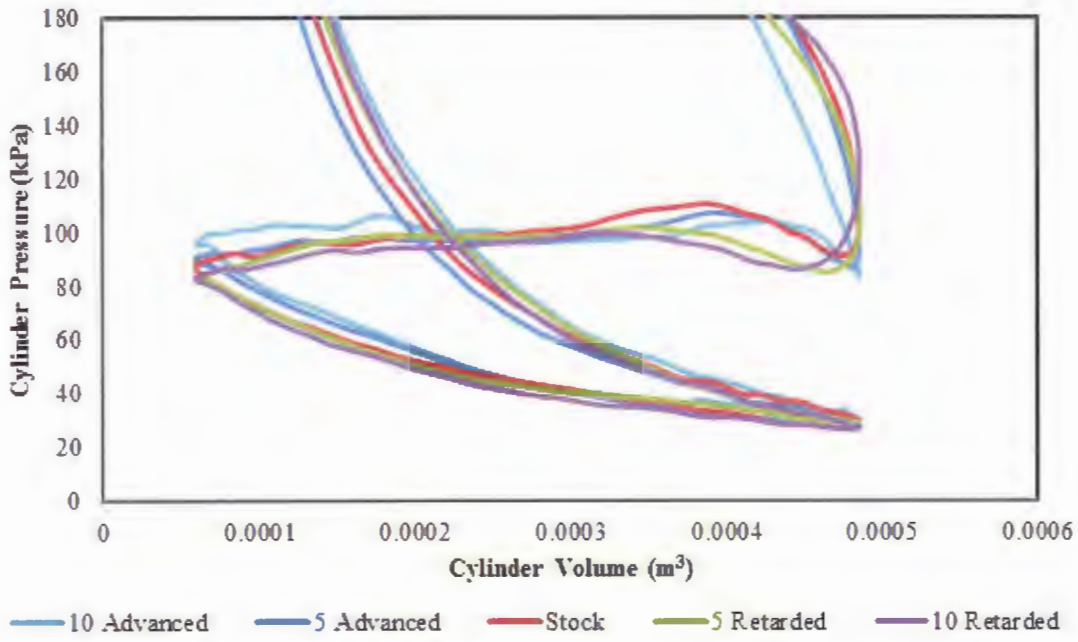

Figure 8.6: Cylinder 1 mode 5 pressure versus volume for all camshaft staging tests

For the idle condition of cylinder 1, (Figure 8.7) it can be seen that the shapes of the pressure traces differ slightly during the expansion and the exhaust stroke. As is the case with mode 4 and mode 5, the effects due to the staging of EVO become minimal as the pressure is already at or below the exhaust pressure at the end of the expansion stroke.

The intake valve closing event has the opposite effect for the idle condition as that for the high speed conditions. Because the piston motion is relatively slow, the inertial filling effects cannot be utilized. As the piston begins to ascend towards TDC of the compression stroke backflow occurs, where the cylinder charge is pushed back through the intake valve and into the intake manifold. This reduces the charge capacity and the overall energy content within the cylinder for each cycle.

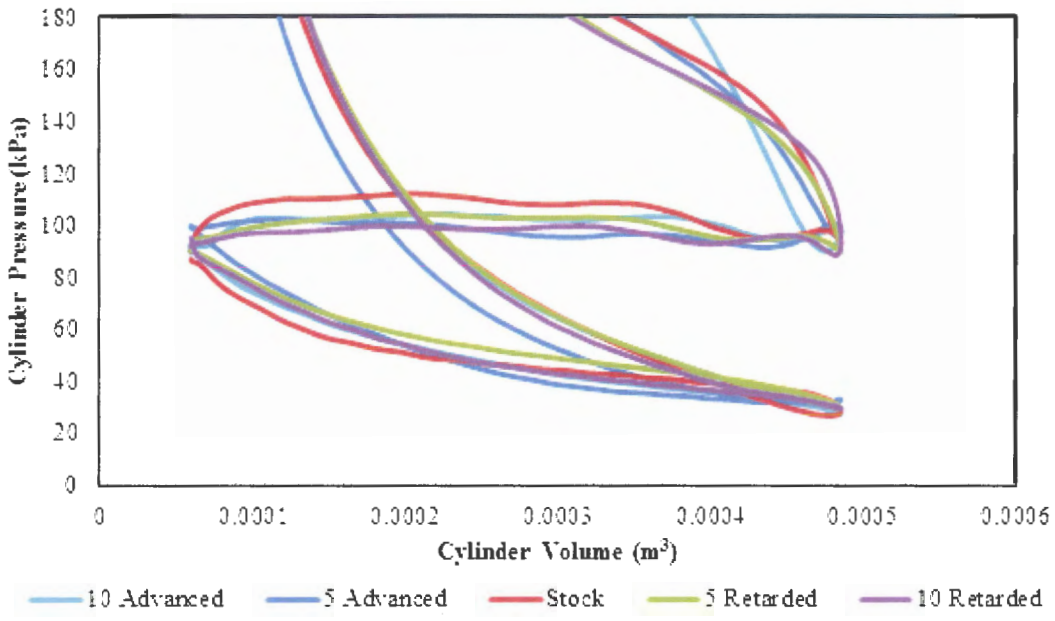

Figure 8.7: Cylinder 1 mode 6 pressure versus volume for all camshaft staging tests

The majority of the trends of cylinder 2 mimic those observed in cylinder 1 and will only be mentioned briefly. Those are the effects of EVO and IVO. The camshaft staging effects that do differ between the two cylinders will, however, be discussed. For example, the effects of staging EVC become apparent for cylinder 2 at the first four high speed modes: Figure 8.8, Figure 8.9, Figure 8.10, and Figure 8.11 as the pressure rise at the end of the exhaust stroke that is expected manifests itself for the advanced timings. This pressure rise speaks to a trapping of exhaust gases in the cylinder at the end of the exhaust stroke and into the beginning of the intake stroke.

Understanding this is important as EVC controls the length of the valve overlap. If EVC were to change with respect to IVO, advancing the timing enough to shorten the overlap helps control the combustion stability at idle and the amount of exhaust gas dilution that occurs at all set points through this period, but advancing it too far increases the pumping work significantly. Again, this will require a balance between the two effects.

Again, for the low load set points, the advancing of the EVO event has little beneficial effect on engine performance as the cylinder pressure during expansion for these modes already reach that of the exhaust manifold pressure as seen in Figure 8.12. Also for this mode, the effects of EVC are no longer prominent as in the previous modes.

For the idle condition, Figure 8.13, it can be seen that the pressure at the end of expansion dips well below that of the exhaust pressure near BDC of the expansion stroke. Again, as for cylinder 1, any alteration in this valve timing has a negligible effect on the pumping work required, but does have a significant effect on the thermal efficiency of the engine set point.

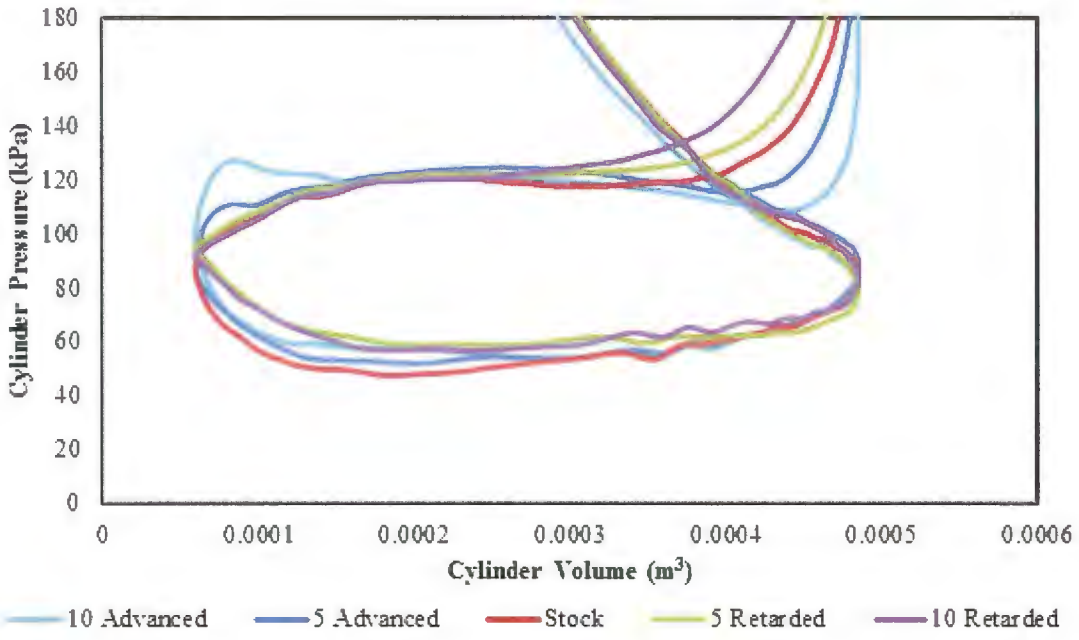

Figure 8.8: Cylinder 2 mode 1 pressure versus volume for all camshaft staging tests

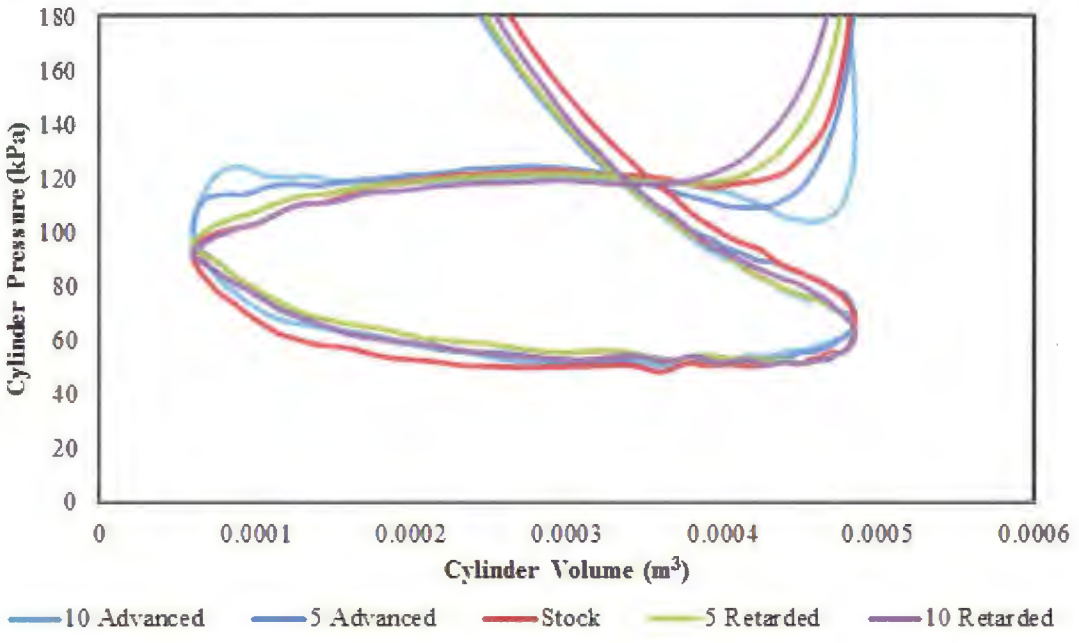

Figure 8.9: Cylinder 2 mode 2 pressure versus Volume for all camshaft staging tests

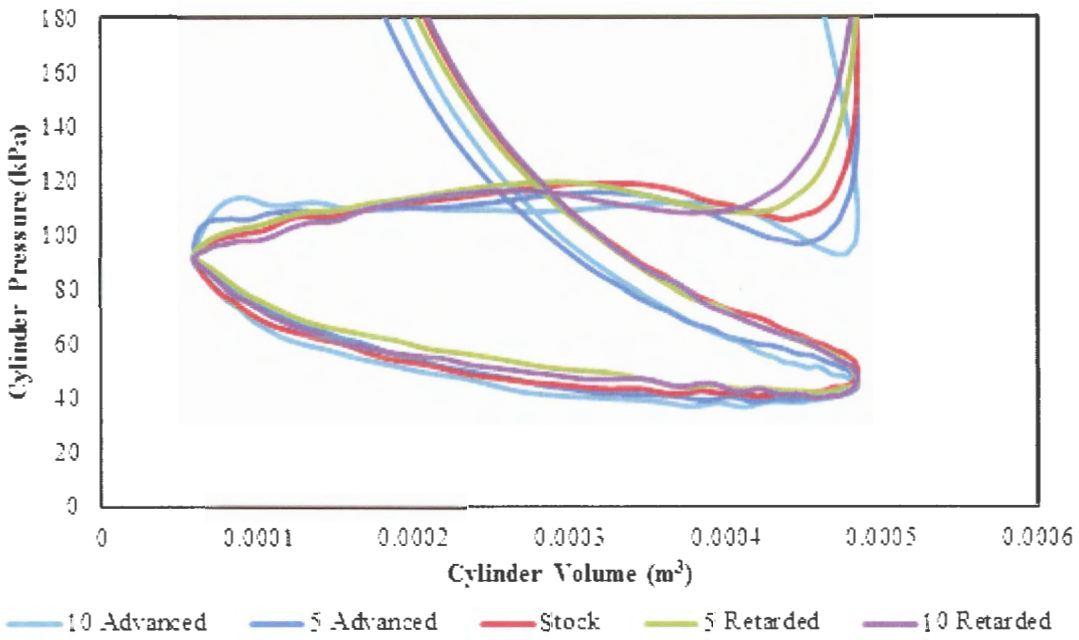

Figure 8.10: Cylinder 2 mode 3 pressure versus volume for all camshaft staging tests

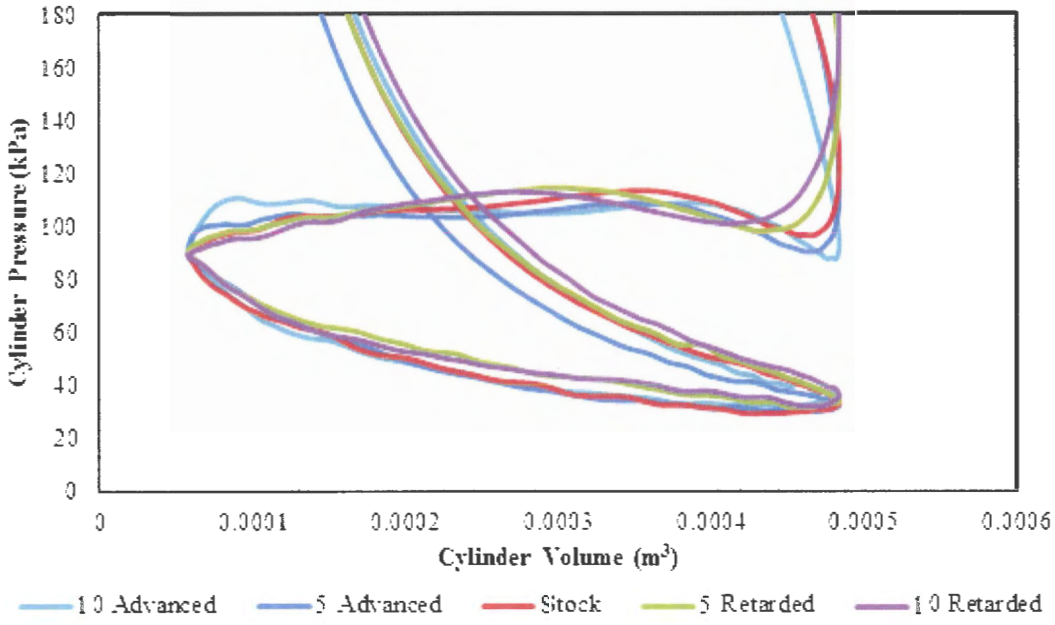

Figure 8.11: Cylinder 2 mode 4 pressure versus volume for all camshaft staging tests

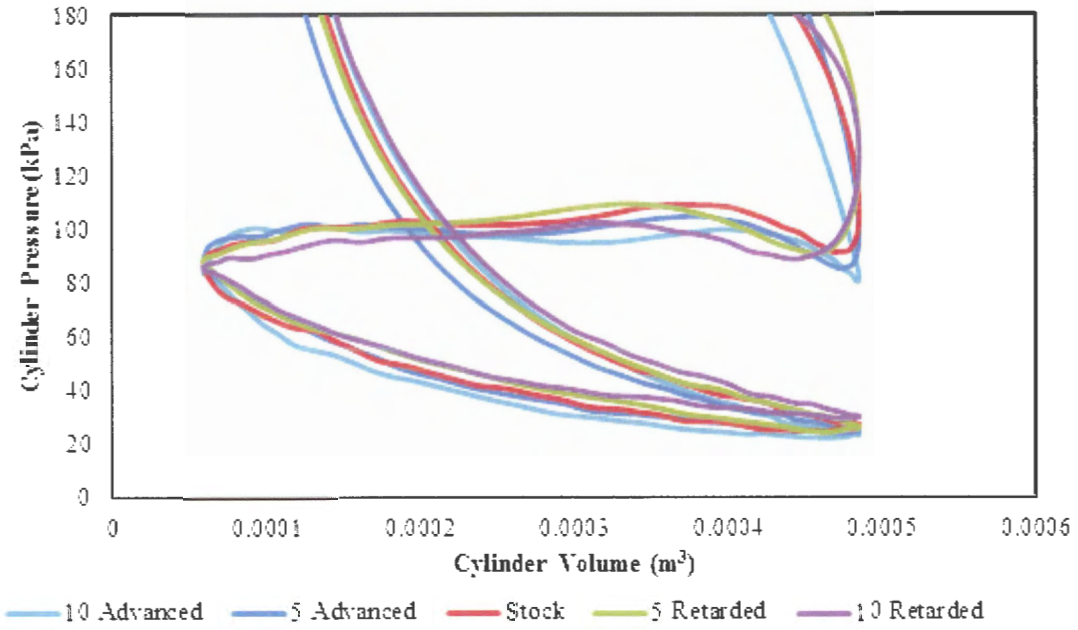

Figure 8.12: Cylinder 2 mode 5 pressure versus volume for all camshaft staging tests

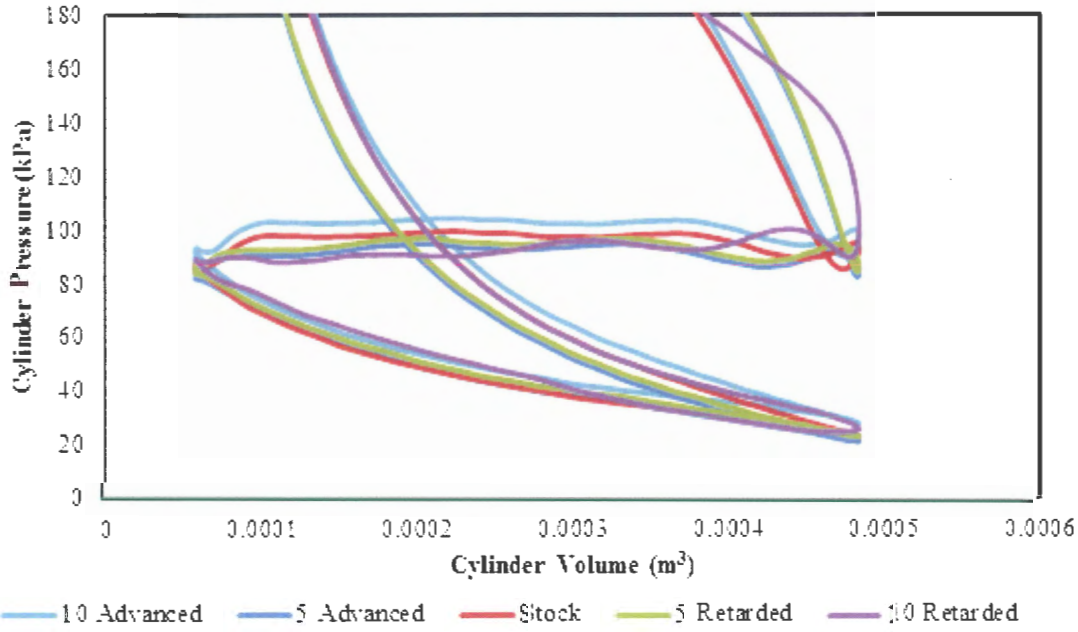

Figure 8.13: Cylinder 2 mode 6 pressure versus volume for all camshaft staging tests

8.2.2 Comparison of Experimental Parameters Based on Cylinder Pressure.

Parameters including torque, power output, pumping mean effective pressure, and net indicated mean effective pressure will be compared between camshaft staging tests. All data presented in the next two sections, with the exception of volumetric efficiency, will be of all 6 modes and for all camshaft staging tests including the stock timing. Some parameters are measured as a function of the whole engine, while others are measured for each cylinder; they will be denoted and discussed accordingly.

Throughout this work, there are two key parameters that characterize an operational set point for an engine: rotational speed and torque. The torque of an engine is a measure of the engine's ability to do work [2], displayed here in N-m. It is calculated as the product of a force measured at the dynamometer anchor point and a moment arm between the center of the dynamometer and the anchor point. The amount of torque an engine can create is dependent on displacement volume and fluctuates directly with engine load. Table 8.1 shows the values of torque obtained from 6-Mode camshaft staging tests and Figure 8.14 is a plot depicting those values. Because torque is measured at the output shaft, it accounts for both cylinders and is presented for the entire engine.

Again, the amount of torque created by the engine decreases with mode even though the same speed set point is maintained. The trend that should be noticed is that even while maintaining the same testing procedure (keeping the same throttle position for each respective mode), higher loads were obtainable for the retarded camshaft timings than those for the advanced camshaft timings. For mode 1, an increase in torque of 5.6% is realized by retarding the camshaft 10 crank angle degrees from stock. The high speed load increase is attributed to a more effective use of the ram effect due to the intake valve

closing later in the compression stroke. The trend reverses itself for the idle set point due to the absence of the ram effect at slow speeds. However, as there is minimal engine loading at this point, the difference in power output becomes negligible; instead, exhaust gas residuals introduced during the valve overlap period, backflow of cylinder charge into the intake manifold and idle stability become the key factors.

Table 8.1: Shaft torque of full engine for 6-Mode camshaft staging tests

	Shaft Torque (N-m)				
	10 Advanced	5 Advanced	Stock	5 Retarded	10 Retarded
Mode 1	49.5	50.3	50.8	52.7	53.8
Mode 2	35.9	36.2	36.6	37.4	39.1
Mode 3	24.1	24.7	24.9	26.3	26.8
Mode 4	14.9	15.7	15.9	16.3	17.0
Mode 5	3.7	3.8	3.8	3.8	4.3
Mode 6	2.6	2.4	2.0	2.2	2.4

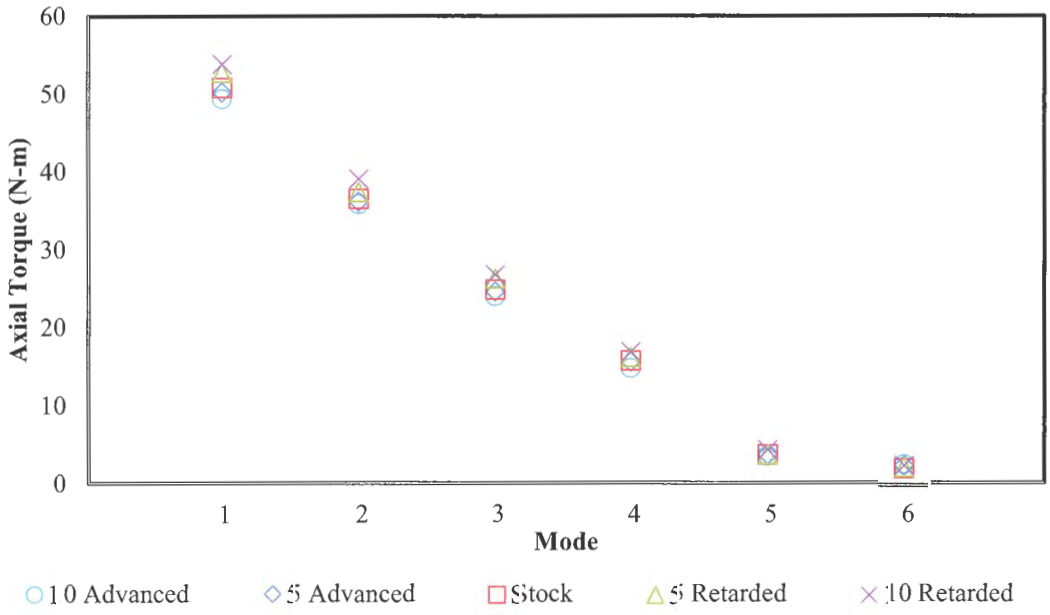

Figure 8.14: Shaft torque comparison for full engine of 6-Mode camshaft staging tests

The shaft output of an engine is a function of both engine speed and torque. It is a measure of the rate at which work is done [2], displayed here in kW. This is essentially the usable power that is transferred from the engine's crankshaft to the load or in this case the dynamometer. As it is a direct function of torque, it follows similar trends for the same reasons. An increase in power of 8% is observed for the most retarded camshaft set point over the stock valve timings. The trends can be seen in Table 8.2 and Figure 8.15

Table 8.2: Shaft output of full engine for 6-Mode camshaft staging tests

	Shaft Output (kW)				
	10 Advanced	5 Advanced	Stock	5 Retarded	10 Retarded
Mode 1	14.6	15.1	15.4	16.1	16.8
Mode 2	11.2	11.6	12.1	12.3	12.7
Mode 3	7.5	7.8	7.8	8.2	8.5
Mode 4	4.3	4.4	4.0	4.8	5.1
Mode 5	1.1	1.2	1.1	1.3	1.4
Mode 6	1.0	0.9	0.7	0.7	0.7

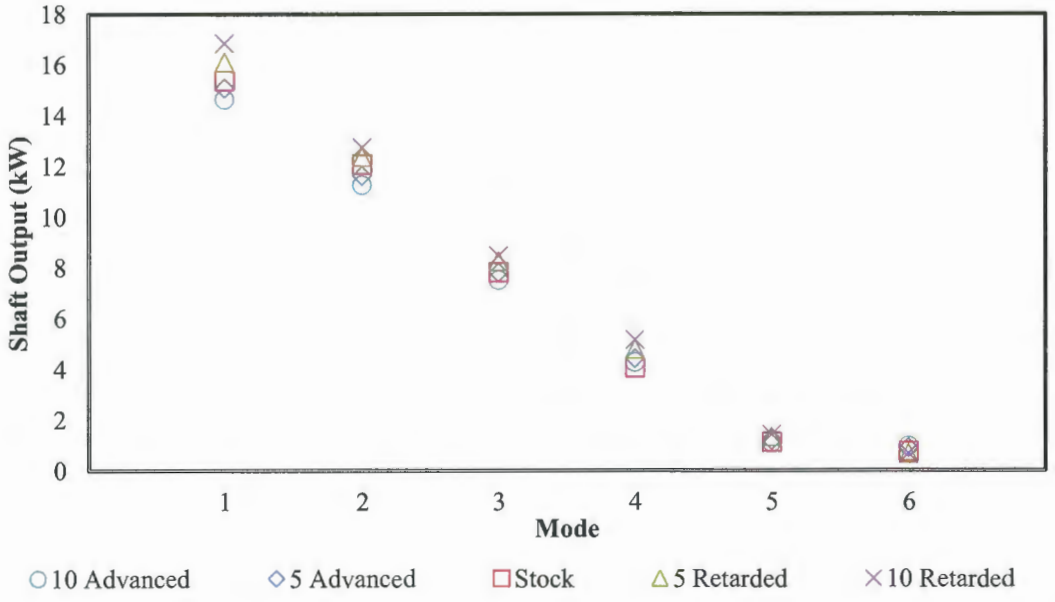

Figure 8.15: Shaft output comparison for full engine of 6-Mode camshaft staging tests

The pumping mean effective pressure, or pumping work, has been discussed several times to this point. It is a measure of the work required by the engine to exhaust the burned charge from and induct the new charge into the cylinder. This is a loss to the engine, so ideally, the pumping work is desired to be small (the smaller the value the more efficient the process). The values of mean effective pressure are calculated from cylinder pressure data; therefore, each cylinder can be analyzed individually. Table 8.3 compares the pumping work of both cylinders for all camshaft staging tests for the 6-Mode data. Figure 8.16 and Figure 8.17 depict the values of Table 8.3 for cylinder 1 and cylinder 2 respectively. By comparing similar modes across different camshaft conditions, an increase in pumping work can be seen as the camshaft is moved from 10 crank angle degrees advanced to 10 crank angle degrees retarded, particularly at the high load set points. The primary cause for this is the high exhaust pressure at the end of the expansion stroke as the camshaft becomes more retarded (the exhaust valve is opening further into the expansion stroke, closer to the exhaust stroke). Also, as the vacuum created between the intake manifold and the cylinder increases, (i.e. the effects of throttling) the intake pressure dips causing the pumping work to increase, though this is an effect that is more dependent on load than on camshaft staging.

The aforementioned trend starts to break down at the lower load set points as the pumping loops become more similar between the camshaft staging tests; the cylinder pressure requires less time to equalize with the manifold pressure due to lower peak cylinder pressures.

A concern that needs to be addressed is that the calculated pumping work, as it progresses through the modes, is atypical of the trends normally observed on automotive

engines. That is, typically, as the engine is throttled the pumping work is expected to increase due to the engine being required to exert more energy to induct the fresh charge. It has already been observed that the intake pressure does decrease with mode, however, the high exhaust pressure at the end of the expansion stroke for the high load modes helps to increase the pumping work. For example, by following the trend in Figure 8.16 it can be observed that for the retarded camshaft setting the pumping work of mode 1 is much higher than the pumping work of mode 5. Recall Figure 8.2 (cylinder 1 mode 1 pressure versus volume for all camshaft staging tests), the pressure at the end of the expansion stroke remains high. Conversely, the cylinder pressure during the same time of the most advanced camshaft timing is much lower (again, a reduction in pumping work). Now, observed the trend in Figure 8.16 for the camshaft staging of 10 crank angle degrees advanced. The pumping work for mode 1 is lower than the pumping work for the more throttled, lower load, modes. This is the trend that would normally be expected.

Table 8.3: Pumping mean effective pressure for all 6-Mode camshaft staging tests

		Pumping Mean Effective Pressure (pmep) (kPa)				
		10 Advanced	5 Advanced	Stock	5 Retarded	10 Retarded
Cylinder 1	Mode 1	41.4	45.1	50.2	54.1	58.7
	Mode 2	44.6	44.6	46.8	49.7	56.5
	Mode 3	48.1	48.3	44.9	47.3	52.0
	Mode 4	50.8	48.3	49.2	50.5	48.9
	Mode 5	48.7	49.7	47.4	48.5	48.7
	Mode 6	50.3	47.2	48.3	46.0	46.8
Cylinder 2	Mode 1	57.9	62.9	66.3	67.0	70.0
	Mode 2	58.3	59.9	64.0	60.5	67.0
	Mode 3	60.2	57.3	58.6	57.9	63.4
	Mode 4	59.8	55.1	57.8	57.1	59.6
	Mode 5	58.3	55.0	58.0	56.2	55.8
	Mode 6	51.6	48.9	47.4	46.8	44.9

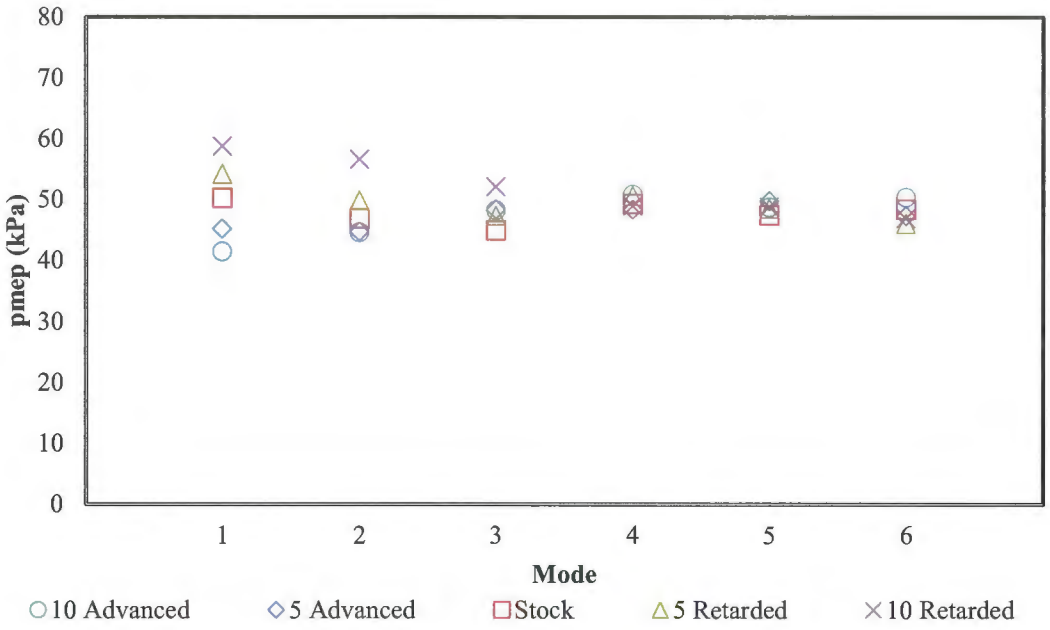

Figure 8.16: Comparison of pumping work between camshaft staging tests for cylinder 1

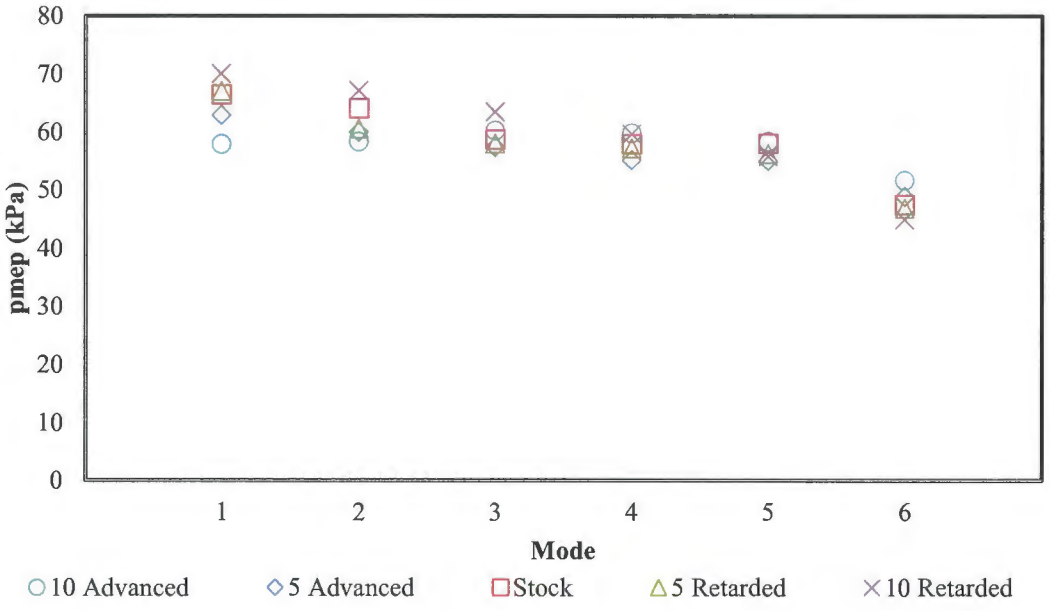

Figure 8.17: Comparison of pumping work between camshaft staging tests for cylinder 2

Similar to those of torque and power, the general trend for imep is that of decreasing with engine load. As with pmep, the value of $imep_{,n}$ decreases with an

advancing of the camshaft, however, it does not decrease to the same degree. The pmep of cylinder 1 decreased by as much as 40% and cylinder 2 by as much as 20% between the most advanced and most retarded camshaft timings, while imep only decreased by 4% for cylinder 1 and 3% for cylinder 2 for mode 1 operation. Similar to the pmep, the trend in imep seems to break down for the higher modes due to minimal engine loading.

Another observation is that imep, by definition, is proportional to the torque produced by then engine (torque divided by displacement volume). However, a greater improvement in torque was observed than that of imep. This is thought to be caused by the fact that the torque is being compared as a function of the total engine output, while the imep is divided into the individual cylinders. As seen previously the performance between the cylinders varies greatly. The calculated values of $imep_{,n}$ are presented in Table 8.4 for both cylinders and depicted in Figure 8.18 and Figure 8.19 for cylinder 1 and cylinder 2 respectively.

Table 8.4: Net indicated mean effective pressure for all 6-Mode camshaft staging tests

		Net Indicated Mean Effective Pressure ($imep_{,n}$) (kPa)				
		10 Advanced	5 Advanced	Stock	5 Retarded	10 Retarded
Cylinder 1	Mode 1	651.4	659.1	670.2	673.0	677.1
	Mode 2	516.4	530.0	548.0	548.2	550.5
	Mode 3	377.4	382.8	380.0	394.2	395.3
	Mode 4	243.6	252.6	255.8	232.9	231.9
	Mode 5	115.5	137.9	166.4	130.6	131.1
	Mode 6	73.0	72.4	75.6	76.6	73.0
Cylinder 2	Mode 1	692.4	706.2	710.3	713.6	715.3
	Mode 2	566.4	570.6	575.5	593.4	595.0
	Mode 3	405.5	410.9	415.6	418.6	420.0
	Mode 4	232.1	265.6	261.6	259.9	272.5
	Mode 5	126.4	153.0	172.1	131.6	153.0
	Mode 6	99.5	103.4	115.4	105.4	99.5

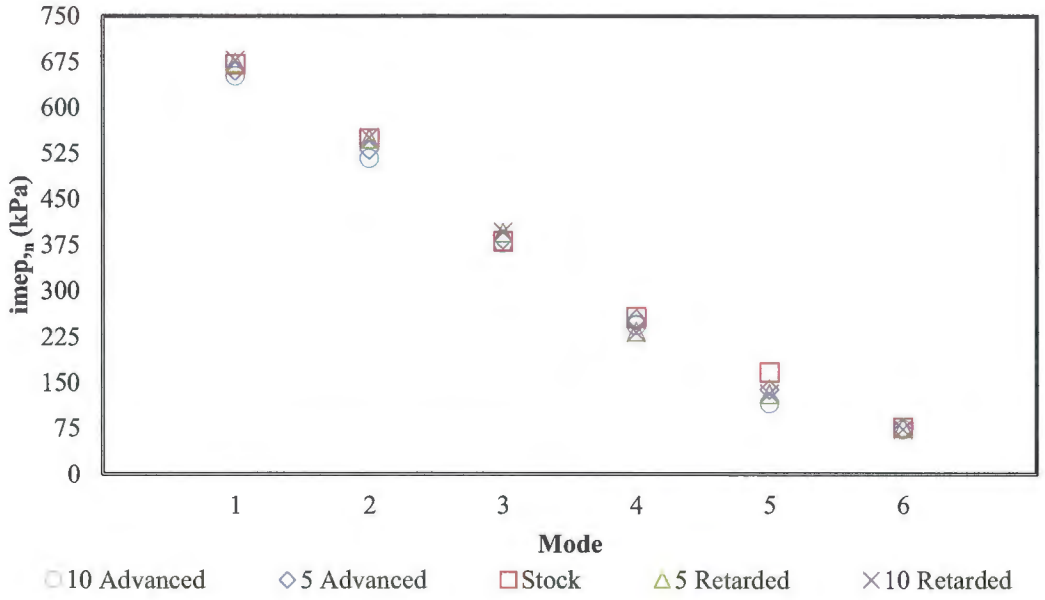

Figure 8.18: Comparison of net imep between camshaft staging tests for cylinder 1

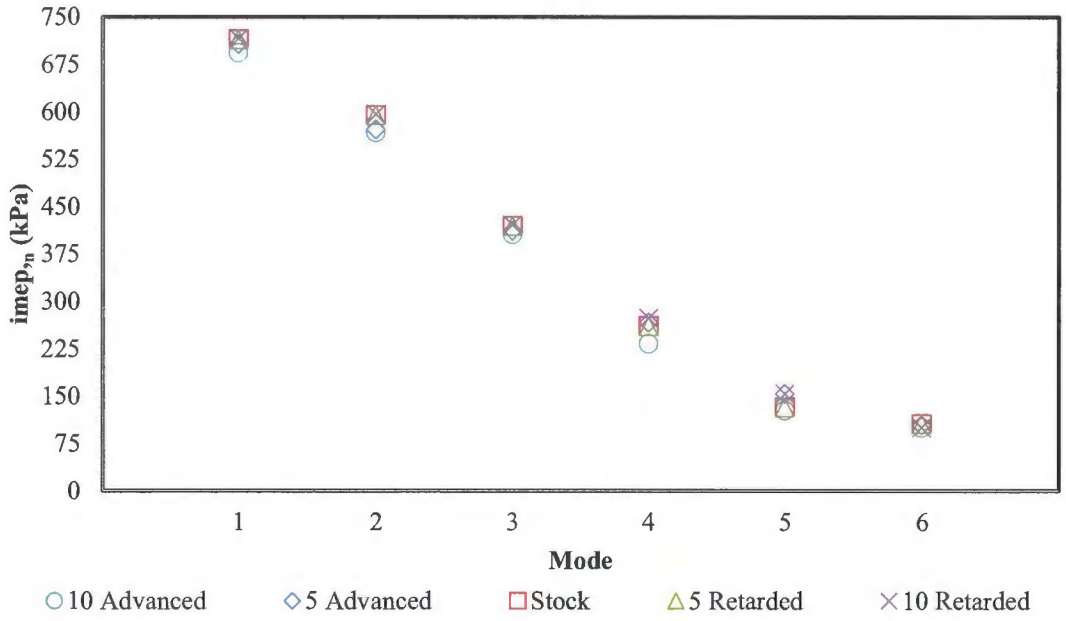

Figure 8.19: Comparison of net imep between camshaft staging tests for cylinder 2

8.2.3 Comparison of Experimental Parameters Based on Energy Flow.

Parameters discussed in this section include the mass flow rate of air, mass flow rate of fuel, air to fuel ratio, exhaust gas temperature, fuel conversion efficiency, specific fuel consumption, and volumetric efficiency. The mass flow rate of air into the engine was measured by the means of a laminar flow element. It provides the average flow rate for the entire engine and is unable to resolve the results into specific cylinders. Therefore, the flow rate of air is presented as the total mean flow rate of air for the engine at an operating point.

The mass flow rate of air decreases with mode as the engine becomes more throttled. It also decreases as the timing of the intake valve closing event is staged from 10 crank angle degrees retarded to 10 crank angle degrees advanced (a 6% decrease in mass flow rate of air is observed for the wide open throttle case). The mass flow rate increases slightly with the advanced camshaft timing for the idle condition as the inertial effects between the intake manifold and cylinder are not strong for low engine speeds. Table 8.5 shows the measured value for mass flow rate of air in kilograms per second for the tested valve timings through all 6-Modes. Figure 8.20 graphically represents the values of Table 8.5 and allows the trends to be easily viewed.

Table 8.5: Mass flow rate of air for full engine 6-Mode camshaft staging tests.

	Mass Flow Rate of Air (kg/s) Both Cylinders				
	10 Advanced	5 Advanced	Stock	5 Retarded	10 Retarded
Mode 1	0.0197	0.0201	0.0204	0.0207	0.0209
Mode 2	0.0164	0.0165	0.0168	0.0175	0.0178
Mode 3	0.0123	0.0124	0.0131	0.0133	0.0139
Mode 4	0.0094	0.0095	0.0098	0.0104	0.0107
Mode 5	0.0084	0.0084	0.0081	0.0090	0.0094
Mode 6	0.0041	0.0041	0.0040	0.0040	0.0038

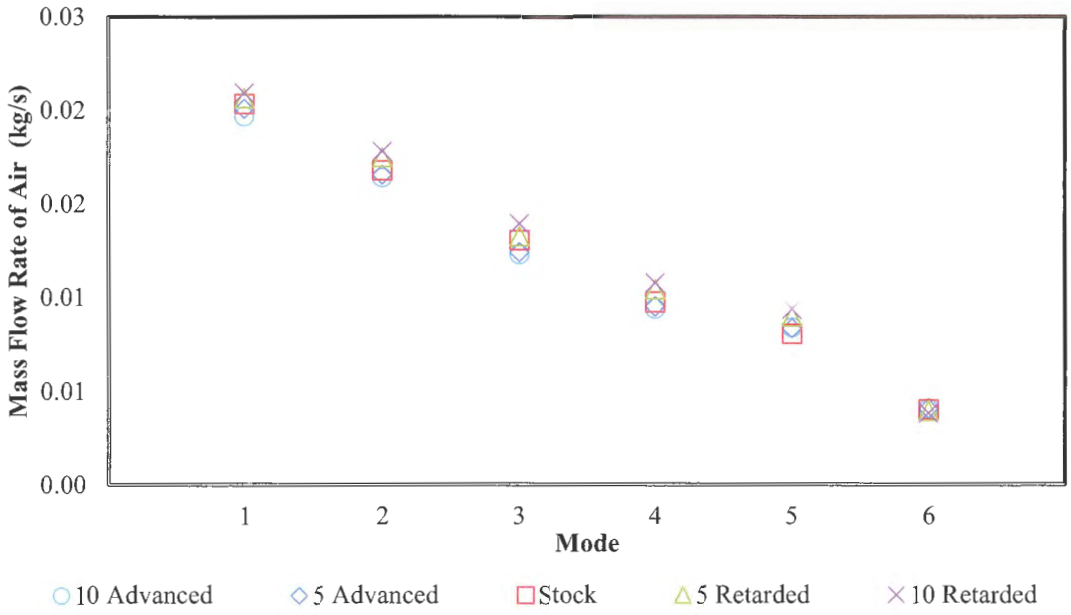

Figure 8.20: Comparison of air mass flow rate between 6-Mode camshaft staging tests

Since the test engine is carbureted and the mass of air pulled through the system is a pressure driven flow, the mass flow rate of fuel and the mass flow rate of air are a coupled entity. The relationship between the mass flow rate of air and the mass flow rate of fuel for a carburetor is based on a ratio of the discharge coefficients and cross sectional areas of the venturi throat and orifice (of the particular carburetor), the density ratio of the fuel and ambient conditions, as well as a ratio of pressure drop between the carburetor and the manifold. So, for an increase in pressure drop in the manifold there is an increase in fuel for a given flow rate of air. This has an effect on equivalence ratio. If the engine was fuel injected, this would not be the case as the injector can be controlled separately to that of the throttle position.

Figure 8.21 shows the intake manifold pressure for the mode 1 operating point of two camshaft locations, 10 crank angle degrees retarded and 10 crank angle degrees

advanced. It can be seen that the intake manifold pressure for the retarded camshaft timing is lower than that of the advanced timing for the majority of the intake valve open period. A pressure rise in the manifold can be seen at the beginning of the induction stroke for the advanced camshaft timing. For this test, the intake valve is open further away from TDC of the exhaust stroke and the exhaust valve is closed closer to TDC of the intake stroke; the pressure rise represents a backflow of exhaust gases into the intake manifold from the cylinder. This dilutes the fresh charge waiting in the intake manifold, decreasing the amount of chemical energy in the cylinder available for the next cycle.

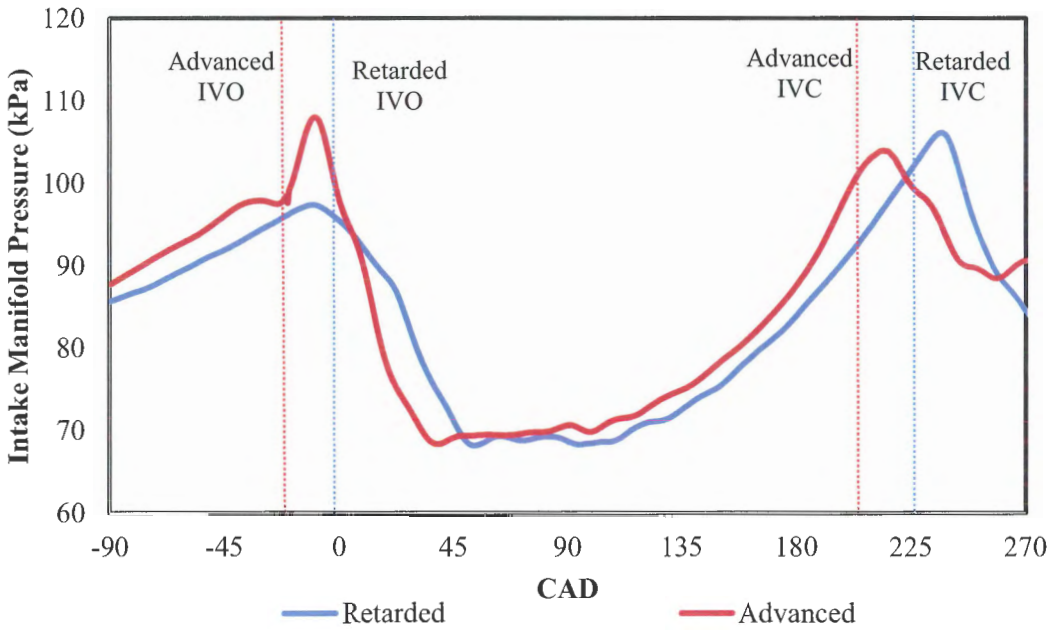

Figure 8.21: Intake manifold pressure for 10 crank angle degrees retarded and 10 crank angle degrees advanced camshaft timings (mode 1)

Table 8.6 contains the measured values of fuel mass flow rate with units of 10^{-3} kg/s. The amount of fuel the engine uses decreases with each mode; again, this is due to the effects of throttling. Also, just as with the mass flow rate of air, the flow rate of fuel

increases as the camshaft is advanced. Figure 8.22 shows the values of Table 8.6 plotted as a function of mode and camshaft setting. Recall that the engine is achieving a higher power output, but it comes at the cost of consuming slightly more fuel.

Table 8.6: Mass flow rate of fuel for full engine 6-Mode camshaft staging tests.

	Fuel Mass Flow Rate ($x10^{-3}$ kg/s) Both Cylinders				
	10 Advanced	5 Advanced	Stock	5 Retarded	10 Retarded
Mode 1	1.72	1.76	1.79	1.83	1.86
Mode 2	1.37	1.39	1.42	1.50	1.54
Mode 3	0.98	1.00	1.07	1.09	1.15
Mode 4	0.75	0.76	0.79	0.85	0.89
Mode 5	0.62	0.63	0.61	0.69	0.73
Mode 6	0.30	0.30	0.30	0.30	0.29

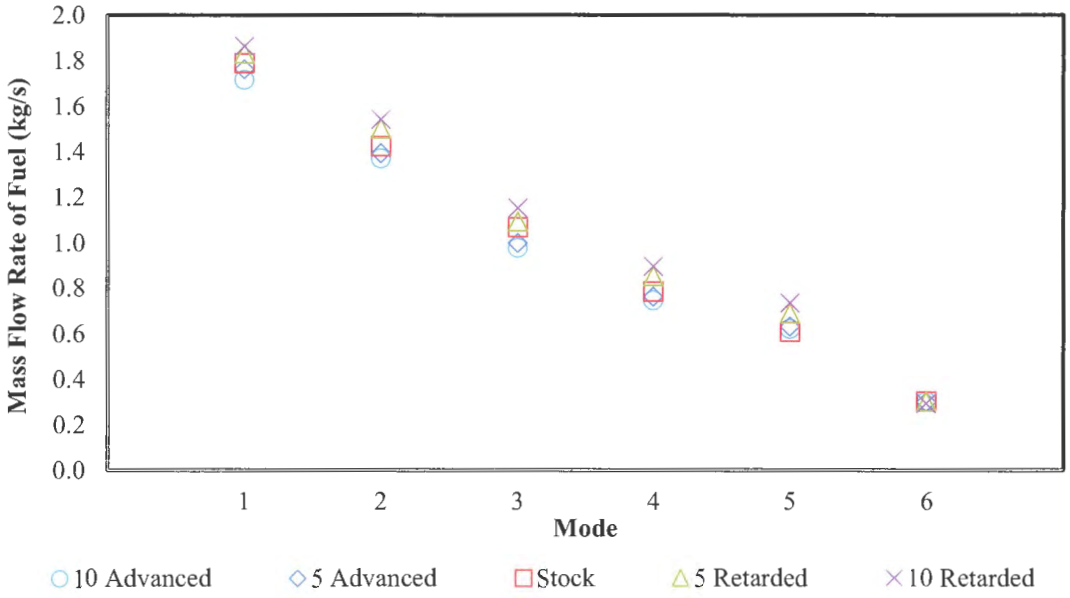

Figure 8.22: Comparison of fuel mass flow rate between 6-Mode camshaft staging tests

Fuel injected engines have the ability to change the amount of fuel introduced to the system every cycle by adjusting the pulse width used to drive the injector. Most fuel

injected spark ignition engines can be run close to a stoichiometric setting to minimize the emissions of the engine. However, stoichiometric operation increases the temperature within the combustion chamber which can cause the air-cooled engines to require additional cooling solutions. Stoichiometric operation can also cause issues when attempting to rapidly adjust speed and load causing unstable combustion and potentially a misfire scenario. Carbureted engines are generally operated with a low air to fuel ratio (A/F less than 14.6, rich operation) to keep the temperature of the engine structure manageable and to allow for a smooth transition between operational modes.

However, rich operation causes issues with emissions as there is generally not enough air to oxidize the fuel completely. This unburned fuel is exhausted; not only is it harmful from an emissions standpoint it is also wasted energy. The air to fuel ratios were recorded by the UEGO sensors located in the exhaust manifold for each cylinder, as discussed in the experimental setup in Chapter 3. These values for both cylinders of the engine for the 6-Mode camshaft staging tests can be seen in Table 8.7 and plotted in Figures 8.23 and 8.24. The air to fuel ratio becomes less rich as the engine is throttled. As the camshaft is staged from 10 crank angle degrees advanced to 10 crank angle degrees retarded engine operation becomes more rich, if only slightly. As described above, this is due to a change in dynamic effects in the manifold by adjusting when flow is introduced with respect to valve lift and piston speed.

This trend is a little peculiar in that generally as the equivalence ratio increases (Air to Fuel ratio decreases) the energy available in the cylinder decreases due to a lack of air. As stated by Heywood [2], for mixtures richer that stoichiometric, a lack of oxygen prevents complete combustion of the fuel carbon and hydrogen and the

combustion efficiency steadily decreases as the mixture becomes richer. The trends observed throughout this work, however, do not follow this. For a camshaft timing of 10 crank angle degrees retarded the air to fuel mixture is more rich than that of 10 crank angle degrees advanced, however, as can be seen up to this point the energy output is higher for the retarded camshaft timings. This is attributed to an increase in charge density; as air is inducted into the cylinder it will expand to fill the volume. As more air is inducted into the cylinder, there is less room to spread out and the density increases. That is, it is a product of there simply being more charge in the cylinder for the retarded timings compared to that of the advanced timings.

Other trends can be extracted from the air to fuel ratio information relating to emissions. The formation of carbon monoxide, CO, increases as the camshaft is retarded. It will be discussed later that when the air to fuel ratio decreases, a smaller fraction of the energy available in the cylinder charge will be released during the combustion process. This is an undesirable effect as the amount of unburned fuel remaining in the cylinder after the combustion process is complete will increase, resulting in more CO products. Carbon monoxide is a product of incomplete combustion, so it is at its greatest when the engine is running at the high speed high load set points and the air to fuel ratio is lowest. Because the test engine is carbureted this is an effect that is difficult to avoid when looking to adjust valve timings.

Again, staging the camshaft or altering the timing of valve events allows for some form of control over the way in which chemical energy is introduced into the engine. This is discussed in great detail in a later section.

Table 8.7: Air to Fuel Ratio for the 6-Mode camshaft staging tests

		Air to Fuel Ratio				
		10 Advanced	5 Advanced	Stock	5 Retarded	10 Retarded
Cylinder 1	Mode 1	11.16	11.11	11.10	11.07	11.03
	Mode 2	11.78	11.65	11.53	11.41	11.33
	Mode 3	12.25	12.20	12.15	12.08	12.07
	Mode 4	12.29	12.30	12.22	12.12	12.05
	Mode 5	13.25	13.05	12.98	12.80	12.53
	Mode 6	13.54	13.89	13.51	13.31	13.13
Cylinder 2	Mode 1	11.81	11.71	11.68	11.51	11.46
	Mode 2	12.12	12.07	12.02	11.91	11.78
	Mode 3	12.94	12.67	12.34	12.22	12.15
	Mode 4	12.83	12.63	12.63	12.30	11.98
	Mode 5	13.76	13.36	13.50	13.25	13.01
	Mode 6	13.30	13.23	13.15	13.10	13.13

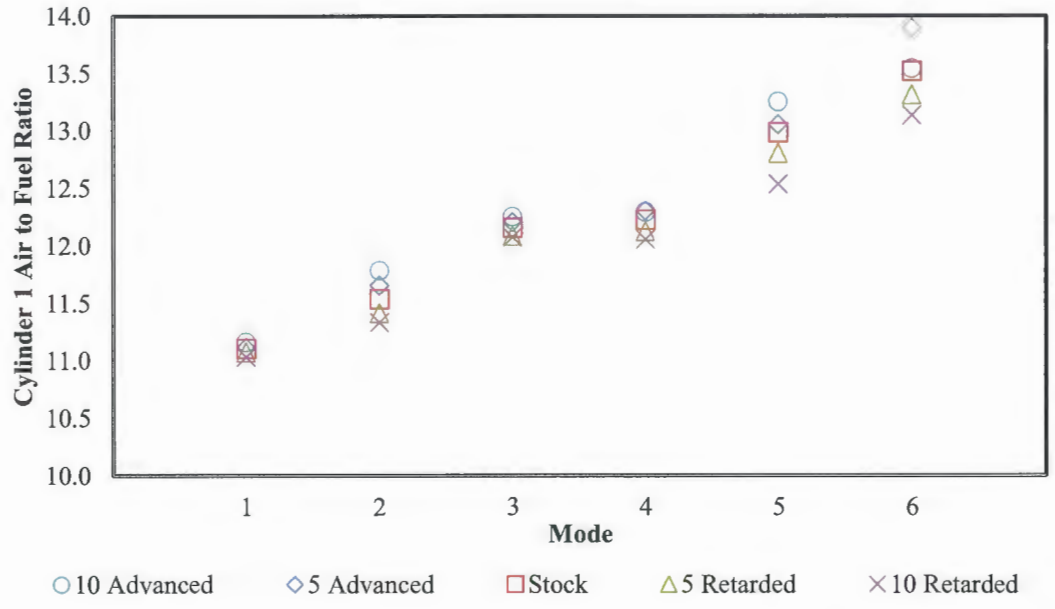

Figure 8.23: Air to fuel ratio for cylinder 1 for 6-Mode camshaft staging tests

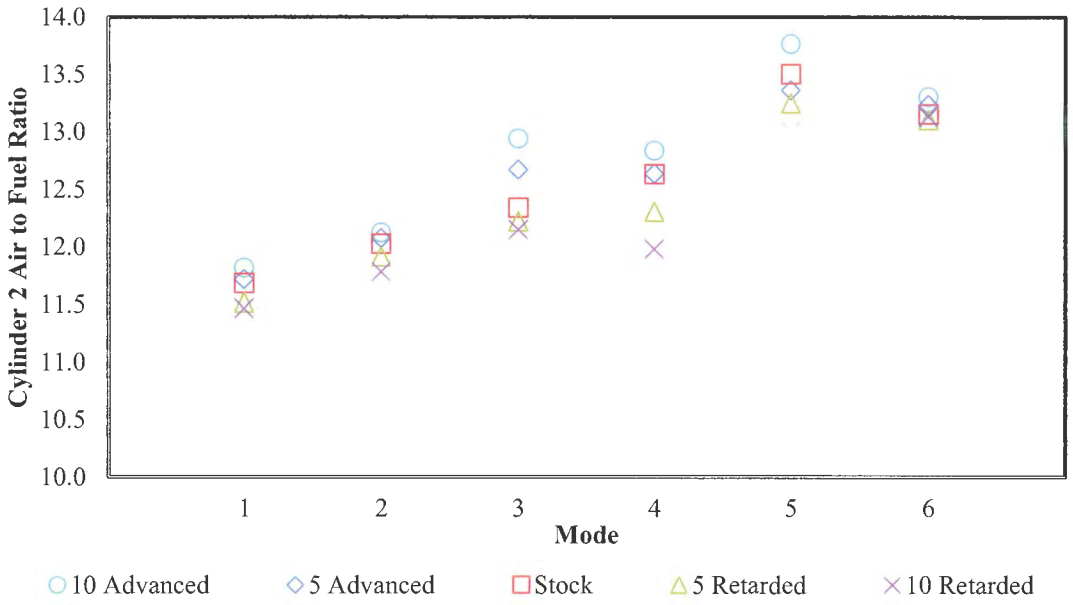

Figure 8.24: Air to fuel ratio for cylinder 2 for 6-Mode camshaft staging tests

The chemical energy introduced into the cylinder, the amount of energy released, and the exhaust valve timing event play a large role in the exhaust gas temperature and a large role in controlling the emissions of an engine. The exhaust gas temperature is used to determine the enthalpy and the sensible energy of the exhaust products, which is discussed in greater detail in a later section. Table 8.8 contains the average exhaust gas temperatures, in Kelvin, of both cylinders for all 6-Mode camshaft staging tests. Figure 8.25 and Figure 8.26 plot those values versus engine mode as a function of camshaft timing for cylinder 1 and cylinder 2 respectively (the y-axis is resolved to show only 800K to 1200K to make apparent the differences). It can be seen that the exhaust temperatures are higher for the high speed low load set points. As was discussed earlier, the air to fuel ratio becomes closer to stoichiometric as the engine becomes throttled. The temperatures of a combustion process that is close to stoichiometric are much higher than

those of a rich combustion process. In fact, the maximum flame temperatures are generally just on the rich side of stoichiometric [2].

However, these changes in temperature are not strictly an air to fuel ratio effect as a change in charge density and spark timing will impact the exhaust gas temperatures. It must be stressed that the test engine operates off of a fixed spark timing that was found by Wildhaber [20] to be far from optimal for all engine operating modes. If the engine were operated at, or close to, a spark timing that allowed for maximum brake torque (the maximum engine torque possible at a fixed speed, mixture composition, and engine load) it would have a great effect on these distributions. Recall, that an alteration in the camshaft has an effect on the mixture composition.

Table 8.8: Exhaust gas temperatures for 6-Mode camshaft staging tests

	Exhaust Gas Temperatures (K)				
	10 Advanced	5 Advanced	Stock	5 Retarded	10 Retarded
Mode 1	997	992	972	955	946
Mode 2	1001	998	990	986	973
Mode 3	1018	1006	1001	1000	994
Mode 4	1041	1035	1027	1022	1014
Mode 5	1033	1017	1009	1000	980
Mode 6	869	865	854	842	828
Mode 1	1001	994	980	965	958
Mode 2	1044	1036	1018	989	983
Mode 3	1033	1028	1019	1005	976
Mode 4	1071	1061	1054	1016	988
Mode 5	1088	1083	1076	1064	1039
Mode 6	976	928	909	883	866

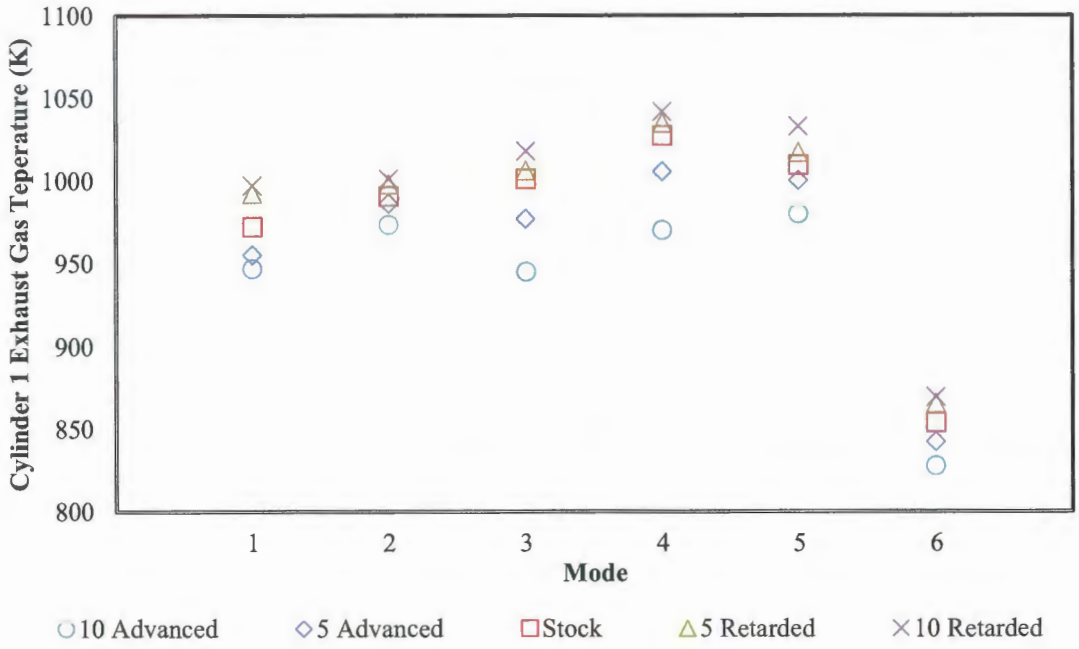

Figure 8.25: Cylinder 1 exhaust gas temperatures for 6-Mode camshaft staging tests

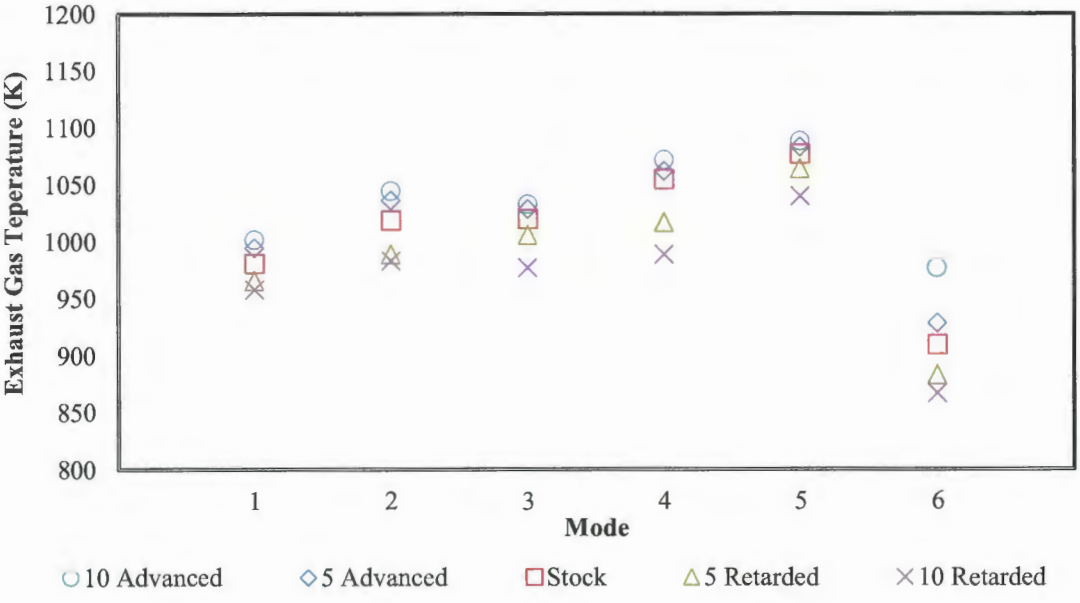

Figure 8.26: Cylinder 2 exhaust gas temperatures for 6-Mode camshaft staging tests

The fuel conversion efficiency of an engine represents the amount of fuel energy that is converted into energy output. It is defined by Equation 8.1 as the power output by the engine divided by the product of the mass flow rate of fuel and the lower heating value of the fuel.

$$\eta_f = \frac{P}{\dot{m}_f Q_{LHV}} \tag{8.1}$$

Because the engine is operated rich, not all the energy supplied is released. Because there is a lack of oxygen available to oxidize the fuel, the combustion efficiency of the engine is less than 1. The combustion efficiency of an engine can be defined as the sum of the enthalpies of the reactants (H_R, referenced at the ambient temperature) minus the sum of the enthalpies of the products (H_P, referenced at exhaust temperature) divided by the product of the mass flow rate of fuel and the lower heating value of the fuel, Equation 8.2. This will be discussed in greater detail later.

$$\eta_c = \left[\frac{\sum_R n_i \overline{h_f^o} - \sum_P n_i \overline{h_f^o}}{(LHV)_f (MW)_f}\right] \tag{8.2}$$

From a first law perspective, as the air to fuel ratio decreases the combustion efficiency decreases, thereby reducing the amount of energy available to be converted into useful work, observed in Table 8.9 and Figure 8.27. However, as witnessed in Table 8.10 and Figure 8.28, the fuel conversion efficiency of the engine increases as the camshaft is staged. Even though the engine is operating slightly more rich under these conditions, it is not enough to offset the increase of charge being inducted to the engine and the increase in power output offsets this phenomena. Keep in mind that as the combustion efficiency decreases the amount of chemical energy that leaves via the exhaust increases. This has an impact on emissions and effects the energy distribution,

discussed in a subsequent section. A reduction in combustion efficiency is an undesired effect.

Table 8.9: Combustion efficiency for 6-Mode camshaft staging tests

	Combustion Efficiency (%)				
	10 Advanced	5 Advanced	Stock	5 Retarded	10 Retarded
Mode 1	72.44	71.76	71.58	70.66	70.25
Mode 2	76.70	75.88	75.10	74.05	73.09
Mode 3	82.60	81.13	79.40	78.53	78.16
Mode 4	82.28	81.41	81.04	79.08	77.29
Mode 5	90.92	88.17	88.50	86.53	84.20
Mode 6	90.14	91.42	89.32	88.17	88.27

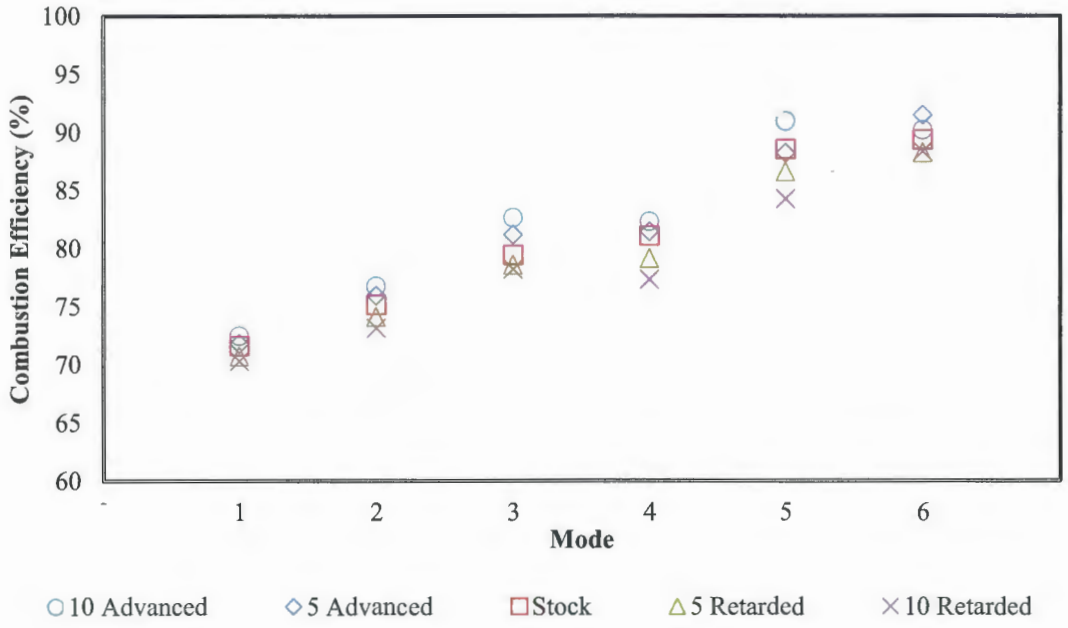

Figure 8.27: Combustion efficiency for 6-Mode camshaft staging tests

Table 8.10: Fuel conversion efficiency for 6-Mode camshaft staging tests

	Fuel Conversion Efficiency (%)				
	10 Advanced	5 Advanced	Stock	5 Retarded	10 Retarded
Mode 1	19.72	19.79	19.88	20.36	20.92
Mode 2	18.97	19.27	19.58	19.05	19.10
Mode 3	17.76	18.05	16.91	17.46	17.01
Mode 4	13.17	13.36	11.91	12.96	13.31
Mode 5	4.10	4.30	4.19	4.45	4.41
Mode 6	7.30	6.81	5.64	5.11	5.23

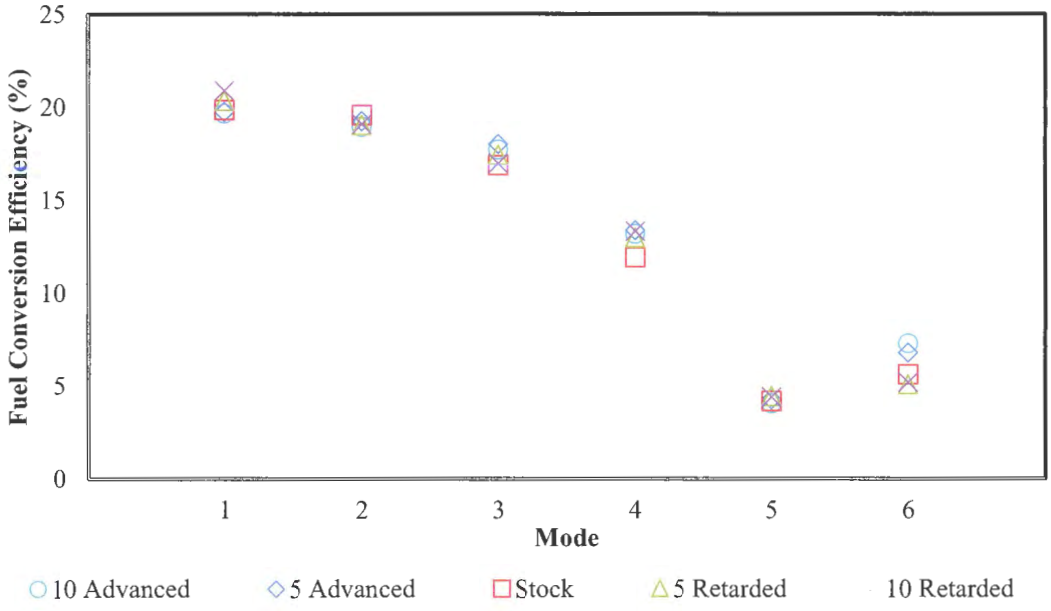

Figure 8.28: Fuel conversion efficiency for 6-Mode camshaft staging tests

Another measure of engine performance is the specific fuel consumption (sfc). It measures how efficiently an engine is using the fuel supplied to produce work [2]. Specific fuel consumption is calculated as the mass flow rate of fuel per unit power output, Equation 8.3.

$$\text{sfc} = \frac{\dot{m}_f}{P} \frac{(g/s)}{(kW)} \tag{8.3}$$

By using a power value measured at the output shaft of the engine, a brake specific fuel consumption term can be used (brake power is the usable power delivered to the load and accounts for all internal engine losses). Heywood [2] states that best values of sfc are about 270(g/kW*hr). The lower the value of sfc, the more efficiently the engine is utilizing the fuel. It can be seen in Table 8.11 and Figure 8.29 that the best case bsfc for mode 1 (high speed high load) occurs at a camshaft staging of 10 crank angle degrees retarded; a value of 398.4 (g/kW*hr), that is a 5 % improvement (or decrease) from the stock value. In general, for the high speed set points (mode 1 through mode 5) the bsfc decreases as the camshaft is staged from advanced to retarded timings. Again, at these lower load set points the engine is becoming more throttled and the amount of chemical energy entering the cylinder is reduced. A greater portion of the energy is used to overcome the losses due to friction at this point and less is used to provide power to the output shaft. Therefore, the power output is low for the amount of fuel consumed.

It can be noted that the dispersion of bsfc between the 10 crank angle degree advanced and 10 crank angle degree retarded camshaft timings increases as the modes progress. That is the difference between the high and low bsfc for mode 1 is 6%, while it is almost 28.3% at mode 6. The adjusting of valve events has a much greater effect on the low load set points, particularly the advanced timings. A contributing factor to this decrease in performance is the excess residuals remaining in the combustion chamber from cycle to cycle. This can be seen in the pressure rise of the intake manifold pressure as the intake valve opens in Figure 8.21 above.

Table 8.11: Brake specific fuel consumption for 6-Mode camshaft staging tests

	Brake Specific Fuel Consumption (g/kW*hr)				
	10 Advanced	5 Advanced	Stock	5 Retarded	10 Retarded
Mode 1	422.5	421.0	419.0	409.3	398.3
Mode 2	439.2	432.3	425.4	437.2	436.1
Mode 3	469.2	461.5	492.5	477.1	489.7
Mode 4	632.8	623.7	699.5	642.7	625.9
Mode 5	2033.2	1936.5	1988.6	1873.1	1888.7
Mode 6	1141.3	1223.7	1477.3	1629.6	1592.7

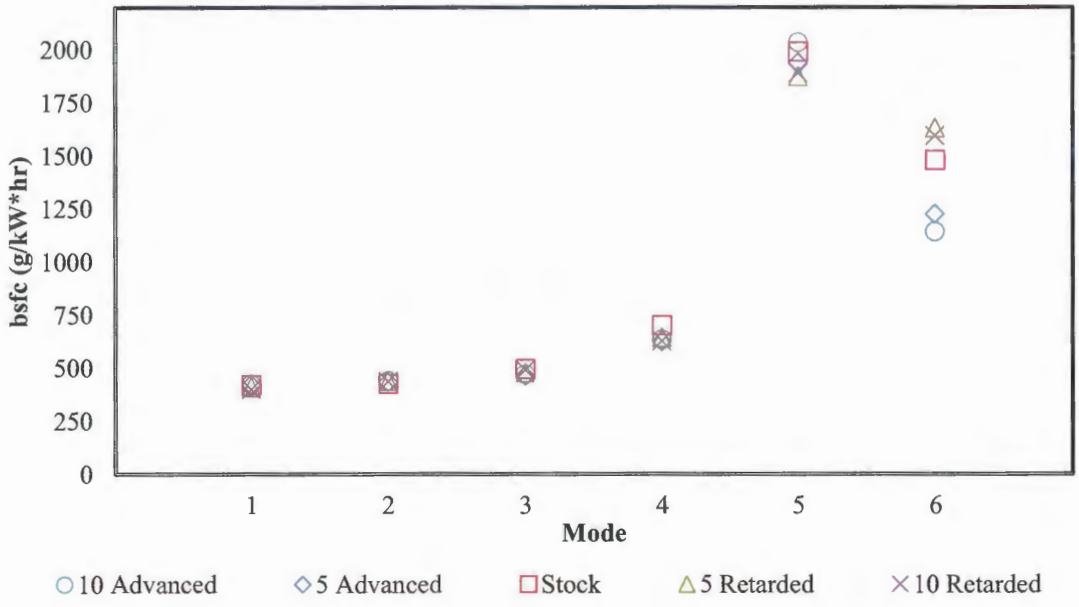

Figure 8.29: Brake specific fuel consumption for 6-Mode camshaft staging tests

The last comparison to be made in this section is the volumetric efficiency between the wide open throttle set point (mode 1) of the camshaft staging tests. Volumetric efficiency provides a means by which to measure the effectiveness of an engine's induction process. It is defined as the volume flow rate of air into the intake system divided by the rate at which the volume is displaced by the piston [2]. Some of

the key parameters that affect an engine's volumetric efficiency are engine speed, fuel characteristics, intake mixture temperature, engine compression ratio, ratio of exhaust to inlet manifold pressure, the design of the intake and manifold ports, the intake and exhaust valve geometry, size, lift characteristics and timings. Within the context of this experimental work, volumetric efficiency will be considered at the highest speed set point (3060 RPM). The only parameter that can be adjusted is the timing of the valve events.

The air to fuel ratio is governed by the carburetor as discussed above and cannot be easily adjusted. The compression ratio requires a change in engine geometry (either the clearance volume or the displacement volume). A redesigned head would be required to alter the valve geometry and valve lift is controlled by the shape of the camshaft lobes and will not be considered for the experimental portion of this work.

Table 8.12 displays the volumetric efficiency calculated with the experimental data for mode 1 of the camshaft staging tests. The increase in volumetric efficiency of 5.5% from 10 crank angle degrees advanced to 10 crank angle degrees retarded is a direct consequence of the ram effect. For low speed, wide open throttle operation, this trend would reverse itself, as backflow into the intake manifold would be detrimental to the volumetric efficiency. One would expect that an increase in valve lift would, if only marginally, increase the high speed volumetric efficiency by allowing the intake valve to remain at the maximum flow area longer (taking into account a restriction due to the port). This is supported by results obtained in steady state flow bench testing. After the valve lift is sufficient enough to create a valve curtain area greater than that of the port cross sectional area, the flow does not increase appreciably. For example, increasing the valve lift from 7.3 mm to 8.3 mm correlates to an increase of air mass flow rate of 0.0296

kg/s to 0.0304 kg/s (an increase of 2.6%). However, while at a valve curtain area less than that of the port cross sectional area an increase in valve lift from 3.1 mm to 4.2 mm correlates to an increase in air mass flow rate of 0.0181 kg/s to 0.0230 kg/s (an increase of 21%).

Also, an increase in valve diameter would aid to increase volumetric efficiency by increasing the flow area available to the cylinder earlier in the induction process. This is supported by the high Mach number that is observed in the steady state flow testing conducted and discussed in Chapter 5.

Table 8.12: Volumetric efficiency comparison for mode 1 of camshaft the staging tests

Volumetric Efficiency (%)	
10 Advanced	77.2
5 Advanced	78.7
Stock	79.4
5 Retarded	80.6
10 Retarded	81.7

The parameters discussed in this section depict some advantages and disadvantages to the advanced and retarded camshaft staging tests. As well as provide trends that exist between the different valve timing locations. By selecting key set points, an engine can be designed to maximize operating efficiency.

8.2.4 Performance of Modified Cylinder Heads for Camshaft Staging Tests.

The modified cylinder heads were tested for each camshaft staging test to determine the improvements in air flow realized due to the modifications made in the port with a shift in valve timing. Table 8.13 and Table 8.14 show the comparisons of the stock and modified heads for the camshaft staging tests of 10 crank angle degrees advanced and 10

crank angle degrees retarded respectively. Table 7.3 in the previous chapter contains the stock camshaft comparisons.

Table 8.13: Comparison of stock and modified heads for the camshaft staging test of 10 crank angle degrees advanced

	Engine Air Mass Flow Rate (kg/s)					
Mode	1	2	3	4	5	6
Modified Heads	0.0205	0.0171	0.0129	0.0099	0.0088	0.0044
Stock Heads	0.0197	0.0164	0.0123	0.0094	0.0084	0.0041
% Increase	3.9%	4.1%	4.7%	5.1%	4.5%	6.8%

It can be seen that by advancing the intake valve opening 10 crank angle degrees the flow rate of the modified head increases appreciably. This result was not realized for the stock camshaft staging test. The increase in cross sectional flow area created by opening the valve earlier allows for the flow to take advantage of the improvements made to the port. Table 8.13 makes a comparison for the camshaft staging test of 10 crank angle degrees retarded.

Table 8.14: Comparison of stock and modified heads for the camshaft staging test of 10 crank angle degrees retarded

	Engine Air Mass Flow Rate (kg/s)					
Mode	1	2	3	4	5	6
Modified Heads	0.0212	0.0181	0.0143	0.0112	0.0098	0.0040
Stock Heads	0.0209	0.0178	0.0139	0.0107	0.0094	0.0038
% Increase	1.4%	1.7%	2.8%	4.5%	4.1%	5.0%

The improvements in air flow realized under the camshaft staging test of 10 crank angle degrees retarded are not as noticeable as those of the advanced camshaft staging

test for the high load set points. Due to the fact that the valve is opening later the cross sectional flow area is smaller during the higher piston speeds. However, the increase in manifold vacuum may make up for this slightly as the improvement for this test was greater than what was observed in the stock camshaft timing test.

8.3 FIRST LAW ENERGY BALANCE

A First Law energy balance provides a useful tool that can be used to determine how and in what quantity energy is being distributed throughout the engine. Energy arrives to the engine in one form: fuel energy. The amount of fuel introduced into the system determines the maximum output the system can achieve at any given time. Once the energy enters the engine, it can leave in several different forms: brake power, sensible exhaust energy, convective energy, and chemical exhaust energy. By observing the law of conservation of energy, the sum of these energy forms must be equal to the fuel energy input. A discussion of each energy form will be presented below along with a comparison of the calculated results of each 6-Mode camshaft staging test.

Many of the input parameters required to perform the First Law energy balance were discussed in the previous section. They are: speed, brake power, air temperature, exhaust temperature, fuel flow rate, air flow rate, air to fuel ratio, and the chemical properties of the fuel. Additionally, the enthalpy of formation of the reactants and products must be obtained at their respective temperatures.

8.3.1 Combustion Stoichiometry. Emissions data were not collected throughout these tests, it is, therefore, difficult to prove an exact energy balance without making some prior assumptions. First, it is known, that within the operating conditions of this test engine, or most carbureted engines for that matter, that the fuel and air mixture being

inducted by the engine is rich. Again, that means there is more fuel then there is available oxygen to oxidize it. So, the first assumption made is that there is no oxygen in the exhaust products. The second assumption is that there is some excess of CO and H_2 present (these are products of incomplete combustion). Also, a reasonable assumption is that there are one-third as many hydrogen molecules as that of carbon monoxide (i.e. $CO=1/3H_2$).

To prove these assumptions are reasonable, a calculation was done where the a priori assumptions were compared to the results of an emissions analysis done by Wildhaber [20] on the same test engine. The energy balance results (sensible energy lost, convective energy, and exhaust chemical energy) compared to within 5% between the two tests. Therefore, the calculated results using the aforementioned assumptions should provide reasonable approximations of emissions of CO and CO_2. However, unburned hydrocarbons (uHC) and NO_x emissions cannot be obtained. The calculations of sensible exhaust energy and chemical exhaust energy should also be accurate.

The global reaction is shown below, Equation 8.4, where the left hand side of the equation accounts for the reactants, that is, the fuel (C_xH_y) and the air (O_2 and N_2). The right hand side of the equation is made of the molecules that are present in the exhaust gas.

$$C_xH_y + a(O_2 + 3.76N_2) = bCO_2 + cCO + dH_2O + eH_2 + fN_2 \qquad (8.4)$$

The coefficients can be calculated by balancing both sides of Equation 8.4. The coefficients associated with the fuel, x and y, are found by assuming a ratio of Hydrogen to Carbon to be 1.87. The coefficient, a, is determined by the air to fuel ratio. Keeping with the second assumption made earlier, the coefficient of H_2, e, can be substituted with

1/3c (the coefficient associated with CO). Equation 8.4 can then be balanced by reducing to four equations (one each for carbon, hydrogen, oxygen and nitrogen) and four unknowns (b, c, d, f). It should be noted that the value of the coefficient 'a' and likewise the coefficients of the products will change with the air to fuel ratio, which is discussed in more detail in a subsequent section.

8.3.2 Energy Pathways. The incoming fuel energy is initially divided up two ways after the combustion process. The energy supplied will either be released during combustion or the alternative, not released. The released energy can then continue down three separate avenues: brake power, sensible exhaust energy, and convective heat transfer. The energy that is not released, coined chemical exhaust energy, is a product of incomplete combustion. The way these pathways split is determined by the air to fuel ratio of the engine. An energy flow diagram can be seen in Figure 8.30, which depicts typical energy flow paths for an internal combustion engine.

Sensible energy and chemical energy do not produce any usable power. Similarly, the convective heat transfer does not provide any useful work. The determination of convective energy flow is made possible with the knowledge that it and brake power are the only energy forms supplied by the chemical energy released during combustion [20].

The effect of staging the camshaft on air to fuel ratio was discussed earlier. As the air to fuel mixture becomes richer the amount of chemical exhaust energy will increase. With a higher combustion inefficiency the temperatures of the combustion process will decrease, therefore, the amount of energy lost to convective heat transfer will decrease. These effects will change the distribution of energy as depicted in Figure 8.30.

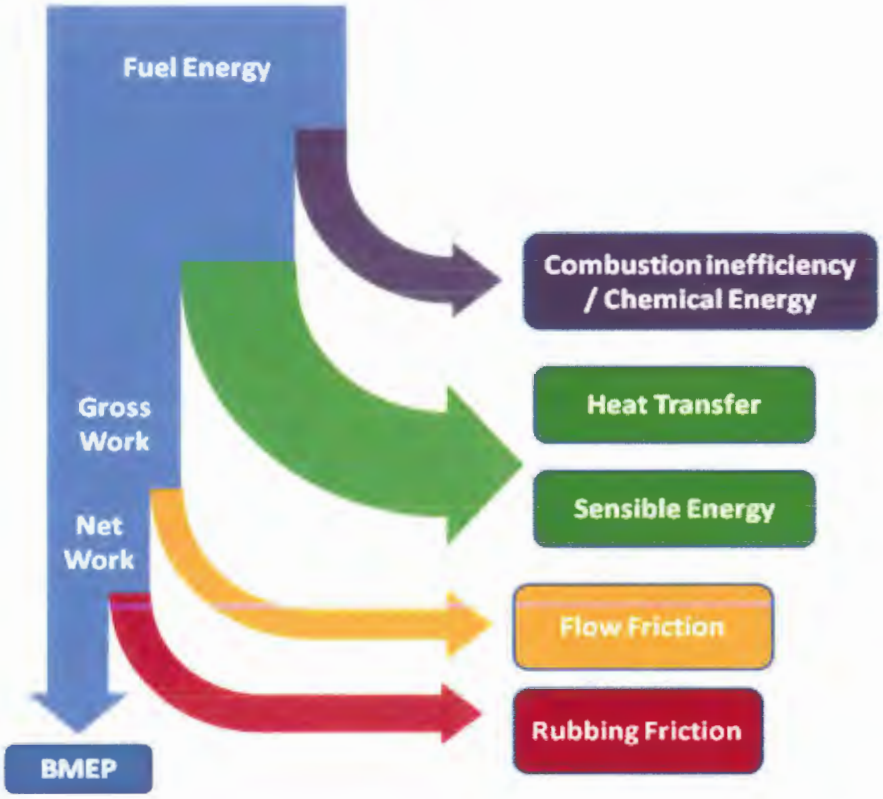

Figure 8.30: Typical energy pathways for an internal combustion engine

8.3.3 Energy Balance Calculations. The energy flow rate into the engine is known by the mass flow rate of fuel and the lower heating value associated with that fuel. The brake power of the engine is measured through the dynamometer, therefore, the amount of fuel used to provide the useful work is known. Sensible exhaust energy lost can be calculated by the sum of the individual enthalpies of the exhaust gas products (on a molar basis) taken at the temperature of the exhaust gas. The loss due to heat transfer is calculated by finding the sum of the enthalpies of the products, as calculated previously, minus the sum of the enthalpies of the reactants, plus the energy due to the brake power.

To determine the chemical exhaust energy, a combustion efficiency term must be calculated (since the mixture is rich all of the energy contained in the fuel will not be released this number will always be less than 1). The combustion efficiency is calculated as the enthalpy of the fuel (referenced at the ambient temperature) minus the contribution of each applicable species in the products, shown earlier in Equation 8.2. That is, those species that contain either a carbon or an oxygen molecule (CO_2, CO, and H_2O). That quantity is divided by the product of the lower heating value of the fuel and the molecular weight of the fuel to obtain a dimensionless efficiency term. The chemical energy, Equation 8.5, is then calculated by the quantity of one minus the combustion efficiency multiplied by the fuel energy input.

$$\dot{E}_{chem} = (1 - \eta_c)(\dot{m}_f)(LHV) \tag{8.5}$$

The energy balance can then be calculated by summing the energy values, and checked by comparing it to the energy supplied,

$$\dot{E}_{fuel} = \dot{W}_b - \dot{Q}_{conv} + \dot{E}_{sens} + \dot{E}_{chem} \tag{8.6}$$

The values of the right hand side of the equation should be very close to that of the left hand side, save for the errors due to rounding the numbers.

8.3.4 Energy Balance Results Between Camshaft Staging Tests. The results obtained through the energy balance calculations are displayed below. Comparisons can be made between each mode of the camshaft staging tests. The distribution of energy, as well as the amount of CO and CO_2 emissions, with respect to camshaft staging tests, will be discussed.

Figure 8.30 to Figure 8.32 represent the distribution of energy for the 6-Mode data for three of the five camshaft staging tests; 10 crank angle degrees advanced, stock,

and 10 crank angle degrees retarded respectively. Those of 5 crank angle degrees advance and 5 crank angle degrees retarded fall in line with the other tests and can be seen in Appendix A, Figures A.5 and A.6. The overall trends in the distribution of energy remain consistent through the 6-Mode data for the camshaft staging tests. However, the actual break down of the percentages does change between tests.

Starting with Figure 8.31, (a camshaft setting of 10 crank angle degrees advanced) it can be seen that 19.68% of the fuel energy supplied is converted into useable power output at the crankshaft. As the load is decreased, the contribution of the brake power decreases. The energy lost to convective heat transfer for mode 1 accounts for 30.55% of the total fuel energy supplied. The contribution increases progressing through the modes, as load is decreased the combustion duration becomes greater, providing more time for convective heat transfer to the cylinder walls. For the low speed set point, the majority of the energy (more than 60%) leaves through convective heat transfer; the burned charge spends more time in the cylinder which, again, allows for more time available for convective heat transfer to occur. The contribution of convective heat transfer decreases slightly as the camshaft is retarded due to lower combustion temperatures; this can also be seen in the decrease of the exhaust gas temperatures as discussed earlier.

It can also be noticed for mode 1, that the chemical exhaust energy makes up 27% of the fuel energy supplied. This increases as the camshaft is retarded to nearly 30%. Again, this chemical energy is the unreleased fuel energy (unburned fuel) and is a product of the engine's air to fuel ratio.

As the camshaft is retarded, the distribution of the energy begins to change slightly (comparing Figure 8.31 to the next camshaft staging tests). Keep in mind that the

amount of energy supplied is increasing as well, see Table 8.6. As the camshaft becomes more retarded, the energy contribution of brake power is increasing and the convective heat transfer is decreasing. But, those two shifts are also associated with an increase in chemical exhaust energy and an increase in sensible exhaust energy

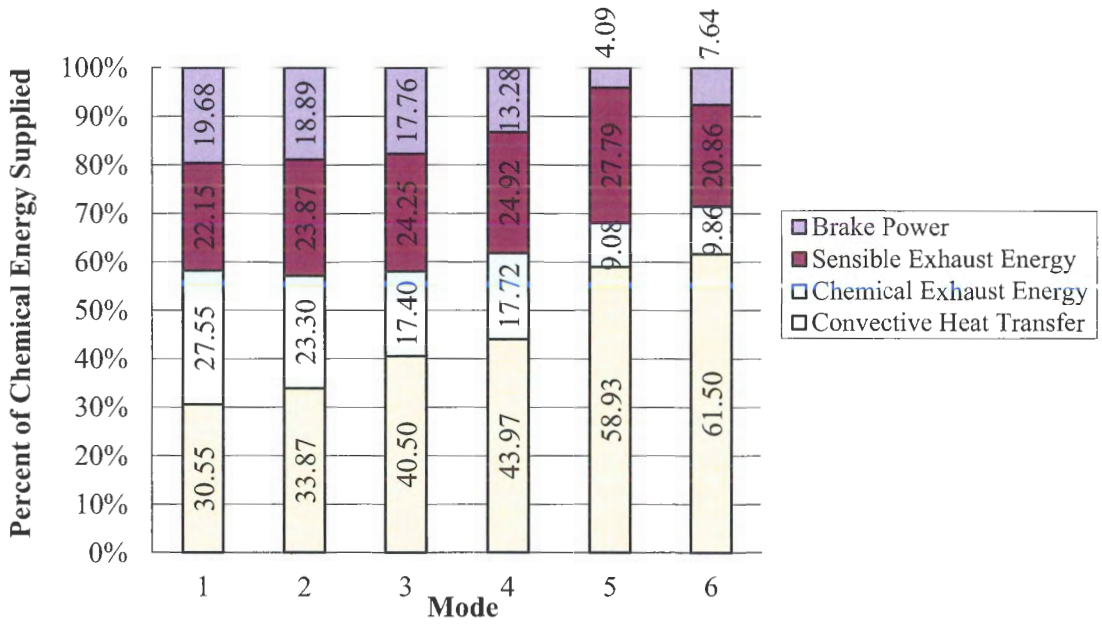

Figure 8.31: 6-Mode energy distribution for camshaft staging of 10 degrees advanced

. Examining the distribution of energy throughout the different modes and various camshaft tests provides insight on how the changes discussed in the previous section are taking place. That is, if the timing of valve events are altered, what effects will manifest themselves in the distribution of the energy pathways due to the amount of chemical energy introduced into the system.

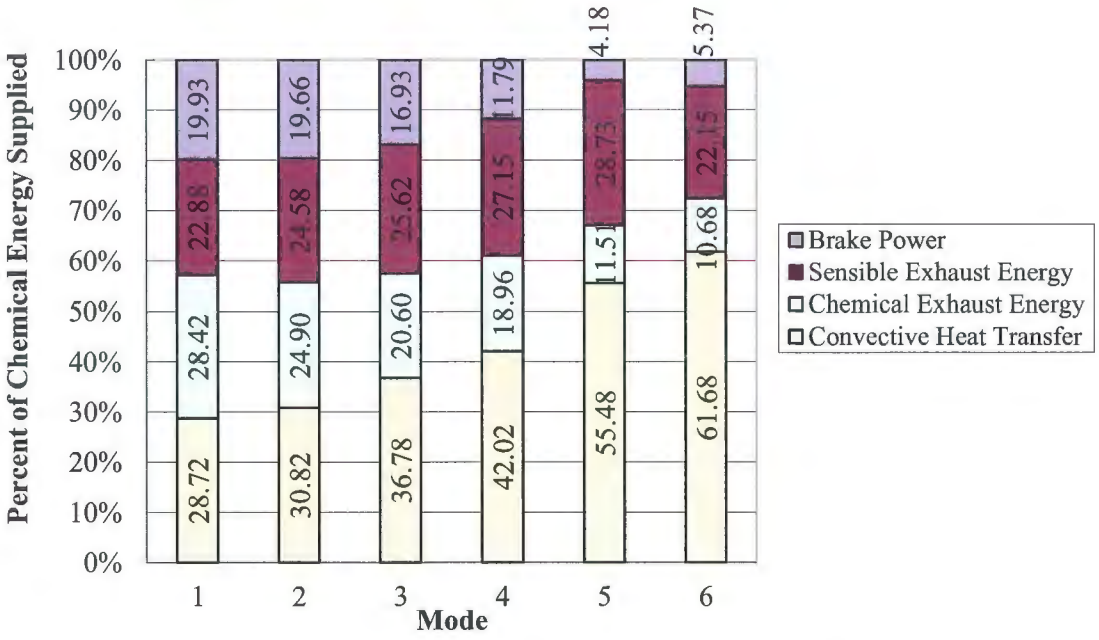

Figure 8.32: 6-Mode energy distribution for the stock camshaft setting

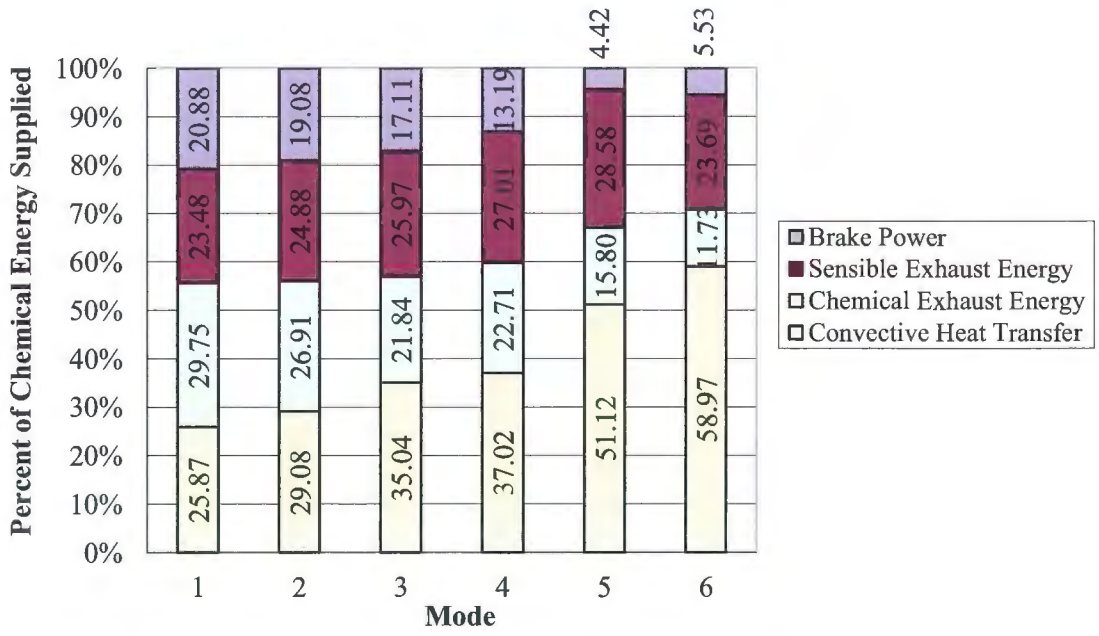

Figure 8.33: 6-Mode energy distribution for camshaft staging of 10 degrees retarded

An energy distribution comparison between the camshaft staging tests at the same operating modes is shown below for the mode 1 and idle set points Figure 8.34 and Figure 8.35 respectively. The other high speed mode set points follow the same trends as those of mode 1 and can be observed in Appendix A, Figures A.7 through A.10. The left axis provides a scale for the different energy pathways, while the right axis represents the fuel energy supplied to the system. Again, the sum of the energy from the different pathways should be equivalent to the energy supplied. The trends that were discussed above, with regards to the energy distribution at different modes, remain the same for the proceeding plots. That is, the brake power, sensible exhaust energy lost, and exhaust chemical energy increase as the camshaft is retarded, while the convective energy decreases as the camshaft is retarded.

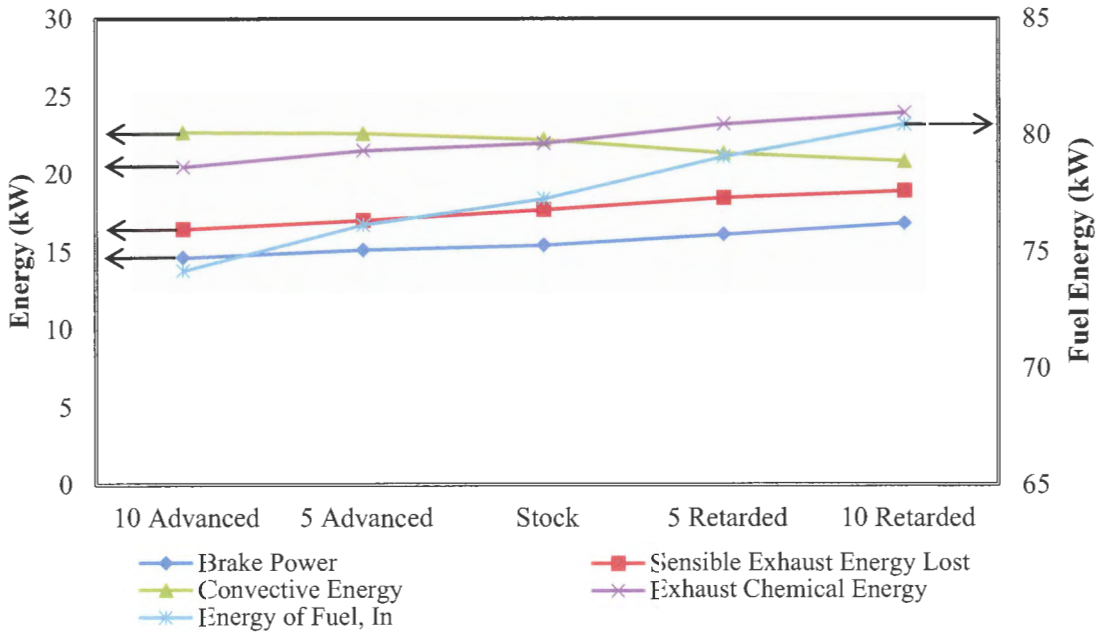

Figure 8.34: Mode 1 comparison of energy for camshaft staging tests

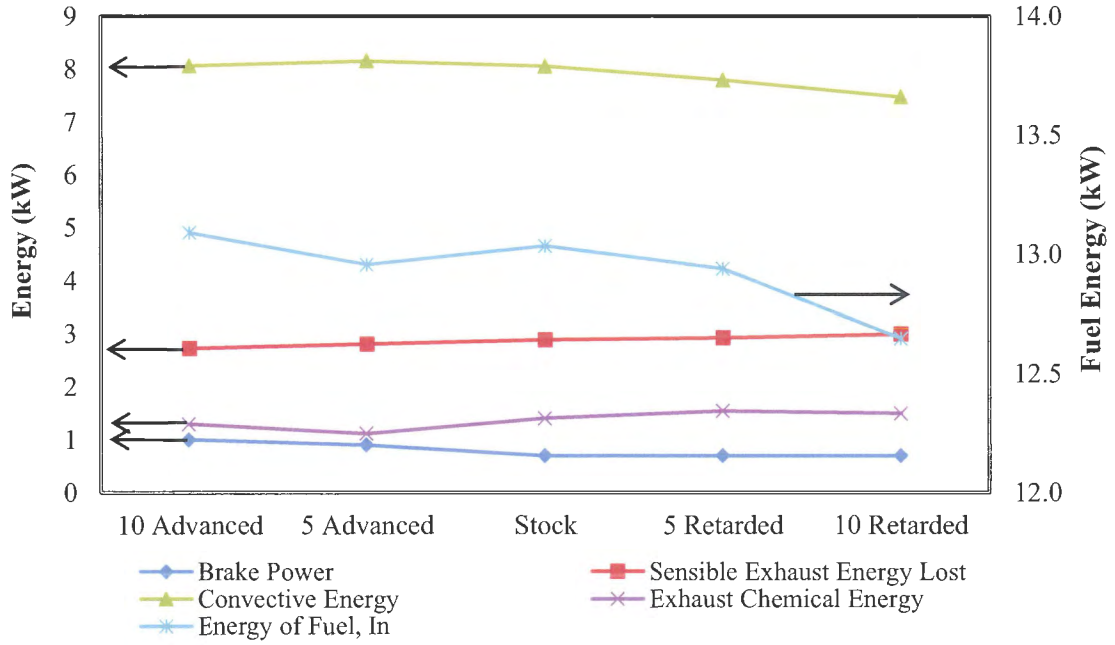

Figure 8.35: Mode 6 comparison of energy for camshaft staging tests

By retarding the camshaft there is an increase in mass flow rate of air, and subsequently, an increase in the mass flow rate of fuel. This increase of flow into the cylinder is directly attributed to the ram effect. Also, by retarding the camshaft the intake manifold pressure dips lower than that of the advanced camshaft, increasing the charge density within the cylinder. By retarding the camshaft the brake power increases as well as the sensible exhaust energy and the chemical exhaust energy. The convective energy decreases as the camshaft is retarded. This is connected to a decrease in air to fuel ratio; as the mixture becomes more rich, combustion temperatures decrease and the amount of heat available for convective heat transfer decreases. The pumping work required of the engine decreases as the camshaft is advanced. The effects of intake valve closing and exhaust valve opening have the greatest effects on the changes in energy distribution.

The camshaft staging tests provide great insight on the consequences of adjusting valve events under various operating conditions. It is, however, limited to the static relationship of the camshaft itself. That is, it is not possible to alter individual valve events in relation to the others. Again, while cutting new camshafts for experimental testing is a viable option, a more simple solution would be to use an engine simulation to assist in the prediction of the performance trends that can be expected when altering individual valve events to their optimum position.

9. ENGINE SIMULATION PROGRAM

9.1 INTRODUCTION TO THE ENGINE SIMULATION PROGRAM

The Stanford Engine Simulation Program (ESP), developed by W.C. Reynolds and expanded upon in collaboration with John Lumley [5], is a comprehensive engine model that simulates the effect of various operating parameters on engine performance. Engine characteristics, such as different speed effects, manifold geometries, valve size and geometry, camshaft profiles, combustion properties, etc., can be altered. The program is capable of outputting parameters such as calculated cylinder pressure data with respect to crank angle degrees, calculated energy flow rates, and calculated mass flow rates among others. Lumley [5] states that parameters can be adjusted to get reasonable agreement with actual engine data, and the model can then be used to study the effects of the proposed design changes.

9.1.1 ESP Governing Models and Assumptions. It is important for an engine model to be able to predict, with sufficient accuracy, what is occurring at the entrance and exit of the cylinder, as well as, what is occurring within the cylinder. The Stanford model uses ordinary differential equations derived from first law energy principles, such as mass and energy balance, a turbulence model equation to describe the turbulence of a fluid, and various algebraic equations to relate the variables.

The geometry of the engine must be initially specified. Characteristics such as bore, stroke, connecting rod length, compression ratio, valve dimensions and lift, and valve timings are vitally important to the model's calculations. These parameters, relative to the test engine, have been discussed in prior sections.

A similar route, as described in Chapter 8, was used to calculate the thermodynamic state of the cylinder contents. The assumption of thermodynamic equilibrium is assumed and dissociation is considered. To assist in the speed of the calculations the enthalpy of formation for the reactants and products is assumed to occur at a fixed pressure; approximately 200 kPa for the reactants and 600 kPa for the products. It is known that these values are a weak function of pressure and a much stronger function of temperature.

Air flow through the manifolds and into the cylinder is calculated in a similar way as that of the flow and discharge coefficient testing discussed earlier. That is, isentropic compressible flow theory is employed and modified with a discharge coefficient for the intake system. Intake and exhaust pressures are specified for a given test. The intake pressure, similar to the real engine tests, determines how throttled the engine is. Intake pressure is specified as the cylinder pressure at BDC of the induction stroke (comparable to where the experimental data is referenced). Backflow from the cylinder to the intake manifold and from the exhaust manifold to the cylinder is considered when the pressure differential between the cylinder and the manifold allows it. However, an assumption is made that the exhaust gas and therefore the backflow of gas out of the exhaust manifold is assumed to be homogeneous. In the case of backflow from the cylinder to the intake manifold, it is assumed that the fresh charge does not mix with the backflow gas.

The user of the model specifics an ignition timing for the test, this provides another parameter that can be adjusted to alter engine performance. A two zone combustion model is utilized. That is, at any given point in the combustion process the cylinder is split into a burned zone and an unburned zone. A turbulence velocity, laminar

flame speed, and flame propagation area are used to determine the burn rate of the mixture. The model considers heat transfer between the in-cylinder charge and the cylinder walls based on a user specified Stanton number.

There are four stages of calculation for the model, they are: compression, combustion (burn), expansion, and the gas exchange. It is assumed that the compression stroke begins when the intake valve closes and ends at the specified time of ignition. The process of expansion begins after the burn stage is complete and ends when the exhaust valve is specified to open. Lastly, the gas exchange process is defined throughout the valve open period. That is, the gas exchange process begins when the exhaust valve is opened and ends when the intake valve is closed. The calculation is achieved by employing a second order Runge-Kutta method with the time step equal to one crank angle degree. Once convergence of the cycle is reached a final cycle is computed and the output parameters can be observed.

9.1.2. ESP Model Limitations. The Stanford Model has certain limitations and weaknesses associated with it. Other industrial engine codes generally use more powerful integration techniques to perform the required calculations. While most codes do not incorporate the same turbulence model as that of ESP, they are capable of performing a chemical calculation for every time step and contain more accurate flame geometry models. This increases the overall accuracy of the engine performance predictions made by the simulation.

Assumptions such as that of the enthalpies being taken at a fixed pressure, while reasonable, will impede on the final accuracy of the model when comparing to experimental results. The gas dynamic model is an unsteady, one dimensional

compressible flow model (similar to the equations used in the steady state flow bench testing) which itself has limited accuracy. The assumption of a homogenous charge is made to decrease the calculation complexity, but it will yield a slight error when comparing with results of experimental engine testing. Also, the model only takes into account a single cylinder of an engine and it is, therefore, impossible to determine the effects that additional cylinders would have on the performance of the first.

9.2 COMPARISON AND RESULTS OF SIMULATED DATA

The primary use for this model is to predict the trends and potential improvements that can be gained by adjusting individual valve events, a task that was not possible to achieve on the test engine. A secondary function of the model is to determine the effects that changing the flow conditions and intake geometry would have on the performance predictions of the simulation. This speaks to parameters that can potentially be adjusted to balance the cylinders. The engine model discussed above was initially set up so that the input parameters matched those of the stock test engine used in this study. Table B.1 in Appendix B provides a list and associated values for the parameters used in the simulation.

9.2.1 Comparison of Experimental and Simulated Data. The intake geometries of the two cylinders differ slightly as discussed in Chapter 4. It was discovered during flow and discharge coefficient testing, discussed in Chapter 5, that the flow conditions through the head differ between the two cylinders. It was also seen in Chapter 7 that the manifold pressures differ between the two cylinders under baseline engine testing. These characteristics were kept in mind when setting up the model for the two cylinders. Below, in Figure 9.1 and Figure 9.2, can be seen a comparison between the Stanford ESP and the

experimental data collected on the test engine. Figure 9.1 compares data of cylinder 1, while Figure 9.2 compares data of cylinder 2.

The pressure predictions of the model match reasonably well with the experimental data. A few differences are obvious, such as the pressure at the end of the expansion stroke. At this point, the simulated pressure deviates for both cylinders while some of the same phenomena are observed (the cylinder pressure dips at the end of the expansion stroke). The cylinder pressure at BDC of the induction stroke behaves differently between the simulation and the test data as well. Because of the way the calculations are performed, the pressure essentially comes to a point before the compression stroke begins; this can be seen in both cylinder 1 and cylinder 2 performance. The pressure during the compression stroke differs between the simulated and experimental data, particularly for cylinder 2.

Along with the variation in the discharge coefficient, the maximum flow area available to the valve can be adjusted to represent the restriction due to the port and throat. This was observed to have an effect on the magnitude of the pumping loops for both cylinder 1 and cylinder 2. Reducing the flow restriction incurred by the port area reduces the pressure drop during the intake stroke, while increasing the flow restriction increased that pressure drop, thereby increasing the pumping work required of the engine and reducing mass flow rate of air.

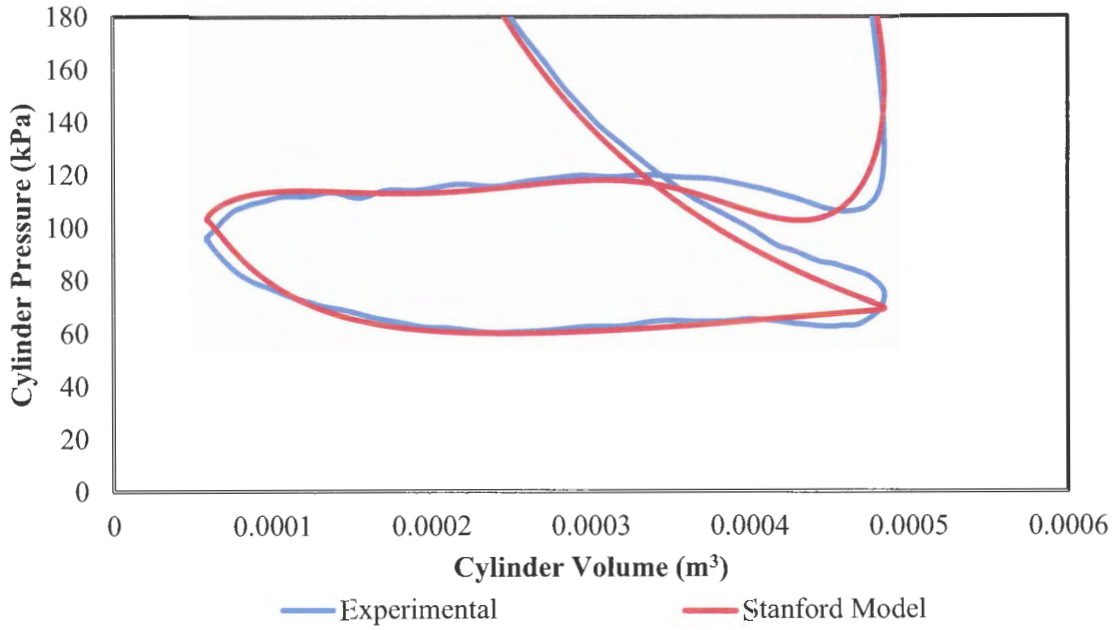

Figure 9.1: Comparison between experimental and simulated data of cylinder 1 mode 1

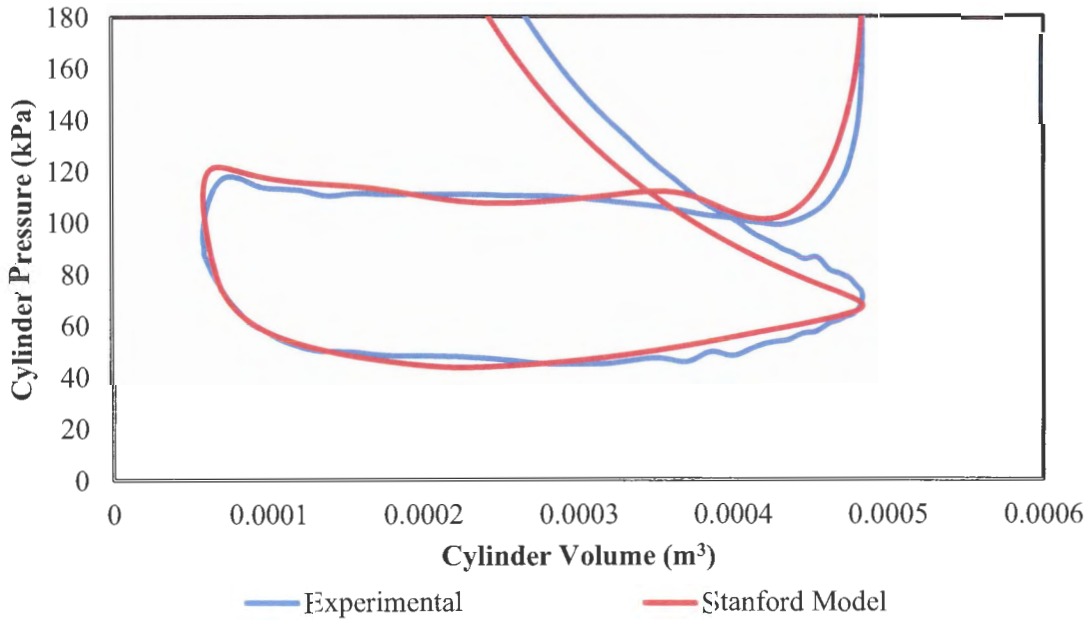

Figure 9.2: Comparison between experimental and simulated data of cylinder 2 mode 1

A second comparison that can be made between the simulation and the experimental data is that of mass flow rate of air inducted into the cylinder. The mass flow rates between the simulated and experimental data can be used to calculate a volumetric efficiency term (η_v). Volumetric efficiency is used to measure the effectiveness of an engine's induction process. It is a characteristic that is generally considered at unthrottled engine operating conditions. It is the air flow under these conditions that constrains maximum engine power. Volumetric efficiency is a function of air mass flow rate, air density, engine displacement volume, and engine speed. The displacement volume is equivalent for both scenarios and the density of air can be manipulated within the simulation to match experimental conditions. A difference between the simulated model and the experimental tests is the engine speed. For mode 1, of the 6-Mode test, the engine speed can vary by as much as ± 20 rpm, while the model can hold a constant speed. The simulated mass flow rate of air can be dependent on the coefficients of friction within the manifold, the restrictions due to the intake geometry, intake valve characteristics, (lift, duration, timing, etc.) and the manifold pressure defined within the model.

Table 9.1 provides a comparison of volumetric efficiency between a simulated stock test and three baseline experimental tests. Recall that volumetric efficiency accounts for both cylinders of the test engine. It is not possible within the realm of these experimental tests to separate the air flow into the respective cylinders. It can be observed that the simulated results match well with the experimental results. With air density and displacement volume held constant and matching the experimental speed as close as possible these results point to a similarity in mass flow rate of air.

Table 9.1: Volumetric efficiency comparison between simulated and experimental tests

Volumetric Efficiency Comparison		
	η_v	% Difference
Simulation	0.804	
Experimental-1	0.795	1.12%
Experimental-2	0.789	1.87%
Experimental-3	0.792	1.49%

A comparison between the pmep of the simulated data and the pmep of the experimental data can also be made. By examining Figure 9.1 and Figure 9.2, it can be seen that the shape of the pumping loops match reasonably well between the simulated and experimental tests. It is, therefore, reasonable to assume that the pumping work of the test would also be similar. Table 9.2 presents the calculated pumping mean effective pressure values for the simulated and experimental tests for both cylinders.

Table 9.2: Comparison of simulated and experimental pumping mean effective pressure

Pumping Mean Effective Pressure Comparison			
	Simulation	Experimental	**%Difference**
Cylinder 1	44.8	46.89	**4.5%**
Cylinder 2	60.18	64.31	**6.4%**

9.2.2 Camshaft Staging Simulation. Below, cylinder 1 and cylinder 2 pressure versus volume diagrams are plotted under three different simulated cases (10 crank angle degrees advanced, stock, and 10 crank angle degrees retarded) and compared to their experimental counterparts. A similar methodology as that of the experimental camshaft staging tests was used for the initial simulated tests. The simulation was run to model the stock engine and then four different camshaft staging scenarios, where all valve timings

were changed by the same amount. The camshaft staging tests consisted of four timings shifted away from the stock timing in different directions: retarded 10 crank angle degrees, retarded 5 crank angle degrees, advanced 5 crank angle degrees, and advanced 10 crank angle degrees. The various effects that these camshaft timings have on engine operation were discussed in great detail in Chapter 8.

Both pressure-volume diagrams are resolved to show strictly the pumping loop and the effects of the four valve events. Cylinder 1 results are plotted in Figure 9.3 and Cylinder 2 results are plotted in Figure 9.4.

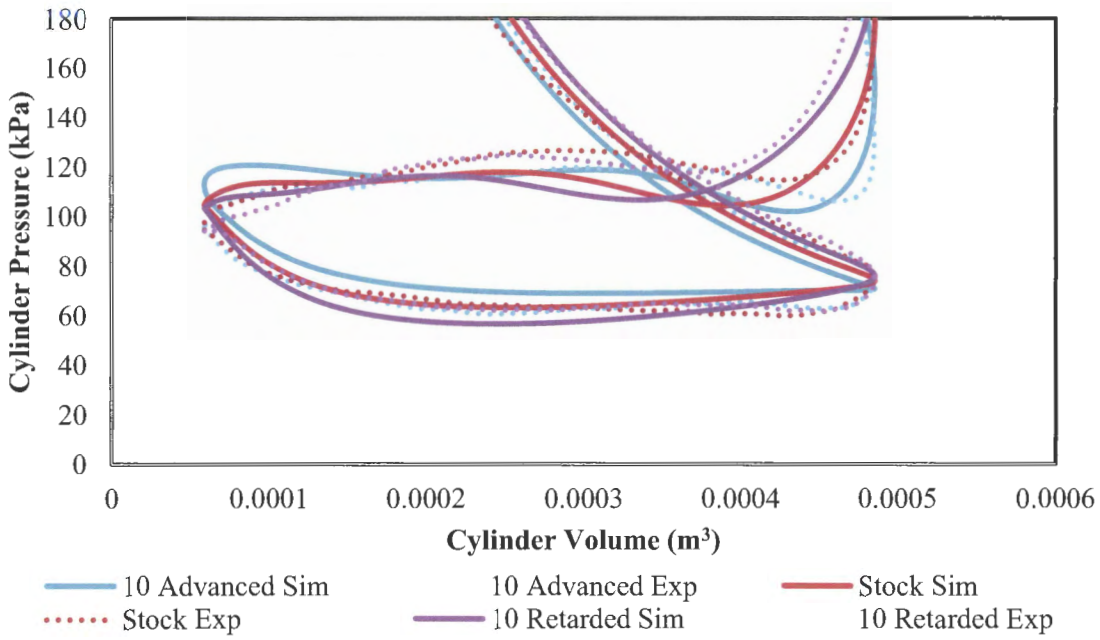

Figure 9.3: Simulated camshaft staging for cylinder 1

Similar results are observed between the camshaft staging tests of the experimental data and the simulated data; particularly those of EVO and IVC. The effects of retarding the exhaust valve closing event can be seen for cylinder 1 in the

simulated tests, where it could not be seen for the experimental tests. That is, there is a pressure rise at the end of the exhaust stroke for the advanced timings.

The simulated data for cylinder 2, Figure 9.4, follows with that of the experimental data as well with some minor discrepancies. At 10 crank angle degrees retarded the cylinder pressure during the valve overlap period decreases for the experimental data, while it remains around the exhaust manifold pressure in the simulation. The trend, due to the EVC event, is slightly more exaggerated for the simulated data then compared to the experimental data. The cylinder pressure during the compression stroke is much higher for the stock and retarded experimental data then for the simulated data.

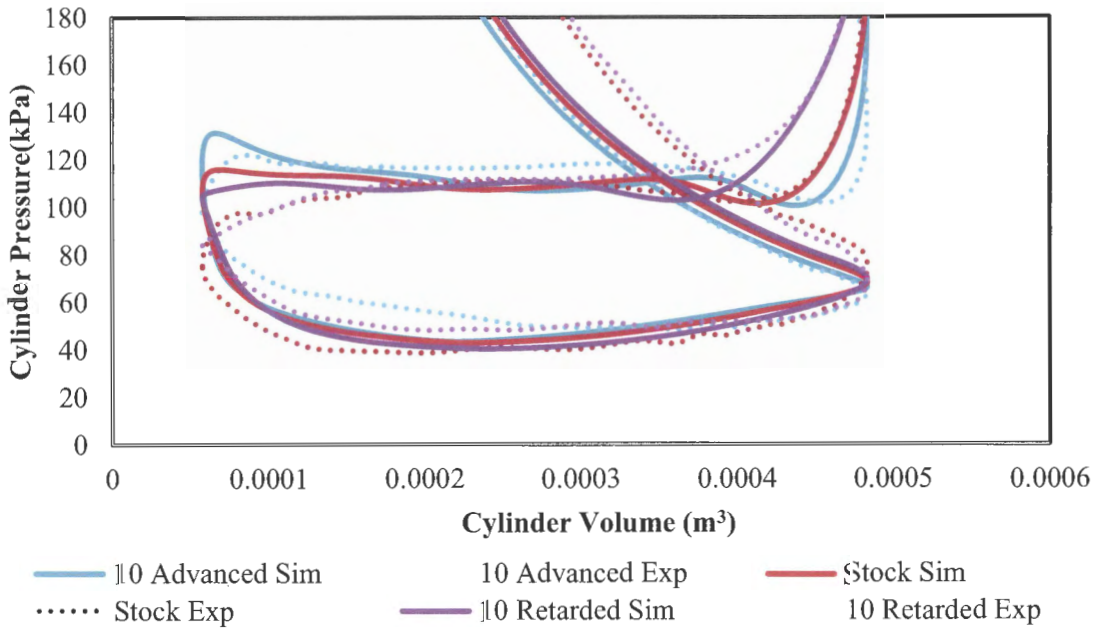

Figure 9.4: Camshaft staging for cylinder 2

Cylinder 2 was simulated under the same speed as cylinder 1. As stated previously, the test for cylinder 2 was run at a slightly lower intake pressure and a slightly higher exhaust pressure to stay consistent with the results obtained via experimental baseline tests. It should be mentioned, that no pressure data in the exhaust manifold was recorded experimentally. That being said, the exhaust pressure of the experimental tests was taken to be equivalent to the cylinder pressure during the middle of the exhaust stroke (for the baseline tests this value stays relatively constant at a pressure just above atmospheric pressure).

A volumetric efficiency comparison between camshaft staging tests can be made for the simulated results, similar to the comparison made at the end of Chapter 8. As can be seen, the model predicts that the volumetric efficiency of the engine increases as the camshaft is retarded.

Table 9.3: Volumetric efficiency comparison of simulated camshaft staging tests

	Volumetric Efficiency (%)
10Advanced	77.5
5Advanced	78.9
Stock	80.4
5Retarded	81.3
10Retarded	82.6

From the culmination of the experimental data and the preliminary simulation results, it can be concluded that simply staging the camshaft will not provide optimal performance. A new cam profile can be designed that advances the exhaust valve opening event, while slightly retarding the exhaust valve closing event; this will require a

longer exhaust valve open period. Minor alterations to the intake valve timings would be beneficial, such as retarding the intake valve closing event slightly.

9.2.3 The Variation of Individual Valve Events. Specific valve timings were analyzed by adjusting one and keeping the other three at the stock timing. The same procedure as stated above was used; that is, four valve timings were considered apart from the stock timing: 10 crank angle degrees retarded, 5 crank angle degrees retarded, 5 crank angle degrees advanced and 10 crank angle degrees advanced. Below, are the results for these simulations for cylinder 2 (similar results are observed for the simulation of cylinder 1). Exhaust valve opening event is represented in Figure 9.5, exhaust valve closing is shown in Figure 9.6, intake valve opening effects are depicted in Figure 9.7, and lastly the effects of intake valve closing are shown in Figure 9.8. Similar results in the individual valve timing tests were observed as those obtained through the camshaft staging tests.

From these simulation results, some preliminary conclusions can be drawn with regards to the valve timing of high speed performance. First, a more advanced exhaust valve open timing could be beneficial to reducing the exhaust pressure in the cylinder to that of the exhaust manifold, within a reasonable time frame. A slightly more retarded exhaust valve closing time could be used to reduce cylinder pressure at the end of the exhaust stroke (more analysis on exhaust back flow will be provided to support this claim). Intake valve opening and closing effects cannot be properly realized on these plots and would be better justified by mass flow rate plots.

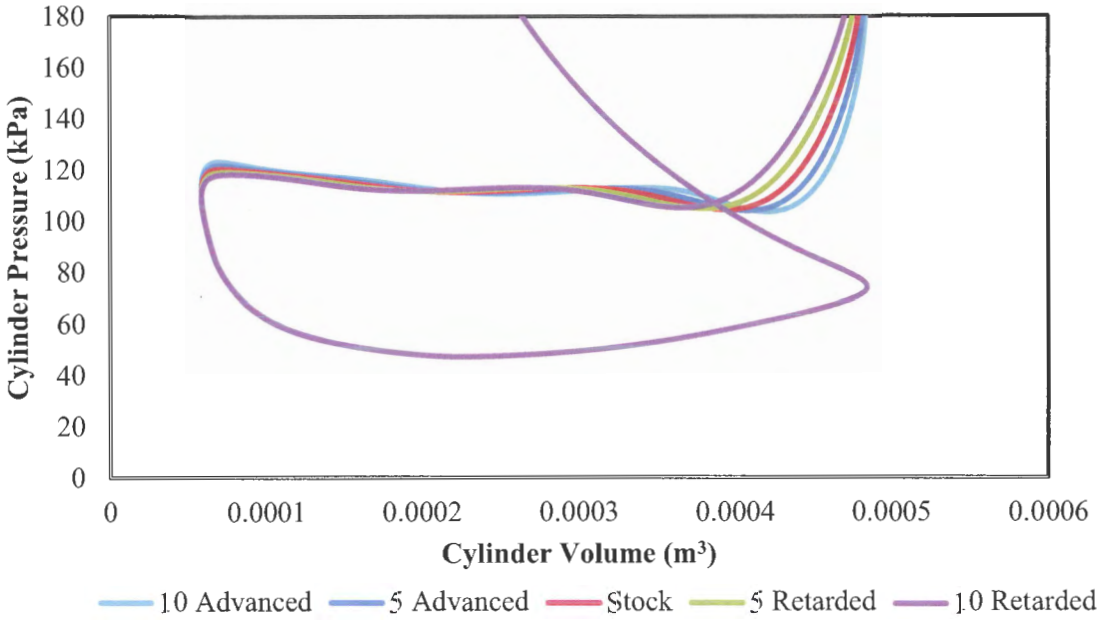

Figure 9.5: Staging of the exhaust valve opening event

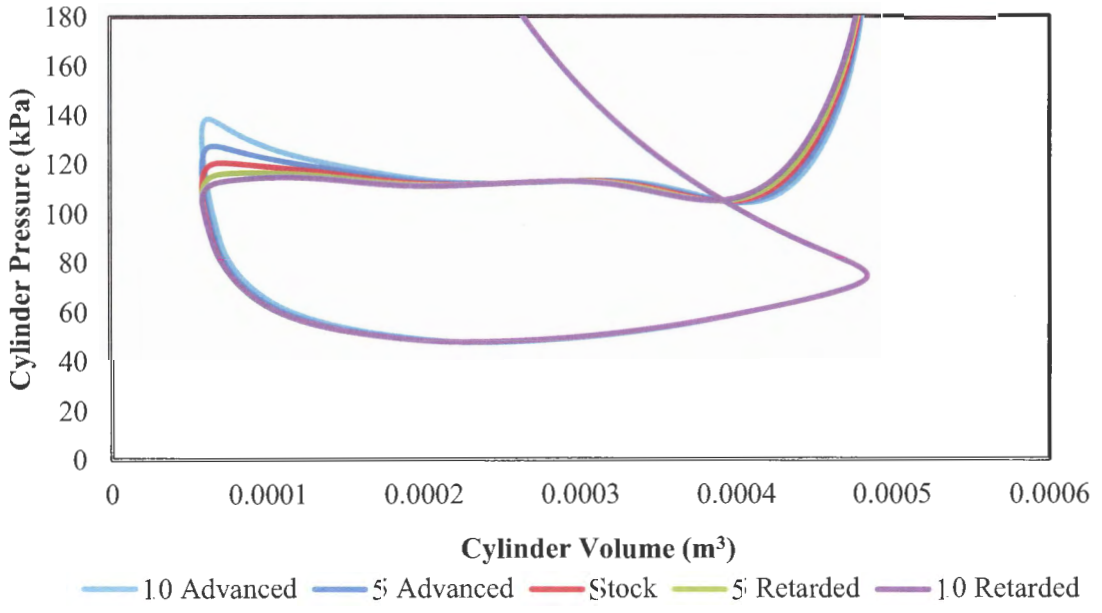

Figure 9.6: Staging of the exhaust valve closing event

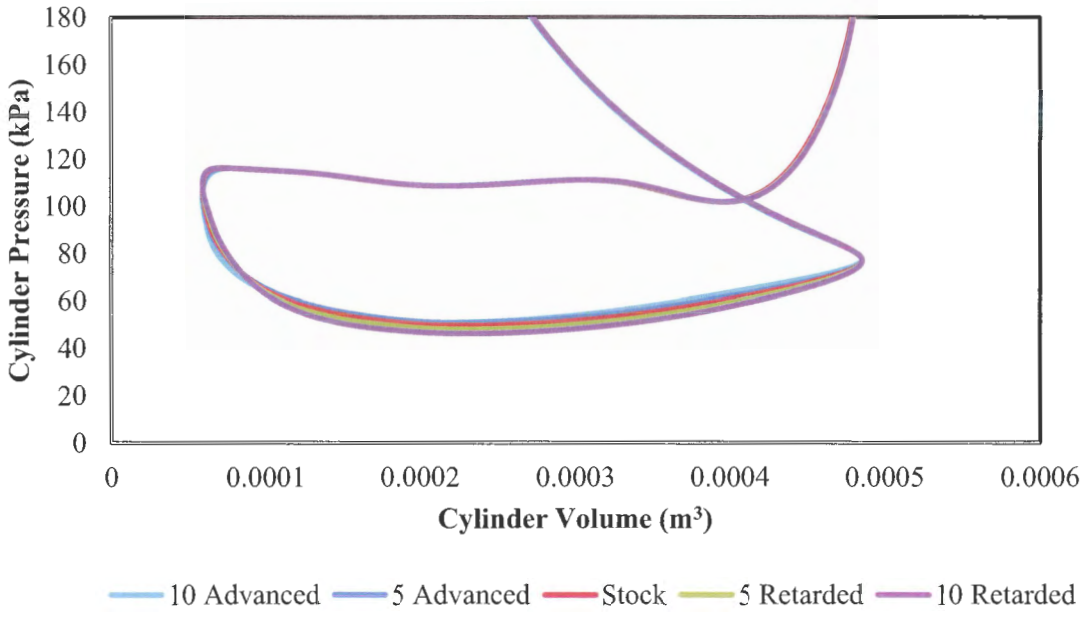

Figure 9.7: Staging of the intake valve opening event

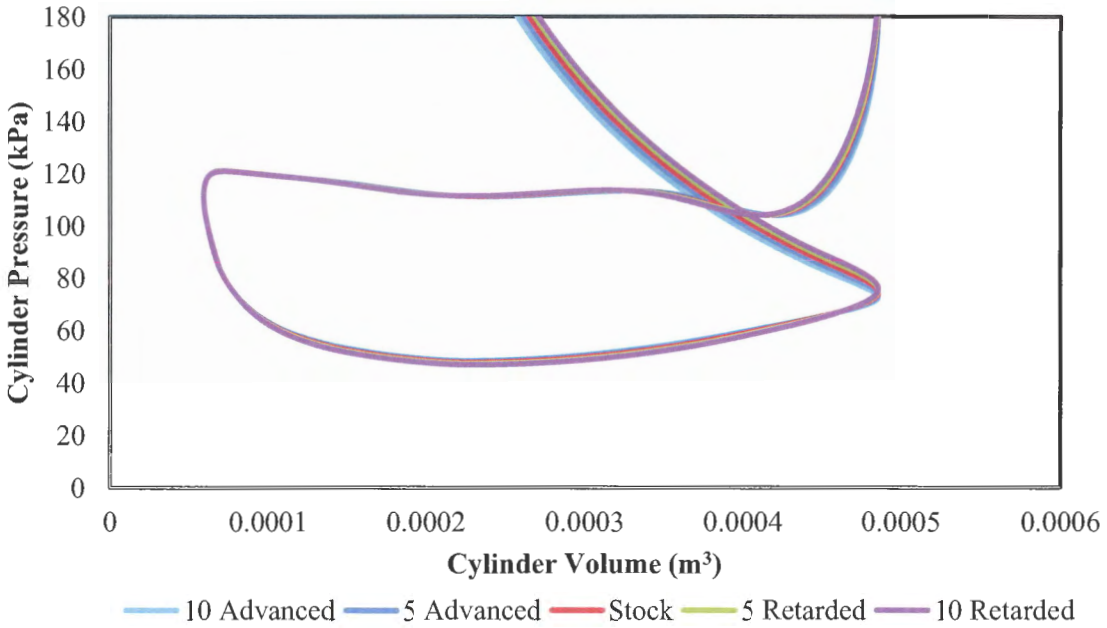

Figure 9.8: Staging of the intake valve closing event

For these tests, only mode 1 operation is represented. Similar trends occur for the subsequent high speed modes. The same trends for low speed, low load operation are observed as those discussed in Chapter 8.

9.2.4 Mass Flow Across System Boundaries. The timing of all four valve events have an effect on the mass flow rate across the system boundaries. Specifically, the timing of the intake valve opening event, the intake valve closing event, and the exhaust valve closing event have an effect on the backflow out of the exhaust manifold into the cylinder and out of the cylinder into the intake manifold. In the case of intake valve opening, backflow occurs between the burned cylinder contents and the fresh charge within the intake manifold. For exhaust valve closing, backflow occurs between the exhaust manifold and the cylinder and ultimately the intake manifold, allowing exhaust gases to dilute the fresh charge. Backflow manifests itself for the intake valve closing event by determining the amount of fresh charge pushed back into the intake manifold during the beginning of compression. The effect of the exhaust valve opening event does not play a role in the back flow of the exhaust gases. However, as discussed earlier, it determines the amount of time available for the blowdown process; it also changes the cross sectional flow area of the valve with respect to the piston velocity. This can have an effect on the mass flow rate of exhaust gases, leaving the cylinder during the exhaust stroke.

For each valve simulation depicted above, the mass flow rates across the valves were calculated for the intake and exhaust processes. The total intake mass trapped in the cylinder for the stock camshaft was calculated to be 3.78×10^{-4} kg and the total exhaust mass was calculated to be 3.75×10^{-4} kg. However, the areas of the plots where backflow

occurs are of primary interest. Accordingly, the plots of mass flow rate will focus on those areas. It should be noted that the amount of backflow makes up only about 1% of the total flow across the valves. However, the amount of backflow between the camshaft staging tests can vary by as much as 100%. The trapezoidal rule was used to analyze the amount of backflow for each test (i.e. integrating from a mass flow rate to total mass trapped value).

In the terms of a thermodynamic analysis, the boundary of the system is taken as the variable volume cylinder and flow through the system is controlled by the variable cross sectional area created by the valves. It should be noted, that a negative intake mass flow rate corresponds to a mass flow rate out of the cylinder and into the intake manifold. A negative exhaust mass flow rate, however, represents a reverse flow from the exhaust manifold into the cylinder. That is, flow from the intake manifold to the cylinder and flow from the cylinder into the exhaust manifold are taken as positive.

First, consider the intake valve open event. It was discussed earlier that this timing does not have a drastic effect on cylinder pressure, but manifests itself in the form of backflow. Below, Figure 9.9 depicts the how altering this timing affects the intake flow as well as the exhaust flow. For advanced timings, the valve is being open earlier in the exhaust stroke; hence, exhaust gases are pushed into the intake manifold diluting fresh charge. The 10 crank angle degrees advanced IVO timing has both an increased flow rate out of the cylinder, as well as, a longer duration. By retarding this event, the amount of exhaust gasses allowed to flow back into the intake manifold from the cylinder and the amount of exhaust gases allowed to escape from the exhaust manifold is drastically reduced. This is a valve timing that is beneficial to engine performance by

occurring closer to TDC, but still allowing time for intake manifold and cylinder pressure equalization to occur.

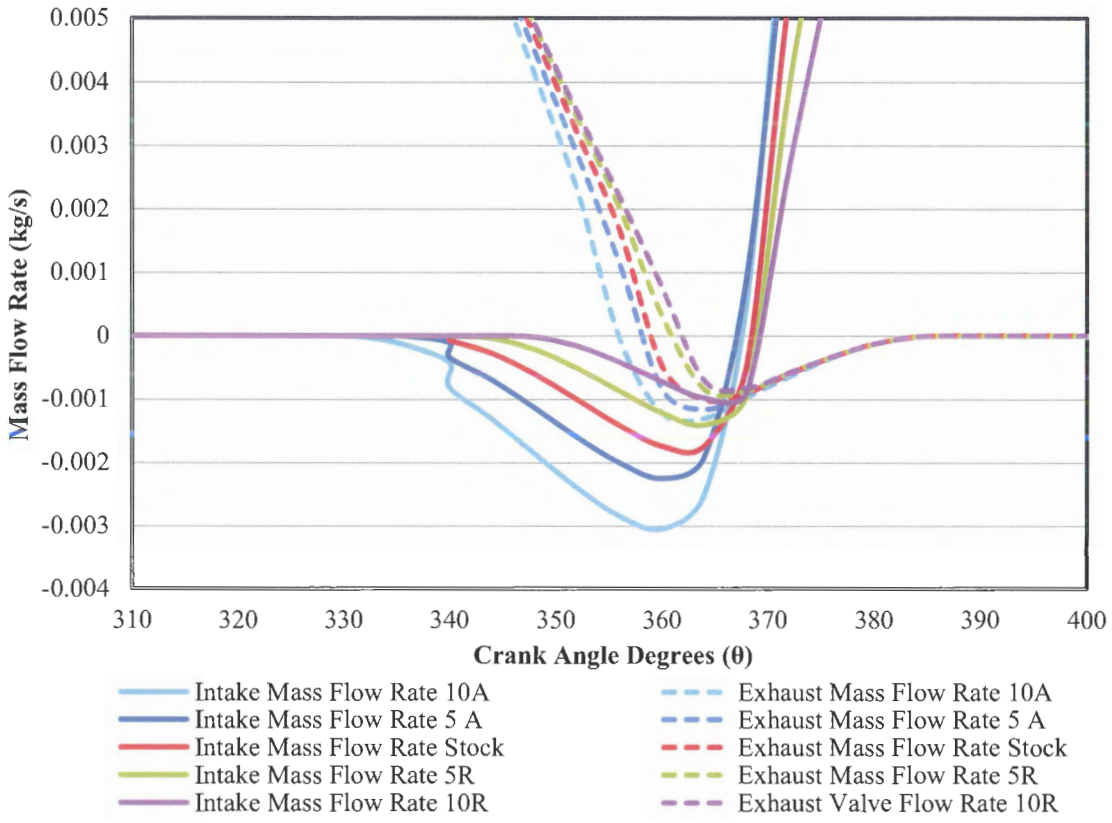

Figure 9.9: Effects of the IVO event on mass flow rate across the valves

Figure 9.10 contains the just intake mass flow rate from the previous plot. For the most advanced timing, the mass trapped (or total mass backflow), was calculated to be -2.99×10^{-6} kg. While the most retarded timing only allowed -4.95×10^{-7} kg of exhaust gases to flow back into the intake manifold. By isolating the intake mass flow rate, it can be observed that after the piston reaches TDC of the exhaust stroke (360 degrees) the mass flow rate between the various valve timings begins to converge. Once the piston

actually begins its induction stroke, (that is, returning to BDC) the intake mass flow rate becomes relatively similar across the different valve timings. Any flow loss realized from advancing this timing will have an opportunity to be regained during the induction stroke; however, the exhaust dilution of the fresh charge will be detrimental to the total energy content of the new cylinder charge.

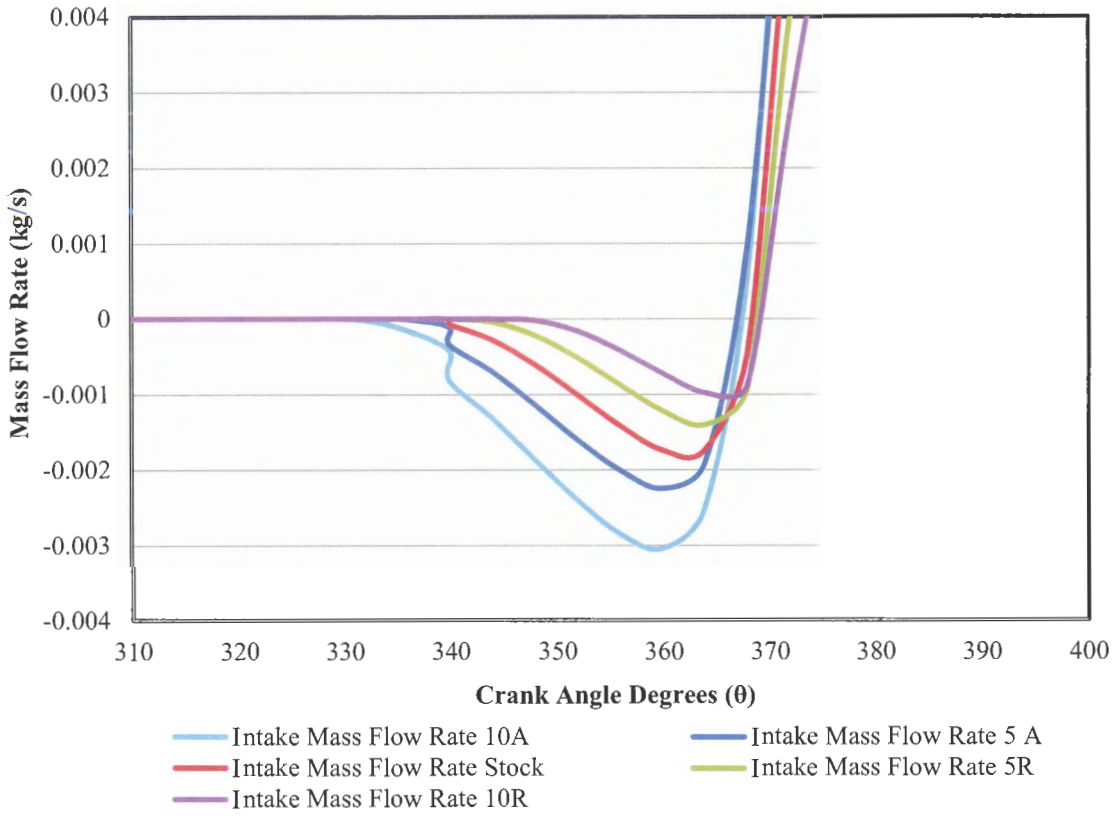

Figure 9.10: Intake mass flow rate for IVO valve event

As seen in Figure 9.9, the timing of IVO also has an effect on the mass flow rate of the exhaust gases. Again, for an advanced IVO, the valve overlap duration is extended. This can be seen on the mass flow rate of the exhaust gases in Figure 9.11.

The flow rate for the advanced valve timings begin to deviate from the stock case. The flow rate of the exhaust gases begin to slow down as the flow area of the intake valve is providing an additional flow path. The flow rate then dips below zero, signifying a reversal of flow out of the exhaust manifold and into the cylinder as the pressure of the manifold becomes greater than the pressure of the cylinder. For the most advanced IVO, the backflow of exhaust gases out of the exhaust manifold and into the cylinder was calculated to be -7.87×10^{-7} kg. The most retarded valve timing realized a backflow of mass equal to -4.10×10^{-7} kg; a reduction of almost 50%.

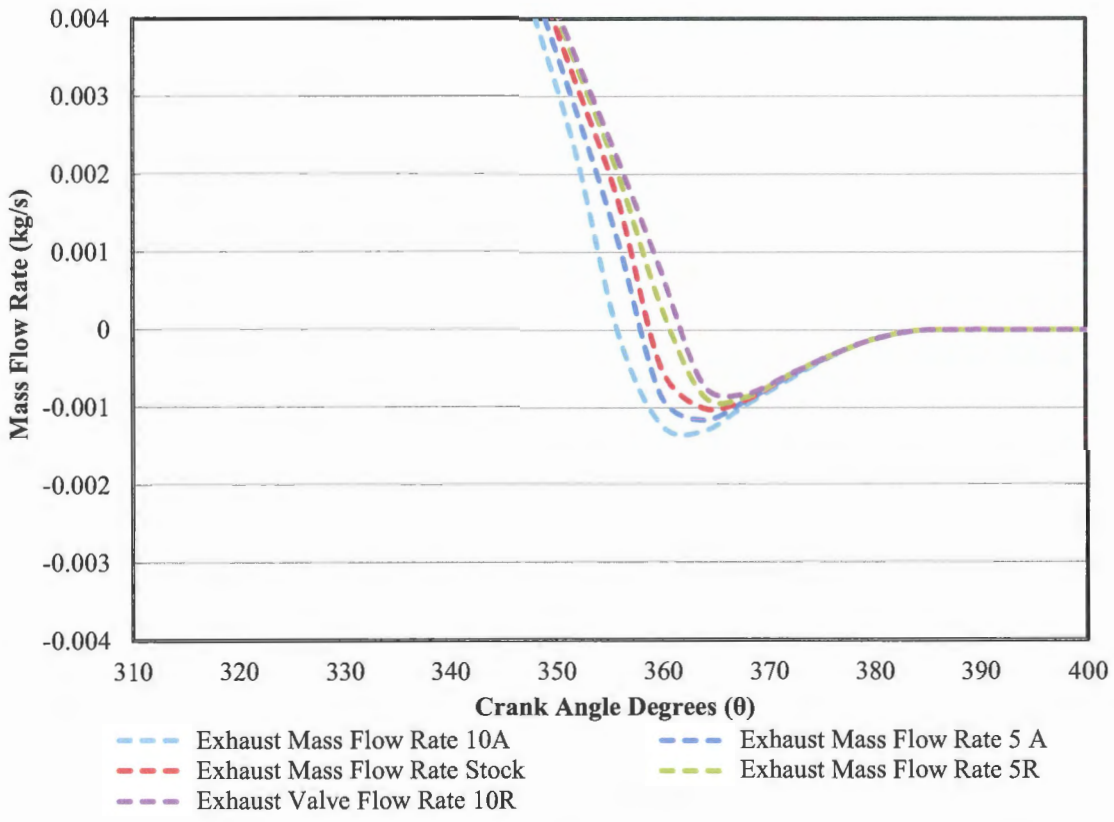

Figure 9.11: Exhaust mass flow rate for IVO valve event

The exhaust valve closing event ends the exhaust process and the valve overlap period. Figure 9.12 depicts the effect of altering the timing of EVC on the intake mass flow rate, while maintaining the stock IVO timing. An increase in intake manifold backflow is seen when the timing of EVC is retarded further into the intake stroke, driven by a pressure differential between the intake and exhaust manifolds and the cylinder. It can be concluded that retarding, or delaying, the exhaust valve closing event will decrease the cylinder pressure around TDC (decreasing pumping work). However, it will result a substantial increase in backflow (higher gas residual).

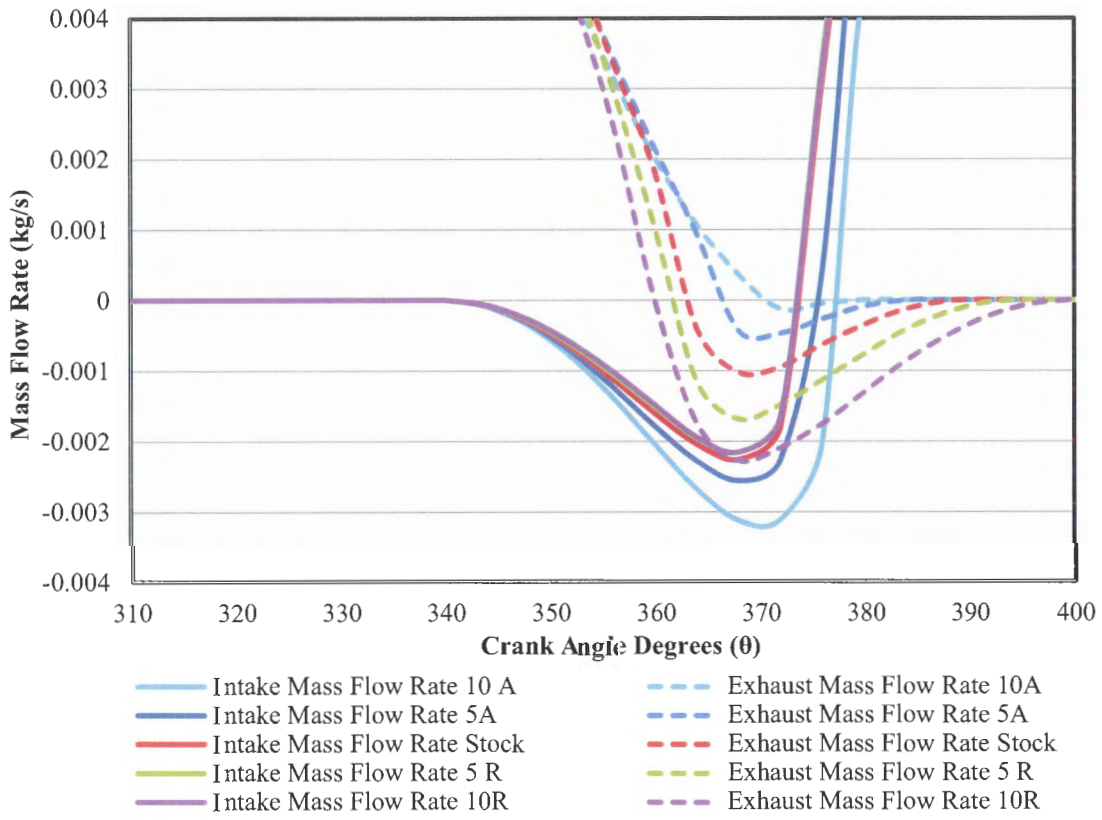

Figure 9.12: Effects of the EVC event on mass flow rate across the valves

By analyzing the intake flow rate, separate from the exhaust flow rate, it can be easily seen that by advancing the exhaust valve closing event, the amount of mass flow rate from the cylinder into the intake manifold increases. This also can be seen on a pressure-volume trace by a rise in peak pressure at the end of the exhaust stroke, see Figure 9.6. Once the EVC event is retarded past the stock valve timing, the reversal of intake mass flow rate no longer changes. The effects of flow out of the exhaust manifold and into the cylinder become dominant. The total mass backflow into the intake manifold due to the EVC event was calculated to be -2.82×10^{-6} kg, while the most retarded (also very similar to the stock) was calculated as -1.59×10^{-6} kg.

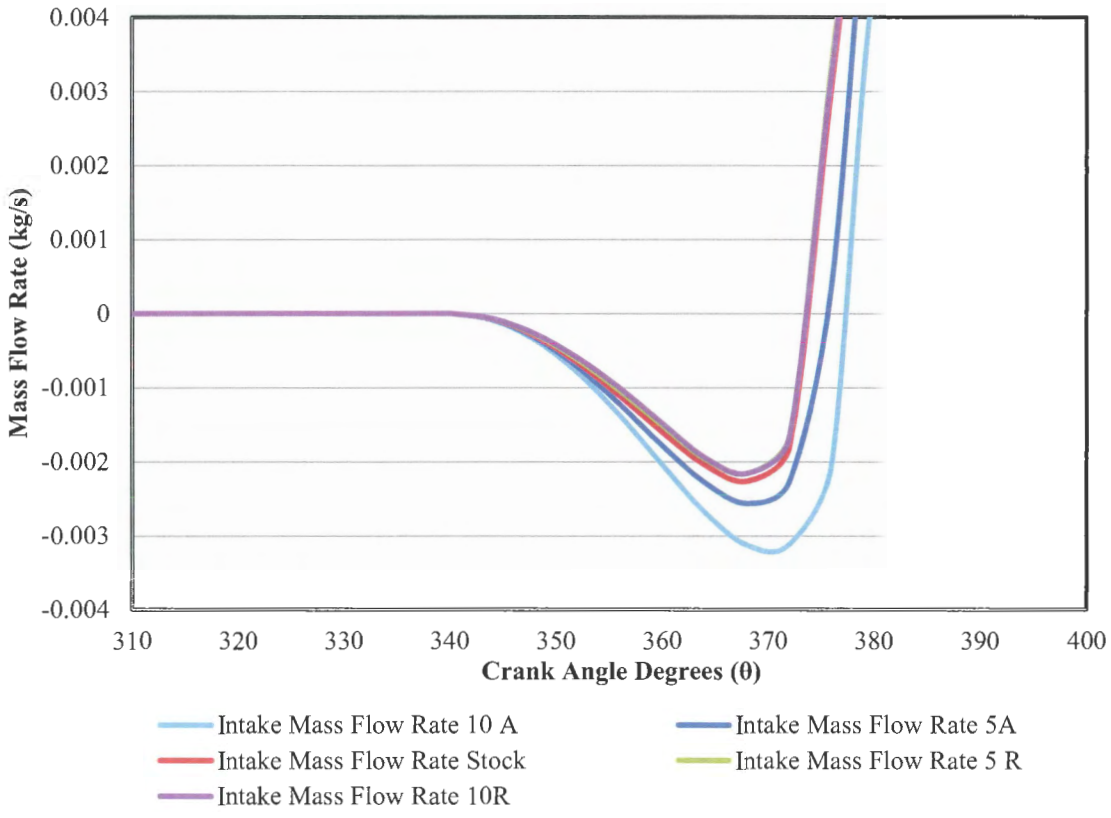

Figure 9.13: Intake mass flow rate for EVC valve event

Retarding the exhaust valve closing event increases the amount of backflow from the exhaust manifold to the cylinder, as observed in Figure 9.14. This is due to the fact that the valve is open further into the induction stroke, so the piston is essentially pulling the exhaust gases out of the exhaust manifold in a similar way as the intake manifold. These exhaust gases will no longer enter the intake manifold; they will simply mix with the fresh charge within the cylinder. The amount of exhaust gases trapped in the cylinder due to an advanced EVC was calculated to be -1.66×10^{-8} kg. The amount of gas trapped due to a retarded timing was calculated to be -1.90×10^{-6} kg. Retarding this timing has a significant effect on the backflow out of the exhaust manifold and into the cylinder.

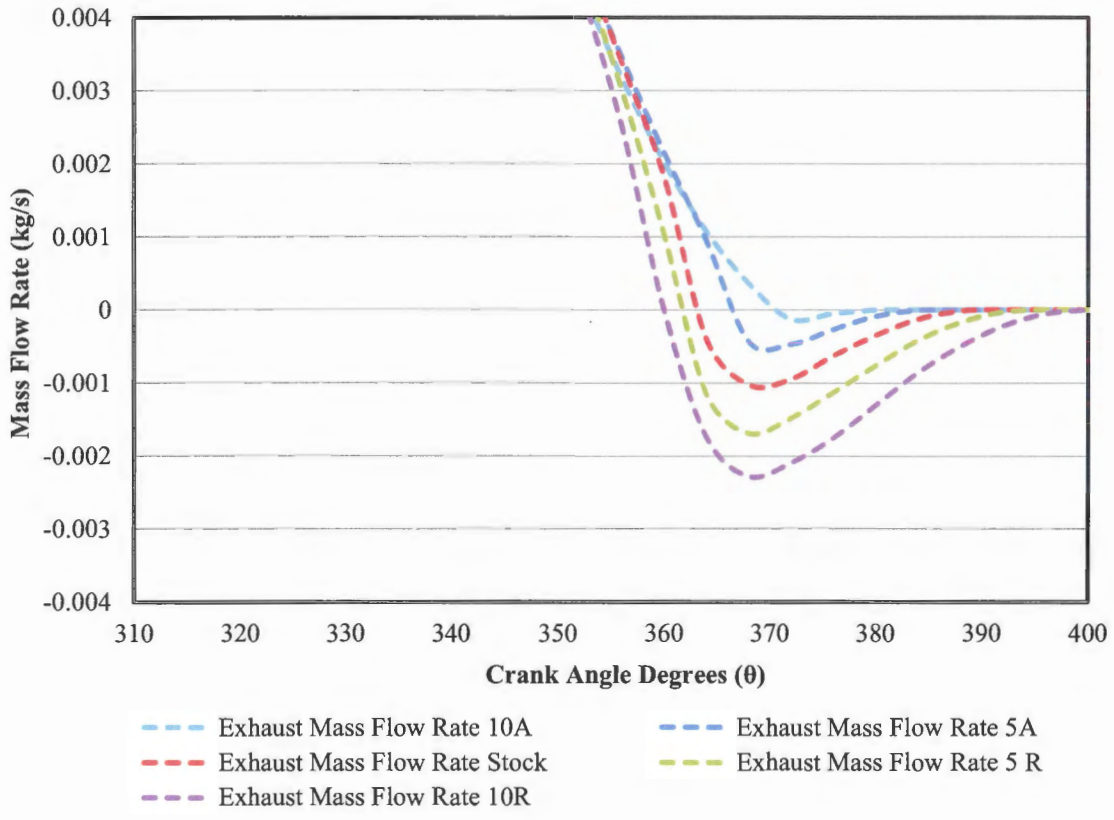

Figure 9.14: Exhaust mass flow rate for EVC valve event

Intake valve closing has the responsibility of ending the induction process and for that matter the gas exchange process. It is also crucial in maintaining a high volumetric efficiency for the engine. By retarding this valve timing, moving it further into the compression stroke, the piston motion causes the cylinder to continue filling, even though the piston has changed directions. It can also cause charge to be pushed back into the intake manifold if left open too long. This reduces cylinder charge and consequently, the available energy. However, advancing this timing too far can restrict the amount of charge inducted.

It can be observed in Figure 9.15, that by retarding the timing of the intake valve closing event the intake mass flow rate remains much higher than those of the stock or advanced cases correlating to a greater quantity of charge entering the cylinder. However, the simulation predicts that back flow out of the cylinder and into the manifold will occur for the retarded timings. A total mass backflow from the cylinder to the intake manifold for the retarded timing was calculated to be -7.60×10^{-6} kg, while it is negligible for the advanced timing.

Within the focus of this investigation a prominent operating condition must be decided. The test engine is primarily run under high speed and high load conditions. If it were more beneficial to design for low speed and low load or even an idle condition, the effects of an advanced valve timing would be desirable.

A large portion of the pumping loop under high speed and high load conditions is made up of the work required to reduce the cylinder pressure to that of the manifold pressure during the expansion stroke. If the cylinder pressure can be reduced to the

exhaust manifold pressure at or slightly before BDC of the expansion stroke, then the work required by the piston to expel the burned gas will be reduced.

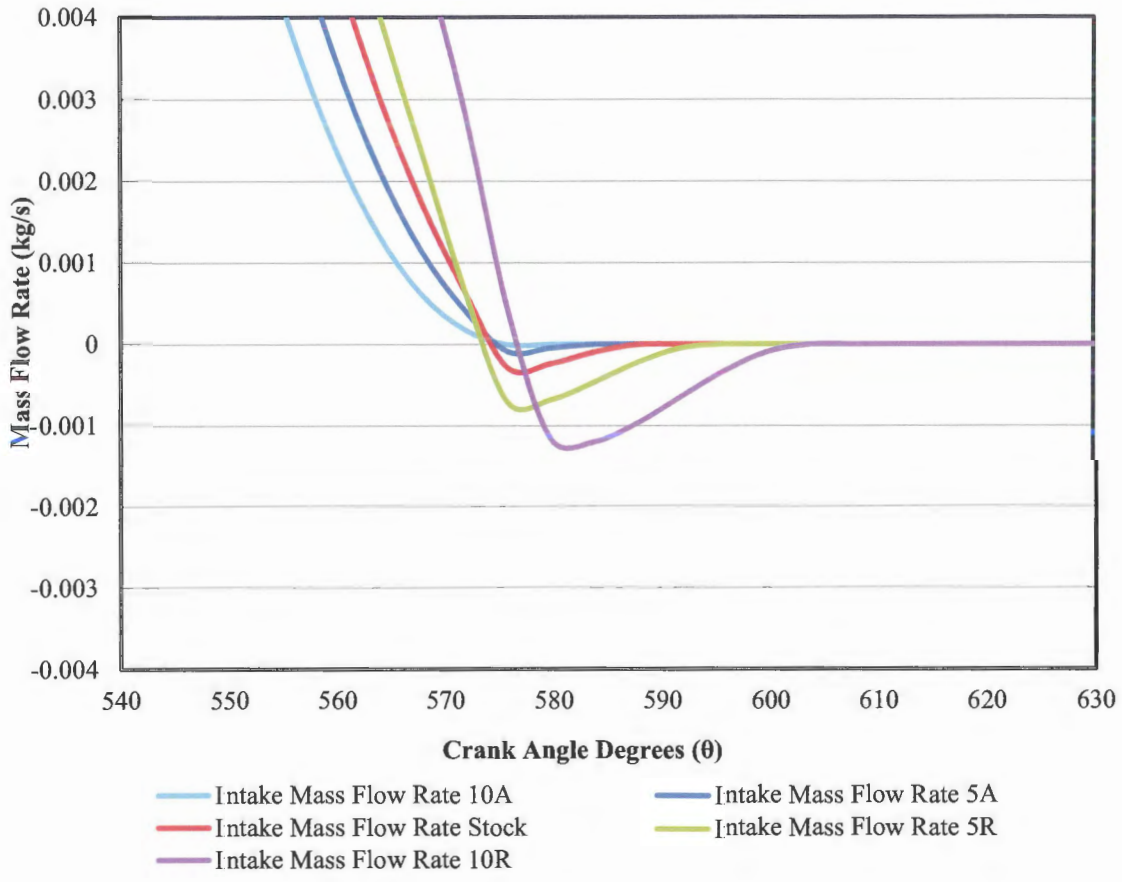

Figure 9.15: Intake mass flow rate for IVC valve event

In order to achieve this, blowdown is employed to make use of a pressure gradient between the cylinder pressure and the exhaust manifold pressure. If EVC is too late in the expansion stroke, the pressure differential will not be great enough to expel the required amount of exhaust gas. EVC, being too early in the expansion stroke, can have a detrimental effect the power output of the engine. Below, Figure 9.16 shows the effect of altering EVC on exhaust mass flow rate. Advancing the valve event timing closer to

TDC of the expansion process yields an increase of mass flow out of the cylinder and into the exhaust manifold earlier in the cycle. By retarding this timing, a higher peak mass flow rate can be seen later in the cycle. However, by retarding this valve event, the time available for the blow down process reduces. This is a balance of reducing the cylinder pressure during the end of expansion, while also increasing the amount of exhaust gas expelled and maintaining a high thermal efficiency. This is fortified by the results seen in Figure 9.5 above.

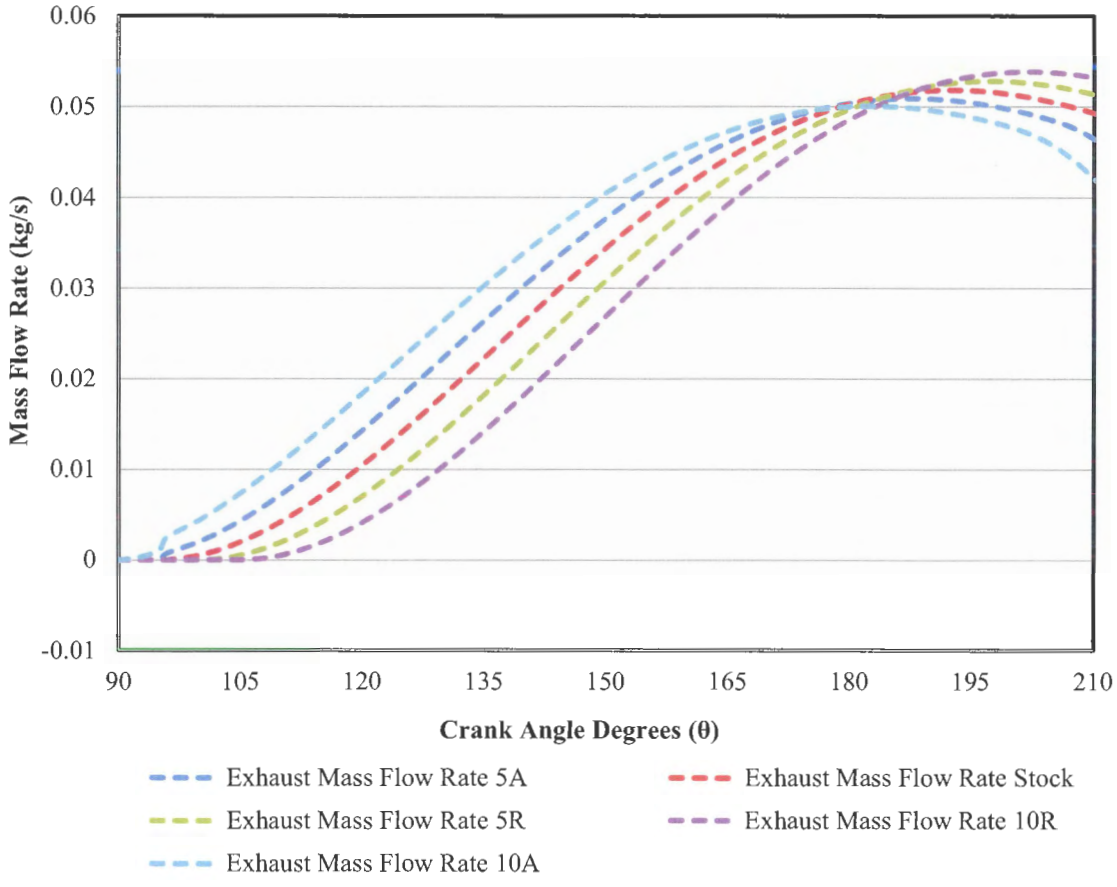

Figure 9.16: Exhaust mass flow rate for EVO valve event

For the test engine, the results from the simulation suggest that it an improvement of 7% in First Law efficiency and a reduction of 12% in pumping work at mode 1 can be gained by retarding the IVO event close to 5 crank angle degrees, advancing the EVC event about 5 crank angle degrees (reducing valve overlap time), retarding IVC by 5 crank angle degrees, and advancing EVO enough (about 5 crank angle degrees) to decrease cylinder pressure at BDC of exhaust but still maintain reasonable efficiency standards. These timings are chosen, not because they provide the best operating conditions at high speed-high loads or idle, but they should provide the best compromise between the two extremes.

This simulation is ultimately used to provide a visualization of the performance effects of altering individual valve timings. It can also be used to determine improvements made by modifying flow conditions of the intake system. It is limited to analyzing one cylinder at a time. In the case of the test engine, it cannot model the effects that one cylinder has on the other as observed through experimental testing.

10. CONCLUSIONS

10.1 METHODS OF ANALYSIS

There are several experiments and techniques described and implemented in this thesis that assist in the determination of intake flow performance for a four stroke spark ignition engine. Intake flow can be analyzed on a steady state flow bench by examining flow coefficients, discharge coefficients, and pressure loss coefficients. Performance characteristics can be gathered through experimental analysis on an engine test stand.

Camshaft staging tests can be used to determine the effects of valve event timings on engine operation. An energy balance approach can be utilized to determine the effects of various tests on the distribution of energy. These experimental analyses, coupled with a simulated engine model, provide a means by which to determine the engine characteristics which best optimize the performance of the engine at various operating conditions.

10.2 OPTIMIZATION OF INTAKE GEOMETRY

For the steady state flow bench tests, it was determined that the port area inside the head accounted for the majority of the losses throughout the intake system. This provides an area of focus, where improvements in performance can be gained. By rounding the corner of the intake port, an increase in flow and discharge coefficients was determined to be close to 8%. Not only did the flow increase under these conditions, the viscous losses as predicted by the pressure loss analysis decreased by almost 7.5% for the high flow conditions , improving the overall efficiency of the induction process.

These improvements were not initially realized under engine testing. However, by advancing the intake valve opening event by 10 crank angle degrees, an improvement of nearly 4% can be realized for the high speed high load set points.

It was also presented that the Mach index of the intake port was found to be close to 0.85 for both cylinder heads over a range of flow conditions. This is a concern, as it was stated that the breathing performance of an engine decreases drastically for a Mach index over 0.5. Even after the modifications were made to the stock engine heads, the Mach index was still observed to be 0.77. This speaks to undersized intake valves for the displacement of the engine. Increasing the diameter of the intake valves would make a larger cross sectional area available to the flow earlier in the intake process. This would, in turn, have the effect of reducing the flow restriction and reducing the amount of work exerted by the engine to induct the charge in the manifold.

10.3 OPTIMIZATION OF VALVE EVENTS

Experimental testing on the engine stand allows for the actual performance of the engine to be captured; both for a stock (baseline) setup and for any alterations made to the engine. For this thesis, a primary objective of engine testing was to determine the improvements that can be gained from changing the valve event timings away from the stock setup.

It was found that by advancing the exhaust valve opening event a reduction of nearly 8% in the pumping work of the engine could be realized. However, moving this timing too far has an effect on the thermal efficiency of the engine. A best case scenario for the test engine was around 5 crank angle degrees advanced from the stock timing.

This provided the reduction in exhaust pressure desired, while still keeping the thermal efficiency high at the lower load set points.

The exhaust valve closing event for the test engine could benefit by being advanced slightly (on the order of 5 crank angle degrees). This would reduce the valve overlap time, helping to control the amount of exhaust gas residuals present. However, it should not be advanced so far that an increase in pumping work is realized.

The intake valve opening event can be retarded slightly from the stock timing to reduce the time it is open during the exhaust stroke. This would have the effect of reducing exhaust gas residuals that enter the intake manifold and dilute the fresh charge. This timing should not be retarded so far as to not allow sufficient time for the cylinder and manifold pressure to equalize before the induction stroke. Through experimental and simulated testing, it was determined that an optimal retardation of this event would be close to 5 crank angle degrees away from the stock timing.

As the major performance area for the engine is at high speed and high load, the timing of the intake valve closing can be retarded to make use of the fluid momentum to increase the amount charge within the cylinder. Higher loads were obtained by the engine under experimental testing for the retarded set points. However, the simulated data suggested that there would be backflow from the cylinder to the intake manifold if the timing were retarded. Even so, the flow rate and ultimately the amount of change in the cylinder at the time of IVC increased. This correlates to an increase in charge density, an overall increase in the output of the engine, and a reduction in specific fuel consumption. Designing for an overall fuel efficiency standpoint, this timing could be retarded as much as 5 crank angle degrees to provide increased high speed and high load

performance while increasing the fuel conversion efficiency of the engine. Retarding this timing too far would lead to a reduction in idle stability of the engine.

If the port areas are altered as the modified heads were, it was found that the flow rate into the cylinder increased for an advanced timing of intake valve open. This can reduce the need for the intake valve closing event to be retarded. By doing this the stability at the low speed operating points would increase while still maintaining improved performance at the high speed operating conditions.

A first law efficiency calculation was performed in Chapter 8. These efficiencies were then multiplied by their respective 6-Mode weighting factors (refer to Table 3.2) and then summed to get an overall weighted efficiency for a camshaft staging test. Table 10.1 provides the resulting values for that calculation

Table 10.1: Weighted fuel conversion efficiency for the camshaft staging tests

	Fuel Conversion Efficiency (%)				
	10 Advanced	5 Advanced	Stock	5 Retarded	10 Retarded
Mode 1 (9%)	19.7	19.8	19.9	20.4	20.9
Mode 2 (20%)	19.0	19.3	19.6	19.1	19.1
Mode 3 (29%)	17.8	18.1	16.9	17.5	17.0
Mode 4 (30%)	13.2	13.4	11.9	13.0	13.3
Mode 5 (7%)	4.1	4.3	4.2	4.5	4.4
Mode 6 (5%)	7.3	6.8	5.6	5.1	5.2
Weighted	15.3	15.5	14.8	15.2	15.2

The values in Table 10.1 are subject to change with some variation in operating condition. However, the general trend between the camshaft staging tests should remain consistent. Because of the weighting factors, the variability between similar tests was not observed to be more than ±0.3% or a change of 1.8% between 6-Mode tests.

The results indicate that without making any prior alterations the best case scenario from a first law efficiency stand point, based on a 6-Mode testing methodology, would be to advance the entire camshaft 5 crank angle degrees.

10.4 SUMMARY OF CONCLUSIONS AND RECOMMENDATIONS

Summarizing all of the conclusions and results, the importance of the areas of focus are as follows:

1. The size of the intake valves are of great concern as they are not scaled appropriately with cylinder bore on the test engine. Increasing the valve diameter will improve the early flow area reducing the restriction.
2. Advancing the timing of the exhaust valve opening event by 5 crank angle degrees away from the stock setting provides an improvement in pumping work by as much as 7.5% at the high load set points while maintaining stable operating conditions at the lower load- high speed tests and at idle.
3. Retarding the timing of intake valve closing by 5 crank angle degrees will improve high load-high speed performance by as much as 4.5% while still maintaining stable operating conditions at idle.
4. Making improvements to the port (i.e. removing any sharp corners) can improve the flow conditions. Viscous flow losses were reduced by as much as 7%. With appropriate intake valve open timing an improvement in mass flow rate of more than 4% can be realized. This can negate the need for retarding the timing of intake valve closing.
5. Due to the way the connecting rods attach to the crankshaft, cylinder 2 is located approximately 2.5 cm lower than cylinder 1. This requires cylinder 2

to have a longer intake port increasing the discharge and flow coefficients, reducing the flow efficiency of the engine. Also, the processes of each cylinder with respect to the other must be considered. Currently on the test engine, the cylinders are phased in such a way that cylinder 1 is assisting cylinder 2 during its induction stroke. This reduces the intake manifold pressure, increasing the pumping work, but also increasing the charge density. The pumping work of cylinder 2 at mode 1 is generally 30% larger than that of cylinder 1, while the overall output of cylinder 2 in the area of 6% greater than that of cylinder 1.

APPENDIX A

ADDITIONAL PLOTS RELATING TO ENGINE TESTING RESULTS

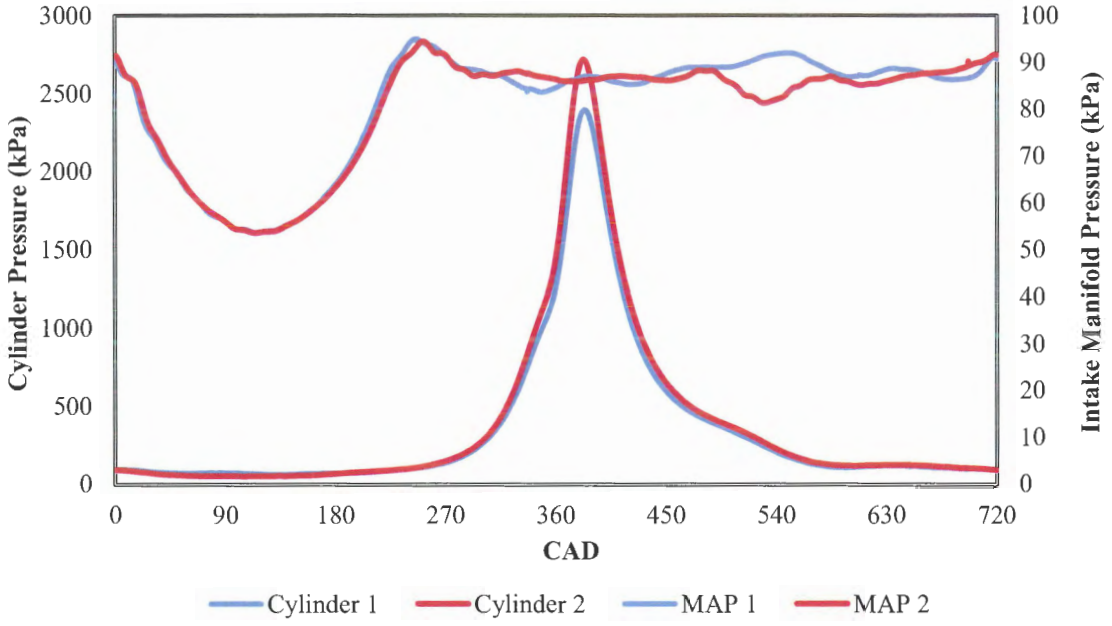

Figure A.1: Cylinder and intake manifold pressure comparison for mode 2 operation

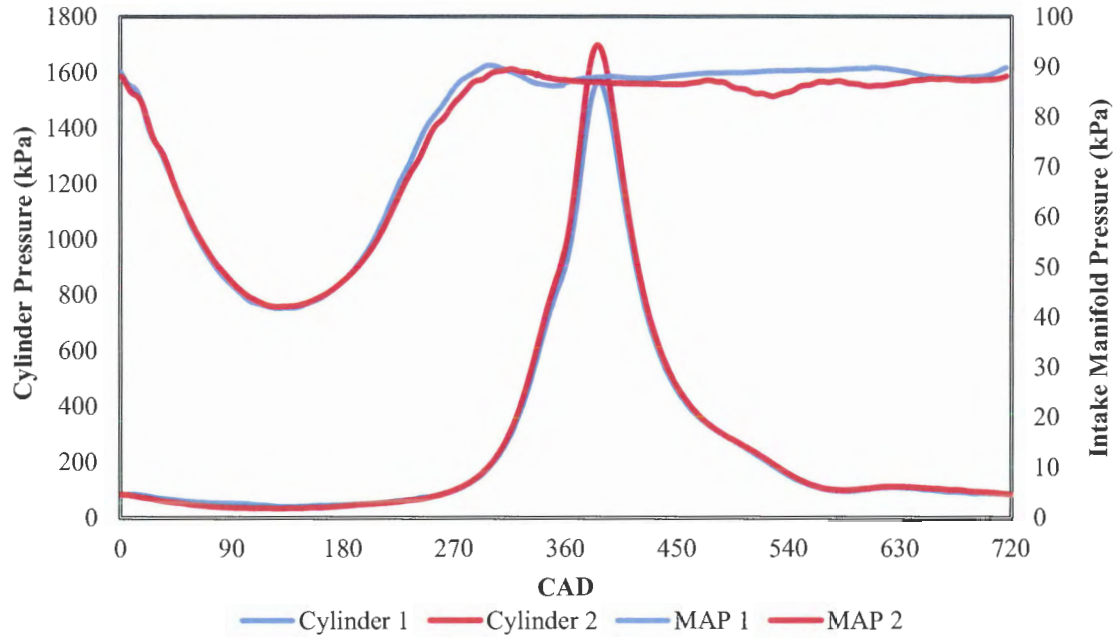

Figure A.2: Cylinder and intake manifold pressure comparison for mode 3 operation

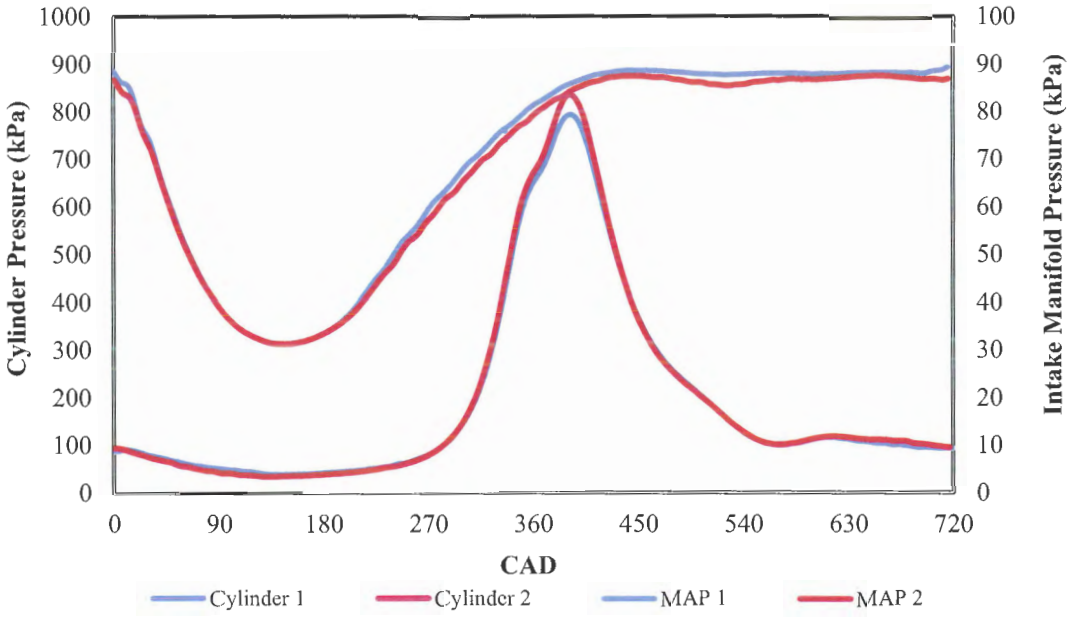

Figure A.3: Cylinder and intake manifold pressure comparison for mode 4 operation

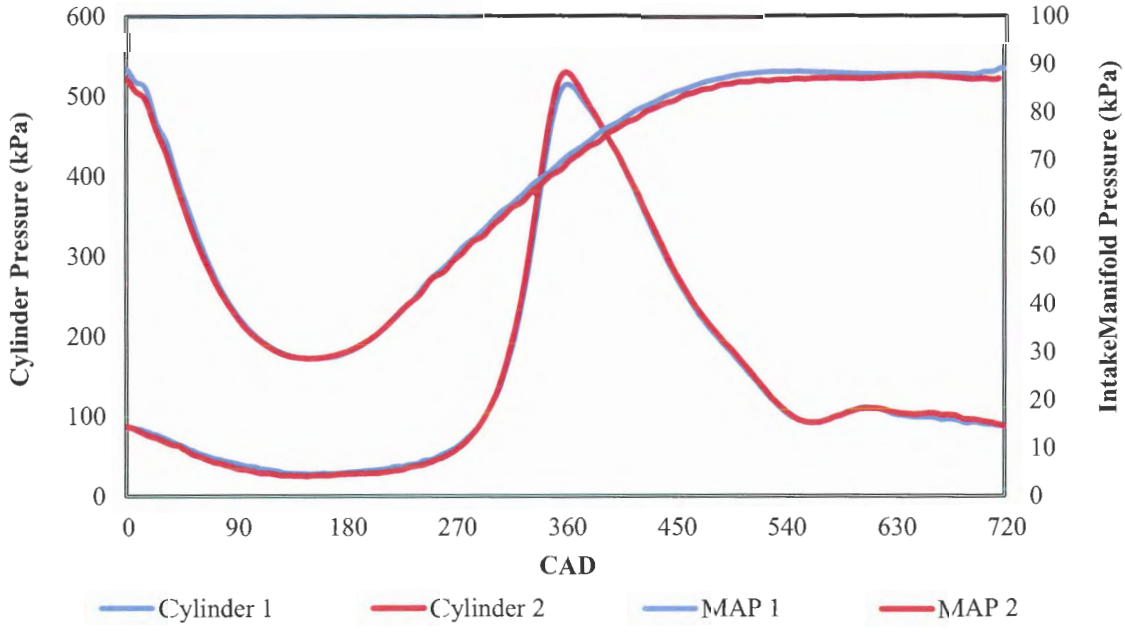

Figure A.4: Cylinder and intake manifold pressure comparison for mode 5 operation

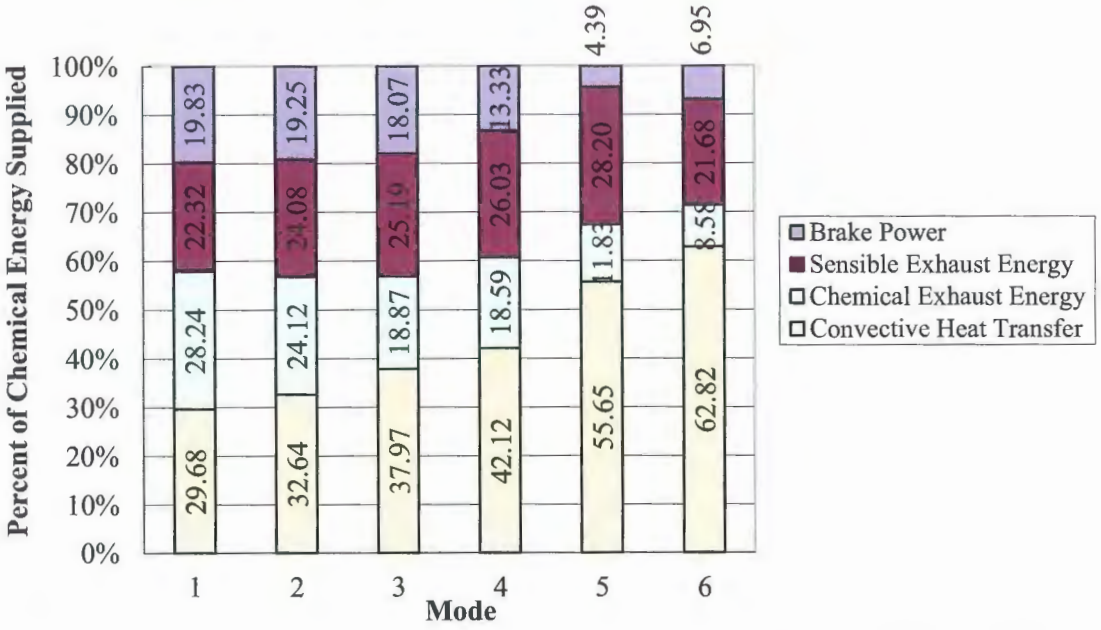

Figure A.5: 6-Mode energy distribution for camshaft staging of 5 degrees advanced

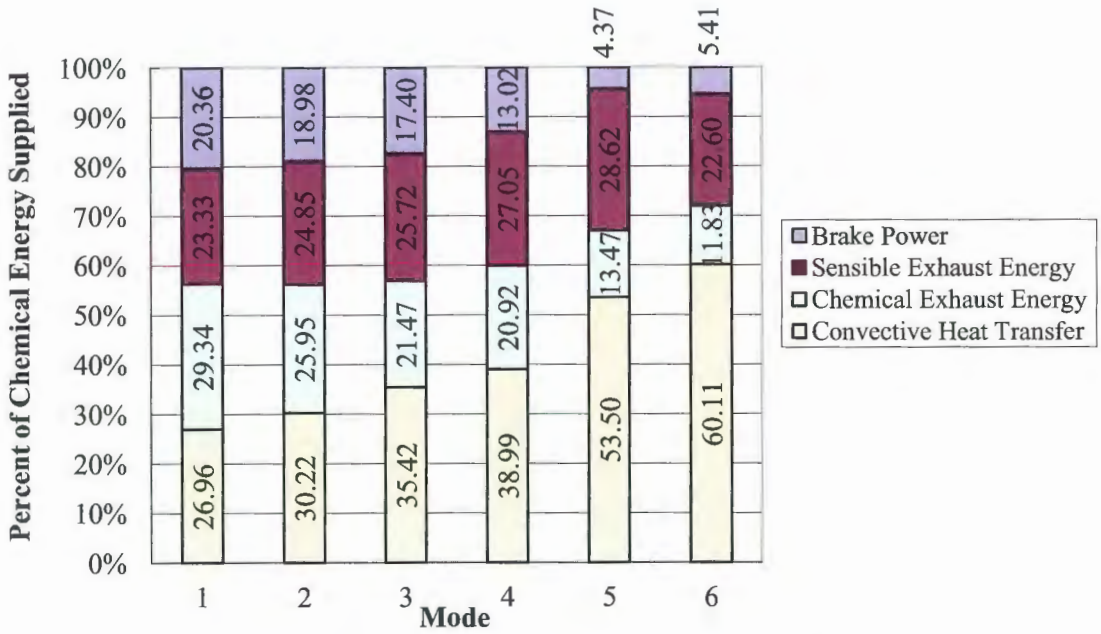

Figure A.6: 6-Mode energy distribution for camshaft staging of 5 degrees retarded

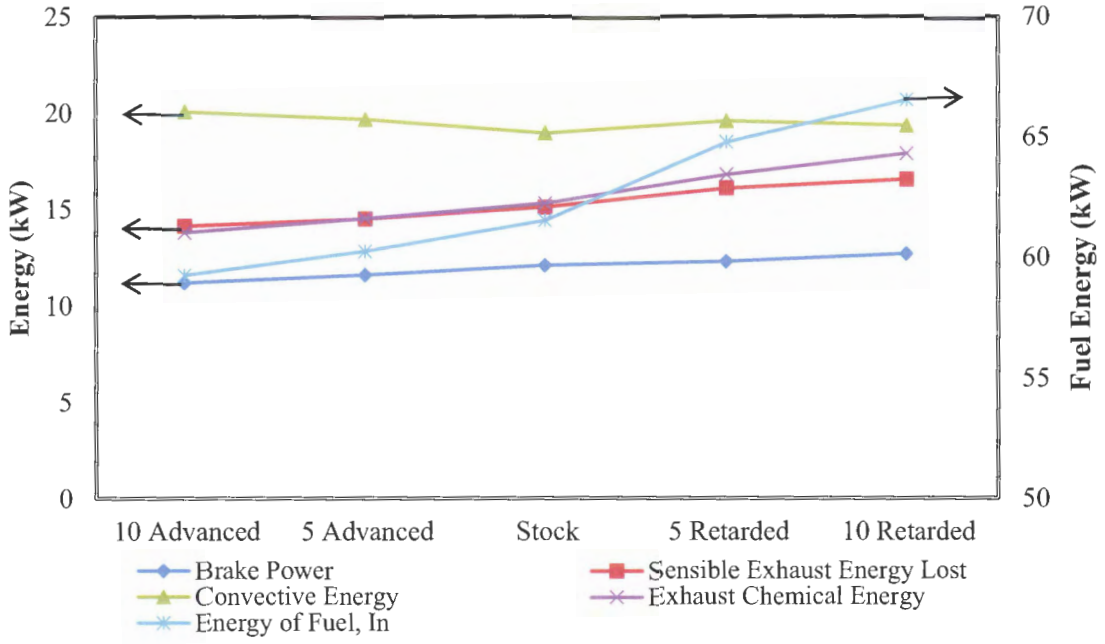

Figure A.7: Mode 2 comparison of energy for camshaft staging tests

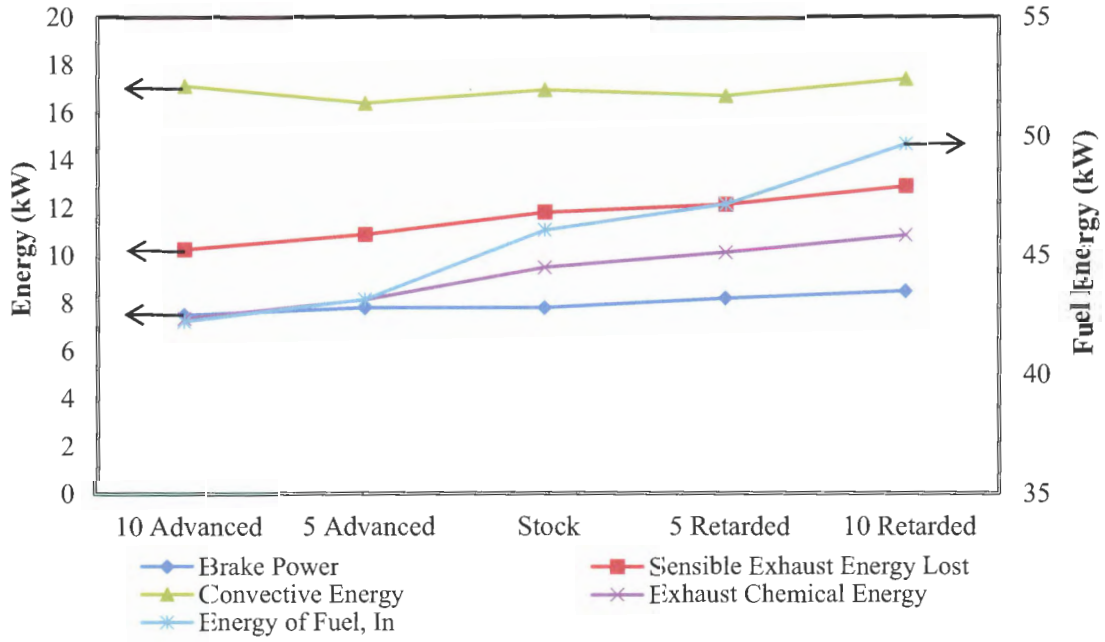

Figure A.8: Mode 3 comparison of energy for camshaft staging tests

APPENDIX B

ENGINE SIMULATION INPUT DATA

Table B.1: Engine simulation input data

ESP: Engine Operating Parameters		
Operating Parameters	**Input**	
RPM	3060	
Firing	702	CA BTDC of Compression
Ambient Conditions:		
Intake Pressure	0.85	atm
Exhaust Pressure	1.1	atm
Amb. Temperature	298	K
EGR	None	
Valve Control		
IVO	353	CA ATDC of Compression
IVC	579	CA ATDC of Compression
EVO	135	CA ATDC of Compression
EVC	367	CA ATDC of Compression
Max intake valve flow area % of reference	67	%
Max exhaust valve flow area % of reference	71	%
Valve Reference Area		
Intake (fully open)	6.06E-04	m^2
Exhaust (fully open)	5.47E-04	m^2
Piston/Cylinder		
Cylinder Bore	0.0845	m
Compression Ratio	8.2	
Piston Stroke	0.076	m
Connecting Rod	0.122	m

Table B.1: Engine simulation input data (continued)

Gas Properties		
Fuel Type	C8H18	Isooctane
Reactants	Fuel, O_2, N_2	1 mol of fuel @ 2atm
Products	CO_2, CO, H_2O, O_2, N_2	6 atm
Valve Flow Model		
$C_{D,\ intake}$	0.428	
$C_{D,intake\ backflow}$	0.428	
$C_{D,\ exhaust}$	0.428	
$C_{D,\ exhaust\ backflow}$	0.428	
Heat Transfer Model		
Stanton Number		
Compression	0.0356	
During burn for unburned gas	0.0356	
During burn for burned gas	0.0356	
During expansion	0.0356	
In-cylinder Hx during gas exchange	0.0356	
Hx from inlet valve flow	0.00237	
Hx from exhaust valve flow	0.00237	
Hx area above piston at TDC/(Bore Area)	1.37	
Hx area for intake jet flow/(Bore Area)	0.5	
Hx area for exhaust jet flow/(Bore Area)	0.5	
Temp of Linear/Piston/Head Hx area	400	K
Temp of Intake Valve-flow Hx area	320	K
Temp of Exhaust Valve Flow area, K	400	K

Table B.1: Engine simulation input data (continued)

Turbulence Model		
(inlet flow turb. Kinetic energy)/(mean flow kinetic energy)	0.2	
(exhaust bkflow. turb. energy)/(mean bkflow. kinetic energy)	0.2	
Factor in turbulence dissipation during compression	0.298	
Factor in turbulence dissipation during burn	0.05	
Factor in turbulence dissipation during expansion	0.298	
Factor in turbulence dissipation during gas exchange	0.298	
Factor in turbulence production during compression	0.00502	
Factor in turbulence production during burn	0.03	
Factor in turbulence production during expansion	0.00502	
Factor in turbulence production during gas exchange	0.00502	
Flame Geometry Model		
Cylindrical Burn		
Flame Propagation Model		
Fraction of mass ignited at ignition	0.02	
laminar flame speed, m/s	0.3	
ration of turbulent flame speed to turbulence velocity	1.5	
fraction of reactants burned (combustion efficiency)	0.8	

Table B.1: Engine simulation input data (continued)

Intake Manifold Properties		
Entrance blockage for intake feeder	0.1	
Discharge blockage fraction for intake Feeder	0	
Entrance blockage fraction for intake runner	0	
Friction factor for inlet feeder	0.002	
friction factor for inlet runner	0.004	
length of intake feeder	0.2	m
length of intake runner	0.4	m
diameter of the intake feeder	0.0381	m
diameter of the intake runner	0.0381	m
volume of intake junction	0	m^3
number of inlet runners from feeder	2	
Exhaust Manifold Properties		
Discharge blockage fraction for exhaust runner	0.1	
Entrance blockage fraction for exhaust collector	0.1	
Discharge blockage fraction for exhaust collector	0.01	
friction factor for exhaust runner	0.002	
friction factor for exhaust collector	0.002	
length of exhaust runner	0.1	m
length of exhaust collector	0.25	m
diameter of the exhaust runner	0.0293	m
diameter of the exhaust collector	0.0986	m
volume of the exhaust junction	0.001	m^3
number of exhaust runners to collector	2	

BIBLIOGRAPHY

[1] Rabbitt, Richard D., "Fundamentals of Reciprocating Engine Airflow Part1: Valve Discharge and Combustion Chamber Effects," SAE Paper 840337, 1984.

[2] Heywood, John B. *Internal Combustion Engine Fundamentals.* New York: McGraw-Hill, Inc. 1988.

[3] Asmus, T.W., "Valve Events and Engine Operation," SAE Paper 820749, 1982.

[4] Xu, Hongming, "Some Critical Technical Issues on the Steady Flow Testing of Cylinder Heads," SAE Paper 2001-01-1308

[5] Lumley, John L. *Engines an Introduction.* New York: Cambridge University Press, 1999.

[6] Young, Donald F., Munson, Bruce R., Okiishi, Theodore H. *A Brief Introduction to Fluid Mechanics*. York, PA: John Wiley & Sons, Inc. 2004

[7] Sherman, R. H., Blumberg, P. N., "Influence of Induction and Exhaust Processes on Emissions and Fuel Consumption in the Spark Ignited Engine," SAE Paper 770880, 1977.

[8] Shelby, Michael H., Stine, Robert A., Warren, Christopher C., "A New Analysis Method for Accurate Accounting of IC Engine Pumping Work and Indicated Work," SAE Paper 2004-01-1262, 2004.

[9] Peng He, Yunqing Li and Jincheng Wang, "Study on the Exhaust System Parameters of a Small Gasoline Engine," SAE Paper 2008-01-1766, 2008.

[10] Poulos, Stephen G., Heywood, John B., "The Effect of Chamber Geometry on Spark-Ignition Engine Combustion," SAE Paper 830334, 1983.

[11] Woshni, G., "A Universally Applicable Equation for the instantaneous Heat Transfer Coefficient in the Internal Combustion Engine," SAE Paper 670931, 1967.

[12] Ham, Yun-Young, Pyongwan, P., "The Effects of Intake Valve Events on Engine Breathing Capability," SAE Paper 912470, 1991.

[13] Burnt, Michael F. J., and Pond Christopher, R., "Evaluation of Techniques for Absolute Cylinder Pressure Correction," SAE Paper 970036, 1997.

[14] Randolf, A.L., "Methods of Processing Cylinder Pressure Transducer Signals to Maximize Data Accuracy," SAE Paper 900170, 1990.

[15] Lancaster, David R., Roger B. Krieger, and John H. Lienesch, "Measurement and Analysis of Engine Pressure Data," SAE Paper 750026, 1975.

[16] Smither, B., McFarlane, I., Drake, T., Ravenhill, P., Allen, P., and Boak, J., "Engine Management System for Fuel Injection System Specifically Designed For Small Engines," SAE Paper 2008-32-0052, 2008.

[17] Figliola, Richard S., Beasley, Donald E. *Theory and Design for Mechanical Measurements*. York, PA: John Wiley & Sons, Inc. 1995.

[18] Cary, Clint W., Wildhaber, Shawn N, Drallmeier, James A., 2009, "Small Engine Design for Fuel Efficiency-Progress Report 1," Missouri University of Science and Technology.

[19] Singh, Avinash, Huck, Cory H. Wildhaber, Shawn N. Drallmeier, James A., 2011, "Small Engine Design for Fuel Efficiency-Progress Report 7," Missouri University of Science and Technology.

[20] Wildhaber, Shawn N., 2011, "Impact of Combustion Phasing on Energy and Availability Distributions of an Internal Combustion Engine," M.S. thesis, Department of Mechanical Engineering, Missouri University of Science and Technology.

VITA

Cory Hannibal Huck was born in Springfield, Missouri on December 12, 1986 to Stanley and Sandra Huck. He graduated from Ozark High School in May of 2005. In December 2009, he received his B.S. in Mechanical Engineering from Missouri University of Science and Technology (formerly known as University of Missouri – Rolla). In January 2010 he joined the Mechanical Engineering Graduate program and in May 2012, received his M.S. in Mechanical Engineering from the Missouri University of Science and Technology. He accepted a position at Cummins, Inc. as an engineer at the Mid-Range Research facility in Columbus, Indiana.